Salt-inducible kinases in normal B-cell differentiation and malignancy

Emily Faye Robinson

Submitted in accordance with the requirements for the degree of

Doctor of Philosophy

The University of Leeds

Leeds Institute of Cancer and Pathology

Section of Experimental Haematology

August 2019

Acknowledgements

Firstly, I would like to take this opportunity to thank my supervisors Dr Gina Doody and Professor Reuben Tooze for their exceptional guidance and support during the past four years, and my funding body Cancer Research UK, without whom this research would not have been possible.

I would also like to express my gratitude to the entire Doody/Tooze lab group who were always on hand to provide advice and discussion. I am particularly thankful to Sophie Stephenson who gave up so much of her time to help both in and out of the lab. I would also like to thank Michelle Campbell for providing her expertise in flow cytometry and helping with mouse experiments until the early hours. Further thanks go to Matthew Care for his bioinformatic analysis of the RNA-sequencing data and my collaborators Nicola Darling and Sir Phillip Cohen for providing tissue from SIK KI mice.

I am also grateful to have met such a fantastic group of friends - Jenny, Sheetal, Nicole and Charlotte. We've laughed, cried and also sworn quite a few times, but their kindness and humour always kept me going.

Final thanks go to my family including my partner Liam, my mum, dad and brother and my grandparents for believing in me and encouraging me throughout my life. This piece of work is dedicated to my late nanna, Patricia Andrews who was immensely proud of my work. Her positive 'can-do' attitude taught me to never give up and inspired my passion for research.

Abstract

The generation of antibody-secreting plasma cells is a step-wise process involving initial B-cell activation and expansion, followed by the persistence of end-stage effector cells that reside in supportive niches. The transition through these stages requires reprogramming for high levels of secretion and adaptation to the bioenergetic demands of immunoglobulin production. To gain insight into the pathways involved, gene co-expression network analysis was applied to temporal data derived from in vitro differentiating human plasma cells. Salt-inducible kinase 1 (SIK1) was identified as a highly connected transcriptional regulator involved in the transition from a cycling plasmablast to a quiescent plasma cell. The SIK subfamily consists of three isoforms; SIK1, SIK2 and SIK3 and belongs to the AMPK-related kinase family. The family has previously been linked to the control of metabolism, in part through controlling dynamic changes in phosphorylation and subcellular localisation of cyclic adenosine monophosphate (cAMP)-regulated transcriptional co-activators (CRTCs) and class II histone deacetylates (HDACs).

To assess the contribution of SIK family kinases during plasma cell differentiation, small molecule SIK inhibitors were utilised. Treatment of primary human B-cells that have activated plasma cell differentiation with the SIK inhibitors lead to a profound reduction in cell viability and these effects were also replicated in a subset of multiple myeloma cell lines. Furthermore, mice with catalytically inactive SIKs demonstrated a decrease in splenic plasma cells at steady state/following in vitro B-cell differentiation and immunisation resulted in alterations in immunoglobulin secretion. Downstream analysis of protein revealed a loss of total class II histone de-acetylase (HDAC) expression in plasmablasts (PBs) and plasma cells (PCs), but not activated B-cells indicative of different downstream mechanisms. Finally, gene expression profiling in PBs and PCs highlighted dramatic changes in genes related to phosphoinositide 3-Kinase (PI3K) signalling, glycolysis and endocytosis indicating profound metabolic collapse.

These novel findings propose that the SIKs play a central, yet complex role in the development and survival of plasma cells through regulating many aspects of differentiation such as growth, proliferation, class switch recombination and glycolysis. Overall, it is reasonable to conclude that plasma cells depend on SIKs for adaptive metabolic programming, thus providing a promising target in the treatment of multiple myeloma which generate extra metabolic requirements to support growth, proliferation and immunoglobulin production.

Table of Contents

List of figures

List of tables

Chapter 1 – Introduction

1.1 The immune system

The role of the immune system is to protect the host from invading pathogens, toxins and allergens, whilst avoiding excessive damage to self-tissues or beneficial microbes. This is achieved through both innate and adaptive responses, which primarily detect structural features of the pathogen that mark it as distinct from host cells.

The innate system predominantly recognises molecular patterns shared by many microbes and toxins that are not present in the mammalian host. Anatomical and physiological barriers as well as non-specific defence mechanisms (inflammation, complement activation, cytokine secretion and phagocytosis) are poised to act rapidly after an encounter, constituting the initial host response. In contrast, the adaptive immune system responds several days after exposure to a pathogen and has the capacity to mount a response to a specific antigen as well as establishing long-term memory. The adaptive system is comprised of highly specialised T- and B-lymphocytes, which express T-cell receptor (TCR) and immunoglobulin (Ig) genes, respectively. Somatic re-arrangement and V(D)J recombination of the gene segments which encode these receptors generates millions of different combinations, thus providing unique antigen specificity (Tonegawa *et al.*, 1974).

T-cell activation is dependent on the interaction with an antigen presenting cell (APC) which displays a processed antigenic peptide bound to a major histocompatibility complex (MHC) class I or class II (Pennock *et al.*, 2013). Once activated, cytotoxic T-cells largely focus on the elimination of pathogen-infected host cells through the release of perforin and granzyme protein families. Helper T cells play a more central role and support the production of cytokines and chemokines that either activate neighbouring cells to perform specific functions or recruit new immune cell subsets to sites of pathogen encounter (Peters *et al.*, 1991; Zhu and Paul, 2008).

In contrast, B-cells directly encounter antigens as three-dimensional structures through the surface B-cell receptor (BCR) and the interaction triggers a complex signalling cascade which results in the generation of plasma cells, effector cells of the B-cell lineage. During this process, the BCR transitions from membrane bound to the secreted immunoglobulin molecule resulting in antigen neutralisation and antibody-mediated cytotoxicity (Geisberger, Lamers and Achatz, 2006).

The signalling events that initiate B-cell differentiation converge on several pathways resulting in both the activation and repression of hundreds of transcription factors and the resultant plasma cell gene expression program. This project will assess the involvement of salt inducible kinases (SIKs) during B-cell differentiation, which have not been previously studied in this context. SIKs belongs to the AMP-activated protein kinase (AMPK) family of kinases and may provide an opportunity for therapeutic targeting in plasma cell malignancies.

1.2 B-cell differentiation

1.2.1 Early B-cell development

B-cells develop from pluripotent haematopoietic stem cells in the bone marrow and differentiate through several maturation stages. The overall process requires the joint action of many cytokines and transcription factors that positively and negatively regulate gene expression (Milne and Paige, 2006; Hardy et al., 2007). In particular, E2A, EBF, PU.1 and Pax5 have been defined as essential in promoting B-cell lineage commitment and differentiation (Nutt and Kee, 2007). At the pre-B cell stage, combinatorial rearrangement of the V, D and J gene segments produces a diverse repertoire of heavy and light immunoglobulin chains encoding the pre-B-cell receptor (LeBien and Tedder, 2008). Subsequent rearrangement of mature κ and λ light chains leads to the expression of both surface IgM and IgD (Vale and Schroeder, 2010). After passing through a control checkpoint, selected B-cells migrate to the spleen and develop into fully mature subsets (Chung, Silverman and Monroe, 2003). Cells then continue to circulate through secondary lymphoid organs such as the spleen and lymph node until encountering a cognate antigen (Shapiro-Shelef and Calame, 2005) which induces a cascade of differentiation events, resulting in proliferation, plasma cell formation and immunoglobulin secretion (Reya and Grosschedl, 1998).

1.2.2 Types of response

The activation of B-cells and thus the generation of antibody secreting cells (ASCs) can be separated into two pathways based on the type of antigen and whether it requires the presence of T-cells to elicit an immune response (Figure 1.1). T-cell independent antigens such as bacterial lipopolysaccharides and polymeric proteins stimulate B-lymphocytes outside of the B-cell follicle through toll-like receptor (TLR) activation or BCR crosslinking. In contrast, a T-cell dependent response arises from both follicular and marginal zone B-cells binding to a cognate antigen, which is displayed on a major histocompatibility complex (MHC) for T-cell recognition and help. ASCs then develop via a two-step process providing both immediate and long-term protection. Initially, an

extrafollicular pathway produces short-lived antibody secreting plasmablasts with moderate affinity. Activated B-cells can also re-enter the B-cell follicle and proliferate, forming an intra-follicular germinal centre (GC) (Nutt *et al.*, 2015). Germinal centres are transient and typically last a few weeks after exposure to antigen. In the dark zone, hundreds of individual clones with functional BCRs undergo a proliferative burst. This is followed by somatic hypermutation in which the hyper-variable region (*VDJ*) of the B-cell immunoglobulin gene is mutated to allow for the production of highly specific antibodies. Following migration to the light zone, affinity maturation and class switch recombination (CSR) occurs to produce antibodies of different immunoglobulin isotypes (Klein and Dalla-Favera, 2008). Consequently, thousands of memory B-cells and plasma cells emerge as soon as one week after antigen encounter providing a range of antigen-specific effector cell types (Tas *et al.*, 2016). The overall process is selective for clones with the highest affinities meaning some rapidly undergo apoptosis whilst others circulate in the blood to initiate and maintain the immune response or migrate to the bone marrow providing serological memory (Morgan, Walker and Davies, 2012).

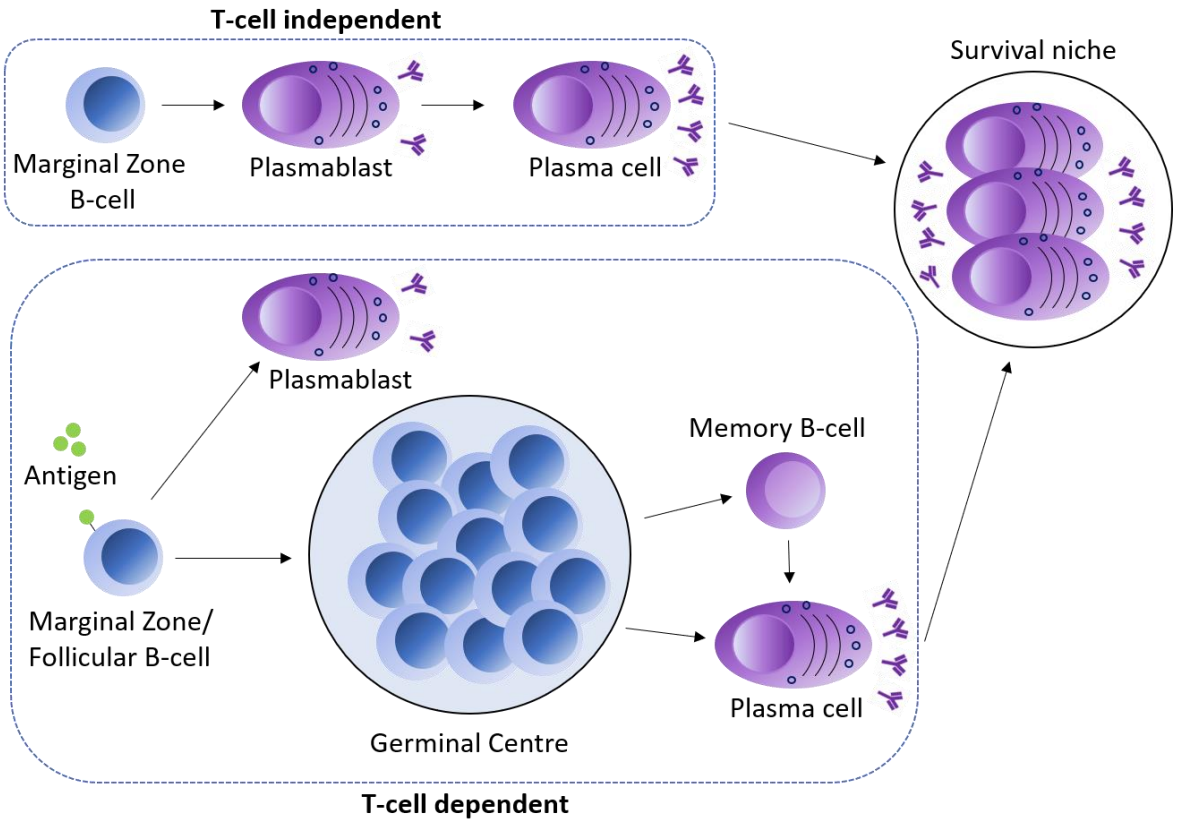

Figure 1.1 T-cell dependent and independent B-cell responses. The differentiation pathways of normal B-cells following antigen encounter. (Adapted from Low *et al.* 2016).

1.2.3 Transcriptional regulation of B-cell differentiation

Transcription factors influence B-cell differentiation by regulating the expression of numerous lineage-specific genes. Fundamentally, the factors that define B-cell and plasma cell identity regulate mutually antagonistic programs to silence B-cell specific programs whilst inducing the expression of plasma cell specific regulators. Figure 1.2 highlights the contribution of several transcription factors to each cellular differentiation state, some of which are outlined below.

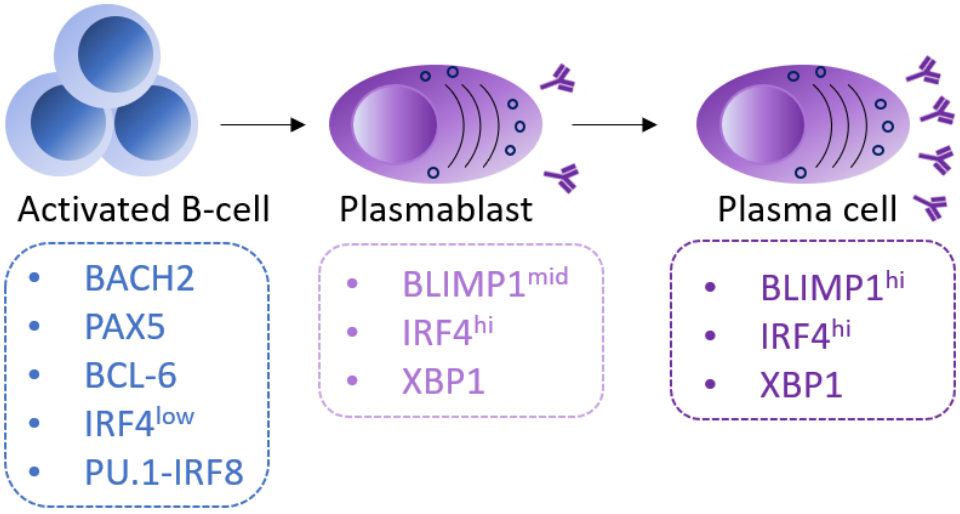

Figure 1.2 Transcription factors that control B-cell differentiation. (Adapted from Nutt *et al.,* 2015).

1.2.3.1 B-cell programme

The overall B-cell gene expression programme is essential for promoting both antigen sensitivity and preventing premature ASC differentiation. PAX5 is central to B-cell maturation through its role in maintaining B-cell identity and immunoglobulin re-arrangement (Holmes, Pridans and Nutt, 2008). BTB Domain and CNC Homolog 2 (BACH2) is a transcriptional repressor essential for BCR-induced proliferation, survival, and cell cycle progression (Miura *et al.*, 2018) and also inhibits plasma cell differentiation by repressing *Prdm1* expression (Muto *et al.*, 2010).

B-cell lymphoma 6 (BCL-6) is a zinc finger transcription factor that predominantly functions as a transcriptional repressor. It is highly expressed in GC B-cells and is essential for GC formation and affinity maturation (De Silva and Klein, 2015). Loss of Bcl6 expression has been shown to impair the upregulation of CXCR4, a chemokine receptor expressed on dark-zone B cells that is critical for the maintenance of GC structural integrity (Kitano *et al.*, 2011).

Myocyte-specific enhancer factor 2B (MEF2B) and MEF2C have distinct roles during B-cell activation. MEF2B is important for early GC formation through activation of Bcl6, whereas MEF2C is crucial for proliferation and survival through upregulation of Bcl2l1 (Ying *et al.*, 2013; Wilker *et al.*, 2008).

Additional factors involved in the B-cell programme include BATF, a transcription factor of the AP-1 family, which is involved in GC structure establishment and class switch recombination (Ise *et al.*, 2011) and c-MYC which is necessary for GC formation and maintenance (Dominguez-Sola *et al.*, 2012; Calado *et al.*, 2012). Finally, the ETS family transcription factor PU.1 and the closely related factor SPIB can form complexes on DNA with IRF4 and IRF8 in B-cells, promoting the normal production of ASCs (Kanno *et al.*, 2005).

1.2.3.2 Plasma cell programme

In order to emerge from the GC reaction, transcriptional re-programming must occur to allow cells to commit to the ASC fate. The ASC transcriptome supports the production of large amounts of immunoglobulin and homing to bone marrow niches. This is achieved through the activation of three well-defined transcription factors – IRF4, BLIMP1 and XBP1.

IRF4 is expressed at low levels during the early stages of B-cell differentiation, however increases upon differentiation. It predominantly acts to repress BCL-6 and activate BLIMP1, thus facilitating the ASC fate (Kallies *et al.*, 2007; Ochiai *et al.*, 2013).

BLIMP1 is one of the most crucial transcription factors during establishment of the plasma cell program and represses key B-cell/GC programme regulators such as SPIB, BCL-6, MYC and PAX5 (Sciammas *et al.*, 2006; Shaffer *et al.*, 2002). It is absent in the early stages of the B-cell lineage but is subsequently expressed in all antibody-secreting cells (ASCs). ASCs must secrete large amounts of immunoglobulin, which causes an increase in metabolic demand and sensitivity to ER stress. Blimp-1 is also essential for normal antibody production due to regulating components of the unfolded protein response (UPR) including X-box binding protein 1 (XBP1) and activating transcription factor 6 (ATF6).

XBP1 is a bZIP protein and is primarily responsible for expansion of the secretory apparatus through remodelling of the endoplasmic reticulum (Tellier *et al.*, 2016b; Todd *et al.*, 2009). Such factors balance protein folding and degradation to overcome the accumulation of unfolded proteins within the ER lumen, maintaining plasma cell survival and functional immunoglobulin secretion.

1.2.4 Bone marrow survival

Following terminal differentiation, plasma cells can migrate to the bone marrow and occupy pro-survival niches for the potential lifetime of the organism (Oracki *et al.*, 2010). Occupancy within such microenvironments is supported by a close interaction with stromal cells as well as neutrophils and eosinophils which have been reported to be the main source of plasma cell survival factors due to the production of IL-6 and CXCL12 (Belnoue *et al.*, 2008; Chu *et al.*, 2011). Furthermore, signalling through A proliferation-inducing ligand (APRIL) and its receptor B-cell maturation antigen (BCMA) has been shown to upregulate expression of the anti-apoptotic protein myeloid cell leukaemia 1 (MCL1) which is known to be essential to ASC survival (Peperzak *et al.*, 2013).

In addition to stromal cells, osteoclasts have been shown to be of crucial importance for the growth and survival of multiple myelomas, providing factors such as BAFF, APRIL and IL-6 (Novak *et al.*, 2004; Abe *et al.*, 2004).

1.2.5 Plasma cell quiescence

The final stage of plasma cell differentiation is accompanied by cell cycle quiescence, which was originally thought to be permanent and irreversible (Chen-Kiang, 2003; Amanna and Slifka, 2010). An alternative replicative self-renewal model proposes that long-lived plasma cells reside in a quiescent state expressing a range of cell cycle regulators, but can be triggered by cellular and immunological cues to promote transient episodes of cell cycle re-entry at a low frequency (Tooze, 2013).

Whilst evidence to support long-lived plasma cell self-renewal is limited, research into haematopoietic stem cells which reside in a quiescent state for prolonged periods of time yet maintain the ability to become activated demonstrates that quiescence is an actively maintained state. For example, quiescent stem cells express metabolic sensors and effectors such as FOXO, HIF1α and LKB1 which are poised to act following metabolic or genotoxic stress. Notably, quiescent stem cells devoid of these pathways have an increased propensity to become activated and fail to maintain the stem cell pool (Cheung and Rando, 2013). This demonstrates that expression of such molecules is essential for the metabolic function and maintenance of quiescent stem cells and gives rise to the idea that similar pathways may regulate plasma cell quiescence.

1.3 Multiple Myeloma

Multiple myeloma (MM) arises from the malignant transformation of plasma cells which accumulate within the bone marrow. The causes remain largely unknown although evidence to suggest that random mutations acquired in a non-linear fashion are selected for based on their clonal advantage and contribute to the heterogenic nature of the disease (Morgan, Walker and Davies, 2012).

1.3.1 Pathogenesis

At present, there is no single conclusion regarding the 'time' of a mutation event during the differentiation pathway. For example, genetic mutations occurring at the B-cell stage include translocations between the Ig heavy chain locus on chromosome 14q32 and one of several oncogenes: *FGFR3*, *MMSET*, *CCND1*, *CCND3* and *MAF*, whereas activating mutations in *MYC*, *KRAS*, *NRAS*, *AKT*, *PI3K*, *XBP1*, *BLIMP1*, *IRF4* and *TP53* occur at the plasma cell stage (Bianchi and Anderson, 2014). Alternatively, it is believed that events driving myeloma could occur at the pre-B cell stage in the bone marrow (Mahindra, Hideshima and Anderson, 2010).

Mutations that arise in mature B-cells can be promoted by genotoxic stress associated with both somatic hypermutation and class switching, highlighting how a cell can be pushed towards malignancy as the result of a normal physiological process. In order to remodel immunoglobulin genes, activation-induced cytidine deaminase (AID) generates DNA double strand break intermediates (Chaudhuri *et al.*, 2003) which are then repaired to preserve genomic integrity (Sherman *et al.*, 2010). During this process, DSBs can translocate with breaks occurring elsewhere in the genome generating aberrant chromosomal translocations (Morgan, Walker and Davies, 2012). To overcome this, cells respond by activating a DNA damage response (DDR) complex that stops neoplasms forming through the induction of apoptosis. In GC B-cells, the DDR is co-ordinated by an ATM serine/threonine kinase which represses the genetic programme associated with B-cell proliferation, self-renewal and differentiation thus stopping the malignant clone from expanding. In some instances, however, the malignant clone escapes this mechanism and proliferates forming cancer (Sherman *et al.*, 2010).

Neoplastic plasma cells subsequently exit the GC and infiltrate the bone marrow to live in close association with bone marrow stromal cells (BMSCs) and extracellular matrix. Myeloma cells release paraproteins (monoclonal antibodies) as well as immunoglobulin light chain fragments. Overall, the pathophysiology is complex and consequences include bone lesions, renal failure and anaemia (Silbermann and Roodman, 2013; Goldschmidt *et al.*, 2000; Birgegård, Gascón and Ludwig, 2006). In

advanced disease, pancytopenia occurs as the result of haematopoietic marrow being replaced by malignant plasma cells (Sridevi *et al.*, 2015).

1.3.2 Treatment

Myeloma is described as incurable although various drug regimens aim to stop further progression and manage symptom control. Targeted and biological therapy includes the 26S proteasome inhibitor bortezomib, (which inhibits the degradation of both short and long-lived proteins thus activating the unfolded protein response) and the immunomodulatory agent lenalomide (which promotes tumour cell apoptosis and inhibits stromal cells found within the tumour microenvironment). Although shown to improve overall survival, toxicity and acquired resistance are problematic meaning therapeutics with increased specificity are required (Mitsiades *et al.*, 2007).

1.4 In vitro generation of plasma cells

Until recently, a model system permitting the in vitro generation of long-lived plasma cells did not exist meaning that the full trajectory of B-cell differentiation and potential mechanisms related to plasma cell transformation could not be readily investigated. Various groups have since addressed this issue, therefore plasma cell differentiation can now be effectively recapitulated in vitro in response to both T-cell derived stimuli such as CD40-L ligation and cytokines (IL-2, IL-21) or TI- signals such as R848 (Jourdan *et al.*, 2009; Cocco *et al.*, 2012; Hanten *et al.*, 2008). Figure 1.3 depicts the in vitro model developed within the Doody/Tooze lab to generate and maintain plasmablasts and plasma cells and highlights the cell surface markers used for identification.

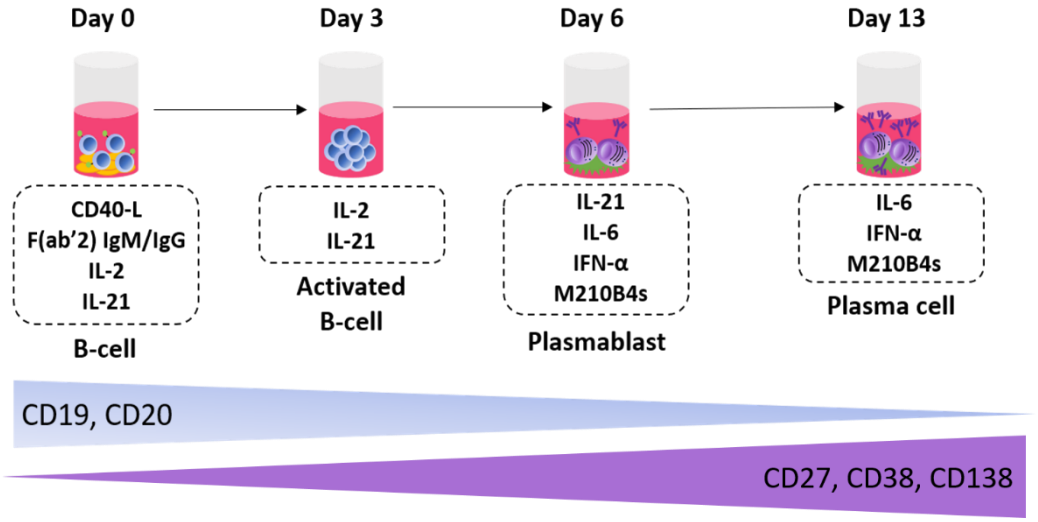

Figure 1.3 In vitro model of B-cell differentiation. Total B-cells isolated from peripheral blood are re-suspended in IMDM with the indicated cytokines and growth factors. Cells are re-fed every 3 days until elective termination occurs.

1.5 Identification of SIK1

Although there is an in-depth understanding of the factors that control commitment to the ASC fate, less is known about the transition between short-lived, cycling plasmablasts and long-lived post-mitotic plasma cells. To investigate which regulatory networks may be involved, the in vitro system described in section 1.4 was used and a 96-hour window encompassing the final transition to quiescence was analysed with a detailed gene expression time-course and weighted gene correlation network analysis (WCGNA) (Care *et al.*, 2016).

As shown in Figure 1.4, salt-inducible kinase 1 (*SIK1*) was identified as a hub gene. Hub genes are centrally located transcriptional regulators with numerous connections and are therefore expected to play important roles in biology (Langfelder and Horvath, 2008). Preliminary data also showed that SIK inhibition resulted in a decrease in the viability of normal human plasma cells. This highlights a potential dependency and suggests that SIKs may co-ordinate terminal differentiation through controlling mechanisms associated with plasma cell survival.

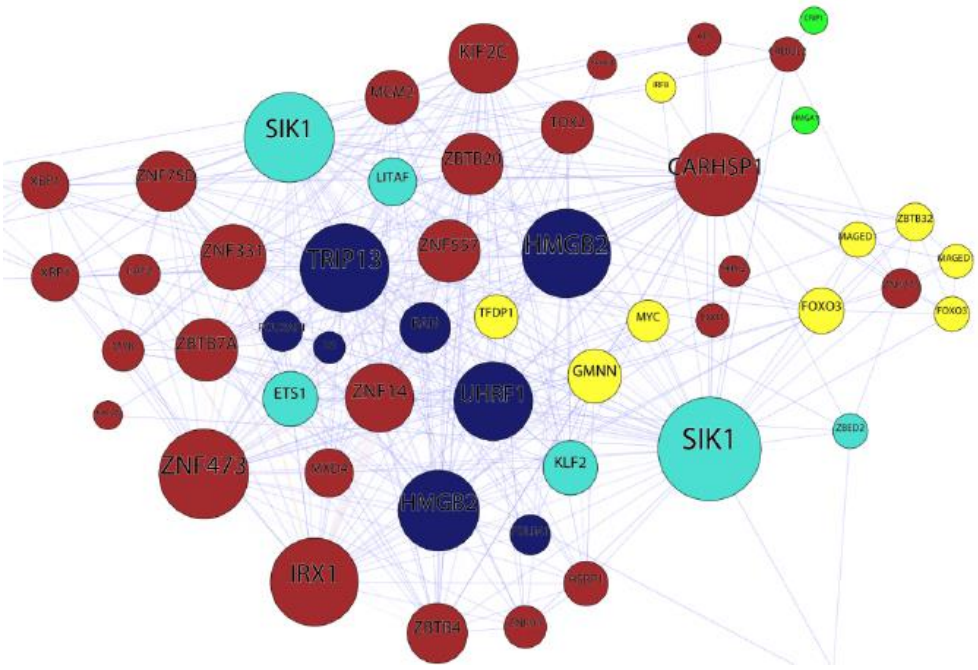

Figure 1.4 Correlation gene network map. Data generated from temporal analysis of an in vitro B-cell differentiation highlighting potentially important control points of plasma cell generation. Edge width shows the Pearson's correlation between each gene and the number of connections per hub gene is represented by node size. (Unpublished data, Matt Care and Nick Barnes).

1.5.1 SIK1 in myeloma

Parsimonious gene correlation network analysis (PGCNA) is a novel bioinformatic tool that can be successfully applied to gene expression data to gain insight into cancer biology and experimental model systems (Care, Westhead and Tooze, 2019). In particular PGCNA improves upon the resolution of biologically significant modules of co-expressed genes compared to other widely used approaches. Using publicly available multiple myeloma datasets, PGCNA generates 26 modules, which map onto known aspects of normal and neoplastic plasma cell biology (Care, Westhead and Tooze, unpublished data). *SIK1* is a member of module 6 which shows the strongest association with overall patient survival. Furthermore, *SIK1* has a median expression value of 97.21% which is comparable with the expression of major plasma cell specific factors such as IRF4 (86.53%), *PRDM1* (94.76%) and *CD38* (98.25%). Thus, SIK1 may be part of a network that either identifies myeloma with a different underlying biology or better response to treatment. This provides rationale for evaluating SIK1 as a potential therapeutic target in the treatment of myeloma.

1.6 AMPK-related kinase subfamily

5’ adenosine monophosphate-activated protein kinase (AMPK) is a regulator of energy homeostasis and exists as a heterotrimeric complex containing one catalytic subunit (AMPKα) and two regulatory subunits (AMPKβ and AMPKγ). More specifically, it is a highly conserved sensor of intracellular adenosine nucleotide levels, which become activated when modest decreases in ATP result in relative increases in AMP or ADP (Mihaylova and Shaw, 2011). In response, catabolic processes such as glycolysis are switched on to generate ATP, whilst anabolic processes such as protein, fatty acid and cholesterol synthesis are switched off.

In silico analysis of the human kinome revealed a group of around 20 kinases with a sequence similar to the kinase domain of AMPKα1/α2. These were subsequently denoted ‘AMPK-related kinases’ and divided into subfamilies comprising BRSKs, NUAKs, MARKs, SIKs and MELK (Manning *et al.*, 2002). With the exception of MELK, AMPK-related kinases have a lysine residue at -2 relative to the T-loop threonine in the kinase domain and are activated by the upstream master kinase liver kinase B1 (LKB1) at a site equivalent to threonine 172 in AMPK (Lizcano *et al.*, 2004).

1.6.1 LKB1 mediated AMPK regulation

LKB1 is a tumour suppressor kinase, discovered as a major cause of the rare Peutz-Jeghers Syndrome. Its activation is governed by a phosphorylation-independent allosteric mechanism, in which it forms a heterotrimeric complex with 2 accessory proteins, STE20-related kinase adaptor (STRAD) and mouse protein 25 (MO25) (Hemminki *et al.*, 1998). The LKB1-AMPK pathway was primarily thought of as an energy sensing pathway, however recent evidence has linked the pathway to fundamental cellular processes including regulation of cell proliferation, cell polarity, migration, transcription and stress/damage responses (Brown, Samarajeewa and Simpson, 2013; Lizcano *et al.*, 2004; Alexander and Walker, 2011).

Studies into the regulation of LKB1 have not been able to show LKB1 complex activation under any stimulating cues leading to the hypothesis that it is constitutively active in cells (Fogarty and Hardie, 2009; Sebbagh *et al.*, 2009). This suggests that the AMPK-related kinases are also constitutively phosphorylated, however with numerous downstream targets little is known regarding what stimuli directs LKB1 to preferentially phosphorylate specific AMPK-related kinases (Woods *et al.*, 2003). It is also important to note that LKB1 can be phosphorylated or post-translationally modified at alternative sites which may indirectly affect the activity of LKB1 towards a substrate by changes in cellular location or binding to an activating subunit (Alessi, Sakamoto and Bayascas, 2006). For example, Lee and colleagues discovered K63-linked ubiquitination of LKB1 as a new post-translational modification event indispensable for LKB1-MO25 interaction, LKB1 activity, and downstream AMPK signalling in cancer cells under energy stress (Lee *et al.*, 2006). Collectively, this proposes a novel and interesting mechanism for conferring signal transduction specificity and control at the kinase substrate level and highlights the complexity of LKB1 mediated AMPK regulation.

1.6.1.1 The role of LKB1 during B-cell differentiation

LKB1 has been described to act as a molecular switch during B-cell differentiation that allows cells to pass through various developmental stages. Antigenic stimulation is proposed to inactivate LKB1, enabling cellular activation and the differentiation of highly proliferative GC B-cells. To exit the GC, DNA double strand breaks which occur during immunoglobulin CSR activate LKB1 to inactivate the downstream substrate CRTC2 and promote the terminal differentiation of GC B-cells into quiescent plasma cells (Figure 1.5) (Waters, Walsh and Teitell, 2015).

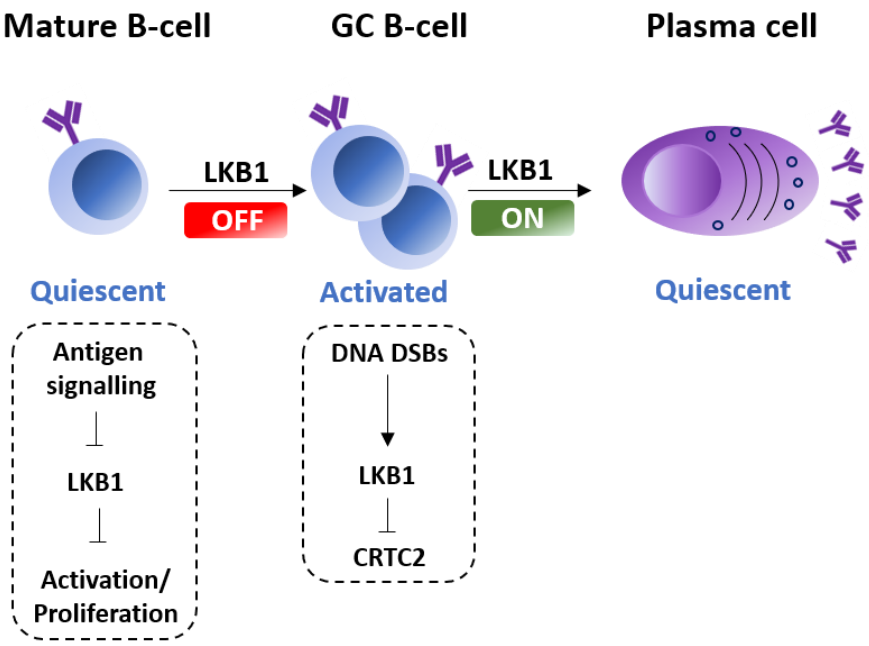

Figure 1.5 Proposed model in which LKB1 acts as a molecular switch to sequentially activate and inactivate B-cells during a T-cell dependent response. (Adapted from Waters, Walsh and Teitell, 2015).

Furthermore, *Lkb1*-deficient B-cells undergo spontaneous B-cell activation and secrete multiple inflammatory cytokines (IL-6 and IL-21), which promote $CD4^+$ T-cell differentiation into T_{FH} cells potentially driving unstimulated GC formation and expansion (Walsh *et al.*, 2015). These results suggest a model in which antigen-triggered LKB1 inactivation in mature B-cells is a physiologic mechanism for modulating the GC reaction through B-cell intrinsic and extrinsic immune system activation.

1.6.1.2 The role of LKB1 in quiescence

As described in section 1.2.5, LKB1 has been implicated as a metabolic sensor in the maintenance of haematopoietic stem cell quiescence and survival. In dendritic cells, LKB1 has been shown to regulate metabolic quiescence by acting as a brake to restrain excessive regulatory T cell (Treg) and Th17 cell responses, thereby promoting protective anti-tumour immunity and maintaining proper immune homeostasis (Wang *et al.*, 2019). Furthermore, Maillet and colleagues recently uncovered a novel role for LKB1 as an essential regulator of hepatocellular quiescence and proliferation during liver regeneration, independently of AMPK (Maillet *et al.*, 2018).

The mechanism(s) for how constitutively active LKB1 regulates quiescence in these cell types remains unclear, although it is conceivable that LKB1 downstream target proteins may be involved. Attempts to elucidate the role of AMPK using *Lkb1* cell-specific knockout models together with complementation or pharmacological activation of AMPK have not been sufficient to reverse the activation and proliferative phenotype suggesting that either LKB1 functions through an AMPK independent mechanism altogether or that an alternative AMPK-related kinase is responsible (Krock, Skuli and Simon, 2011; Blagih, Krawczyk and Jones, 2012). An attractive alternative is the SIK family kinases which have overlapping downstream substrates and functions as highlighted in Figure 1.6.

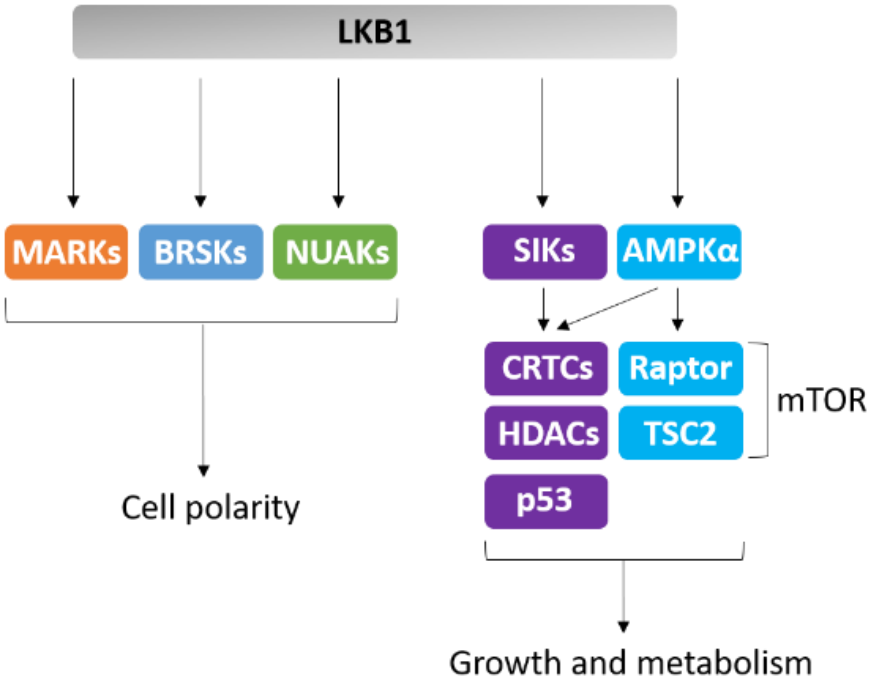

Figure 1.6 LKB1 is a master kinase that activates 13 kinases of the AMPK subfamily. (Adapted from Shackelford and Shaw, 2009).

1.6.2 Alternative mechanisms of AMPK regulation

In addition to LKB1, alternative mechanisms of AMPK regulation include phosphorylation by protein kinase A (PKA) which inhibits AMPK by phosphorylating S173 of the α1-subunit. This blocks upstream kinases such as LKB1 and CaMKK2 from phosphorylating threonine 172 (Djouder *et al.*, 2010).

CAMKK2 can also phosphorylate AMPK to significantly enhance enzymatic activity. Recent studies have indicated the involvement of CaMKKβ/AMPK signaling in metabolic regulation including appetite control (Anderson *et al.*, 2008), amino acid starvation-induced autophagy (Ghislat *et al.*, 2012) and cancer growth (Frigo *et al.*, 2011).

Furthermore, ubiquitination inhibits AMPK by inducing its degradation, however the exact mechanisms underlying this are unclear. This can be seen with WW domain-containing E3 ubiquitin protein ligase 1 (WWP1) which mediates the degradation of the AMPK α2-subunit through ubiquitination in the presence of high glucose levels (Lee *et al.*, 2013).

1.7 SIKs

SIK1, the founding member of the SIK subfamily was discovered in the adrenal glands of rats fed with a high salt diet (Wang *et al.*, 1999). Subsequent homology searches then led to the identification of SIK2 and SIK3. All three isoforms are monomeric and contain an N-terminal kinase domain bearing an LKB1 phosphorylation site, a central SNF1 protein kinase homology (SNH) domain, and a long C-terminal extension with several potential protein kinase A phosphorylation sites (Figure 1.7) (Katoh *et al.*, 2004). SIK1 is located on chromosome 21, whereas SIK2 and SIK3 are located on chromosome 11.

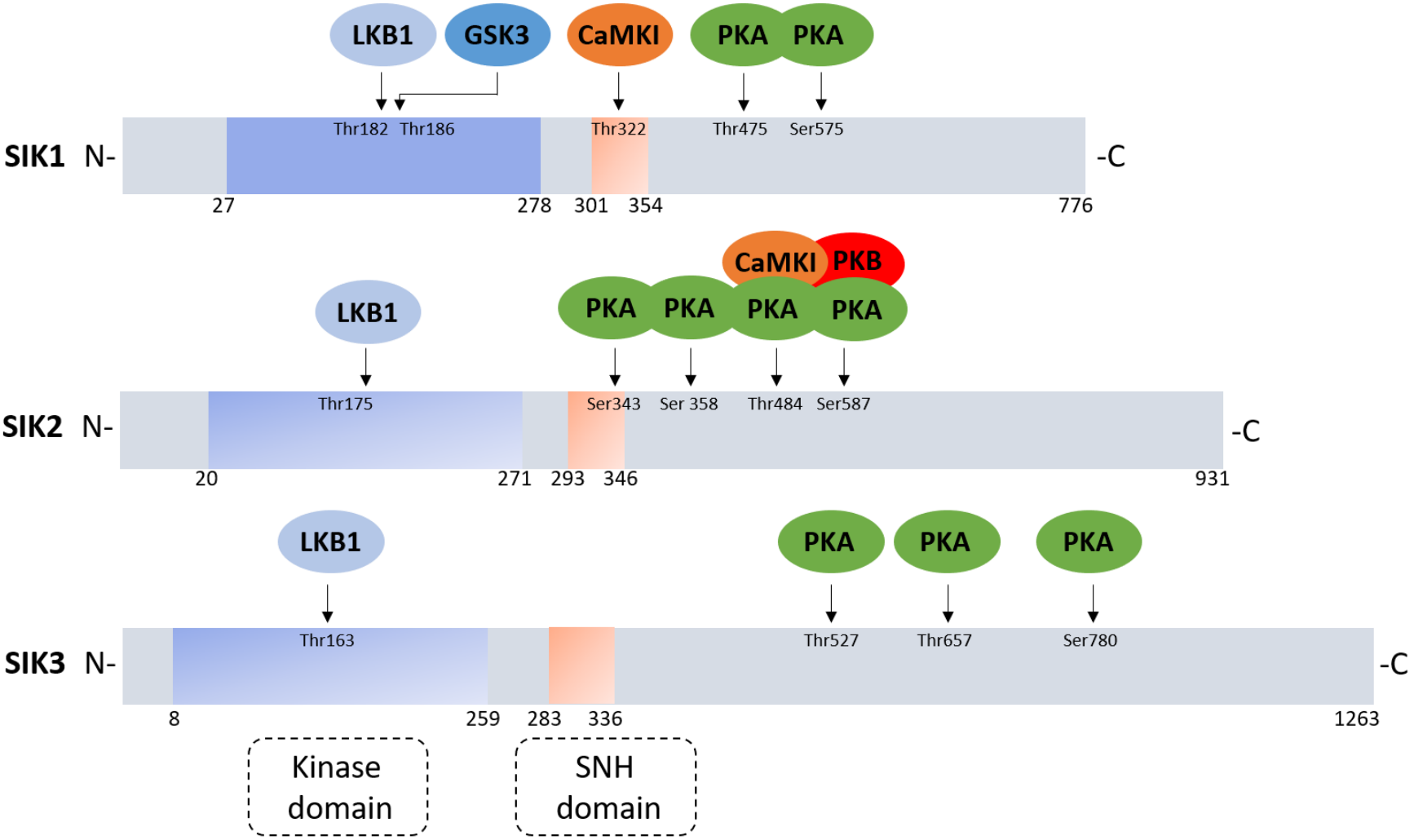

Figure 1.7 Domain structure and reported phosphorylation sites of SIK isoforms. Structure of SIK1, SIK2 and SIK3 highlighting reported upstream kinase regulation. (Adapted from Sakamoto *et al.*, 2018).

1.7.1 Tissue distribution of SIK isoforms

All three isoforms are broadly expressed. SIK1 is most abundantly present in the adrenal cortex and pineal gland as well as dendritic and myeloid cells (Feldman *et al.*, 2000). Furthermore, *SIK1* is a rapidly inducible gene, whose mRNA expression is regulated by multiple stimuli including high dietary salt intake, adrenocorticotropic hormone, signaling glucagon signaling and circadian rhythms (Wang *et al.*, 1999; Lin *et al.*, 2001; Koo *et al.*, 2005; Jagannath *et al.*, 2013). In contrast, SIK2 and SIK3 are ubiquitously expressed with the highest SIK2 levels in adipose tissue and the highest SIK3 expression in the brain (Wein *et al.*, 2018).

1.7.2 Regulation of SIKs

Unlike AMPK, SIKs do not respond to nucleotides, but instead are regulated by extracellular signals, through complex LKB1-dependent and independent mechanisms. LKB1 activates all three SIK isoforms through phosphorylation of a threonine residue in the activation loop of the kinase domain (Sakamoto *et al.*, 2018). Recent studies have shown that reduced levels of SIK1 are associated with poor outcome in cancers, resulting in an invasive cellular phenotype with increased metastatic potential. For example, the LKB1-SIK1 signalling pathway is suppressed in ovarian carcinoma cells, which leads to the activation of transforming growth factor β (TGF-β) mediated epithelial-mesenchymal transition (EMT). In contrast, upregulation of LKB1 promoted SIK1 expression and markedly suppressed the growth and aggressiveness of ovarian cancer cells (Hong, Zhang and Yang, 2018). Furthermore, in gastric adenocarcinoma cells, gastrin-mediated signalling has been shown to induce phosphorylation of LKB1 at Ser428 and SIK1 at Thr182, thus reducing cell migration (Selvik *et al.*, 2014). Alternatively, fasting stimuli specifically control the kinase activity of LKB1 and establish the LKB1-SIK3 pathway as a converging point between feeding and fasting signals to control lipid homeostasis (Choi, Lim and Chung, 2015).

Signals that increase intracellular cAMP levels lead to protein kinase A (PKA)-mediated SIK family member phosphorylation (Screaton *et al.*, 2004) which does not alter SIK intrinsic kinase activity but instead promotes an interaction between SIK and 14-3-3 proteins (Berggreen *et al.*, 2012). This association leads to conformational changes and/or shifts in SIK cytoplasmic distribution that block the ability of these kinases to access and phosphorylate their substrates (Sonntag *et al.*, 2017). For example, in myeloid cells, prostaglandin E2 (PGE_2) signalling through PKA leads to SIK inhibition and a loss in CRTC3 phosphorylation driving IL-10 expression (MacKenzie *et al.*, 2013a). In addition, the cAMP-PKA-SIK2 signalling pathway acts as a tumorigenic mechanism in pancreatic tumour cells. Suppression of SIK2 mediated by PKA inhibits the phosphorylation of its downstream CREB-regulated transcriptional co-activator (CRTC) resulting in nuclear translocation and gene transcription. This promotes lipids absorption and synthesis, and the

abundant lipids in tumour cells provide substrates for structural, signalling, and metabolic purposes (Chen *et al.*, 2019). In contrast, PKA signalling in part by phosphorylation of Thr475 been shown to directly elevate *Sik1* transcripts as well as increasing the accumulation and stabilization of SIK1 protein thus supporting the differentiation of myogenic progenitor cells (Stewart *et al.*, 2013a). Furthermore, phosphorylation of Ser575 (SIK1) and Ser587 (SIK2) in response to treatment with adrenocorticotrophic hormone (ACTH) or PKA activators has been shown to promote nuclear exportation of SIKs suggesting that changes in SIK cellular localisation may also play regulatory roles (Takemori *et al.*, 2002).

Finally, activation of SIK1 in response to moderate increases in intracellular sodium requires elevations in intracellular calcium via activation of a reverse Na^{+}/Ca^{2+}-exchanger (NCX). This is followed by activation of calmodulin kinases (CaMK), leading to SIK1 phosphorylation of the T322 residue and increased SIK1 activity (Stenstrom *et al.*, 2009). Alternatively, Ca2+/calmodulin-dependent protein kinase I/IV are capable of phosphorylating SIK2 at Thr484 in cortical neurons, resulting in SIK2 degradation and CREB-dependent neuroprotective gene expression (Sasaki *et al.*, 2011).

1.7.3 Molecular mechanism of SIK-regulated gene transcription

To mediate a biological effect, the SIKs control gene expression via phosphorylation of transcriptional co-factors. Phosphorylation creates an interaction with 14-3-3 adaptor proteins which results in cytoplasmic sequestration and the potential to be ubiquitinated and degraded by the 26S proteasome (Dentin *et al.*, 2007). Alternatively, inhibition of the SIKs through PKA-mediated phosphorylation or small-molecule inhibitors abolishes the interaction with 14-3-3 and the substrate/co-factor is free to translocate into the nucleus where it can activate or repress gene transcription (Figure 1.8) (Altarejos and Montminy, 2011).

The SIK signalling pathway has not been fully elucidated, however there is emerging data to suggest that it plays both a positive and negative role through numerous downstream substrates, some of which are outlined below.

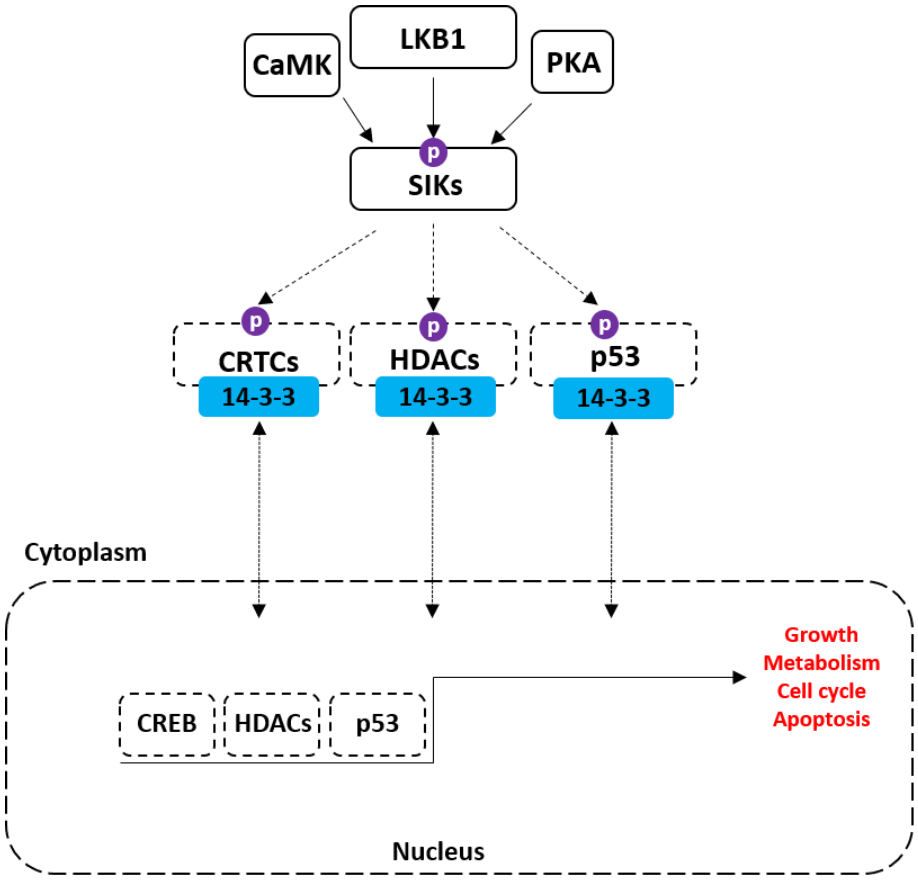

Figure 1.8 Schematic diagram of SIK regulation.

1.7.3.1 CREB-CRTC

cAMP response element (CRE)-binding protein (CREB) is a multi-faceted transcription factor regulating the expression of around 4000 target genes (Zhang *et al.*, 2005), which collectively exert a substantial impact on metabolism, cell proliferation and the immune response (Oh *et al.*, 2013; Ravnskjaer *et al.*, 2007; Siu and Jin, 2007). Activation is achieved through a group of transcriptional co-activators termed CREB-regulated transcriptional co-activators (CRTCs) (Iourgenko *et al.*, 2003). The family consists of three isoforms, CRTC1, CRTC2 and CRTC3. CRTC2 and CRTC3 have been shown to play roles in gluconeogenesis (Patel *et al.*, 2014), lipid metabolism (Han *et al.*, 2015) and macrophage polarisation (Luan *et al.*, 2015) whereas CRTC1 has been implicated in neuronal function including long term memory (Parra-Damas *et al.*, 2017) and circadian rhythm (Sakamoto *et al.*, 2013).

The SIKs are known to phosphorylate all three CRTC isoforms at various serine residues, however the literature predominantly reports the interaction between CRTC2 and CRTC3. In mice, depletion of SIK2 leads to the accumulation of larger adipocytes due to the hyperactivation of a CREB-CRTC2–dependent transcriptional program. This contributes to reduced insulin signalling highlighting the role of the SIK-CRTC-CREB pathway in regulating whole-body glucose metabolism (Park *et al.*, 2014). Furthermore, it has been shown in hepatocytes that following activation of the PI3K/AKT pathway through feeding, there is cAMP mediated phosphorylation of SIK2 resulting in disrupted CREB-dependent gene transcription (Dentin *et al.*, 2007).

SIK inhibition using HG-9-91-01 causes CRTC2 dephosphorylation resulting in increased glucose production comparable to that seen with glucagon stimulation (Patel *et al.*, 2014). This identifies SIKs as a potential target in the treatment of diabetes. SIKs also restrict the formation of regulatory macrophages and inhibition induces striking increases in many of the characteristic markers of regulatory macrophages, greatly stimulating the production of IL-10 and other anti-inflammatory molecules. This occurs through dephosphorylation of CRTC3, which enhances a gene transcription program controlled by CREB, highlighting the role of SIKs in resolving inflammation (Clark *et al.*, 2012).

Interestingly, CRTC2 has been shown to accumulate in the cytoplasm where it regulates a gene program that controls B-cell differentiation, including efficient termination of the GC reaction and antibody secretion. Over-expression of a constitutively active CRCT2 in B-cells causes a marked increase in proliferation and decrease in soluble IgG production, and in GC-derived B-cell lymphomas CRTC2 inactivation is disrupted. Overall, these findings place CRTC2 in a regulatory pathway that controls GC exit and plasma cell differentiation and provides rationale for future studies to interrogate the role of CRTC2 as a potential oncogenic factor (Sherman *et al.*, 2010).

1.7.3.2 Class II HDACs

Histone deacetylases (HDACs) predominantly modify histones by removing acetyl groups. Class IIa HDACs (HDAC 4/5/7/9) are recruited to specific promoters by sequence-specific DNA-binding proteins, with a subsequent de-acetylation of local chromatin resulting in repression of transcription (Wang, Qin and Zhao, 2014). Additionally, many non-histone targets can be post-translationally modified by dynamic acetylation, altering protein-protein interaction, intracellular localisation, enzymatic activity and stability. In particular, protein acetylation has been defined as playing a regulatory role in the transcriptional regulation of metabolism. Thus, HDACs function beyond the epigenetic control of gene expression (Ellmeier and Seiser, 2018).

HDACs have been implicated in the reprogramming of metabolically active cells including hepatocytes and adipocytes. For example, fasting or treatment with the fasting hormone glucagon leads to rapid dephosphorylation of hepatic class IIa HDACs, resulting in nuclear accumulation (Mihaylova and Shaw, 2013). In contrast, insulin is able induce the phosphorylation and corresponding nuclear exclusion of class IIa HDACs by activating SIK3 (Wang *et al.*, 2011). Following SIK inhibition, pro-inflammatory cytokines produced by macrophages were repressed through HDAC4 activation and p65-NF-κB de-acetylation and an increase in IL-10 secretion was seen following stimulation with TLR2/4 agonists, promoting SIK as a resolver of inflammation (Lombardi *et al.*, 2016).

The LKB1-SIK pathway phosphorylates HDACs at conserved motifs, stimulating 14-3-3 binding. For example, SIK2 activates MEF2-dependent transcription and relieves repression of myogenesis by the HDACs. This signalling module upstream from class IIa deacetylases is important for regulating cellular programs controlled by MEF2 and other transcription factors (Walkinshaw *et al.*, 2013). Furthermore, a domain-focused CRISPR screen revealed an essential role for LKB1 and its SIK effectors (SIK3, in a partially redundant manner with SIK2) to maintain MEF2C function in acute myeloid leukaemia (AML). Targeting of LKB1 or SIK3 diminishes histone acetylation at MEF2C-bound enhancers and deprives leukaemia cells of this essential transcription factor, highlighting how an oncogenic factor can be disabled by targeting of upstream kinases (Tarumoto *et al.*, 2018).

HDAC9 is expressed in B-cells and its overexpression has been observed in B-lymphoproliferative disorders and B-cell non-Hodgkin lymphomas (B-NHL). It is thought to contribute to lymphomagenesis by altering pathways involved in growth and survival as well as modulating BCL6 activity and p53 tumour suppressor function. Such findings provide rational for therapeutic approaches based on HDAC inhibitors (Gil *et al.*, 2016). Interestingly, combination treatment with HDAC inhibitors and proteasome inhibitors/immunomodulatory drugs shows remarkable anti-myeloma activity in both preclinical and clinical settings (Harada, Hideshima and Anderson,

2016). Taken together, it is possible that SIK inhibitors promote HDAC degradation in an analogous manner to HDAC inhibitors in the treatment of B-cell and plasma cell malignancies through hyper-acetylation.

Finally, it is important to note that cells can utilise multiple substrates downstream of the LKB1-SIK pathway. For example, Wein and colleagues showed that SIK2 utilises both CRTC2 and HDAC4/5 in osteocytes. Parathyroid hormone (PTH) signalling leads to PKA-mediated phosphorylation of SIK2, which inhibits its cellular activity. This in turn reduces phosphorylation of HDAC4/5 and CRTC2 by an unknown phosphatase and subsequent nuclear translocation. As a result, HDAC4/5 block MEF2C-driven SOST expression, whilst CRTC2 enhances CREB-mediated RANKL gene transcription forcing PTH to link bone resorption and bone formation (Wein *et al.*, 2016).

1.7.3.3 Additional substrates

Additionally, SIK1 has been shown to be capable of modulating p53 phosphorylation in response to cell detachment (anoikis). Cheng and co-authors demonstrated SIK1 activated by LKB1 suppresses metastasis and invasion in a human mammary epithelial cell line due to p53-mediated apoptosis through pro-apoptotic Bax and Puma (Cheng *et al.*, 2009).

In hepatocellular carcinoma (HCC), SIK1 phosphorylates the silencing mediator of retinoic acid and thyroid hormone receptor (SMRT) at threonine Thr1391, which disrupts the binding of β-catenin to the transducin-beta-like protein 1 (TBL1)/transducing-beta-like 1 X-linked receptor 1 (TBLR1) complex, thereby inactivating the Wnt/β-catenin pathway. This highlights the role of SIK1 as a negative regulator of HCC (Qu *et al.*, 2016).

Finally, activated SIK2 has been shown to play a dual role by augmenting AMPK-induced phosphorylation of acetyl-CoA carboxylase and activating the PI3K/AKT pathway through p85a-S154 phosphorylation. This regulates both fatty acid oxidation and cancer cell proliferation/survival and offers an important therapeutic opportunity in preventing abdominal metastasis in ovarian cancer (Miranda *et al.*, 2016).

1.8 Small molecule SIK inhibitors

The majority of previous studies use small-molecule SIK inhibitors to establish the role of SIKs. SIKs are unique among the AMPK-related kinases due to a small threonine residue situated at the gatekeeper site. As such, small molecule inhibitors (HG-9-91-01) target both the ATP-binding site and small hydrophobic pocket created by the additional amino acid residue. HG-9-91-01 also inhibits a number of protein tyrosine kinases that possess a threonine residue at the gatekeeper site, including Src family members (Src, Lck, and Yes), BTK, and the FGF and Ephrin receptors (Clark *et al.*, 2012). To overcome this, Sundberg and colleagues used HG-9-91-01 as a starting point to develop improved analogues, yielding a novel probe 5 (YKL-05-099). YKL-05-099 displays increased selectivity for SIKs versus other kinases and enhanced pharmacokinetic properties, providing a useful probe to also investigate SIK function in vivo (Sundberg *et al.*, 2016).

Compounds such as HG-9-91-01 and YKL-05-099 represent invaluable starting points in both the understanding of SIKs and in the treatment of various diseases, however efforts for structure-based drug design are currently limited by the lack of SIK crystal structures.

1.9 Aims

Preliminary data suggests that SIKs, in particular SIK1, may play a central role in the development and survival of plasma cells. The conversion to a plasma cell is accompanied by adaptive metabolic reprogramming to support high-level immunoglobulin secretion and maintain energy homeostasis. The hypothesis states that SIKs are activated by LKB1 due to DNA double strand breaks and/or low nutrients and play a distinct role from AMPK in regulating plasma cells. Furthermore, CRTC2 inactivation (or other downstream substrates) could be essential to plasma cell survival and longevity. Finally, SIKs could provide a new therapeutic target in the treatment of plasma cell malignancies such as multiple myeloma which generate extra metabolic requirements due to continuous growth, division and immunoglobulin production.

Therefore, the aim of this project will be to:

1. Investigate the expression, regulation, and function of SIKs in both primary human B-cells and multiple myeloma cell lines using small molecule inhibitors.
2. Investigate the regulation of downstream substrates (CRTCs and class II HDACs).
3. Develop an in vitro system for the generation of murine plasma cells and evaluate the impact of SIKs on B-cell populations, plasma cell differentiation and immunoglobulin production using SIK kinase inactive mice.

Chapter 2 - Materials and Methods

Human

2.1 Molecular cloning

2.1.1 Plasmids

Human *SIK1* (NM_173354.3) with an N-terminal HA epitope tag was purchased from GenScript and cloned into pIRES2-EGFP (Clontech) using XhoI and EcoRI (Appendix 1). Human *SIK1* in pIRES2-EGFP was used as a template for site-directed mutagenesis to create the mutants K56M, S575A and T182A. pCMV5-SIK2, pCMV5-SIK3, pCMV5-SIK1 T182D, pCMV5-SIK1 T103M and pCMV5-SIK1 T103Q were purchased from the MRC PPU (Medical Research Council, Protein Phosphorylation and Ubiquitylation Unit) and sub-cloned into pIRES2-EGFP using BamHI and EcoRI (Appendix 2).

Table 2.1 Constructs

Construct	Plasmid vector	Effect of mutation	Reference
HA-SIK1	pIRES2-EGFP	-	-
HA-SIK2	pIRES2-EGFP	-	-
HA-SIK3	pIRES2-EGFP	-	-
HA-T103M SIK1	pIRES2-EGFP	Drug resistant	(Clark *et al.*, 2012)
HA-T103Q SIK1	pIRES2-EGFP	Drug resistant	(Clark *et al.*, 2012)
HA-T182D SIK1	pIRES2-EGFP	Prevents activation	(Tang *et al.*, 2013)
HA-T182A SIK1	pIRES2-EGFP	Prevents activation	(Hashimoto *et al.*, 2008)
HA-K56M SIK1	pIRES2-EGFP	Kinase dead	(Tang *et al.*, 2013)
HA-S575A SIK1	pIRES2-EGFP	Constitutively active	(Henriksson *et al.*,

2.1.2 Site directed mutagenesis

pIRES2-HA-SIK1 was mutated at several sites including K56M, S575A and T182A using the QuickChange II site-directed mutagenesis kit (Agilent) outlined below. Mutations were confirmed by Sanger sequence (Source BioScience).

2.1.3 Primers

Primers were designed using the QuikChange Primer Design Program (Agilent) with a melting temperature of ≥78°C (table 2.2).

Table 2.2 Mutagenic primers

Mutation	Forward Primer 5'-3'	Reverse Primer 3'-5'
K56M	CGCAGGTTGCAATAATGATAATTGATAAAACA	TGTTTTATCAATTATCATTATTGCAACCTGCG
S575A	GACGGCGGGCGGCGGACACCTCA	TGAGGTGTCCGCCGCCCGCCGTC
T182A	AGAGCCTCTGTCCGCGTGGTGTGGGAG	CTCCCACACCACGCGGACAGAGGCTCT

2.1.4 Reaction mix

The sample reaction was prepared with the reagents and volumes outlined in table 2.3.

Table 2.3 Mutant strand synthesis reaction

Reagent	Volume
10X Reaction Buffer	5µL
DNA Template	2µL (40ng)
Forward Primer	1µL (125ng)
Reverse Primer	1µL (125ng)
dNTP	1µL
High fidelity DNA Polymerase	1µL
dH_2O	39µL

2.1.5 Thermal cycling

PCR (Polymerase chain reaction) was performed using the conditions outlined in table 2.4 with a thermocycler (Tprofessional; Biometra).

Table 2.4 Thermal cycling conditions

Segment	Cycles	Temperature (°C)	Time (Seconds)
1	1	95	30
2	16	95	30
		55	60
		68	300
Ice for 2 minutes			

DpnI restriction enzyme was added to the PCR product for 1 hour at 37°C to remove any template DNA. Plasmids were stored at 4°C until transformation.

2.1.6 DNA digestion with restriction endonucleases

Restriction digests were performed on plasmids using the volumes and endonucleases outlined in table 2.5 and 2.6. Reaction mixtures were incubated at 37°C for 1 hour. Parent vectors were treated for a further 20 minutes with CIP (Calf intestinal phosphatase; New England Biolabs) to prevent re-ligation.

Table 2.5 Reaction mixture for DNA digestions

Reagent	Volume
DNA	4µL
Buffer 10X	5µL
BSA	0.5 µL
Restriction endonuclease 1	1µL
Restriction endonuclease 2	1µL
dH_2O	38.5µL

Table 2.6 Restriction endonucleases

Enzyme	Restriction site 5'-3'	Manufacturer
XhoI	C*TCGAG	New England BioLabs
EcoRI	G*AATTC	New England BioLabs
BamHI	G*GATCC	New England BioLabs

2.1.7 Agarose gel electrophoresis

Digests were visualised using a 0.7% agarose gel and ethidium bromide (EtBr) staining. 0.7% (w/v) of agarose was dissolved in 1X TBE buffer (89mM Tris-base, 80mM boric acid, 2mM EDTA) with the addition of two drops of ethidium bromide (0.625mg/mL, Fisher Scientific). DNA mixed with a buffer containing 40% sucrose, 30% (v/v) glycerol and food colouring was loaded on to a gel and run at 100V for 1 hour. Molecular weight ladders (100bp or 1kb; New England Biolabs) were included for size recognition. Gels were imaged using the Geldoc XR system (Bio-Rad).

2.1.8 DNA extraction

Fragments of interest were excised from each gel using a scalpel. DNA elution was performed using the QIAquick® Gel Extraction Kit following the manufacturer's instructions (QIAGEN).

2.1.9 Ligation

DNA fragments generated from restriction digests were ligated to a parent vector using T4 DNA ligase (Invitrogen) to produce a complete plasmid. The reaction mixture outlined in table 2.7 was incubated at room temperature for 2 hours.

Table 2.7 Reaction mixture for ligation

Reagent	Volume
Vector	1µL
Insert	4µL
5X Ligase Buffer	1µL
T4 Ligase	0.5µL
dH_2O	3.5µL

2.1.10 Transformation of bacterial cells

5µL of the ligation material was added into 50µL DH5α (E.coli) competent cells and incubated on ice for 20 minutes. The reaction mixture was then heat shocked at 42°C for 45 seconds and placed onto ice for a further 2 minutes. For recovery, 200µL SOC media (Super optimal broth) (2% tryptone, 0.5% yeast extract, 10mM NaCl, 2.5mM KCl, 10mM $MgCl_2$, 10mM $MgSO_4$ and 20mM glucose) was added and the cells were grown at 37°C for 1 hour on a shaking platform. Cells were then plated on LB (Luria-Bertani) agar containing kanamycin or ampicillin overnight at 37°C.

2.1.11 Plasmid purification

Bacterial colonies were picked and inoculated in LB broth (1% (w/v) bactopeptone, 0.5% (w/v) NaCl, 0.5% (w/v) yeast extract, pH 7.5) supplemented with either ampicillin/kanamycin overnight at 37°C on a shaking platform. Plasmid DNA was purified using a miniprep or midiprep kit (QIAGEN) depending on amount of DNA required for sequence verification, further cloning or cell transfection. DNA was quantified using a NanoDrop™ spectrophotometer (ND-1000; ThermoScientific).

2.2 Cell culture

2.2.1 Cell lines

Human multiple myeloma cell lines (OPM2, KMS11, U266, RPMI8226, JIM1, JJN3, KMS18 and H929) and monocytic cell lines (U937, RAW.264 and THP-1) were obtained from the American Type Culture Collection (ATCC). The human cervical epithelial cell line (HeLa) was used for transfections. Cell lines were authenticated using standard short tandem repeat based techniques (CRUK Cancer Centre Genomics Facility). Cells were routinely cultured in RMPI-1640 medium (Invitrogen) supplemented with 10% heat-inactivated fetal bovine serum (PAA Laboratories, Inc.) at 37°C in a humidified atmosphere of 5% CO_2.

2.2.2 Population and ethics

Whole blood was obtained from healthy volunteers and collected in EDTA (ethylenediaminetetraacetic acid) tubes following informed consent. Approval for the study was granted by the Leeds (East) NHS Research Ethics Committee, REC reference number 07/Q1206/47.

2.2.3 *In vitro* differentiation of human plasma cells

Table 2.8. List of cytokines/growth factors used to generate human plasma cells

Cytokine/ Growth Factor	Stock Concentration	Final Concentration	Supplier
hIL-2	10,000 units/mL	20 units/mL	Roche
hIL-21	100µg/mL	50ng/mL	Peprotech
F(ab')$_2$ anti-IgM/IgG	1.2mg/mL	10µg/mL	Jackson Laboratories
R848	1mg/mL	1µg/mL	InvivoGen
Amino Acids	50X	20µl/mL	Sigma
Lipid Mix	200X	5µL/mL	Sigma
Tx Hybridoma	-	11µL/mL	Gentaur
hIL-6	100,000ng/mL	10ng/mL	Peprotech
hIFN-α	1x10^7 units/mL	100 units/mL	Peprotech
APRIL	100µg/mL	100ng/mL	Caltag
γ-secretase inhibitor L-685,458	1mg/mL	1µg/mL	Sigma-Aldrich

Irradiated CD40-L expressing murine L cells

Murine L cells stably transfected with human CD40-L (CD154) were irradiated twice on ice using 25 Gray for 45 minutes with gentle mixing in-between. Following irradiation, 100µL of cells were stained with anti-CD154 and assessed using flow cytometry to confirm CD40-L expression. 1x10^6 cells were prepared in 1.5mL freezing vials and stored at -80°C.

24h prior to the processing of samples, 1 vial (per sample) of irradiated CD40-L cells was thawed and washed with 15mL Iscoves Modified Dulbecco's Medium (IMDM) containing 10% HIFBS (heat-inactivated foetal bovine serum) and β-Mercaptoethanol (1 mM). Following washing, cells were re-suspended in 12mL complete IMDM media and plated into a 24-well plate (0.5mL/well; 6.25x10^4/well). The plate was incubated at 37°C in a humidified atmosphere with 5% CO_2.

Day 0

50mL of human peripheral blood was collected in EDTA tubes and diluted 1:2 with room temperature phosphate buffered saline (PBS). 17mL of lymphoprep was added to a 50mL tube and 34mL of the diluted blood was layered on top. The tubes were centrifuged at 1159 x g for 20 minutes at 18°C using an acceleration value of 5 and no brake in an Eppendorf 5810R centrifuge. Post centrifugation, the buffy coat containing mononuclear cells was aspirated using a Pasteur pipette and transferred to a 50mL tube containing ice-cold PBS. The cells were washed three times with cold PBS and once with MACS buffer (1x PBS, 0.5% FBS, 2mM EDTA). Total

peripheral blood mononuclear cells (PBMCs) were counted using trypan blue and a haemocytometer.

B-cells were isolated by magnetic labelling using a memory B-cell isolation kit (Miltenyi Biotech). Cells were labelled with an antibody cocktail followed by microbeads and subsequently separated using an LD column in a magnetic field. B-cell purity was confirmed by flow cytometry (95% $CD19^+$ $CD20^+$). Cells were counted and re-suspended in the appropriate volume of IMDM to achieve $2.5x10^5$ cells/mL/well of a 24 well plate. To stimulate cells in a T-dependent manner, 500µL of IMDM containing 2X cytokines (IL-2, IL-21) and the anti-B-cell receptor $F(ab')_2$ anti-IgM/IgG plus 500µL of B-cells were added on top of the CD40-L cells and placed at 37°C in a humidified atmosphere of 5% CO_2. To stimulate cells in a T-independent manner, cells were incubated with IL-2, IL-21, $F(ab'_2)$ anti-IgM/IgG and R848 (TLR7/8 agonist).

Day 3

Activated B-cells were collected and counted using trypan blue. Cells were re-suspended in IMDM with 1x cytokines and growth factors (IL-2, IL-21, amino acids, Tx-Hyb, and lipids). Cells were re-plated at a density of $1x10^5$/mL/well of a 24 well plate.

Day 6

The stromal cell line M2-10B4 was irradiated using 57 Gray for 57 minutes. M2-10B4s were trypsinised and re-suspended at a concentration of $1x10^6$ cells/12mL IMDM containing 1.7X cytokines/growth factors (IL-21, IL-6, IFN-α, lipid, amino acids, Tx-Hyb). 0.7mL was then seeded per well ($8.3x10^4$ cells/well) of a 12-well plate. Plasmablasts were collected and counted using trypan blue and re-seeded into transwells with 1x cytokines/growth factors (IL-21, IL-6, IFN-α, lipid, amino acids, Tx-Hyb) at a density of $5x10^5$ cells/0.5mL/transwell.

Following a review of the conditions, differentiations carried out towards the end of the project were altered from day 6 onwards. Instead of the M2-10B4 stromal layer, IFN-α and TxHyb, cells were cultured with APRIL and a gamma secretase inhibitor (GSI, L-685458; Sigma) as well as IL-6, IL-21, lipids and amino acids in 96 well plates ($1x10^5$ cells/0.2mL/well) to improve plasma cell survival.

Long term culture

Every 3-4 days, half of the IMDM was removed and replaced with fresh IMDM containing 1x cytokines/growth factors (either IL-21, IL-6, IFN-α, lipids, amino acids, Tx-Hyb or IL-21, IL-6, APRIL, GSI, lipids and amino acids). At day 13, IL-21 was removed from the culture. Cells were re-fed until elective termination occurred.

2.2.4 Phenotypic analysis of differentiating B-cells

Approximately 2x10^5 cells per sample were stained with the antibodies indicated in Table 2.9. Cells were centrifuged at 500 x g for 5 minutes before being washed with MACS buffer (PBS, 0.5% BSA) To block non-specific staining, 25µL of blocking buffer (932µL MACS buffer/10% BSA, 16.6µL human IgG; Sigma, 50µL normal mouse serum) was added per sample and incubated for 15 minutes at 4°C. Cells were stained with the antibody mixture for 15 minutes at 4°C. Cells were then washed and re-suspended in MACS buffer and phenotype was evaluated using flow cytometry (CytoFLEX S). Data was analysed using FlowJo software (BD). To account for and adjust spectral overlap between fluorophores, single-colour compensation was applied using anti-mouse Ig, κ CompBeads™ (BD). Non-specific staining was identified using isotype controls.

Table 2.9 Antibodies used for the staining of differentiating B-cells

Antibody	Fluorophore	Clone	Supplier	Volume
CD19	PE	HIB19	Miltenyi	2µL
CD20	e450	2H7	eBioscience	2µL
CD27	FITC	M-T271	BD	2.5µL
CD38	PE-CY7	HB-7	BD	0.5µL
CD138	APC	44F9	Miltenyi	2µL

2.2.4.1 Gating Strategy

B-cells were gated firstly on forward vs. side scatter characteristics. Doublets were excluded by plotting area against height. Live-dead discrimination was based upon staining with 7-AAD (7-aminoactinomycin D) against forward scatter (Figure 2.1).

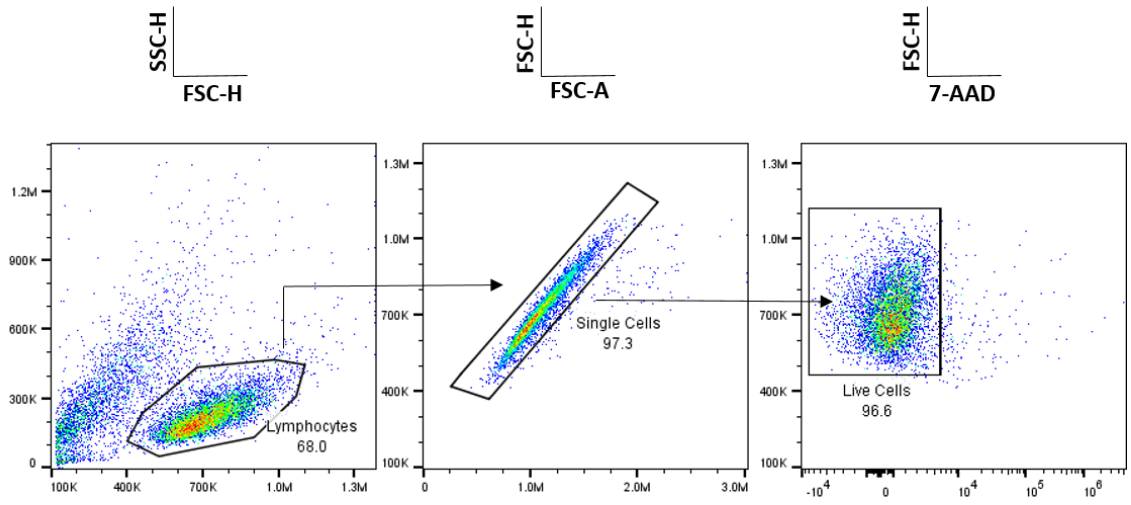

Figure 2.1 Gating strategy for phenotypic analysis.

2.2.5 Concentration-response assays

All inhibitors were dissolved in DMSO (dimethyl sulfoxide) at a concentration of 10mM and stored at -20°C. Inhibitors were diluted to the appropriate concentration in either RPMI1640 or IMDM directly before use.

Compound	Target	Source
HG-9-91-01	SIKs	MRC PPU
MRT199665	AMPK	MRC PPU
YKL-05-099	SIKs	MedChemExpress
Dasatinib	BCR/Abl, Src, c-Kit, Ephrin receptors	Cell Signaling
Ibrutinib	BTK	Janssen Biotech
Bortezomib	Proteasome	Selleckchem

Table 2.10 List of inhibitors used in concentration-response assays.

2.2.5.1 Cell viability

Apoptosis was measured by flow cytometry for externalised phosphatidylserine and cell permeability by adding 100µL of 1X binding buffer (eBioscience) containing 5µl of Annexin V (FITC; BD) and 5µL of 7-AAD (PerCP-Cy5-5-A; BD) to each sample. Apoptotic cells were classified on being either single positive for Annexin V (early-mid apoptosis) or double positive for both AnnexinV and 7-AAD (mid-late apoptosis) (Figure 2.2).

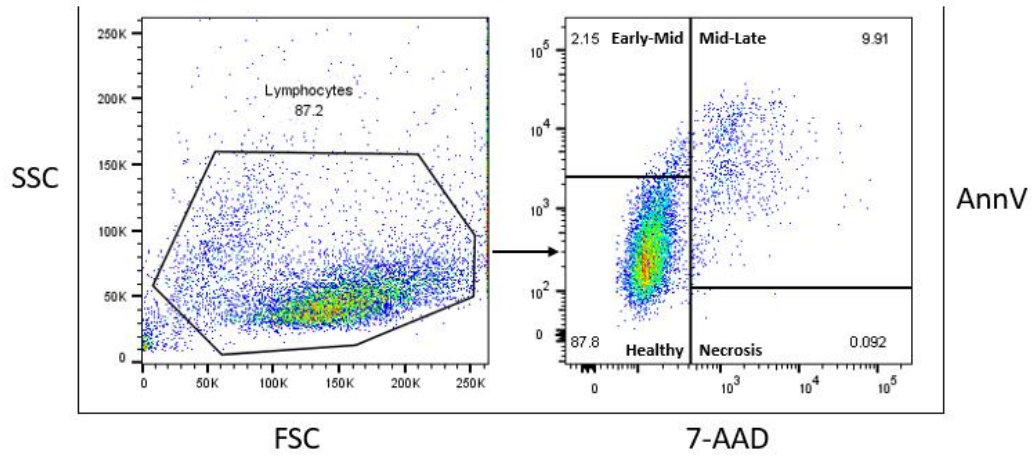

Figure 2.2 Gating strategy used to identify the percentage of apoptotic cells in myeloma cell lines.

2.2.5.2 Cell number

Calculation of absolute cell number by flow cytometry was performed using a ratiometric method based on the addition of a known number of CountBright™ beads (Thermofisher) to the cell sample. Single viable cells were identified using doublet discrimination and a live/dead stain. Cell number was then calculated from the cell-to-microbead ratio using the equation in Figure 2.3.

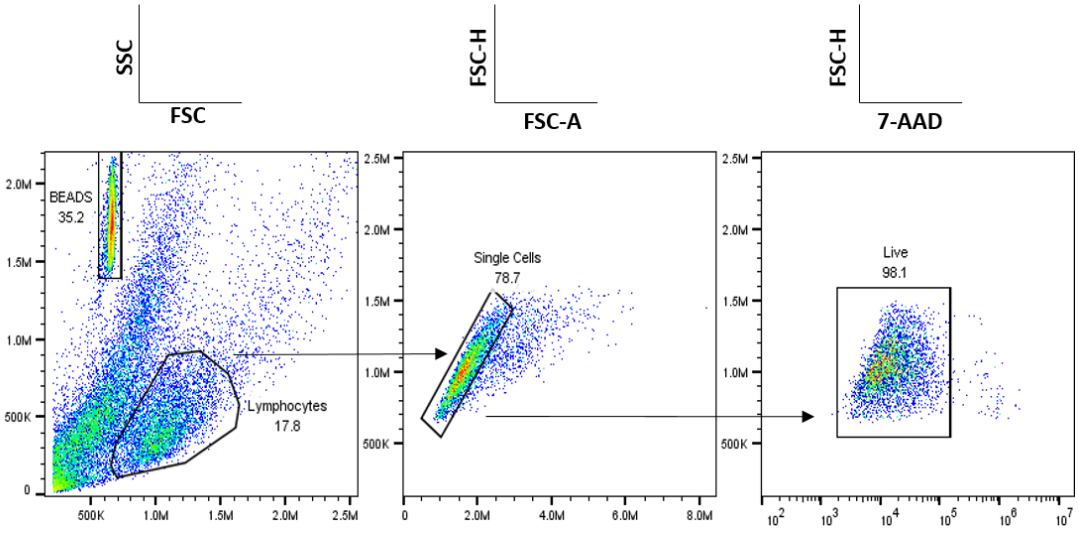

$$\frac{\#\text{Cell events}}{\#\text{Bead events}} \times \frac{\#\text{Beads}}{\text{Sample volume}}$$

Figure 2.3 Gating strategy and equation used to calculate absolute cell number in both myeloma cell lines and primary differentiating cells.

2.2.5.3 Statistical analysis

The number of repeats for each experiment varied and are given in the figure legends. Comparison of means was carried out using a Student t-test and error bars indicate standard deviation (SD) from the mean. Analysis was conducted using GraphPad Prism software.

2.2.6 Plasmid transfection

To assess the various pIRES2-HA-SIK constructs, plasmids were transfected into HeLa or HEK-293T cells. Cells were seeded into 6 well plates, grown until 80% confluent and transfected with 1µg of appropriate DNA using GeneJuice® transfection reagent (Millipore) and Opti-MEM™ serum free media (Thermofisher). Cells were incubated overnight at 37°C and transfection efficiency was assessed by GFP (green fluorescent protein) expression. Following successful transfection, cells were either counted or lysates were taken for downstream assays such as immunoblotting.

The polymeric transfection reagents TransIT-Jurkat, TransIT-X2 and TransIT-2020 were used to transfect myeloma cell lines with pmaxGFP (Lonza). Myeloma cell lines were seeded at a density of $3x10^5$ cells/well in a 6-well plate and transfected with a solution containing TransIT reagent (7.5µL), Optimem SFM (250µL) and pmaxGFP (2.5µg). Cells were analysed at 24h, 48h and 72h post-transfection using flow cytometry.

2.2.7 Nucleofection

Electroporation of myeloma cell lines was carried out as follows: $2x10^6$ cells were re-suspended in solution V, L or C (Lonza) depending on the cell type containing 10µg of plasmid or 2-8µM siRNA (small interfering RNA) duplexes (Ambion). The appropriate electrical current was applied using a Nucleofector™ device (Amaxa) and cells were transferred into 12 well plates containing RPMI supplemented with 10% FBS. Cells were analysed 24h, 48h and 72h post-nucleofection using flow cytometry and lysates were taken for immunoblotting.

Electroporation of primary cells stimulated in a T-independent manner was carried out using Ingenio electroporation solution (Mirus). $6x10^6$ cells were re-suspended in 100µL Ingenio solution containing 2µg/mL pmaxGFP or 10ug of plasmid and IL-2, IL-21, $F(ab')_2$ anti IgM/IgG and R848 and electroporated (Amaxa) using program U-15. Electroporated cells were transferred into a 6-well plate containing fresh IMDM. Cells were analysed 24h, 48h and 72h post-nucleofection using flow cytometry.

2.3 Techniques for protein analysis

2.3.1 Nuclear and cytoplasmic extraction

Cells were centrifuged at 200 x g for 3 minutes and the supernatant was removed leaving the cell pellet as dry as possible. The following ratios (200:11:100µL) were used for CER I (Cytoplasmic Extraction Reagent I): CER II (Cytoplasmic Extraction Reagent II): NER (Nuclear Extraction Reagent) respectively (NE-PER™ kit; ThermoFisher).

Ice-cold CER I was added and the tube was vortexed for 15 seconds to fully re-suspend the cell pellet. The tube was incubated on ice for 10 minutes. Ice-cold CER II was added, vortexed for 5 seconds and incubated on ice for 1 minute. The tube was vortexed again and centrifuged for 5 minutes. The supernatant (cytoplasmic extract) was immediately transferred to a clean, pre-chilled tube and placed on ice. To extract the nuclear fraction, the insoluble pellet was re-suspended in ice-cold NER. The tube was vortexed for 15 seconds and placed on ice. Vortexing was repeated every 10 minutes for a total of 40 minutes. The tube was centrifuged for 10 minutes and the supernatant (nuclear extract) was transferred to a clean, pre-chilled tube. Extracts were stored at -80°C until required for downstream assays.

2.3.2 Immunoprecipitation

Following overnight transfection of expression constructs into HeLa cells, proteins were isolated using immunoprecipitation. Cells were lysed in RIPA (radioimmunoprecipitation assay) buffer (10mM Tris HCl, pH 8.0, 1mM EDTA, 1% Triton X-100, 0.1% sodium deoxycholate, 0.1% SDS, 140 mM NaCl) containing protease inhibitors for 10 minutes on ice. 200µL of each extract was incubated with 1µg antibody overnight at 4°C on a rotating wheel. The protein-antibody complex was then precipitated with 20µL of protein A Sepharose beads for 2 hours at 4°C. The extract was then washed 3 times with RIPA buffer and centrifuged at 800 x g for 1.5 minutes at 4°C. The sample was boiled for 5 minutes with 20µL 2X gel loading buffer containing β-mercaptoethanol. Samples were then subjected to SDS-PAGE (sodium dodecyl sulfate–polyacrylamide gel electrophoresis) and immunoblotting for protein detection.

2.3.3 SDS Polyacrylamide Gel Electrophoresis (PAGE) and Immunoblotting

Cells were washed in ice-cold PBS and lysed in Laemmli buffer (4% SDS, 20% glycerol, 10% 2-mercaptoethanol, 0.004% bromophenol blue and 0.125 M Tris HCl). Proteins were separated on 5-12% SDS-polyacrylamide gels and transferred to a nitrocellulose membrane in transfer buffer (25mM Tris base, 192mM glycine, 20% methanol). Membranes were blocked in wash buffer (TBS-T; 50 mM Tris-HCl, pH 7.5, 150 mM NaCl, 0.1% Tween-20) containing 5% skimmed milk for 1 hour at room temperature and incubated overnight at 4°C in 5% BSA/TBS-T with the

appropriate primary antibody. On the following day, membranes were incubated in secondary antibody (1:20,000) for 1 hour at room temperature. Unbound antibody was removed with TBS-T. Horseradish peroxidase (HRP) was detected with enhanced chemiluminescent substrate (ECL; Thermofisher) and the signal was visualised using a gel doc imager (BioRad) or exposed to film (Amersham Hyperfilm ECL; GE Healthcare) and developed using an X-ray developer (SRX-101A).

2.3.3.1 Commercial antibodies

Table 2.11 Antibodies used in immunoblotting

Antibody	Host	Source	Clone/Cat Number	Dilution
SIK1	Rabbit	ProteinTech	51045-1-AP	1:1000
SIK2	Rabbit	Cell Signaling	D28G3	1:700
SIK3	Sheep	MRC PPU	S373D	1:700
CRTC2	Rabbit	ProteinTech	12497-1-AP	1:750
HDAC4	Rabbit	ProteinTech	17449-1-AP	1:1000
HDAC4	Rabbit	Cell Signaling	D8T3Q	1:1000
HDAC5	Rabbit	Cell Signaling	D1J7V	1:1000
HDAC6	Rabbit	Cell Signaling	D21B10	1:1000
HDAC7	Rabbit	Cell Signaling	D4E1L	1:1000
IRF4	Rabbit	Santa Cruz	H-140	1:1000
MEF2	Rabbit	Santa Cruz	C-21	1:1000
HA	Rabbit	Sigma	H6908	1:1000
β-actin	Mouse	Sigma	A1978	1:100,000

2.3.3.2 Polyacrylamide gels

Table 2.12: The composition of polyacrylamide gels used

Gel	Tris Buffer	dH_2O	Polyacrylamide	10% APS	Temed
10% Resolving	1.25mL	2.05mL	1.7mL	30µL	5µL
7.5% Resolving	1.25mL	2.46mL	1.25mL	30µL	5µL
Stacking	1.25mL	3.25mL	0.5mL	30µL	5µL

2.4 Techniques for analysis of gene expression

2.4.1 RNA extraction

To extract RNA, cells were lysed in 800µL of Trizol®. 160µL of chloroform was added and the mixture was inverted. Cells were then centrifuged at 160 x g for 15 minutes at 4°C to ensure separation of the aqueous and organic phases. The top aqueous layer containing RNA was transferred to a new Eppendorf and 10µg of RNAse free glycogen was added. To precipitate the RNA, 400µL isopropanol was added to each sample and incubated for 10 minutes at room temperature. Samples were then centrifuged at 160 x g for 10 minutes at 4°C. The precipitate was then washed 3 times with 1000µL of 75% ethanol to remove any remaining salts and air-dried. RNA was dissolved in dH_2O (20-45µL) and heated for 10 minutes at 55°C. Samples were then treated with DNase I (DNA-*free*™, Ambion) for 1 hour at 37°C. Following this, 5µL of DNase inactivation reagent was added and samples were incubated for 2 minutes. Concentration and purity was quantified using a NanoDrop™ (Thermofisher).

2.4.2 cDNA synthesis

Mix 1 (1µL OligoDT, 1µL dNTPs, 3µL RNase free water) was added to 1µg of RNA and incubated at 65°C for 5 minutes. Mix 2 (4µL 5X RT buffer, 2µL $MgCl_2$, 2µL DTT, 1µL RNase OUT, 0.25µL SuperScript™II, 0.75µL RNase free water) was added and incubated at 42°C for 1 hour followed by 70°C for 15 minutes to terminate the reaction. RNase H was added to the mixture and incubated at 37°C for 20 minutes. All reagents for cDNA synthesis were purchased from Invitrogen.

2.4.3 TaqMan®

The PCR reaction mixture (1µL 20X TaqMan® gene expression assay, 10µL TaqMan® universal master mix, 100ng cDNA template and 5µL RNase free water) was inverted several times and briefly centrifuged. Plates were sealed and loaded into the RT-PCR machine (Stratagene mx3005p; Agilent) and exposed to the parameters in table 2.13. ΔCT values were used to calculate relative mRNA expression of SIK1 (Hs00545020_m1), SIK2 (Hs01568566_m1) and SIK3 (Hs00228549_m1) which were normalised to the gene expression of the control, *PPP6C* (Hs00254827_m1).

Table 2.13 RT-PCR thermal cycling parameters

Segment	Cycles	Temperature (°C)	Time (Seconds)
1	1	95	600
2	40	95	30
		60	60

2.4.4 RNA-sequencing

Libraries were sequenced on a NextSeq500 platform (Illumina) using 75-base pair single-end sequencing. Fastq files were assessed for initial quality using FastQC, trimmed for adapter sequences using TrimGalore and aligned to GRCh38.p12 (Gencode release 28) with STAR aligner using twopassMode (Dobin *et al.*, 2013). Transcript abundance was estimated using RSEM and imported into R using txImport and then processed using DESeq2 (Li and Dewey, 2011; Soneson, Love and Robinson, 2015; Love, Huber and Anders, 2014). Using DESeq2 rLog transformed data, exploratory analysis of biological replicates was carried out using correlation heatmaps and MDS (all genes) and PCA (500 most variant genes). Differential gene expression was determined using DESeq2, quality visualised using MA plots and shrinkage of log fold estimated using the apeglm method (Zhu, Ibrahim and Love, 2018). rLog transformed data was exported for downstream visualisations using the GENE-E package. All bioinformatic analysis was performed by Dr Matthew Care.

Table 2.14 Programs used for bioinformatic analysis

Program	Version	Link
FastQC	v0.11.8	https://www.bioinformatics.babraham.ac.uk/projects/fastqc/
TrimGalore	v0.6.0	https://www.bioinformatics.babraham.ac.uk/projects/trim_galore/
STAR	v2.6.0c	
RSEM	v1.3.0	
R	v3.5.1	
txImport	v1.10.1	
DESeq2	v1.22.2	
GENE-E	v3.0.21	https://software.broadinstitute.org/GENE-E/

Mouse

2.4.5 Animals/ethics

C57BL/6 mice were obtained from SBS (St James Biomedical Services; University of Leeds) and Nicola Darling (University of Dundee). All procedures were performed under the approved UK Home Office project license in line with the Animal (Scientific Procedures) Act 1986 and in accordance with the UK National Cancer Research Institute Guidelines for the welfare of animals.

2.5 In vitro culture system

2.5.1 B-cell isolation

Tissue was harvested from C57BL/6 mice aged between 6-12 weeks old that had been maintained in specific-pathogen-free (SPF) conditions. Spleens were gently forced through the nylon mesh of a 70µm cell strainer (Fisher Scientific) using the end of a 5mL syringe (BD Plastipak). Single cell suspensions were re-suspended in 5mL PBS and carefully layered onto 5mL lympholyte-M (Cedarlane) in a 15mL tube. Cells were centrifuged (Eppendorf 5810R centrifuge) at 1159 x g for 20 minutes at 18°C using an acceleration value of 5 and no brake and the mononuclear cells were removed using a Pasteur pipette. Cells were then washed in PBS twice at 4°C.

To isolate murine B-cells, several negative selection kits were tested. Optimisation led to the use of two different kits depending on the required cell type. The magnetic pan B-cell isolation kit II (Miltenyi Biotech) containing a cocktail of biotinylated CD3ε, CD4, CD8a, CD49b, Gr-1, and Ter119 antibodies was used for the isolation of both B1 and B2 murine B-cell subsets. Cells were counted using counting slides (TC-10 Automated Cell Counter, BioRad) and re-suspended in MACS buffer. Appropriate volumes of FcR block, pan B-cell antibody cocktail, MACS buffer and microbeads were added. Cells were added to an LS column within a magnetic field and the unlabelled flow through was counted.

The EasySep™ mouse B-cell isolation kit (STEMCELL Technologies) containing CD43 was used to isolate B2 cells. Counted cells were re-suspended in recommended medium (PBS, 2% FBS, 1mM EDTA) and appropriate volumes of rat serum, antibody cocktail and streptavidin RapidSpheres™ were added. Cells were added to 'The Big Easy' magnet for 2.5 minutes and the enriched cell suspension was poured into a new tube and counted.

Following both isolation protocols, B-cells were phenotyped to ensure purity (>95% $B220^+$ $CD138^-$) before being added into culture.

2.5.2 Cytokines and growth factors

The culture systems were developed over time using various different cytokines and growth factors to derive conditions based upon both TLR (Toll-like receptor) and BCR (B-cell receptor) engagement. Table 2.15 outlines all of the cytokines tested; however, as described in the results section some of these were not included in the final two systems. To note, human reagents were used when recognised by murine receptors (recombinant APRIL and IL-21).

Table 2.15: List of cytokines and growth factors tested to differentiate murine B-cells

Cytokine/Growth Factor	Final	Supplier
mIL-4	50ng/mL	Miltenyi
mIL-5	50ng/mL	Miltenyi
mIL-6	10ng/mL	Miltenyi
hIL-21	50ng/mL	Peprotech
hAPRIL	100ng/mL	Caltag
γ-secretase inhibitor L-685,458	1µg/mL	Sigma-Aldrich
LPS 0111:B4	5-7.5µg/mL	Sigma-Aldrich
CpG ODN2395	10µg/mL	InvivoGen
sCD40-L	5µg/mL	Peprotech
$F(ab')_2$ anti-IgM/IgG	12µg/mL	Jackson
Amino Acids	20µL/mL	Sigma-Aldrich
Lipids	5µL/mL	Sigma-Aldrich

2.5.2.1 Irradiated CD40-L expressing murine L cells

Irradiated CD40-L were prepared as described in section 2.2.3.

2.5.3 Optimised culture conditions

Day 0

For BCR signalling, isolated B-cells were seeded in 24 well plates at $2.5x10^5$ cells/mL (0.5mL/well; $1.25x10^5$ cells/well) with CD40-L expressing murine L cells, $F(ab')_2$ anti-IgM/IgG, IL-4 and IL-5 for 2 days.

For TLR signalling, B-cells were seeded at the same density as above with CD40-L expressing murine L cells, LPS, IL-4 and IL-5.

Day 2

On subsequent days, both mechanisms followed the same steps. On day 2, cells were removed from the CD40-L cells and transferred across to new 24 well plates.

Day 4

On day 4, plasmablasts were re-seeded in IL-6, APRIL, amino acids and lipids at $5x10^5$ cells/mL in 96 well plates (0.2mL/well; $1x10^5$ cells/well). Cells were fed with fresh media every 3-4 days containing APRIL, IL-6, amino acids and lipids. Feeding was carried out until elective termination occurred.

2.5.4 Phenotypic evaluation

Approximately $1x10^6$ cells per sample were washed with MACs buffer (PBS, 0.5% BSA) and re-suspended in 1µL Fc block (BD) for 10 minutes. Antibodies were added and the cells were incubated for a further 15 minutes. Cells were then washed in MACS buffer and re-suspended in 300µL MACS buffer. 5µL of 7-AAD was added immediately before samples were analysed using flow cytometry (CytoFLEX S).

Table 2.16 List of antibodies used for cell phenotyping by flow cytometry

Antibody	Fluorophore	Clone	Supplier	Volume
B220	PE	RA3-6B2	Miltenyi	5µL
CD138	APC	REA104	Miltenyi	5µL
BCMA	FITC	REA550	Miltenyi	5µL
TACI	BV421	8F10	BD	2µL

2.6 Validation of the culture system

2.6.1 Blimp-1 reporter mice

B-cells from Blimp-1-Venus spleens (Morgan *et al.*, 2009; Ohinata *et al.*, 2008) were isolated and cultured using both TLR and BCR signalling in vitro culture conditions. Blimp-1 expression was monitored throughout the differentiation using flow cytometry (525/40 bandpass filter).

2.6.2 CFSE staining

Cell division was assessed using Carboxyfluorescein succinimidyl ester (CFSE). Cells were washed and re-suspended in PBS containing 5% HIFBS. CFSE dissolved in DMSO was added at a final concentration of 10µM. Cells were mixed and incubated at room temperature for 5 min. A sample was taken and stored at 4°C overnight to establish maximal CFSE loading. Labelled cells were washed three times with PBS containing 5% HIFBS and re-suspended in culture medium as required. CFSE expression was analysed on subsequent days using flow cytometry (525/40 bandpass filter).

2.6.3 2-NBDG Uptake

To measure glucose uptake, cells were equilibrated in low glucose (1g/L) DMEM for 1 hour. The fluorescent glucose analogue 2-NBDG (200µg/mL) was added and the cells were analysed using flow cytometry (525/40 bandpass filter) as described in Lam et al (Lam *et al.*, 2018).

2.6.4 IgM and IgG ELISA quantification

Buffers

- ELISA coating buffer (0.05M Carbonate-Bicarbonate) pH 9.6
- ELISA wash solution (50mM Tris, 0.14M NaCl, 0.05% Tween 20) pH 8.0
- ELISA blocking buffer (50mM Tris, 0.14M NaCl, 1% BSA) pH 8.0
- Sample/conjugate diluent (50mM Tris, 0.14M NaCl, 1% BSA, 0.05% Tween 20) pH 8.0
- Enzyme substrate: TMP (Trimethoprim)
- ELISA stop solution: 0.18, H_2S0_4

Mouse IgM

ELISAs (enzyme-linked immunosorbent assays) were performed according to the manufacturer's instructions for the Mouse IgM Quantification Set (E90-101, Bethyl Laboratories, Inc). 96 well plates were coated with 100µL of affinity purified antibody (1:100) for 1 hour at room temperature. The antibody solution was then removed and each plate washed 5 times with ELISA wash solution. 200µL of blocking solution was added to each well overnight at 4°C to prevent non-specific binding. Following incubation, blocking solution was removed and wells were washed a further 5 times with wash solution. The standards (1-10) were diluted using sample/conjugate diluent according to Table 2.17.

Table 2.17 Concentration of IgM ELISA standards

Standard	ng/mL	RS10-101-6	Sample Diluent
1	1000	4µL	2mL
2	500	500µL from std 1	500µL
3	250	500µL from std 2	500µL
4	125	500µL from std 2	500µL
5	62.5	500µL from std 2	500µL
6	31.25	500µL from std 2	500µL
7	15.63	500µL from std 2	500µL
8	7.813	500µL from std 2	500µL
9	3.906	500µL from std 2	500µL
10	0	Blank	500µL

Samples were diluted to a concentration predicted to fall within the standards' range. 100µL of each standard/sample was added to the appropriate well and incubated for 1 hour at room temperature. Plates were then washed 5 more times with wash solution. 100µL of 1:75,000 horseradish peroxidase (HRP)-conjugated detection antibody (A90-101P-34) was added to each well and incubated for 1 hour at room temperature. Plates were washed 5 times with wash solution and 100µL of 3,3',5,5'-tetramethylbenzidine (TMB) substrate was added to each well. Plates were incubated in the dark for up to 15 minutes, however for concentrated samples this was reduced significantly. The reaction was stopped using 100µL of stop solution (0.18M H_2SO_4) and the concentrations were quantified using a plate reader (Cytation 5, BioTek) and standard curve analysis software (ELISAkit Ltd).

Mouse IgG

IgG quantification was performed in an analogous manner to IgM quantification using the Mouse IgG Quantification Set (E90-131, Bethyl Laboratories, Inc). The standards (1-10) were diluted using sample/conjugate diluent according to Table 2.18. 1:100,000 HRP conjugated IgG-Fc antibody (A90-131P) was used for detection.

Table 2.18 Concentration of IgG ELISA standards

Standard	ng/mL	RS10-101-6	Sample Diluent
1	5000	5µL	9.5mL
2	500	100µL from std 1	500µL
3	250	500µL from std 2	500µL
4	125	500µL from std 2	500µL
5	62.5	500µL from std 2	500µL
6	31.25	500µL from std 2	500µL
7	15.63	500µL from std 2	500µL
8	7.813	500µL from std 2	500µL
9	3.906	500µL from std 2	500µL
10	0	Blank	500µL

2.6.5 Gene expression profiling

2.6.5.1 RNA sequencing

B-cells were isolated using the EasySep™ mouse B-cell isolation kit (STEMCELL Technologies) and differentiated using both TLR and BCR culture conditions. RNA was extracted as described in section 2.4.1. RNA-sequencing and bioinformatic analysis was carried out as described in section 2.4.4.

2.6.6 Phenotypic analysis of immune cell populations in SIK kinase inactive mice

2.6.6.1 Processing of tissue

Spleens and femurs were harvested from C57BL/6 mice. Single cell suspensions were created using the end of a 5mL syringe (BD Plastipak) and a 70µm cell strainer (Fisher Scientific) to gently force the spleen through the nylon mesh. Bone marrow was extracted from femurs by flushing with PBS using a 25G needle (BD). Following several washes with PBS, cells were counted using the trypan blue exclusion method with a haemocytometer. $2x10^6$ cells were taken for each phenotypic stain.

2.6.6.2 Staining panels

Mononuclear cells were re-suspended in 50µL of brilliant violet stain buffer (BD Bioscience) and 1µL Fc receptor block (BD Bioscience). The respective antibody mixes outlined below were added and samples were run on an LSRII 4 laser flow cytometer (BD Bioscience).

Table 2.19: Antibodies using for the staining of B-cell populations in the bone marrow

Antibody	Fluorophore	Clone	Supplier	Volume
CD138	APC	281-2	Miltenyi	5µL
B220	PE	RA3-6B2	Miltenyi	5µL
CD43	PER-CP5.5	S7	BD	1µL
IgM	BV421	R6-60.2	BD	5µL
IgD	BV605	11-26C.2a	BD	5µL
Ly51	PE-CY7	6C3	BioLegend	5µL

Table 2.20: Antibodies used for the staining of PBMC populations in the spleen

Antibody	Fluorophore	Clone	Supplier	Volume
CD3ε	FITC	145-2C11	BioLegend	1µL
CD4	APC FIRE 750	GK1.5	BioLegend	1µL
CD8	PE-CY7	53-6.7	BioLegend	1µL
B220	PE	RA3-6B2	Miltenyi	5µL
CD138	APC	281-2	Miltenyi	5µL

Table 2.21: Antibodies used for the staining of B-cell populations in the spleen

Antibody	Fluorophore	Clone	Supplier	Volume
B220	PE-CY7	RA3-6B2	BD	5µL
IgM	BV421	R6-60.2	BD	5µL
IgD	BV605	11-26c.2a	BD	5µL
CD43	PER-CP5.5	S7	BD	5µL
CD138	APC	281-2	BD	5µL
CD21	APC-CY7	7E9	BioLegend	5µL
CD23	BV510	B3B4	BD	5µL

2.6.6.3 Compensation

To account for and adjust spectral overlap between the fluorophores in each staining panel, single-colour compensation was applied. Each individual antibody was added to a droplet of UltraComp eBeads™ (eBioscience) and run on a compensation program on the LSRII.

2.6.6.4 Gating Strategies

To ensure all populations were identifiable including those with smaller numbers, 1 million events were recorded for all stains. Fluorescence minus one (FMO) and isotypes were used to set the following gates.

Early B-cell development in the bone marrow

To look at the early developmental stages of B-cells, cells were separated into Hardy fractions (Hardy *et al.*, 1991). B-cells ($B220^+$ $CD138^-$) were sub-gated on Ly51 and CD43 to separate fractions A-C and D-F. Further sub-gating with IgD and IgM allowed for the resolution of fractions D, E and F (Figure 2.4).

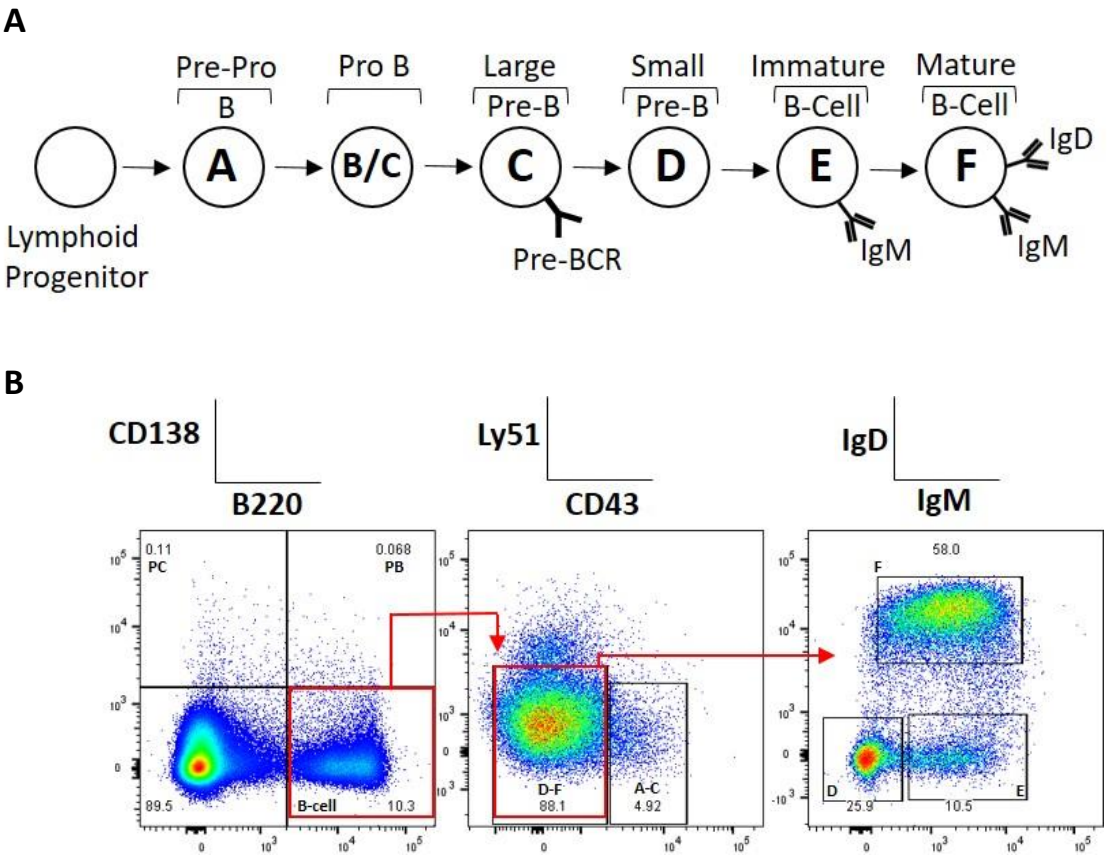

Figure 2.4 (A) Schematic diagram of early B-cell development in the bone marrow and 'Hardy Fraction' classification (B) Gating strategy used to separate cells into Hardy fractions.

PBMC populations in the spleen

Cells were separated into B- and T-cell populations using B220 and CD3ε. Non B/T-cells were characterised as $B220^{-}CD3\varepsilon^{-}$. Further separation into plasmablasts and plasma cells was achieved using CD138 and helper and cytotoxic T-cells using CD4 and CD8 (Figure 2.5).

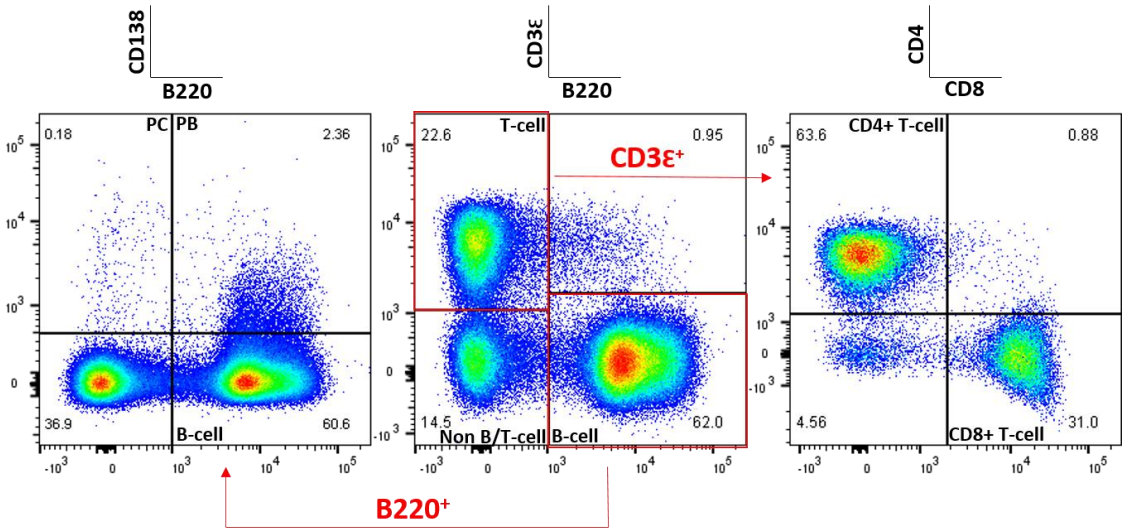

Figure 2.5 Gating strategy used to separate splenic PBMCs into B and T-cell populations.

Mature B-cell populations in the spleen

To distinguish mature B-cell populations in the spleen, $B220^+$ cells were gated on IgM and CD21. IgM^+CD21^+ cells were further gated on B220 and CD23 to resolve marginal zone (MZ) B-cells and IgM^- cells were further gated on IgD and CD23 to resolve follicular (FoB) and transitional (TZ) B-cells (Figure 2.5).

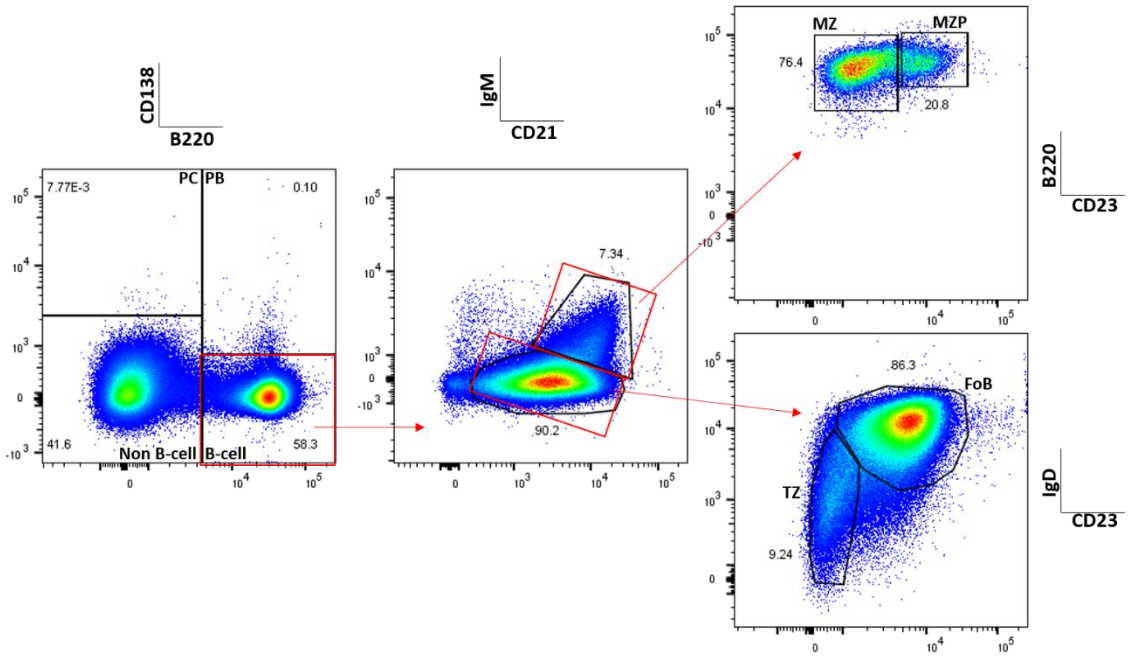

Figure 2.6 Gating strategy used to identify mature B-cell populations in the spleen.

2.6.7 NP-Specific ELISA following NP-Ovalbumin immunisation

96 well plates were coated with 100µL per well 10µg/mL NP(>20)-BSA or 2µg/mL NP(1-9)-BSA for 2 hours at room temperature. Plates were washed three times with ELISA wash solution (PBS/0.05% Tween). Plates were blocked (1% BSA/PBS) with 200µL per well for 1 hour at room temperature. Serum samples from NP-ovalbumin (OVA) immunised mice were diluted four-fold starting at 1:200. 50µL of each sample was added and incubated overnight at 4°C. Plates were washed three times. 50µL biotinylated IgG1 (BD Biosciences) was added to each well for 1 hour at room temperature. Plates were then washed three times. 50µL avidin-HRP was added to each well for 1 hour at room temperature. Plates were washed three times. 50µL TMB (3,3',5,5'-Tetramethylbenzidine; Bethyl Laboratories) was added to each well and incubated for approximately 5 minutes in the dark. 50µL stop solution (H_2SO_4) was added and the plate was read within 15 minutes at 450nm. The dilution series was plotted in an excel spreadsheet. Using an excel macro-file, an optical density-reading (OD) was chosen in the linear range and the endpoint titre was calculated.

Chapter 3 - Effect of SIK inhibition on human differentiating B-cells and multiple myeloma cell lines

The SIK subfamily is comprised of three isoforms (SIK1, SIK2 and SIK3) which belong to the AMP-activated protein kinase (AMPK) family. Although each isoform differs in length, structures are similar with a serine-threonine kinase domain at the N-terminal end, a sucrose-nonfermenting 1 (SNF-1) kinase homology domain in the middle, and a domain containing a protein kinase phosphorylatable serine residues at the C-terminal end (Okamoto, Takemori and Katoh, 2004). The kinase domain is essential to SIK activity and is catalysed by the upstream master kinase LKB1 through phosphorylation of the T-loop (Lizcano *et al.*, 2004). Furthermore, 14-3-3 isoforms can bind directly to the T-loop after phosphorylation by LKB1, resulting in enhanced catalytic activity and cytoplasmic localization of SIK (Al-Hakim *et al.* 2005). Alternatively, cAMP signalling and subsequent protein kinase A (PKA)-dependent phosphorylation can induce inhibitory 14-3-3 protein binding through conformational changes and/or shifts in SIK cytoplasmic distribution that block the ability to access and phosphorylate key substrates (Sonntag *et al.* 2017).

Over the past 10 years, the role of SIKs has been characterised in numerous cell types using small-molecule inhibitors and loss of kinase activity has revealed common downstream effectors such as CRTCs and HDACs. For example, SIK inhibition has been shown to promote the formation of regulatory macrophages through downstream CRTC2 dephosphorylation and subsequent CREB interaction, stimulating the production of IL-10 and other anti-inflammatory molecules (Clark *et al.* 2012). In hepatocytes, inhibition activates a similar pathway to enhance gluconeogenic gene expression and glucose production (Patel *et al.* 2014). Alternatively, inhibition in melanocytes resulted in an increase in MITF transcription (a well-known target of HDACs) promoting the biosynthesis of eumelanin (Mujahid *et al.*, 2017). Taken together, this suggests upstream control of SIK activity provides an opportunity to integrate diverse extracellular cues into changes in gene expression.

Gene co-expression network analysis of the maturation phase between a plasmablast and plasma cell identified *SIK1* as a highly connected hub gene suggesting that it was likely to play an important role in the biology of these cells. With this in mind, it was important to understand the function of SIKs in primary human differentiating B-cells. Furthermore, the effect of inhibition on multiple myeloma cell lines was also evaluated to investigate its potential as a therapeutic target. Two commercially available pan-SIK inhibitors HG-9-91-01 and YKL-05-099 were initially tested as well as the generic AMPK inhibitor, MRT19965.

3.1 Tracking *SIK* expression in differentiating B-cells by RNA-sequencing

Despite identifying *SIK1* as a hub gene, weighted gene correlation network analysis (WGCNA) does not distinguish the expression level of a given gene, but how well it correlates with the expression of other genes and so as further evidence for the preferential expression of *SIK1* during plasma cell differentiation, the relative FKPM (fragments per kilobase of exon per million fragments mapped) for *SIK1*, *SIK2* and *SIK3* were determined by RNA-sequencing which spanned all stages of the in vitro culture system.

Examination of the expression levels showed that *SIK1* transcripts increased rapidly during the transition from an activated B-cell (day 3) to a plasma cell (day 13) and this was maintained at high levels in fully mature cells. Alternatively, *SIK2* was barely detectable throughout the time course, whereas *SIK3* was expressed at moderate levels, but did not fluctuate (Figure 3.1).

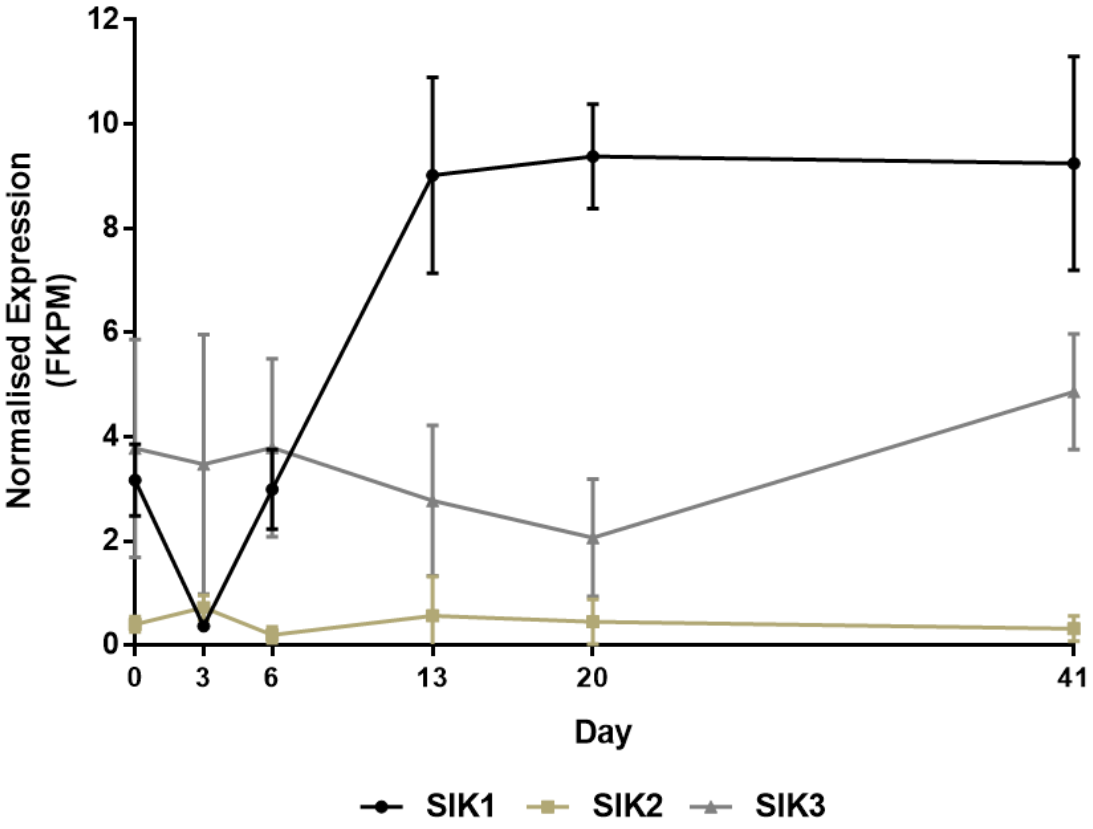

Figure 3.1 Relative mRNA expression of SIK family members during in vitro B-cell differentiation. RNA-sequencing was performed on samples from the indicated time points. Data is derived from 3 human donors and shown as mean ± SD. Data kindly provided by Mario Cocco and Matt Care.

3.2 Evaluation of SIK expression in differentiating B-cells

To confirm RNA expression patterns, it was important to ascertain the protein level of all 3 isoforms during B-cell differentiation. Interestingly, SIK1-3 expression was virtually undetectable in resting B-cells (day 0). Following stimulation with CD40-L, $F(ab')_2$ anti-IgM/IgG, IL-2 and IL-21, cells upregulated all 3 isoforms, however as differentiation occurred, the expression pattern of each isoform varied. SIK1 was readily detectable for the duration of the culture, whereas SIK2 was expressed only at the earlier time points. The expression of SIK3 was highest between day 1 and day 6, but small amounts of protein were also detectable at day 10 and 13 (Figure 3.2).

It is important to point out that mRNA and protein assessment was carried out in different donors and therefore the data does not reflect a direct comparison of the same cells. Furthermore, appendix 3 demonstrates that the SIK1 antibody can recognise SIK1 in HeLa cells transfected with either SIK2 or SIK3. This could suggest that either the SIK1 antibody is not isoform specific, or that HeLa cells express considerable levels of SIK1 and therefore interpretation of protein levels must be done so with caution. Additionally, it is well known that SIKs are controlled by activation status through regulatory proteins such as LKB1 and PKA (Al-Hakim *et al.*, 2005; Wein *et al.*, 2018) and therefore gene expression and total protein expression may be of less relevance in this context.

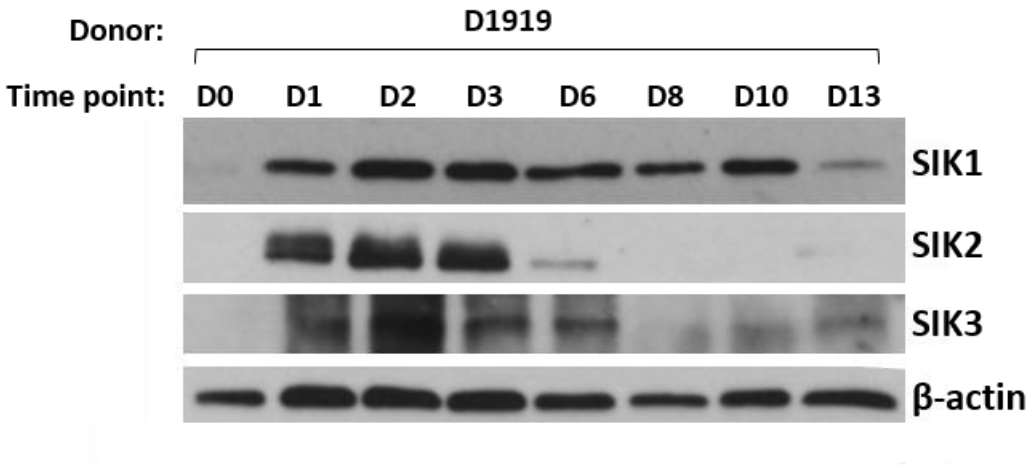

Figure 3.2 Endogenous expression of SIK family members in differentiating B-cells. Protein samples were harvested at the indicated time points, loaded on a 10% gel and transferred to a nitrocellulose membrane. Membranes were probed with antibodies for SIK1, SIK2 and SIK3. β-actin was used as a loading control. Blots are representative of expression assessed in 2 separate donors.

3.3 Inhibition of SIKs during plasma cell differentiation

The overall expression data are compatible with a requirement for SIK activity in either the generation or maintenance of plasma cells. To investigate the role of SIKs during terminal B-cell differentiation, the pan-SIK inhibitor HG-9-91-01 was used to block downstream signalling pathways. Primary cells were exposed to the small molecule inhibitor at various stages of the in vitro differentiation system (Figure 3.3). Following a 3 day incubation, cells were stained using antibodies against CD19, CD20, CD27, CD38 and CD138 and analysed by flow cytometry. Cell number was also recorded and normalised to a DMSO control to assess cell survival.

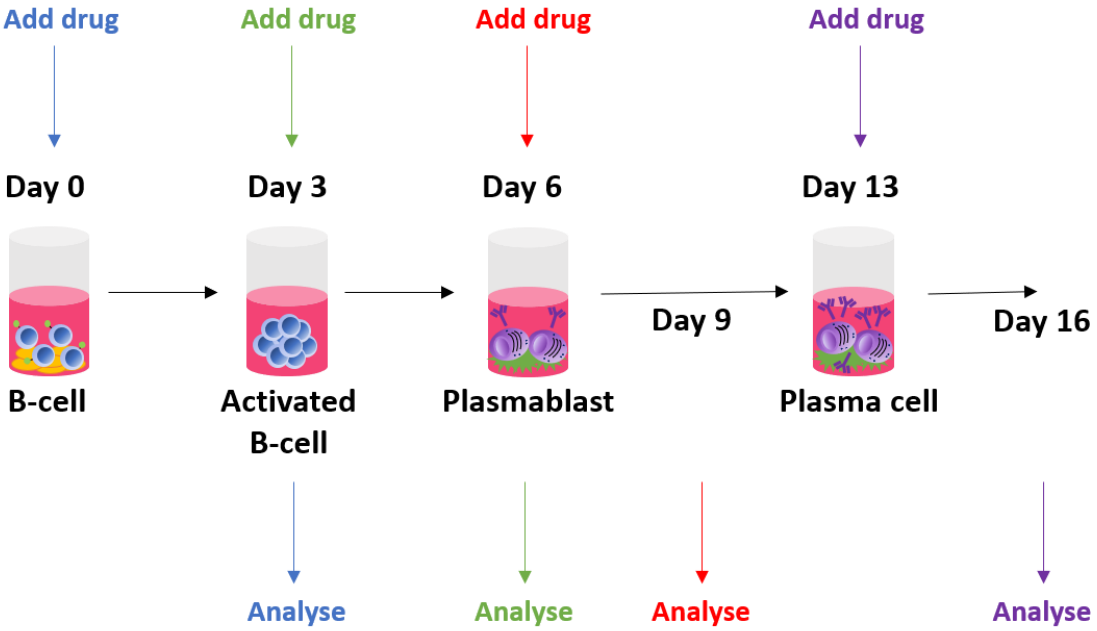

Figure 3.3 Schematic diagram highlighting time points at which HG-9-91-01 was added. Cells were incubated with DMSO or HG-9-91-01 (1µM) for 3 days. Samples were stained using antibodies against CD19, CD20, CD27, CD38 and CD138 and analysed using flow cytometry. Cells were counted using CountBright Beads™.

3.3.1 SIK inhibition on resting B-Cells (Day 0)

As SIK protein was undetectable in resting B-cells, it was assumed that cells would be unresponsive to SIK inhibition due to the small molecule inhibitor being unable to bind to the substrate. To test this hypothesis, HG-9-91-01 was added to resting B-cells for 3 days. As expected, cell counts revealed no significant difference between cells treated with DMSO or HG-9-91-01 across the 4 donors (Figure 3.4).

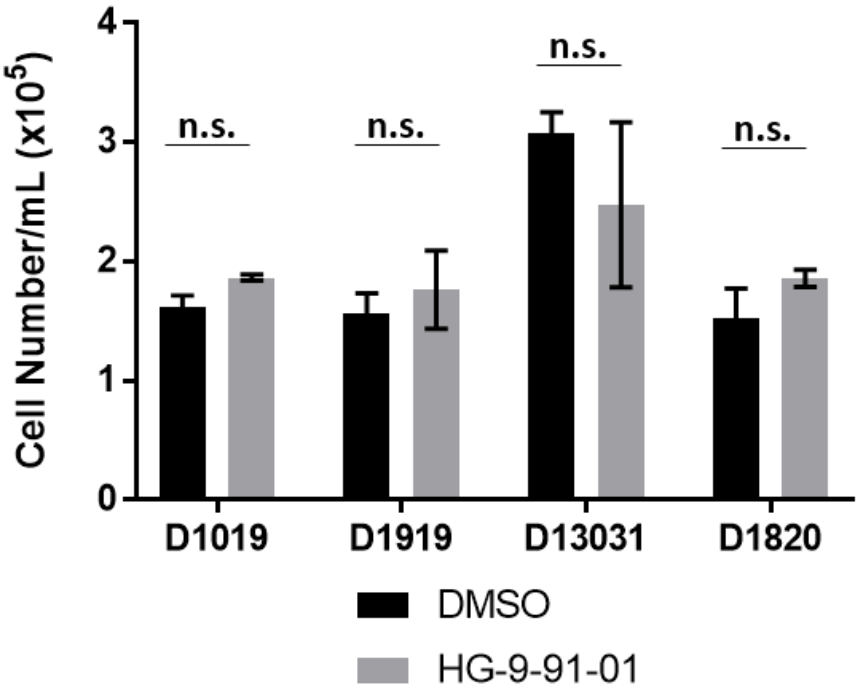

Figure 3.4 Assessing the impact of SIK inhibition on resting B-cell number. Total B-cells isolated from 4 donors were treated with DMSO or HG-9-91-01 (1µM) along with CD40-L, F(ab')$_2$, IL-2 and IL-21. On day 3, cells were counted using CountBright Beads™. Values are expressed as the mean ± SD. Significance was calculated using a paired t-test ($p<0.05$).

Phenotypic assessment of cardinal markers was also carried out following the 3 day incubation. Histogram plots identified a slight decrease in CD19 and an increase in CD38 expression, however this was inconsistent across the 4 donors (Figure 3.5) suggesting that resting B-cells do not rely on SIK kinase activity for activation or early differentiation.

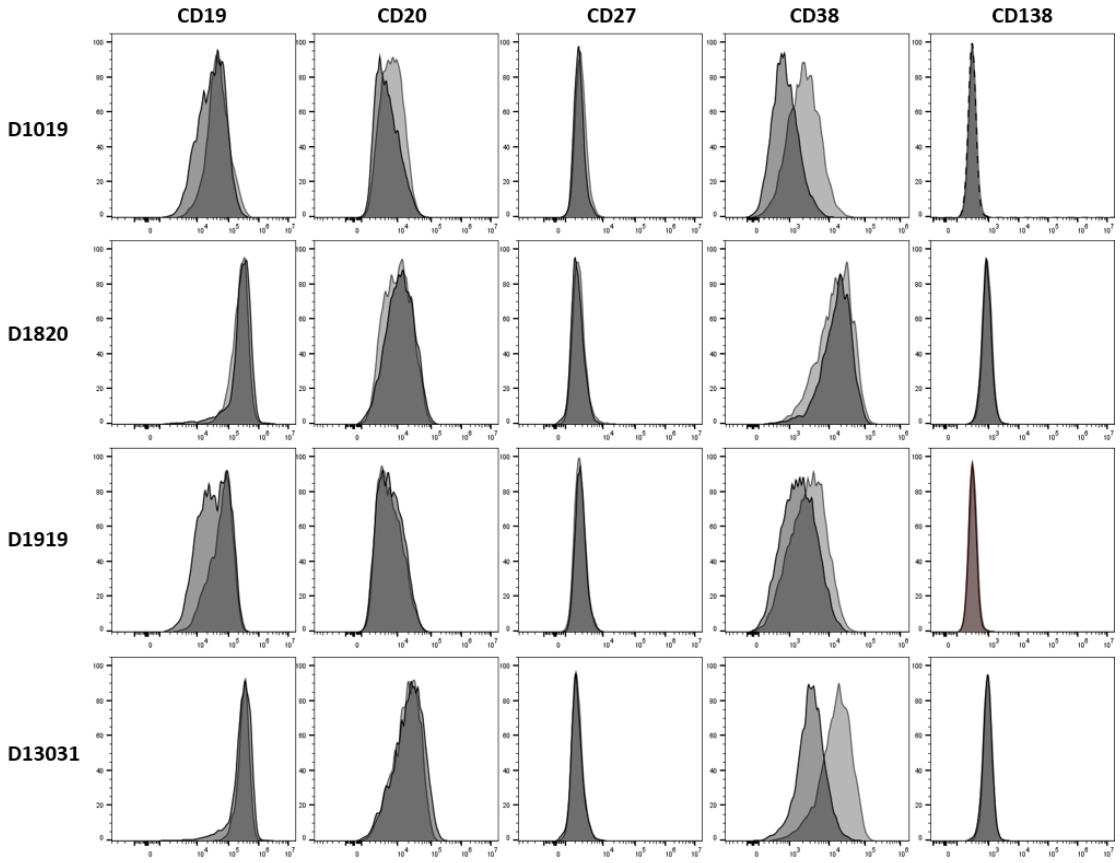

Figure 3.5 Assessing the impact of SIK inhibition on resting B-cell phenotype. Total B-cells isolated from 4 donors were treated with DMSO or HG-9-91-01 (1µM) along with CD40-L, $F(ab')_2$, IL-2 and IL-21. On day 3, cells were stained using antibodies against CD19, CD20, CD27, CD38 and CD138 and analysed by flow cytometry. Histograms represent DMSO (*dark grey*) and HG-9-91-01 (*light grey*) treated cells.

Although resting B-cells were initially unaffected by the loss of SIK kinase activity, it was important to establish if cells would be impacted at a later time point. For this, cells were washed at day 3 to remove the inhibitor and cultured as per normal conditions until terminally differentiated. Flow cytometry evaluation revealed minimal differences in phenotype across the 3 time points (Fig 3.6A) and cell counts were also similar (Fig 3.6B).

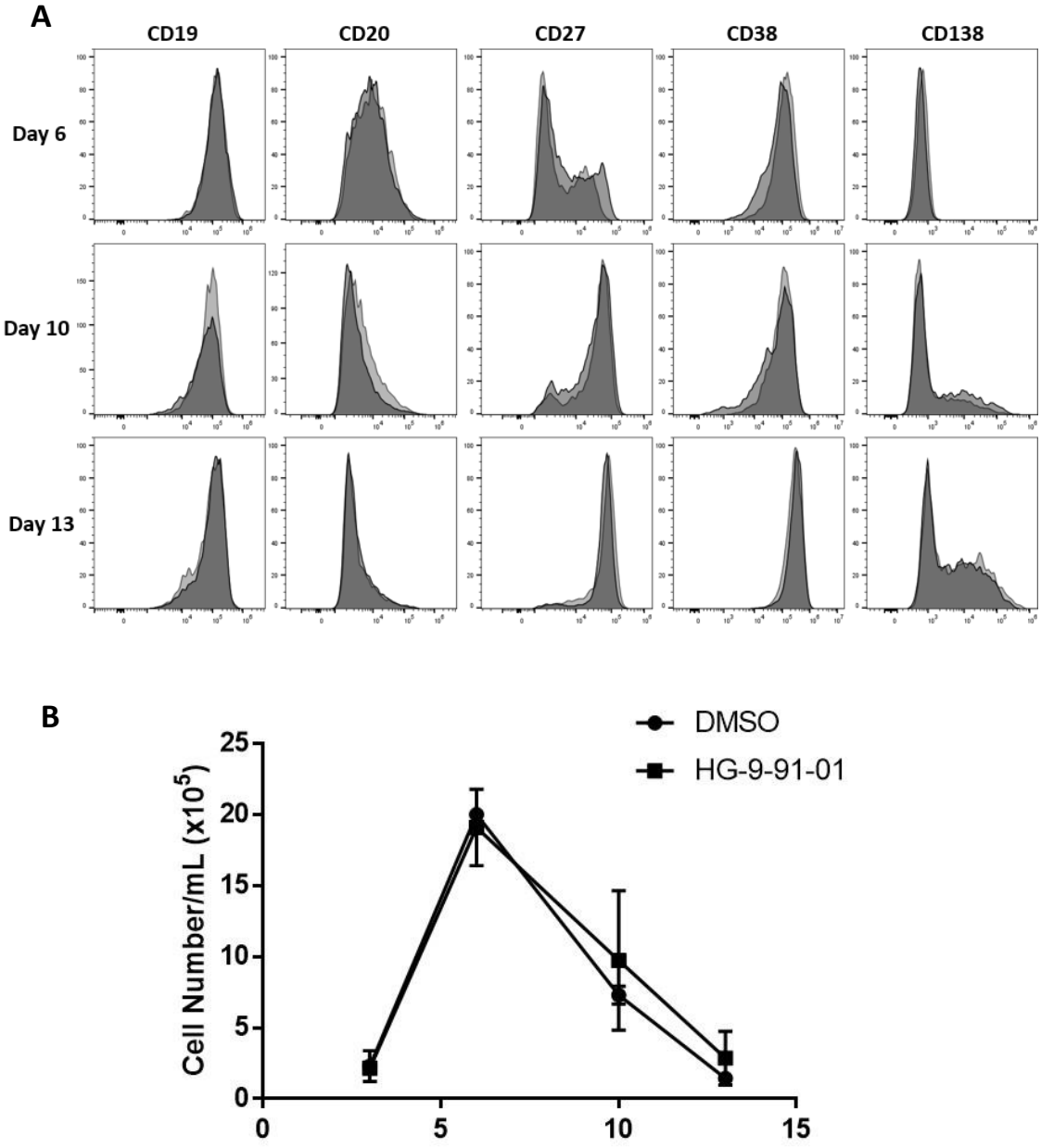

Figure 3.6 Assessing the ability of B-cells to terminally differentiate following SIK inhibition. (A) Total B-cells isolated from 2 human donors were treated with DMSO or HG-9-91-01 (1µM) for 3 days along with CD40-L, $F(ab')_2$, IL-2 and IL-21. At day 3, cells were washed and re-suspended in IL-2 and IL-21. At day 6, cells were re-suspended in IL-6, IL-21, lipids and amino acids and re-fed every 3 days. At day 6, 10 and 13, cells were stained using antibodies against CD19, CD20, CD27, CD38 and CD138. Histograms represent DMSO (*dark grey*) and HG-9-91-01 (*light grey*) treated cells. (B) Cells were counted using CountBright Beads™. Values are expressed as the mean ± SD for 2 human donors.

3.3.2 SIK inhibition on activated B-cells (Day 3)

Following exposure to antigen, activated B-cells undergo rapid expansion with previous work demonstrating that cells can undergo up to 4 divisions in the first 3 days of the in vitro system (Cocco *et al.*, 2012). Whilst the impact of SIK inhibition on resting cells was minimal, there was a significant decrease in cell number (80-90%) during the activated B-cell to plasmablast transition in all 4 donors (Figure 3.7).

It is important to note that the number of DMSO treated cells increased by roughly 1 log over the 3 day incubation, whereas HG-9-91-01 treated cells had counts similar to the seeding density ($1x10^5$ cells/mL) suggesting that inhibition could have affected proliferative capacity or viability. The data is also consistent with the western blot shown in Figure 3.2, in which all SIK isoforms were expressed at high levels on day 3 suggesting that SIKs play an important role during the early stages of becoming a plasma cell when cells are experiencing high levels of proliferation.

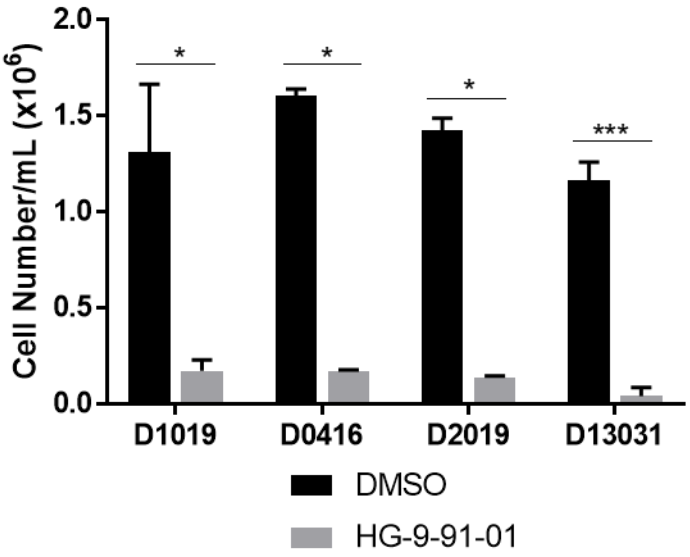

Figure 3.7 Assessing the impact of SIK inhibition on activated B-cell number. Cells were cultured with DMSO or HG-9-91-01 (1µM) in addition to IL-2 and IL-21. After 72h, samples were taken and counted using CountBright Beads™. Values are expressed as the mean ± SD. Significance was calculated using a paired t-test (* = p<0.05; ** = p<0.01; *** = p<0.001).

With a potential effect on proliferation, it was important to determine if any striking phenotypic alterations also occurred following SIK inhibition. The most observable difference after HG-9-91-01 exposure was an increase in the percentage of cells expressing both CD27 and CD38. There was no effect on CD138, as would be expected at this early time point (Figure 3.8).

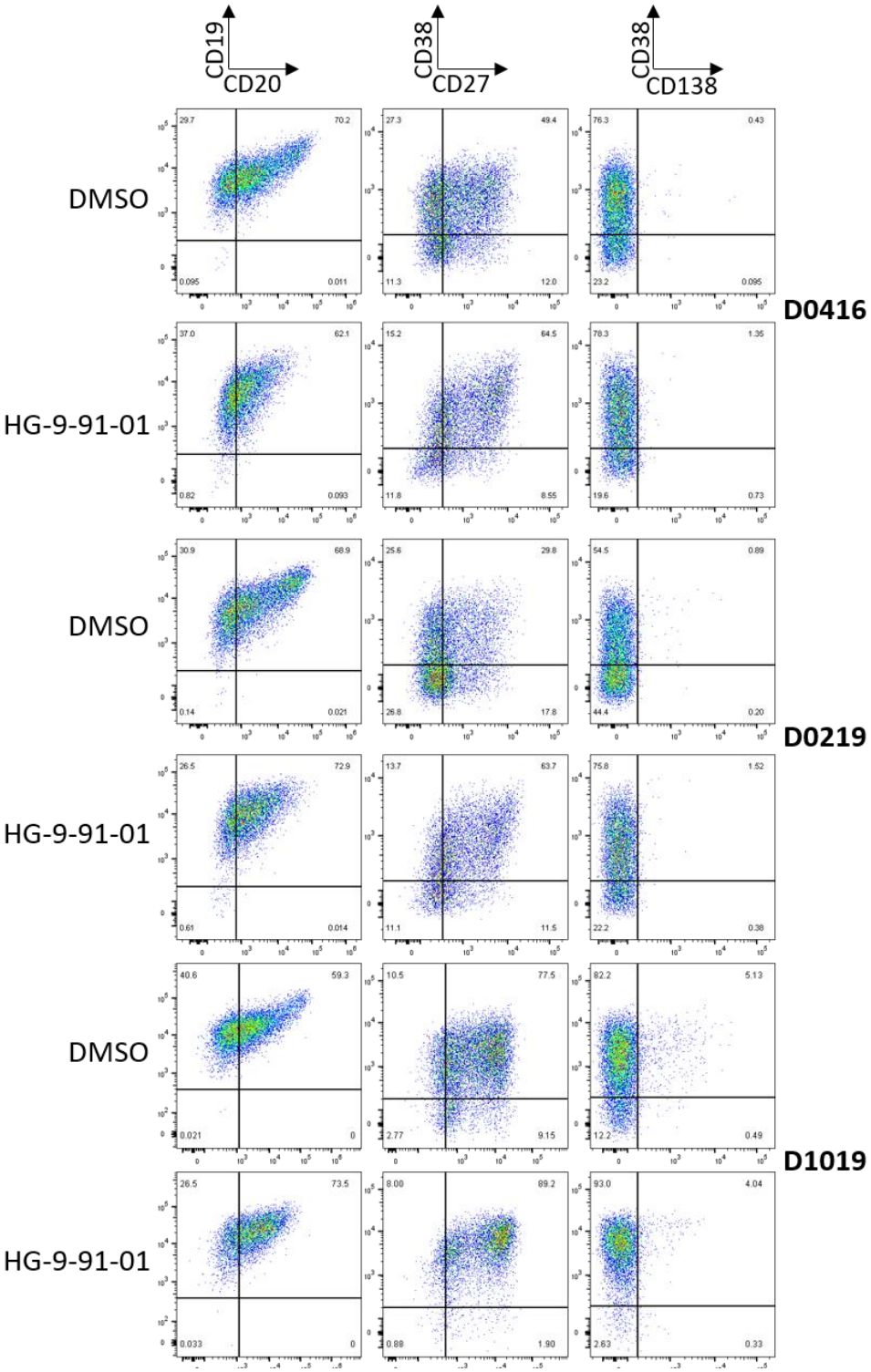

Figure 3.8 Assessing the impact of SIK inhibition on activated B-cell phenotype. Cells were cultured with DMSO or HG-9-91-01 (1µM) in addition to IL-2 and IL-21 for 3 days. After 72h, samples were stained with antibodies against CD19, CD20, CD27, CD38 and CD138 and analysed using flow cytometry.

3.3.3 SIK inhibition on plasmablasts (Day 6)

Following clonal expansion, activated B-cells initiate a differentiation program that turns them into short-lived, cycling plasmablasts (Brynjolfsson *et al.*, 2018). This is accompanied by a dynamic change in gene expression profile including the silencing of B-cell transcription factors such as *Pax5*, *Bach2* and *Bcl6* and the activation of plasma cell specific factors such as *Irf4*, *Prdm1* and *Xbp-1* (Tellier *et al.*, 2016; Shi *et al.*, 2015). Furthermore, changes in cell surface phenotype occur including downregulation of CD19 and CD20 and upregulation of CD27, CD38 and CD138 (Tarte *et al.*, 2003; Kaminski *et al.*, 2012). As plasmablasts are distinct from activated B-cells, it was necessary to assess SIK requirement at this time point.

Following SIK inhibition, there was a significant decrease in cell number across all 3 donors (Figure 3.9). As cells treated with DMSO did not demonstrate extensive proliferation in relation to the seeding density (1x10^6/mL), it is conceivable that SIK inhibition caused a reduction in cell viability at this time point.

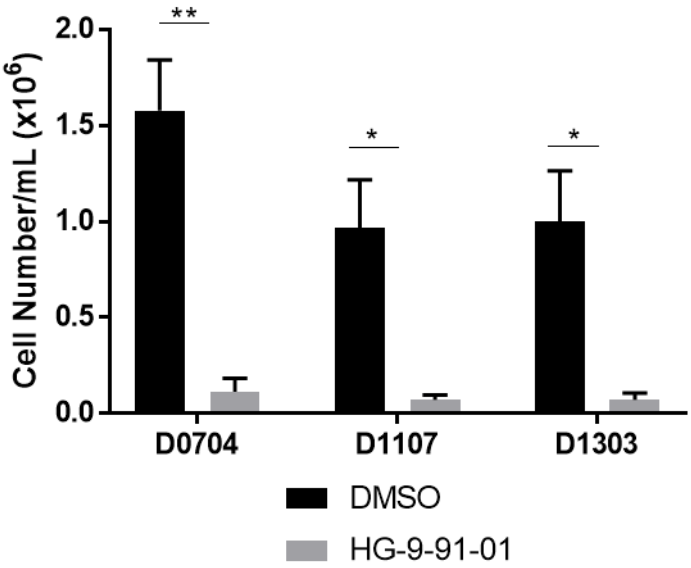

Figure 3.9 Assessing the impact of SIK inhibition on plasmablast cell number. Cells were cultured with DMSO or HG-9-91-01 (1µM) in addition to IL-6, IL-21, IFN-α, M210B4 stromal cells, lipids and amino acids for 3 days. After 72h, samples were taken and counted using CountBright Beads™. Values are expressed as the mean ± SD. Significance was calculated using a paired t-test (* = p<0.05; ** = p<0.01).

Phenotypic characterisation revealed an increase in cells that retained CD20 following SIK inhibition, whereas cells positive for both CD38 and CD27 decreased. This could suggest that a small population of cells which are phenotypically more 'B-cell like' survive preferentially when SIK kinase activity is compromised. However, amongst the population that were $CD38^{+}CD27^{+}$, cells treated with HG-9-91-01 demonstrated higher expression levels of both markers, which could be consistent with accelerated differentiation in a proportion of surviving cells (Figure 3.10).

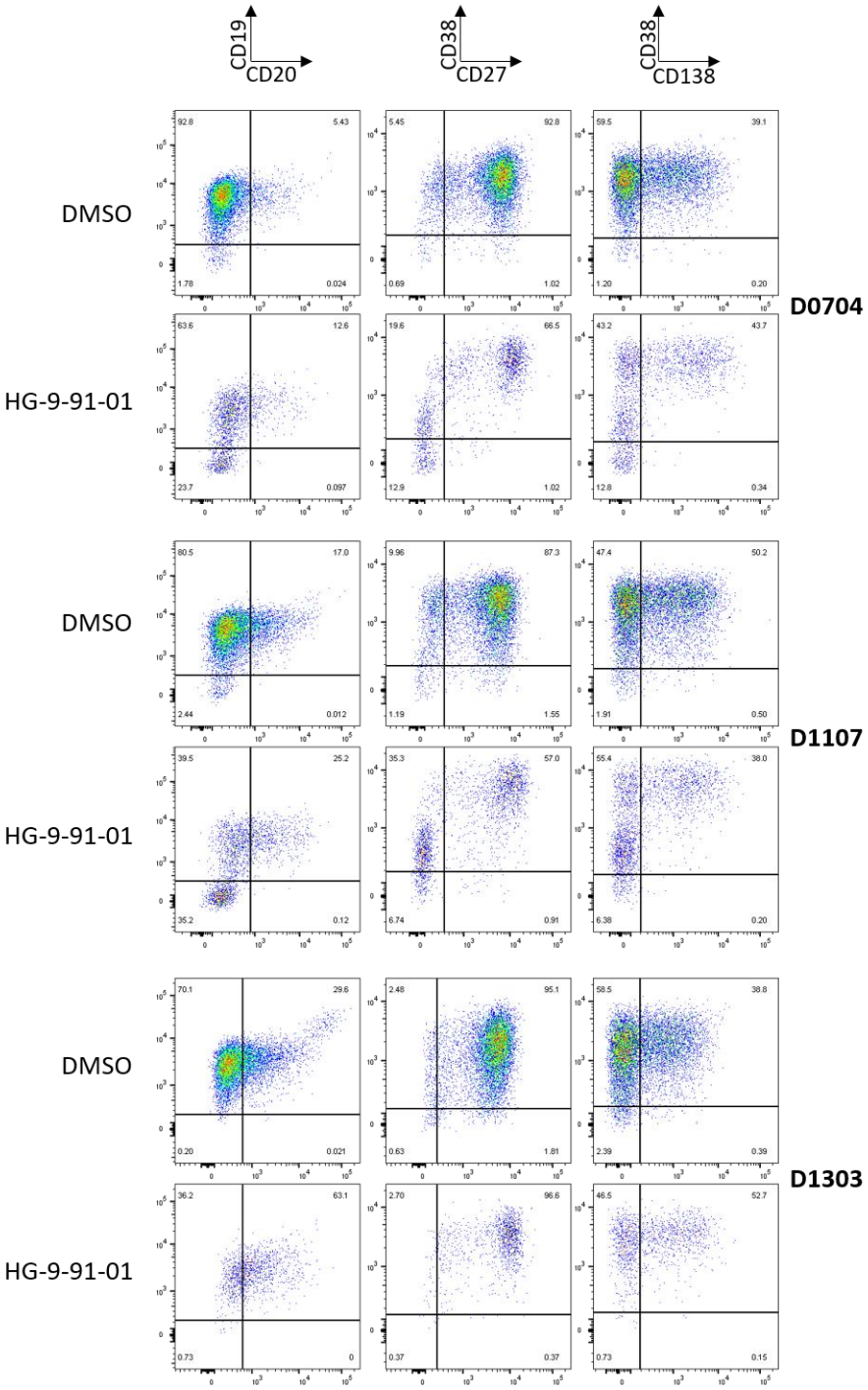

Figure 3.10 Assessing the impact of SIK inhibition on plasmablast phenotype. Cells were cultured with DMSO or HG-9-91-01 (1μM) in addition to IL-6, IL-21, IFN-α, M210B4s, lipids and amino acids for 3 days. After 72h, samples were stained with antibodies against CD19, CD20, CD27, CD38 and CD138 and analysed using flow cytometry.

3.3.4 SIK inhibition on plasma cells (Day 13)

The final stage of differentiation (plasmablast to plasma cell) is accompanied by further changes in gene expression profile and phenotype as well as an exit from cell cycle (Chen-Kiang, 2003). Data generated by colleagues within the lab suggests the transition to a plasma cell occurs around day 10 within the in vitro system, therefore SIK inhibition was performed on day 10 cells. Following loss of SIK kinase activity, there was a significant decrease in cell number across all 4 donors (Figure 3.11). As plasma cells have exited cell cycle, it is likely that in a similar manner to plasmablasts, SIK inhibition caused a reduction in cell viability.

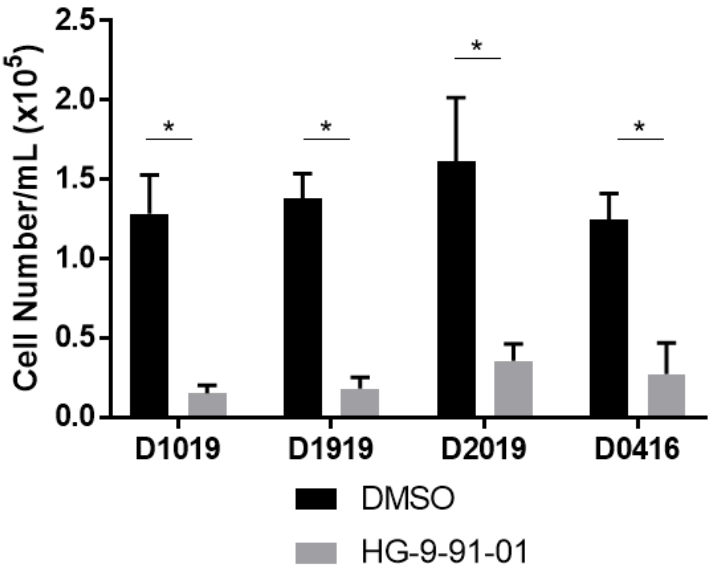

Figure 3.11 Assessing the impact of SIK inhibition on plasma cell number. Cells were cultured with DMSO or HG-9-91-01 (1µM) in addition to IL-6, IL-21, IFN-α, M210B4s, lipids and amino acids for 3 days. After 72h, samples were taken and counted using CountBright Beads™. Values are expressed as the mean ± SD. Significance was calculated using a paired t-test (* = $p<0.05$).

Flow cytometry comparison of day 13 cells was difficult due to there being a limited number of cells after SIK inhibition. Of the few cells that remained, there were no striking differences between cardinal marker expression (Figure 3.12).

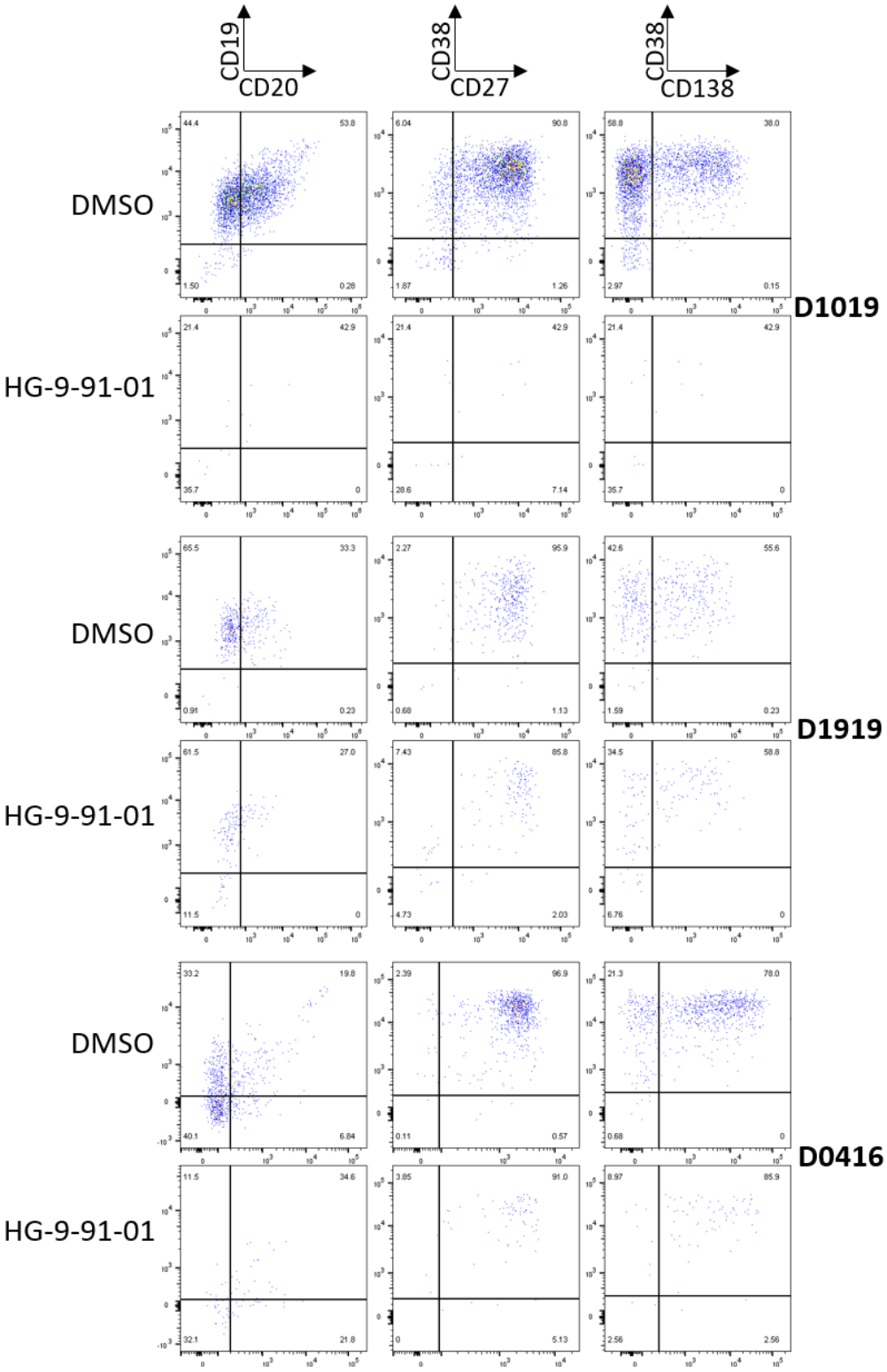

Figure 3.12 Assessing the impact of SIK inhibition on plasma cell phenotype. Cells were cultured with DMSO or HG-9-91-01 (1µM) in addition to IL-6, IL-21, IFN-α, M210B4s, lipids and amino acids for 3 days. After 72h, samples were stained with antibodies against CD19, CD20, CD27, CD38 and CD138 and analysed using flow cytometry.

3.3.5 SIK inhibition on plasma cells cultured in bone marrow niche conditions

Although plasma cells cultured with IL-6, IL-21, IFN-α, lipids and amino acids were sensitive to SIK inhibition, it was necessary to determine if factors critical for long-lived plasma cell survival such as BAFF and APRIL (Benson *et al.*, 2008) could alter this. B-cell maturation antigen (BCMA) acts as a receptor for both BAFF and APRIL, however recent work has shown it can be cleaved from the cell surface by γ-secretase (Laurent *et al.*, 2015). With this in mind, a gamma secretase inhibitor (GSI) was included. Different combinations of these factors were added to cells in addition to IL-6, lipids and amino acids.

Overall survival was low when IFN- α, BAFF and APRIL (H98) were added alone, however this improved considerably when GSI was included in addition to BAFF or APRIL. SIK inhibition resulted in a decrease in cell number across all conditions (apart from BAFF), suggesting that long-lived plasma cell survival factors were not able to decrease sensitivity to inhibition (Figure 3.13).

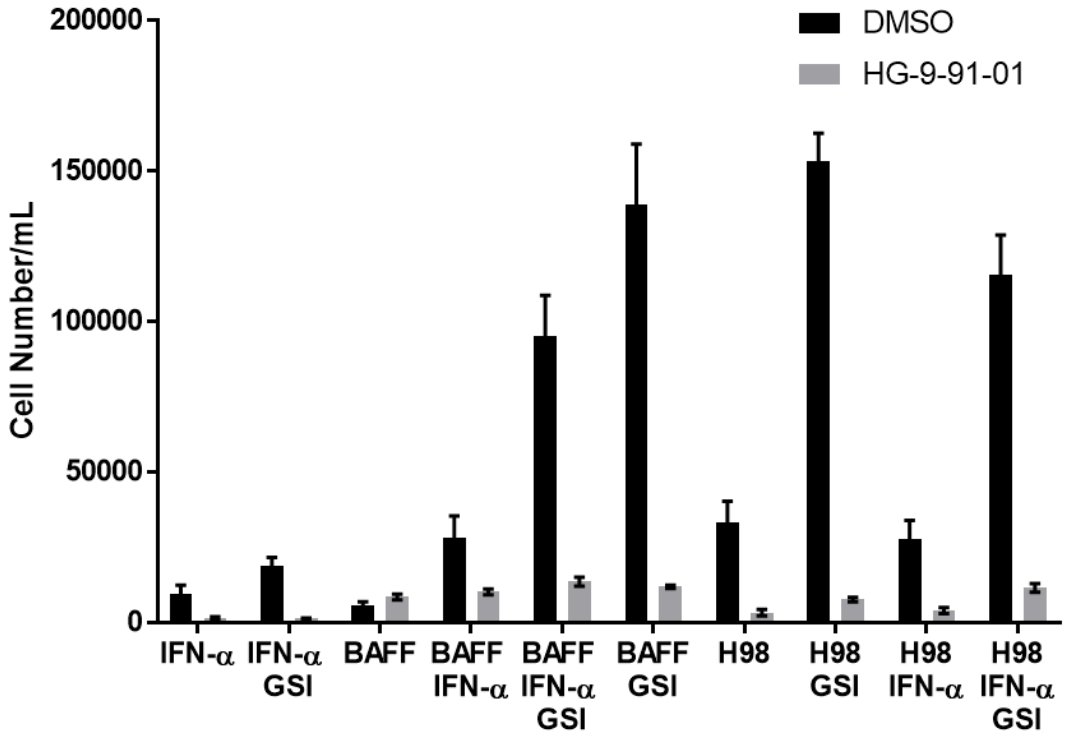

Figure 3.13 The impact of SIK inhibition on plasma cell number cultured with survival factors. Day 13 cells were cultured with DMSO or HG-9-91-01 (1μM) in addition to IL-6, IL-21, M210B4s, lipids and amino acids and various survival factors for 3 days. After 72h, samples were taken and counted using CountBright Beads™. Values are expressed as the mean ± SD for 2 human donors.

3.3.6 Time-course analysis

Prior inhibition experiments were performed using a 3 day (72h) incubation period, however for downstream analysis it was important to establish the relationship between time exposed to the inhibitor and survival. As seen in Figure 3.14, the concentration of HG-9-91-01 that had been used in previous experiments (1µM) decreased survival by over 20% from as early as 24 hours, suggesting that SIK inhibition exerts its effect almost immediately. Viability then decreased in a time-dependent manner until 96 hours.

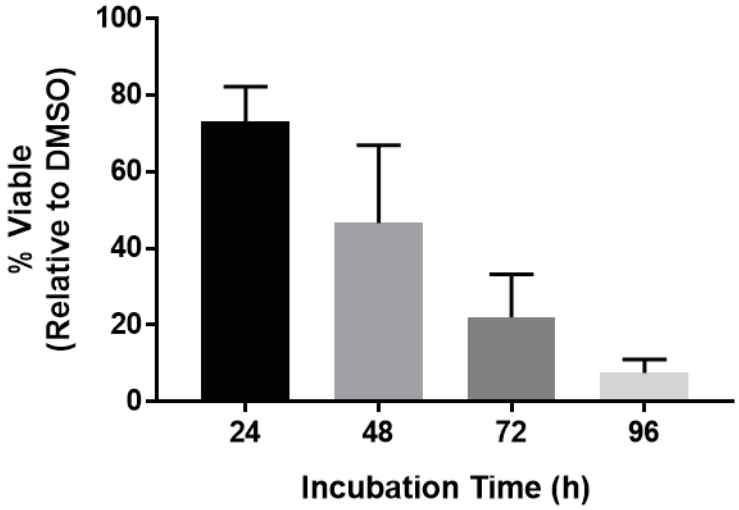

Figure 3.14 The impact of SIK inhibition on plasmablast cell number across a time-course. Day 6 plasmablasts were cultured with DMSO or HG-9-91-01 (1µM) in addition to IL-6, IL-21, IFN-α, M210B4s, lipids and amino acids for 4 days (96h). At 24h intervals, samples were taken and counted using CountBright Beads. Values are expressed as the mean ± SD for 2 human donors.

In the same experiment, samples were evaluated for marker expression to determine whether certain phenotypic profiles were present prior to the decrease in viability. The most compelling observation occurred at 48h post-inhibition in which there was considerable downregulation of all markers. Interestingly by 72h, the majority of these cells had disappeared suggesting that marker downregulation was a predecessor of cell death. By 96h, the small percentage of cells that remained had a similar phenotype to the control cells, although there was a decrease in the percentage of cells expressing CD138 and a small population of cells still displayed increased marker downregulation (Figure 3.15).

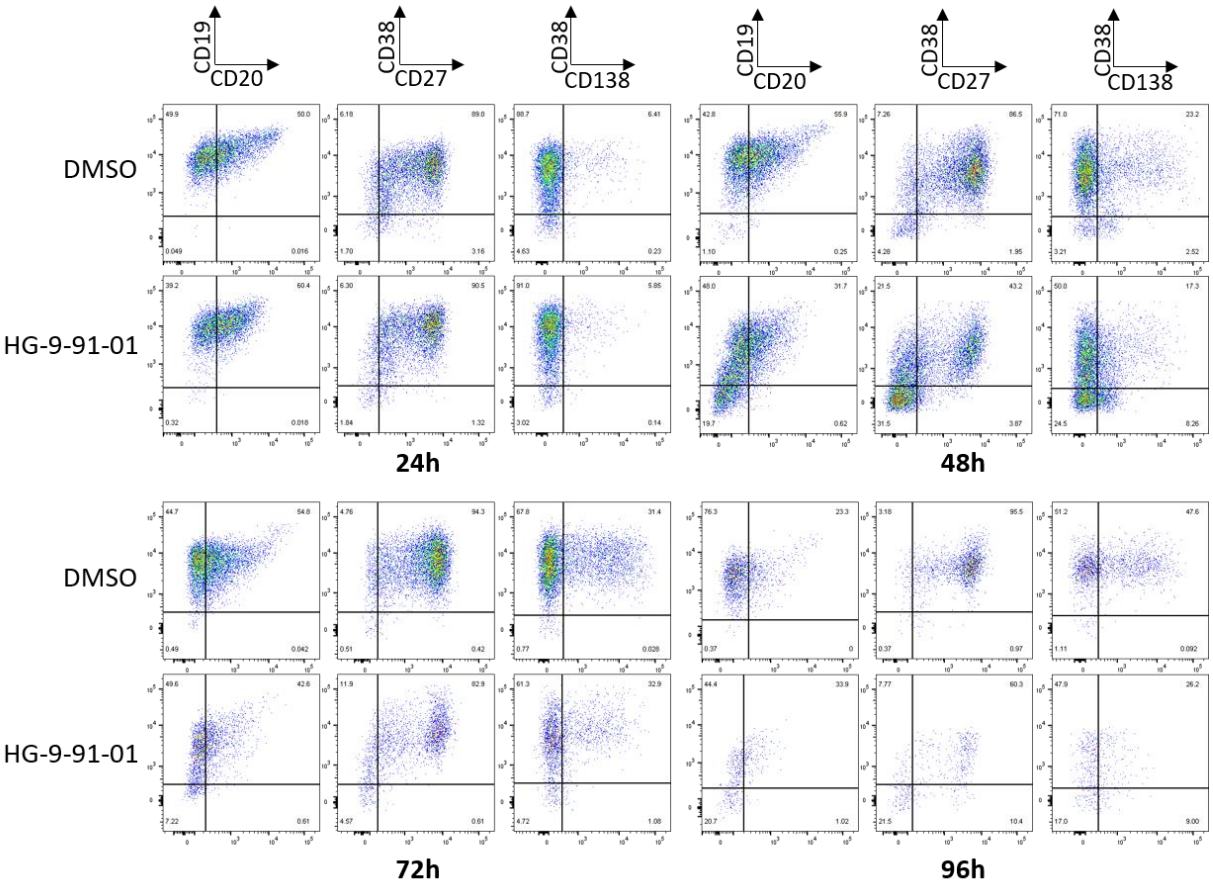

Figure 3.15 The impact of SIK inhibition on phenotype across a time-course. Day 6 plasmablasts were cultured with DMSO or HG-9-91-01 (1µM) in addition to IL-6, IL-21, IFN-α, M210B4s, lipids and amino acids for 4 days (96h). At 24h intervals, samples were stained with antibodies against CD19, CD20, CD27, CD38 and CD138 and analysed using flow cytometry. Results are representative of 2 donors.

3.3.7 SIK inhibition on T-independent stimulated plasmablasts

During an immune response, B-cell proliferation and differentiation is initiated through either BCR or TLR activation depending on the type of antigen present (Lanzavecchia, 1985; Treanor, 2012; Buchta and Bishop, 2014). The data presented so far in this chapter has utilised BCR signalling to stimulate B-cells in a T-dependent manner, however it is also important to assess sensitivity to SIK inhibition in cells stimulated with T-independent stimuli. This is because SIK inhibition has been shown to negatively regulate TLR signalling, in part through the inactivation of cAMP-regulated transcriptional co-activators (CRTCs) blocking pro-inflammatory cytokine production and increasing IL-10 secretion in human monocytes, macrophages, and DCs (Lombardi *et al.*, 2016; Clark *et al.*, 2012).

Day 6 cells activated with the TLR7/8 agonist R848 in addition to IL-2, IL-21 and F(ab')$_2$ anti-IgM/IgG were exposed to either DMSO or HG-9-91-01 for 3 days. Cell number decreased significantly following SIK inhibition in a similar manner to cells activated through the BCR (Figure 3.16). This suggests that regardless of the type of B-cell activation, differentiating cells have a dependency on SIK kinase activity for survival.

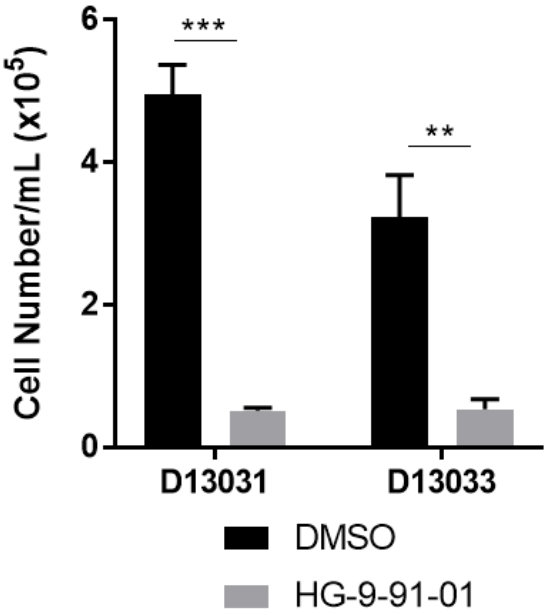

Figure 3.16 The impact of SIK inhibition on TI stimulated plasmablasts. Cells were stimulated at day 0 with R848, IL-2, IL-21 and F(ab')$_2$ anti-IgM/IgG. On day 3, cells were washed and re-suspended in IL-2 and IL-21. On day 6, cells were cultured with DMSO or HG-9-91-01 (1µM) in addition to IL-6, IL-21, IFN-α, lipids and amino acids for 3 days. On day 9, cells were counted using CountBright Beads™. Results are expressed as the mean ± SD. Significance was calculated using a paired t-test (* = $p<0.05$; ** = $p<0.01$; *** = $p<0.001$).

3.3.8 Therapeutic potential in ASC populations

As the data suggests that SIKs are a requirement of plasma cell survival, they could provide an attractive target in diseases where expansion of plasma cells is problematic, such as multiple myeloma. Currently, the proteasome inhibitor bortezomib is administered to patients with myeloma as a single agent or in combination with other therapies and although not curative, a recent systematic review has confirmed its effectiveness in prolonging overall and progression free survival (Scott *et al.*, 2016).

With that being said, it was of interest to compare the efficacy of HG-9-91-01 with bortezomib on day 6 plasmablasts. After a 3 day incubation, cell counts revealed similar decreases in cell viability relative to the DMSO control (between 90-95%) (Figure 3.17). Although not an in-depth investigation, this bolsters the idea that SIKs could be useful as a therapeutic target in multiple myeloma.

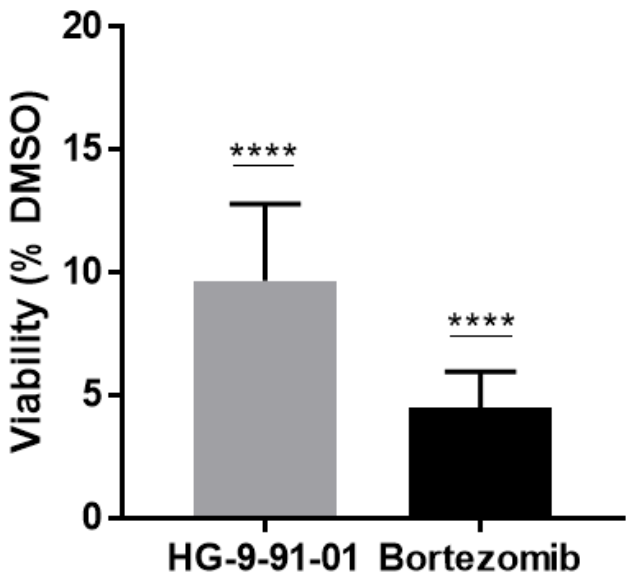

Figure 3.17 A comparison of proteasome and SIK inhibition on day 6 plasmablast survival. Day 6 plasmablasts were cultured with DMSO, HG-9-91-01 or Bortezomib (1µM) in addition to IL-6, IL-21, IFN-α, M210B4s, lipids and amino acids for 3 days. On day 9, cells were counted using CountBright Beads and viability was measured as a percentage of the DMSO control. Results are expressed as the mean ± SD for 3 human donors. Significance was calculated between DMSO and HG-9-91-01 or Bortezomib treated cells using a paired t-test (* = $p<0.05$; ** = $p<0.01$; *** = $p<0.001$ **** = $p<0.0001$).

3.3.9 Concentration-response and time-course relationships

With the potential to be a therapeutic, basic pharmacodynamic assessment of HG-9-91-01 was carried out. Establishing whether a small molecule inhibitor acts in a concentration and time-dependent manner is useful because it allows various conclusions to be drawn. For example, predictions can be made about the intensity of action whilst increasing the dose and IC50s can be generated to compare the potency of different drug prototypes in the same system. Furthermore, saturating doses can be identified in which a maximal response is obtained. This is essential when it comes to determining safety and means the best candidate can be taken forward for pre-clinical testing.

With this in mind, concentration-response curves were generated at different time points during the differentiation. On day 6 plasmablasts, as little as 16nM HG-9-91-01 resulted in a considerable reduction (25%) in cell viability. Furthermore, viability continued to decrease in a concentration-dependent manner (Figure 3.18).

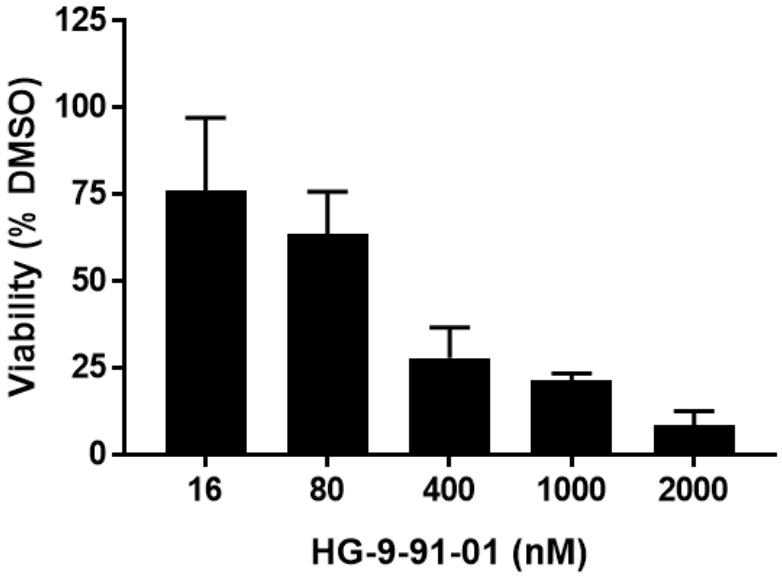

Figure 3.18 Assessing the impact of HG-9-91-01 concentration on plasmablast survival. Day 6 plasmablasts were cultured with increasing concentrations of DMSO or HG-9-91-01 in addition to IL-6, IL-21, IFN-α, M210B4s, lipids and amino acids for 3 days. On day 9, cells were counted using CountBright Beads™ and viability was measured as a percentage of the DMSO control. Results are expressed as the mean ± SD for 2 human donors.

Activated B-cells were also exposed to increasing concentrations of HG-9-91-01 and viability was recorded at both 48h and 72h post-inhibition. Cells responded in a time-dependent manner over a 72 hour period. Once again as concentration increased, viability decreased in a concentration-dependent manner. To note, the maximal response in this experiment occurred after 72h using 2μM HG-9-91-01, however it is plausible that a higher concentration or increased exposure time could reduce viability further due to the small percentage of cells still remaining.

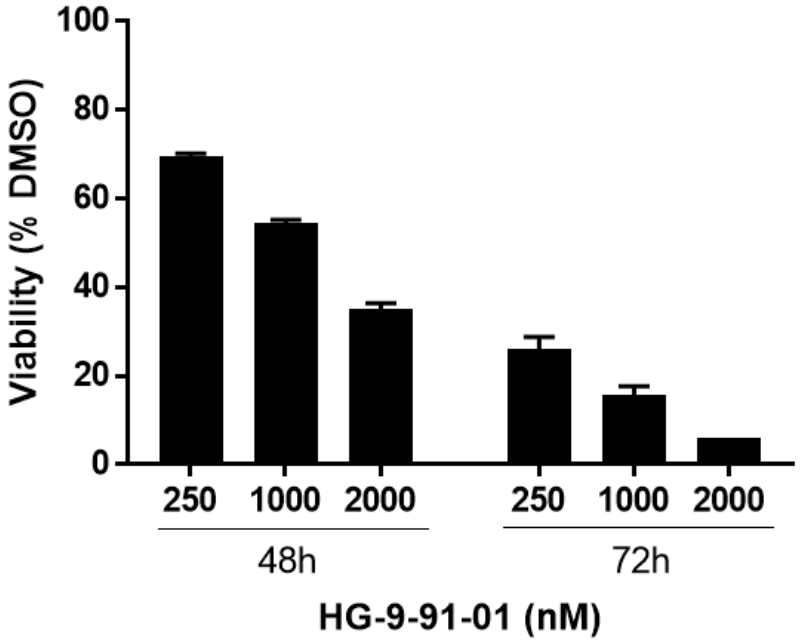

Figure 3.19 Assessing the impact of HG-9-91-01 concentration and exposure time on activated B-cell survival. Day 3 activated B-cells were cultured with increasing concentrations of DMSO or HG-9-91-01 in addition to IL-2 and IL-21 for 3 days. On day 6, cells were counted using CountBright Beads™ and viability was measured as a percentage of the DMSO control. Results are expressed as the mean ± SD for 2 human donors.

3.4 Impact of SIK inhibition on multiple myeloma (MM) cell lines

3.4.1 Analysis of myeloma cell line growth characteristics

With the idea that SIKs may be targetable in myeloma, the next step was to assess SIK inhibition in a variety of myeloma cell lines. With different cell lines to test, it was vital to determine whether growth characteristics were comparable to allow correct interpretation of the data. Figure 3.20 shows that cell lines underwent uniform cell growth and increased roughly 10-fold over the course of 3 days.

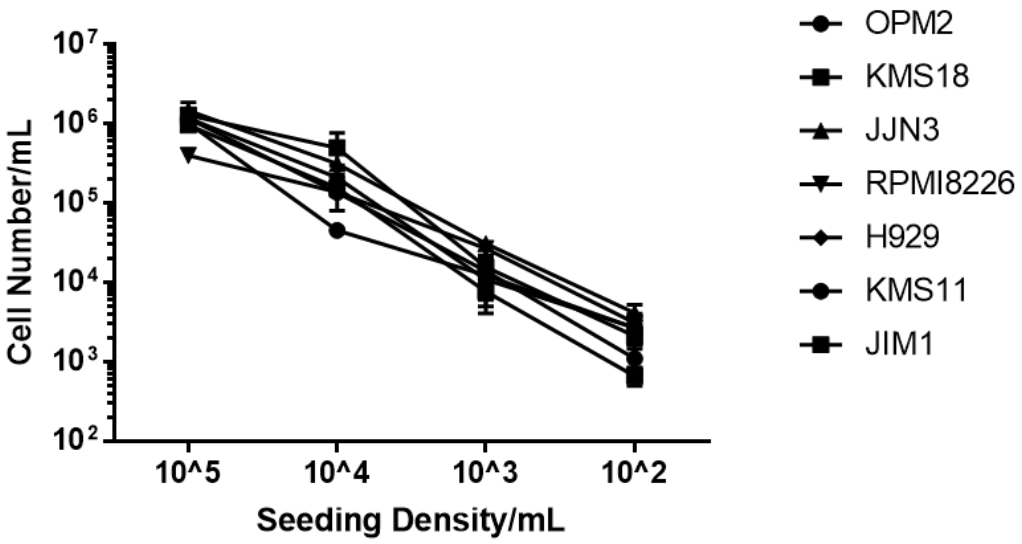

Figure 3.20 The impact of seeding densities of cell growth. Cells were seeded at increasing densities ($1x10^{2-5}$) in RPMI-1640. On day 3, samples were collected and counted using CountBright™ beads.

Following viability assessment, 5 cell lines survived better when seeded at $1x10^5$ cells/well and 3 cell lines survived better when seeded at $1x10^4$ cells/well in a 12-well plate (Figure 3.21). To overcome this, it was decided that all cell lines would be seeded at $5x10^4$ (roughly half way between the two optimal densities) in further experiments meaning that cell death could be attributed to small molecule inhibitors and not spontaneous apoptosis or media depletion.

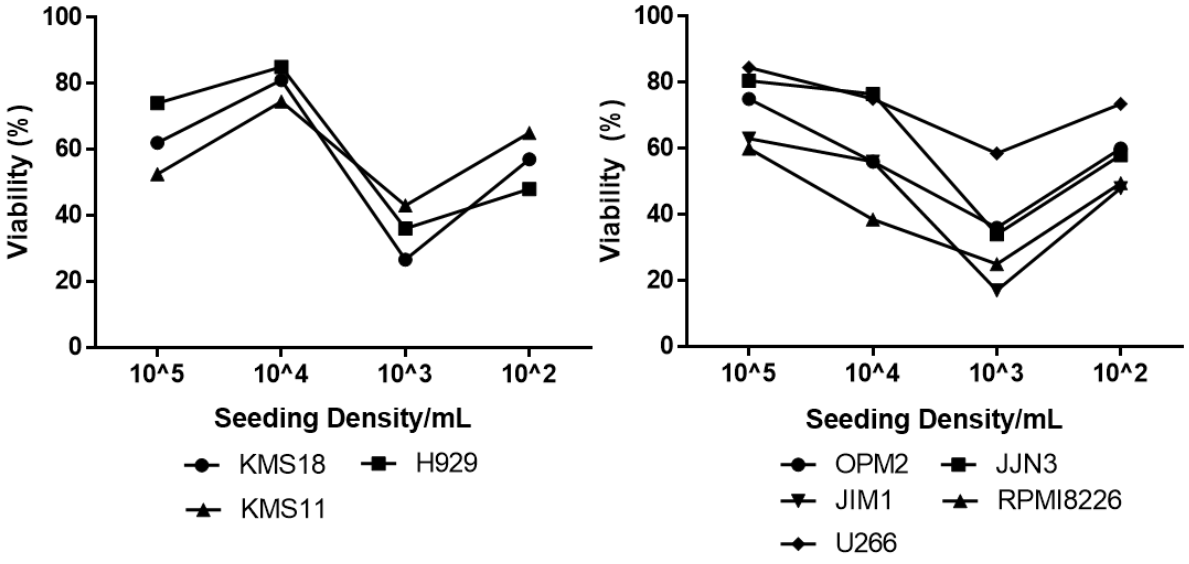

Figure 3.21 The impact of seeding densities on cell viability. Cells were seeded at increasing densities ($1x10^{2-5}$) in RPMI-1640. On day 3, cells stained with Annexin V and analysed using flow cytometry.

3.4.2 SIK inhibition on MM cell line viability

Using the optimal conditions determined in Figure 3.21, experiments were then performed using incremental concentrations of the SIK inhibitor HG-9-91-01, and MRT19965 which potently inhibits most of the AMPK-related kinases to determine the impact on cell viability.

The assay confirmed that the AMPK inhibitor, MRT19965 induced profound apoptosis in a concentration-dependent manner across all cell lines. HG-9-91-01 also induced apoptosis, however the reduction in viability differed between myeloma cell lines. For example at the higher concentrations, the viability of KMS11 and OPM2 reduced by over 95% whereas for U266, RPMI8226, JIM1, JJN3 and KMS18 this was closer to 60-70%. Interestingly, HG-9-91-01 had little effect on H929 with 75% of the population remaining viable following inhibition (Figure 3.22).

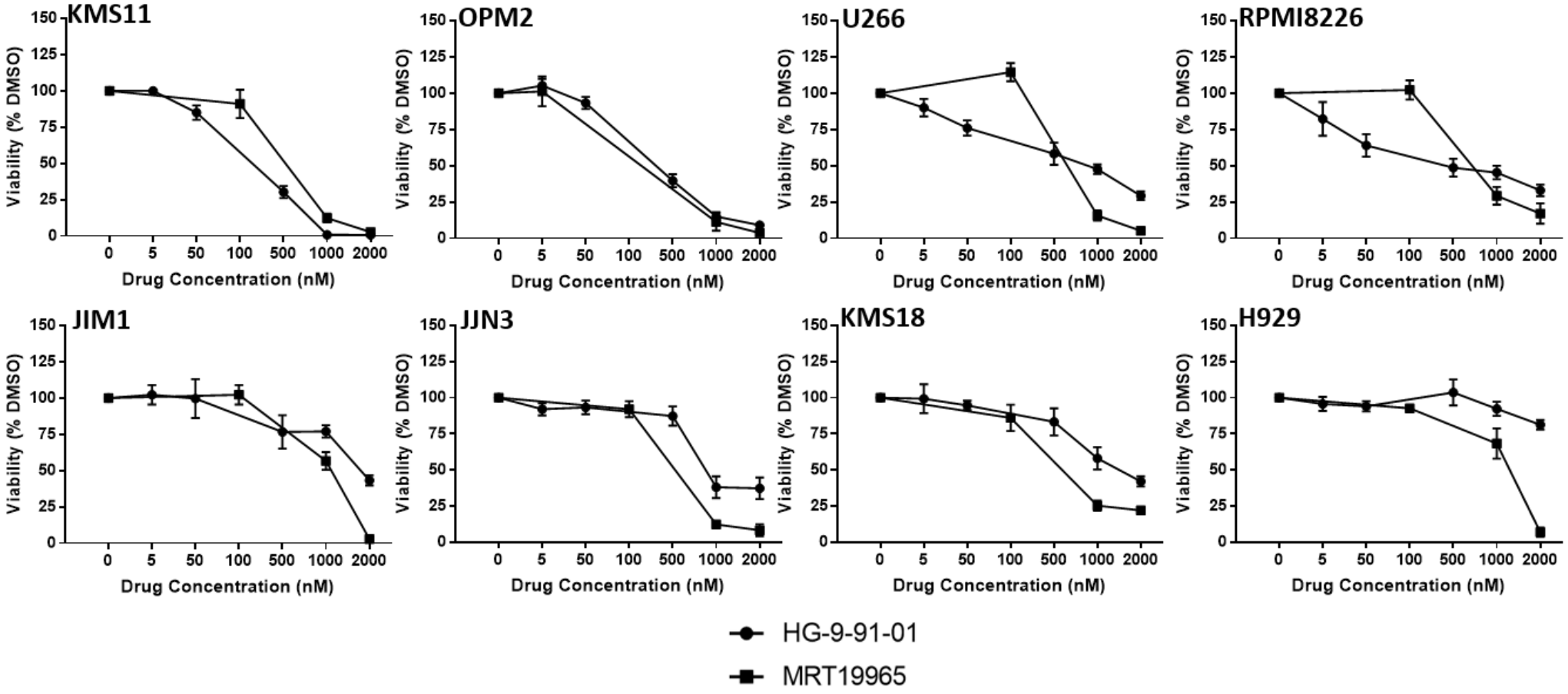

Figure 3.22 The impact of SIK and AMPK inhibition on multiple myeloma viability. Concentration-response curves were generated using increasing concentrations (5-2000nM) of HG-9-91-01 and MRT19965 for 3 days. Cells were stained with antibodies to Annexin V and 7-AAD and analysed using flow cytometry. The percentage of healthy cells was normalised to a DMSO control and expressed as the mean ± SD.

3.4.3 SIK inhibition on MM cell number

To further validate the results seen with annexin V staining, it was necessary to investigate the effect of SIK inhibition on myeloma cell number. Similar results were obtained using MRT19965 and cell number was reduced by over 95% at the highest concentration (2μM), however U226 was slightly less sensitive. HG-9-91-01 also had a similar effect on cell number with KMS11 and OPM2 seeing the largest decrease. JJN3 appeared more sensitive to SIK inhibition when measuring cell number, however U226, RPMI8226, JIM1, KMS18 and H929 had near identical results (Figure 3.23).

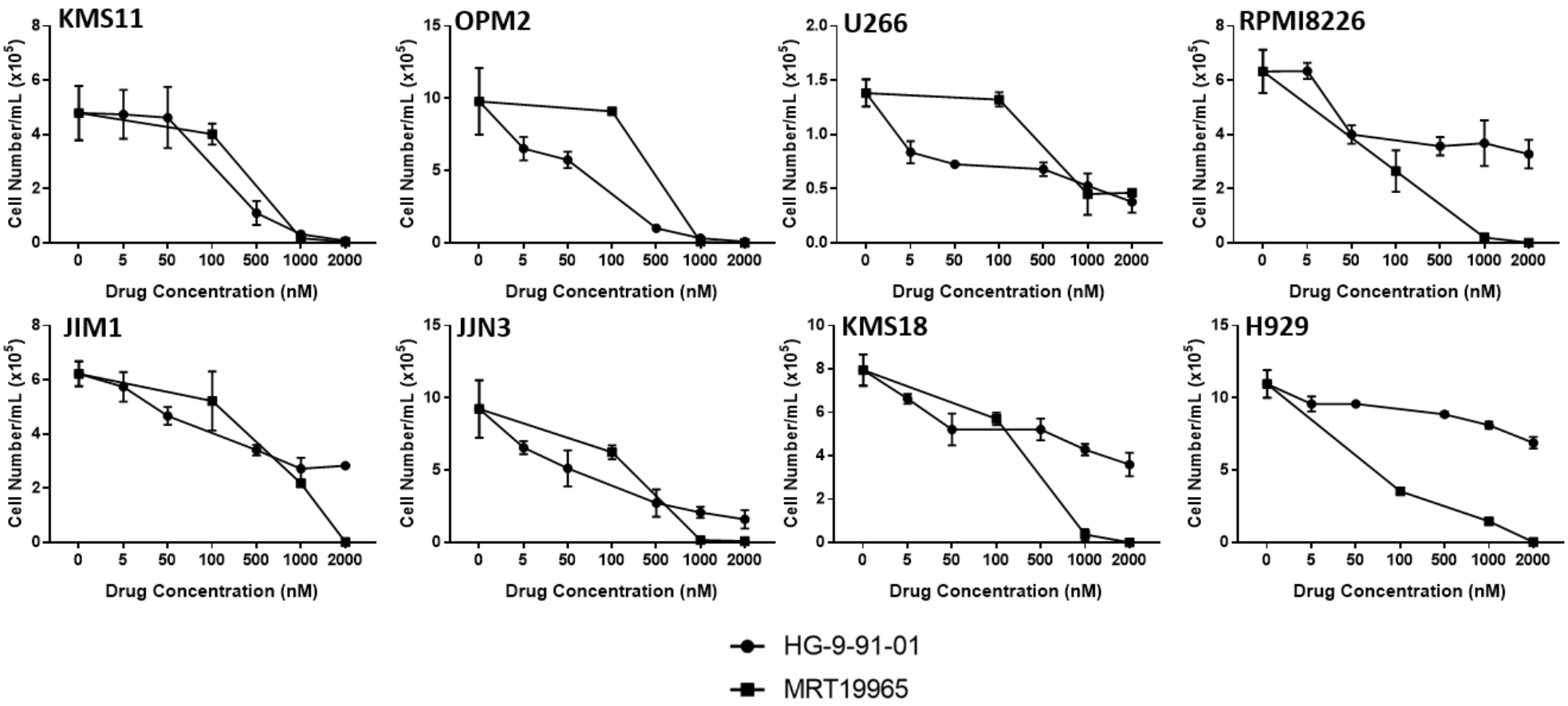

Figure 3.23 The impact of SIK and AMPK inhibition on multiple myeloma cell number. Concentration-response curves were generated using increasing concentrations (5-2000nM) of HG-9-91-01 and MRT19965. On day 3, samples were taken and counted using CountBright Beads™ and normalised to a DMSO control. Results are expressed as the mean ± SD.

3.4.4 Time-course relationship for MM cell lines

To support the time-course data seen in primary cells, a similar experiment was carried out in HG-9-91-01 sensitive and resistant myeloma cell lines. Once again, SIK inhibition had an effect after just 24h in both KMS11 and OPM2, but not H929. In the 3 cell lines, viability decreased in a time-dependent manner, however this was more prominent in KMS11 and OPM2 as would be expected (Figure 3.24).

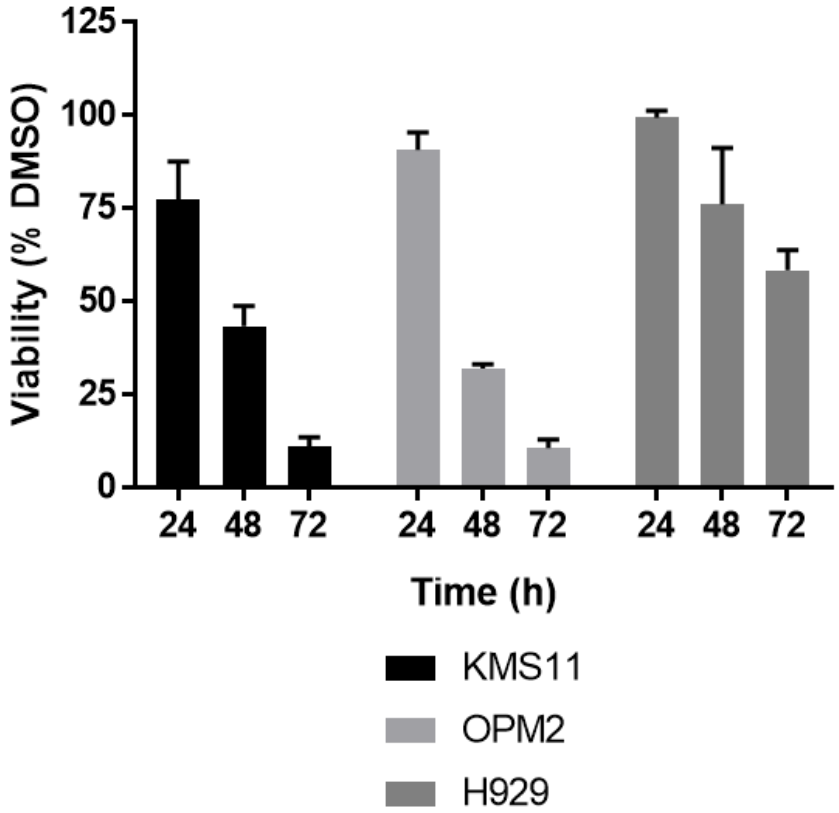

Figure 3.24 The impact of SIK inhibition on myeloma cell number across a time-course. KMS11, OPM2 and H929 were cultured with DMSO or HG-9-91-01 (2µM) for 3 days (72h). At 24h intervals, samples were taken and counted using CountBright Beads™. Results were normalised to a DMSO control and expressed as the mean ± SD.

3.4.5 Therapeutic efficacy in MM cell lines

To further investigate SIKs as a therapeutic target for myeloma, it was of interest to assess the relative sensitivity to bortezomib in the 3 cell lines both sensitive and resistant to HG-9-91-01. Interestingly, the proteasome inhibitor was effective across all 3 cell lines reducing viability by over 99%, whereas SIK inhibition reduced viability by 90% in KMS11 and OPM2, and by just 10% in H929 (Figure 3.25). Although myeloma cell lines originate from different patients and therefore have different underlying genetic abnormalities, they are all vulnerable to proteasome inhibition. This however does not appear to be the case for SIK inhibition and therefore further experiments will try to uncover the underlying mechanism that may account for these differences.

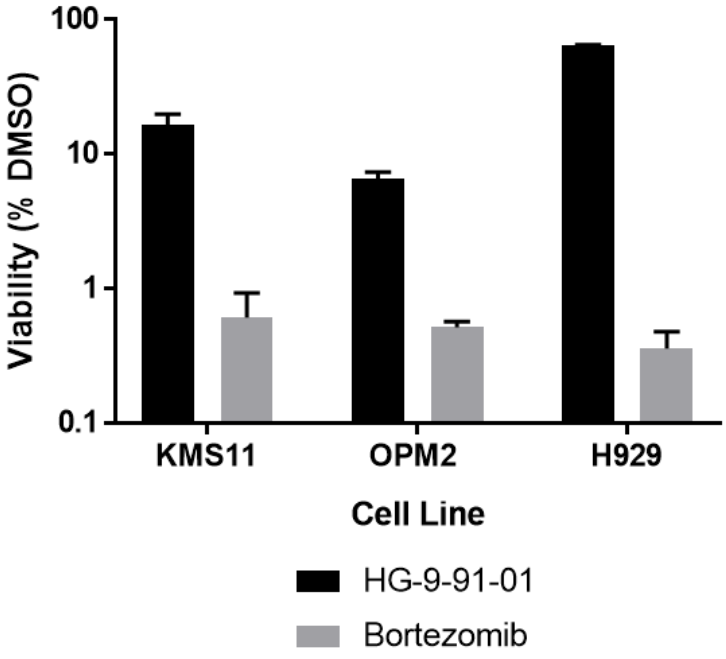

Figure 3.25 Comparing the effects of proteasome inhibition and SIK inhibition on myeloma cell lines. KMS11, OPM2 and H929 were cultured with bortezomib or HG-9-91-01 (2µM). Following a 3 day incubation, samples were taken and counted using CountBright Beads™. Results were normalised to a DMSO control and expressed as the mean ± SD.

3.4.6 Evaluation of SIK family member expression in MM cell lines

To gain further insight into SIK dependency, a Western blot was performed on the multiple myeloma cell lines used in the concentration-response assays. Recent work by Zhou and colleagues showed that endogenous SIK2 protein expression correlated inversely with the IC_{50} value of the SIK inhibitor ARN-3236 indicating that cells with relatively high SIK2 protein expression are more sensitive to treatment with the SIK2 inhibitor (Zhou *et al.*, 2017). This prompted the suggestion that cell lines could have particular expression patterns which may account for the differences seen in sensitivity to SIK inhibition.

Firstly, antibody specificity for SIK1-3 was tested on HeLa cells transfected with SIK vectors (Appendix 3). Immunoblot analysis revealed that each cell line expressed at least one SIK isoform. For example, OPM2 predominantly expressed SIK2 whereas KMS11 predominantly expressed SIK1. Notably, no correlation could be observed between the expression of a specific SIK isoform and sensitivity to SIK inhibition, however the results seemed to suggest that sensitivity may correlate with total SIK expression. For example, sensitive cell lines such as OPM2 and KMS11 expressed high levels of just one isoform, whereas cell lines that were increasingly resistant displayed high levels of at least 2 and in some cases all 3 isoforms (Figure 3.26).

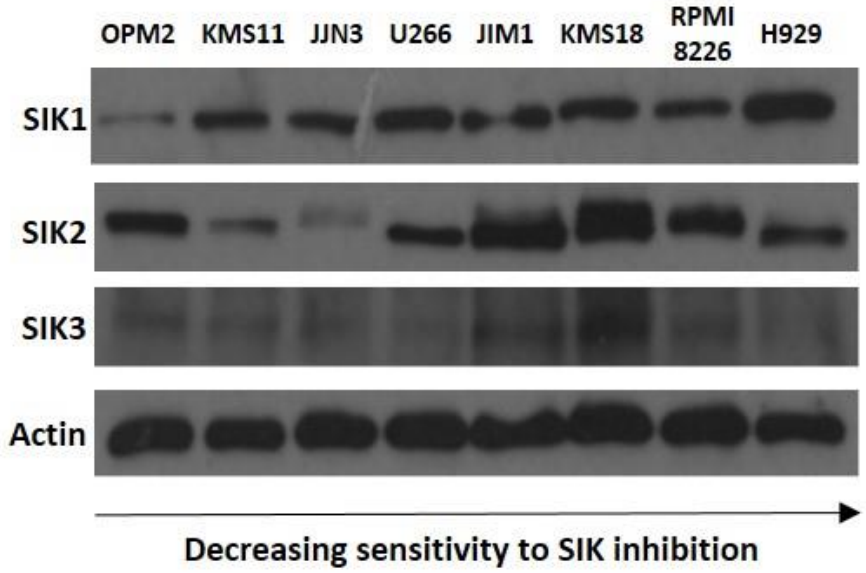

Figure 3.26 SIK expression in multiple myeloma cell lines by immunoblot. Proteins were loaded on a 10% SDS-PAGE gel and transferred to a nitrocellulose membrane. Each membrane was probed with either SIK1, SIK2, or SIK3. β-actin was used as a loading control.

3.4.7 Assessment of SIK1 kinase domain sequence

As SIK protein expression offered little explanation, alternative options were explored to try and understand what may confer sensitivity and resistance to HG-9-91-01. This included sequencing of the SIK1 kinase domain in 7 of the MM cell lines. As depicted in Figure 3.27, the inhibitor binds to a threonine residue (T182) denoted the gate-keeper site which is possessed only by the SIK kinase family. As myeloma cell lines harbour extensive mutation profiles, it was deemed possible that a mutation in the gatekeeper site could explain the variation in sensitivity to SIK inhibition. The threonine residue is encoded by the amino acid sequence 'ACT' and therefore primers were designed to sequence around this.

					*													
MARK1	L	Y	L	V	M	E	Y	A	S	G	G	E	V	F	D	Y	L	V
MARK3	L	Y	L	I	M	E	Y	A	S	G	G	E	V	F	D	Y	L	V
MARK2	L	Y	L	V	M	E	Y	A	S	G	G	E	V	F	D	Y	L	V
MARK4	L	Y	L	V	M	E	Y	A	S	A	G	E	V	F	D	Y	L	V
SIK1	L	Y	I	V	T	E	F	A	K	N	G	E	M	F	D	Y	L	T
SIK2	L	Y	L	V	T	E	Y	A	K	N	G	E	I	F	D	Y	L	A
SIK3	I	Y	L	V	T	E	Y	A	S	G	G	E	I	F	D	H	L	V
NUAK1	I	V	I	I	M	E	Y	A	S	K	G	E	L	Y	D	Y	I	S
NUAK2	I	V	I	V	M	E	Y	A	S	R	G	D	L	Y	D	Y	I	S
BRSK1	L	Y	L	V	L	E	H	V	S	G	G	E	L	F	D	Y	L	V
BRSK2	L	Y	L	V	L	E	H	V	S	G	G	E	L	F	D	Y	L	V
AMPK	I	F	M	V	M	E	Y	V	S	G	G	E	L	F	D	Y	I	C
MELK	I	F	M	V	L	E	Y	C	P	G	G	E	L	F	D	Y	I	I

Figure 3.27 Sequence alignment of AMPK-related kinases. The gatekeeper site is indicated using an asterisk (Adapted from Clark *et al.* 2012).

Following optimisation of the PCR conditions, gel fragments were cut out, purified and sent off for Sanger Sequencing (Source BioScience). Sequencing tracks were then compared against the NCBI *SIK1* sequence (NM_173354.4) using pairwise sequence alignment (EMBOSS Needle). The sequence obtained following *SIK1* kinase domain sequencing (orange highlight) showed no mutations at the gatekeeper site (ACT) across the 7 cell lines tested (Figure 3.28). This suggests that inhibitor binding capability is not accountable for the differences observed regarding sensitivity. Interestingly OPM2 possessed a difference in two residues just before the gatekeeper site meaning the amino acid sequence would change from a valine to a serine.

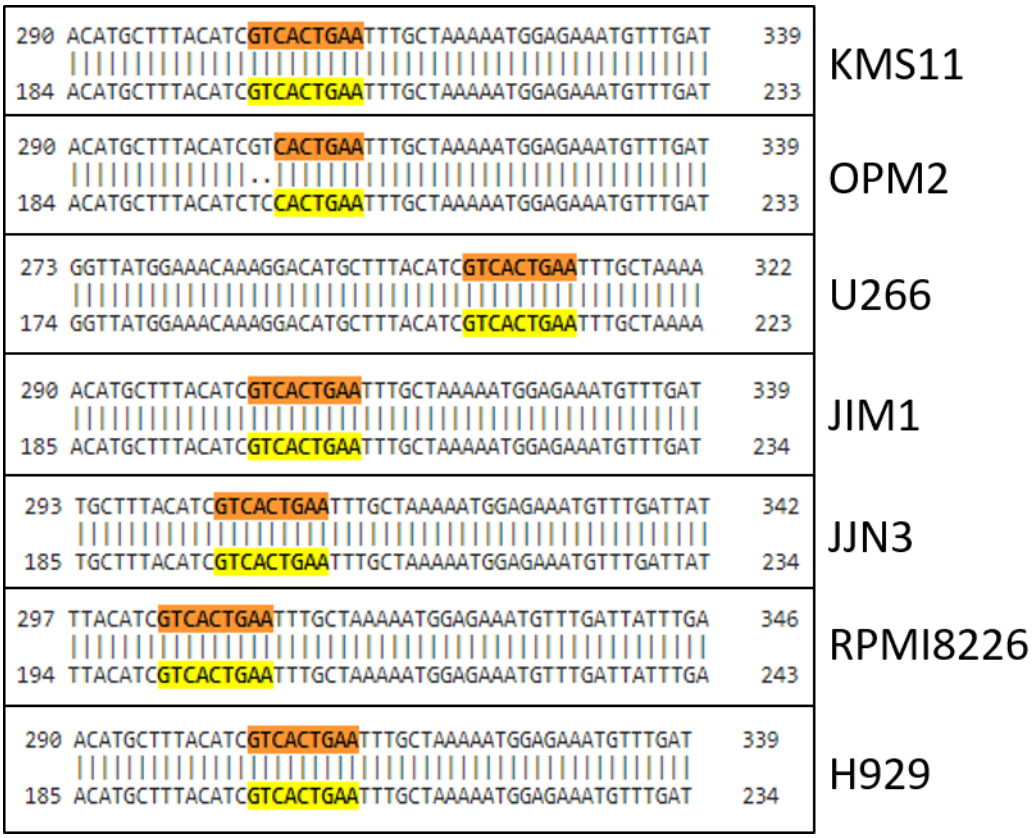

Figure 3.28 Assessing SIK1 gatekeeper site sequence in myeloma cell lines. Sequences obtained following *SIK1* kinase domain sequencing (orange highlight) and the sequence taken from the NCBI website (yellow highlight) were compared using pairwise sequence alignment (EMBOSS Needle).

3.5 SIK inhibition in monocytes

The SIK family has been shown to participate in various roles through use of the inhibitor HG-9-91-01 on cell types including macrophages, dendritic cells, melanocytes and hepatocytes (Clark *et al.*, 2012; Sundberg *et al.*, 2014; Mujahid *et al.*, 2017; Patel *et al.*, 2014). In the majority of these studies, the SIKs act as a molecular 'switch' impacting downstream gene expression, however there have been no previous reports of SIK inhibition causing cell death. Although cell death has not been described as consequence, SIK2/SIK3 knockouts have been shown to cause a growth arrest in AML cell lines (Tarumoto *et al.*, 2018) and depletion of SIK2 decreases entry into cell cycle in ovarian cancer cells (Ahmed *et al.*, 2010),

To confirm that the inhibitor was working as anticipated, it was deemed necessary to add HG-9-91-01 and MRT19965 to various monocytic cell lines and primary cells where SIKs have not been reported to cause cell death. Surprisingly, THP-1 cells responded in a concentration-dependent manner to both SIK and AMPK inhibition. In contrast, U937 and RAW264.7 did not respond to SIK inhibition, however were sensitive to AMPK inhibition (Figure 3.29).

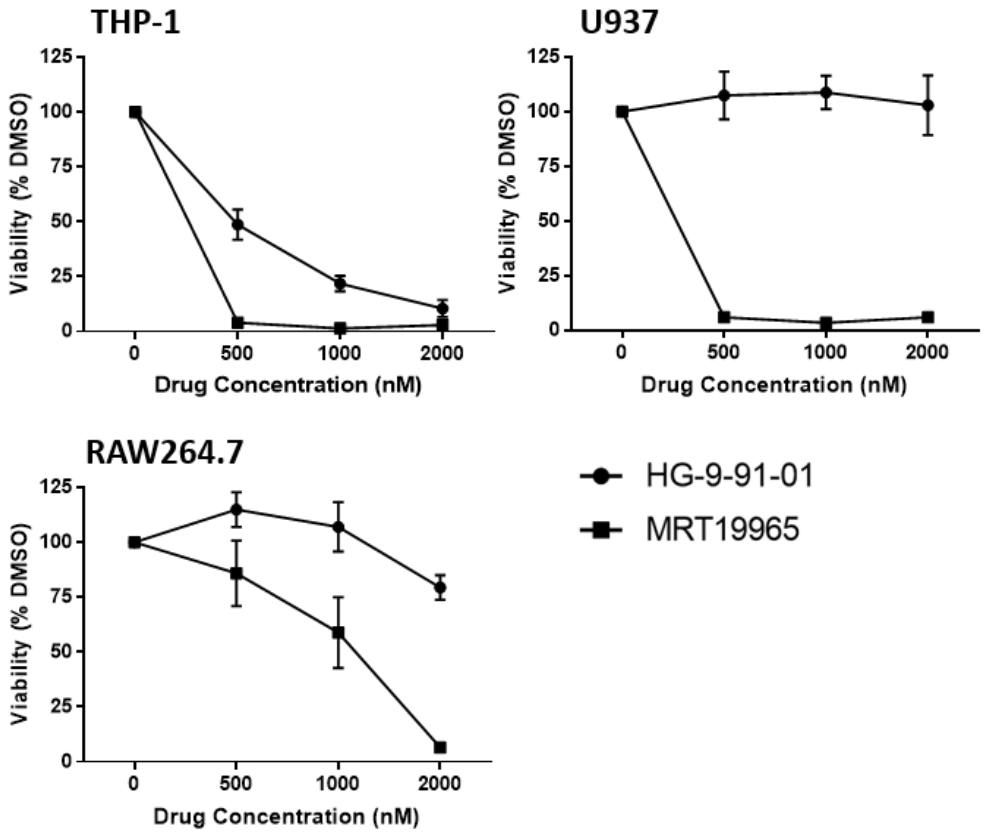

Figure 3.29 Assessing the impact of SIK and AMPK inhibition on monocytic cell line survival. Concentration-response curves were generated using increasing concentrations (500-2000nM) of HG-9-91-01 and MRT19965. On day 3, samples were taken and counted using CountBright Beads™ and normalised to a DMSO control. Results are expressed as the mean ± SD.

In addition to cell line investigation, primary monocytes were isolated from peripheral blood and exposed to HG-9-91-01 or MRT19965 for 3 days. Interestingly, SIK inhibition resulted in an increase in the number of viable cells whereas AMPK inhibition had no effect relative to the DMSO control (Figure 3.30).

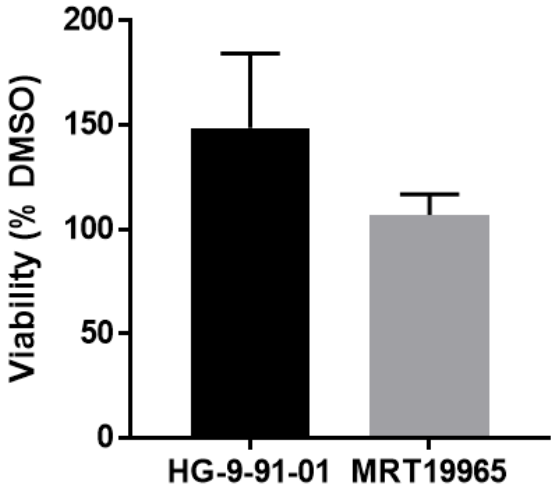

Figure 3.30 The impact of SIK and AMPK inhibition on primary monocyte survival. Monocytes were incubated with DMSO, HG-9-91-01 or MRT19965 (2μM). On day 3, samples were taken and counted using CountBright Beads™ and normalised to a DMSO control. Results are expressed as the mean ± SD for 2 human donors.

3.6 Validation of SIK inhibitor selectivity

Inhibitor screening for HG-9-91-01 across a large selection of different protein kinases highlighted activity against Src, YES1 (Src kinase), ephrin receptor A4 and BTK (Clark *et al.*, 2012). As off-target effects could affect interpretation of the previous data, it was important to use inhibitors against these kinases in the same cell types to determine whether reduction in viability was attributable to the SIK family.

3.6.1 MM cell lines

KMS11, OPM2 and H929 myeloma cell lines were chosen to investigate the effects of dasatinib (Src inhibitor) and ibrutinib (BTK inhibitor) on cell number in comparison to HG-9-91-01. Similar to the effects of HG-9-91-01, KMS11 and OPM2 were relatively sensitive to dasatinib with around 50% reduction in viability whereas H929 displayed only a 25% decrease (Figure 3.31).

Dasatinib has previously been shown to block proliferation, survival, adhesion, migration, and angiogenic potential in myeloma patient samples (Facon *et al.*, 2009; Coluccia *et al.*, 2007) and although developed originally as an inhibitor of the protein tyrosine kinase Bcr-Abl and Src kinase family, has recently been shown to target salt-inducible kinases (Ozanne, Prescott and Clark, 2015). As a result of this, trying to rule out Src kinase family interaction following SIK inhibition in myeloma cell lines is difficult and the only way to overcome this would be through the use of an alternative inhibitor or SIK knockdowns. Interestingly, all 3 cell lines were unaffected following BTK inhibition with ibrutinib and viability remained upwards of 90%, ruling out an off-target effect of BTK.

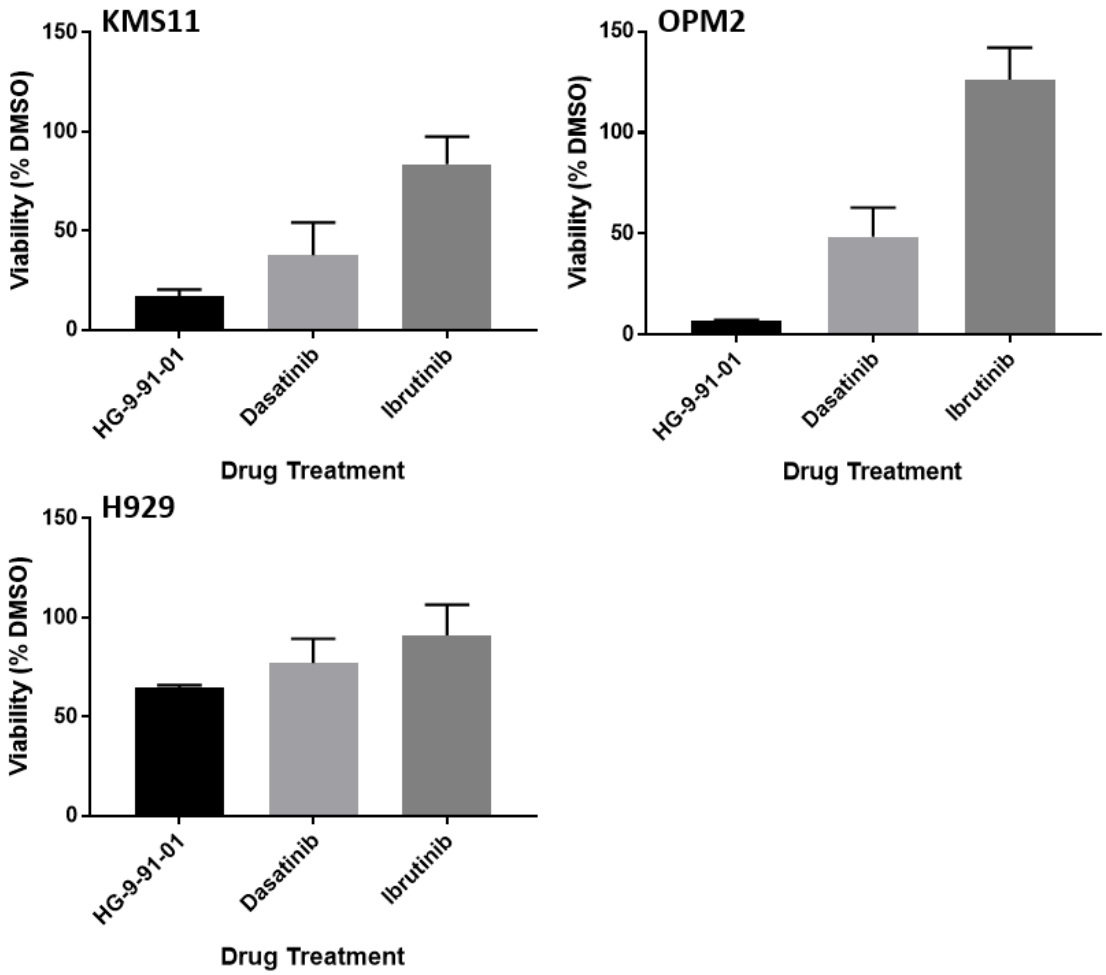

Figure 3.31 Assessing off-target effects of HG-9-91-01 in myeloma cell lines using Src family kinase and BTK small molecule inhibitors. Myeloma cell lines were incubated with DMSO, HG-9-91-01, dasatinib or ibrutinib (2μM) for 3 days. Samples were counted using CountBright Beads™ and normalised to a DMSO control. Results are expressed as the mean ± SD.

3.6.2 Primary Plasmablasts

To explore the role of off-target effects further, primary plasmablasts were exposed to dasatinib and ibrutinib for 3 days. Following SIK inhibition, there was a 85-90% decrease in cell viability, whereas for Src inhibition this was closer to 50% (Figure 3.32A). As seen already in the cell lines, ibrutinib did not have a negative impact and instead caused an increase in cell number relative to the DMSO control. This was surprising as Tai and colleagues demonstrated that PCI-32765, an oral and selective BTK inhibitor, blocked in vivo MM cell growth in the SCID-hu mouse model of myeloma bone disease (Tai *et al.*, 2012; McCune *et al.*, 1988). To further investigate the increase in cell number, cells were phenotyped, however no differences in cardinal marker expression were observed (Figure 3.32B).

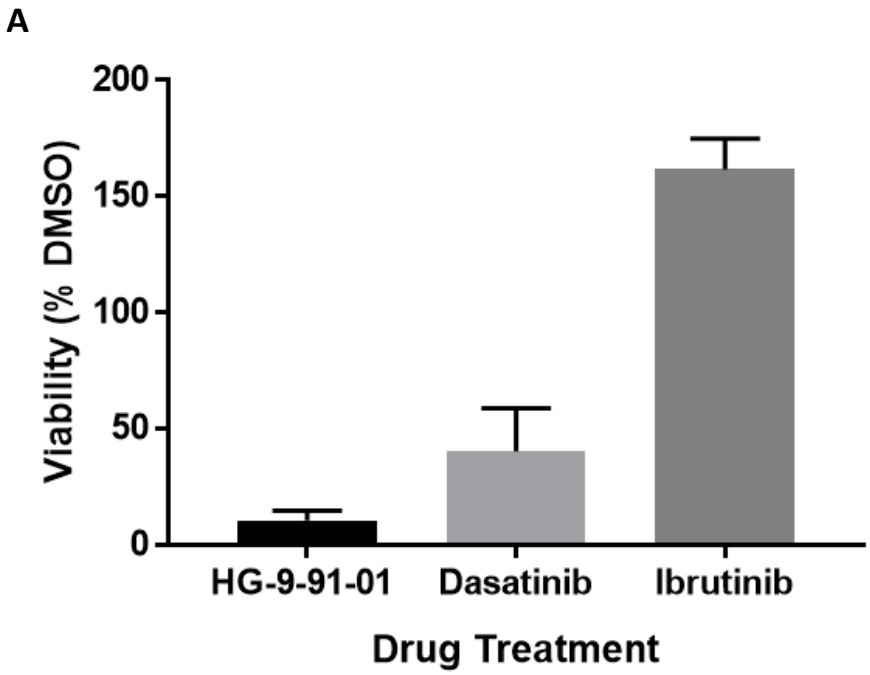

B

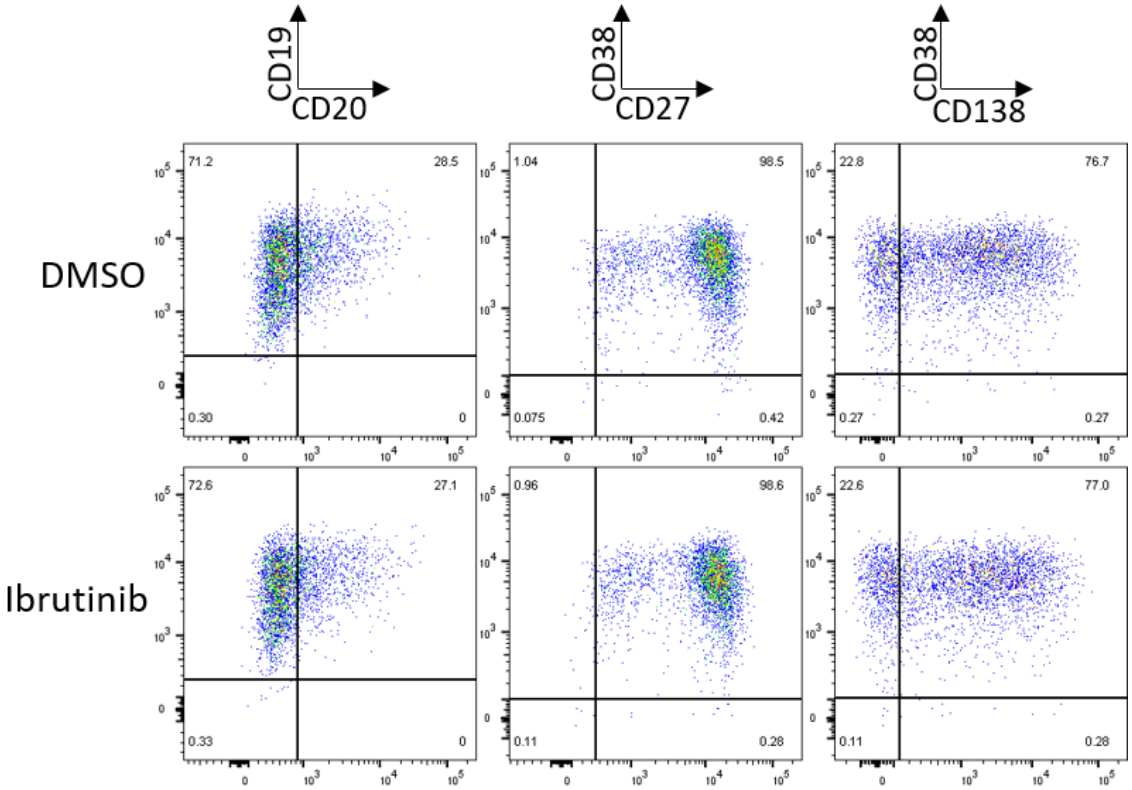

Figure 3.32 Assessing off-target effects of HG-9-91-01 in primary plasmablasts using Src family kinase and BTK small molecule inhibitors. Day 6 plasmablasts were incubated with HG-9-91-01, dasatinib or ibrutinib (2μM) for 3 days in addition to IL-6, IL-21, IFN-α, M210B4s, lipids and amino acids. On day 9, (A) samples were counted using CountBright Beads™ and normalised to a DMSO control. Results are expressed as the mean ± SD for 2 human donors. (B) Samples were stained with antibodies against CD19, CD20, CD27, CD38 and CD138 and analysed using flow cytometry.

3.6.3 HG-9-91-01 resistant vectors

An alternative approach to highlight that the observed effects of a compound are attributable to 'on-target' activity, is to show that the inhibitor action disappears when a drug-resistant mutant kinase is expressed in place of the wild-type (Cohen, 2010). Mutation of the gatekeeper threonine to an alternative amino acid such as glutamine has been shown to make SIKs 1000-fold less sensitive to HG-9-91-01 (Clark *et al.*, 2012). As SIK1 is thought to be the dominant isoform in the B-cell lineage, both wild-type (pIRES2-EGFP SIK1) and HG-9-91-01-resistant mutants of SIK1 (T103M and T103Q) were transfected into HeLa cells and then treated with DMSO, HG-9-91-01 or MRT19965.

Initially results appeared promising as there was no decrease in viability in cells transfected with SIK1 T103M or SIK1 T103Q and treated with HG-9-91-01. However, when analysing the wild-type kinase results, there was also very minimal reduction in cell viability which is not what was expected. This suggests that either the pIRES2-EGFP vector or SIK1 overexpression alters sensitivity to SIK inhibition or HeLa cells were not sensitive to SIK inhibition (Figure 3.33).

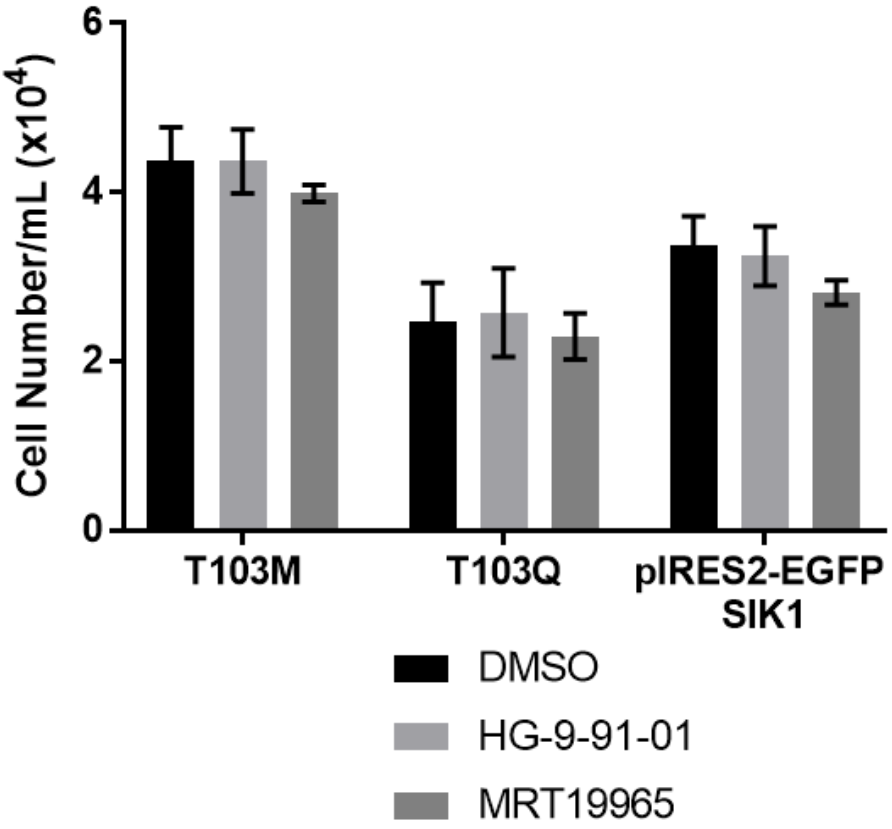

Figure 3.33 SIK1 drug-resistant mutants in HeLa cells. pIRES2-EGFP SIK1 wild-type or pIRES2-EGFP drug-resistant mutants were transfected into HeLa cells using GeneJuice®. After 24h, cells were treated with DMSO, HG-9-91-01 or MRT19965 (2µM). Following a 3 day incubation, cells were counted using CountBright Beads™. Results are expressed as the mean ± SD.

Given the previous result, a concentration-response experiment was carried out on HeLa cells to determine whether HG-9-91-01 worked in a similar manner to both primary differentiating B-cells and myeloma cell lines. Surprisingly, HeLa cells were less responsive to HG-9-91-01 and a high concentration of 4μM was only able to reduce viability by 40%. This demonstrates that HeLa are not suitable for this experiment and therefore it should be repeated in an alternative cell type, more sensitive to HG-9-91-01 (Figure 3.34).

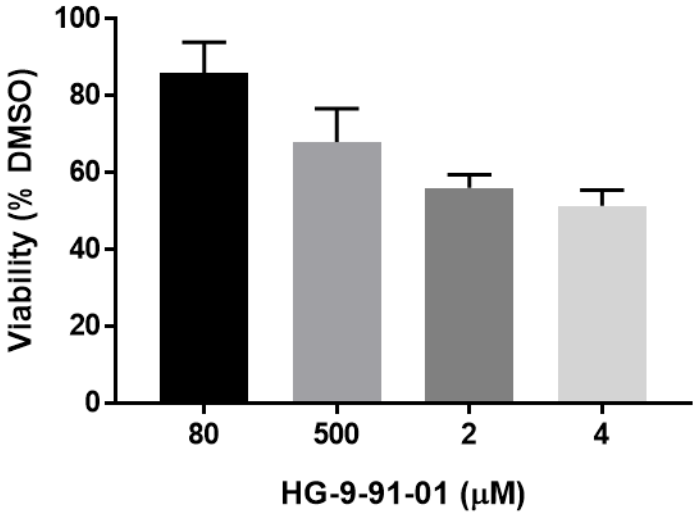

Figure 3.34 The impact of SIK inhibition on HeLa cell survival. HeLa cells were seeded at $3x10^5$ cells/mL and incubated with increasing concentrations of HG-9-91-01. Following a 3 day incubation, cells were counted using CountBright Beads™ and normalised to a DMSO control. Results are expressed as the mean ± SD.

3.6.4 YKL-05-099 on MM cell lines

Originally, a lack of small-molecule SIK inhibitors meant that off-target effects had to be accepted, however over the past few years various attempts have been made to try and improve these compounds. Sundberg and colleagues used HG-9-91-01 as a starting point to develop improved analogues, yielding a novel probe 5 (YKL-05-099) which displays increased selectivity for SIKs versus other kinases and enhanced pharmacokinetic properties allowing for the study of SIK function in vivo (Sundberg *et al.*, 2014).

To determine whether YKL-05-099 behaved in a manner comparable to HG-9-91-01, a concentration-response experiment was carried out on cell lines both sensitive (KMS11 and OPM2) and resistant (H929) to HG-9-91-01. As seen in Figure 3.35, YKL-05-099 acted in a concentration-dependent manner across all 3 cell lines. Furthermore, the results confirmed what had been seen in previous experiments with KMS11 and OPM2 being sensitive and H929 being resistant to SIK inhibition. Interestingly, the reduction in viability for KMS11 and OPM2 observed with YKL-05-099 was slightly less than with HG-9-91-01 which may be attributable to the improved kinase selectivity of YKL-05-099.

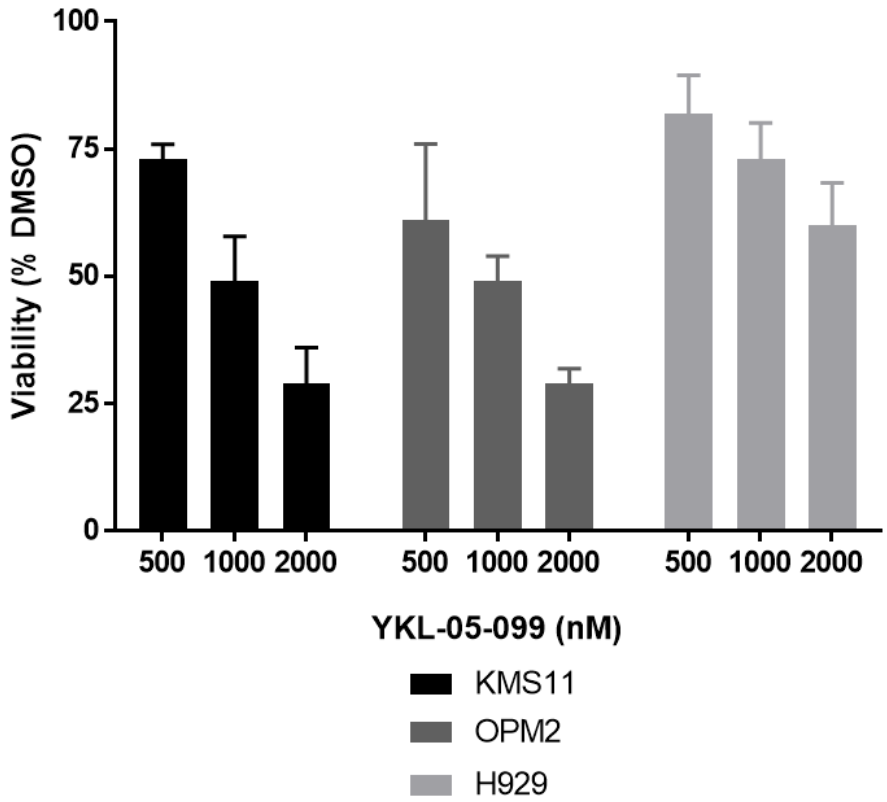

Figure 3.35 Assessing the impact of SIK inhibition (YKL-05-099) on myeloma cell line survival. Increasing concentrations of YKL-05-099 were added to KMS11, OPM2 and H929. Following a 3 day incubation, cells were counted using CountBright Beads™ and normalised to a DMSO control. Results are expressed as the mean ± SD.

3.7 *SIK* expression in MM patient samples

Although cell lines are a useful tool to study biological processes, results do not always accurately replicate primary cells due to reasons such as genetic drift and manipulation which can affect phenotype and responsiveness to stimuli (Kaur and Dufour, 2012). In order to strengthen the findings, primary cells from MGUS and multiple myeloma patients with varying percentages of neoplastic cells were obtained and *SIK* family kinase expression was examined using a TaqMan assay. Variation occurred between samples (Figure 3.36A), however compared to the healthy control, patient samples had high levels of *SIK1*, intermediate levels of *SIK2* and low levels of *SIK3* (Figure 3.36B).

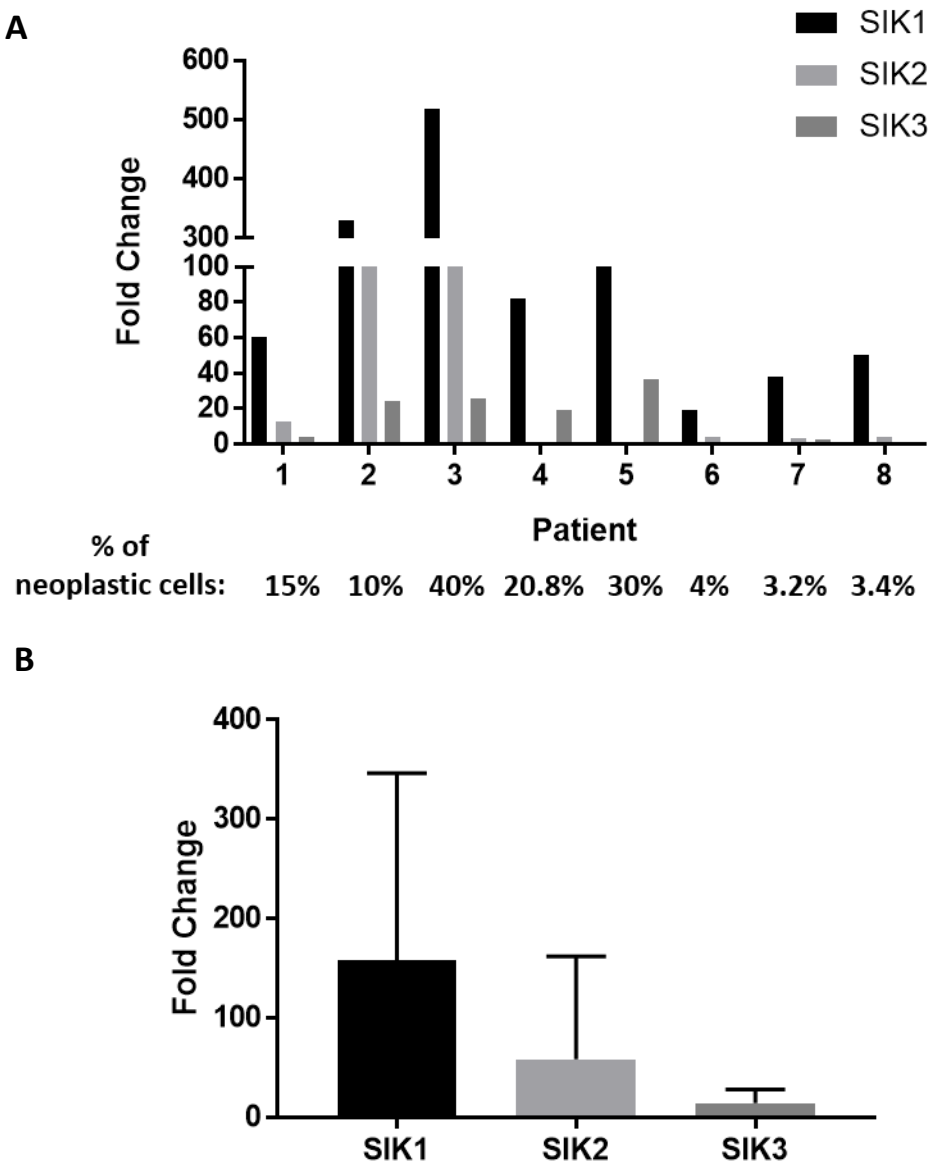

Figure 3.36 Evaluating SIK expression in MGUS and multiple myeloma primary samples using qPCR. (A) The expression of SIK1, SIK2 and SIK3 was evaluated in patient samples using a TaqMan assay. ΔCT values were calculated for each probe and then normalised using a 'healthy' sample. (B) Average SIK1, SIK2 and SIK3 ΔCT values are expressed as the mean ± SD for 8 biological replicates.

3.8 PKA-mediated signalling

Although SIK activity is primarily mediated by LKB1 T-loop phosphorylation, signals that increase intracellular cAMP levels have also been shown to enhance PKA-mediated SIK family member phosphorylation (Screaton *et al.*, 2004) which can further control cellular function. For example, SIK2 is regulated by the cAMP–PKA pathway through phosphorylation of Ser358, resulting in the binding of SIK2 to 14-3-3 proteins and a subsequent relocalisation to the cytosol with no effect on intrinsic kinase activity (Henriksson *et al.*, 2012). In myocytes, removal of cAMP priming stimuli led to the dephosphorylation of SIK1 (S577) and (T475) causing SIK1 translocation to the nucleus where it was degraded by the proteasome (Stewart *et al.*, 2013b). This demonstrates how cAMP-PKA signalling can regulate the ability of SIKs to phosphorylate their substrates.

In line with the work carried out Patel and colleagues in which the cell-permeable cAMP analogue Bt_2-cAMP was shown to have a similar effect to SIK inhibition on hepatocytes (Patel *et al.*, 2014), day 6 plasmablasts were incubated with Bt_2-cAMP. It seemed possible that similar to SIK inhibition in primary cells, a decrease in cell number would occur. After a 3 day incubation, it was evident in both donors that Bt_2-cAMP had no effect on cell number (Figure 3.37). The lack of a defined control readout of cAMP activity makes it difficult to determine whether the Bt_2-cAMP successfully stimulated cAMP-PKA signalling, however the results suggest that cAMP does not regulate SIK activity in plasmablasts.

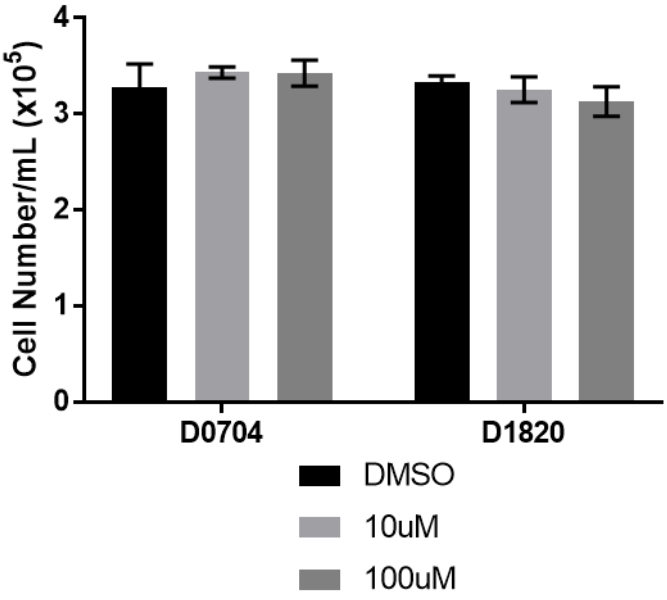

Figure 3.37 Assessing the impact of cAMP signalling on plasmablast cell number. Day 6 plasmablasts were cultured with Bt_2-cAMP (10µM/100µM) in addition to IL-6, IL-21, IFN-α, M210B4s, lipids and amino acids for 3 days. After 72h, samples were taken and counted using CountBright Beads™.

3.9 Further assessment of SIK function

Use of the SIK inhibitors, HG-9-91-01 and YKL-05-099 have so far demonstrated the importance of SIK kinase activity in cells undergoing terminal differentiation. Although meaningful, it is possible that alternative targets of HG-9-91-01 already described could be contributing to the decreased viability observed in both primary cells and myeloma cell lines. As RNA-sequencing and WGCNA identified *SIK1* as the most relevant SIK isoform, both gain-of-function and loss-of-function experiments were necessary to enhance the previous results. To this end, numerous transfection optimisation experiments were carried out for the delivery of both SIK1 vectors and siRNA into myeloma cell lines and primary B-cells.

To ensure that the vectors expressing wild-type or mutant human SIK1 (K56M, T182D, S575A, T103M, T103Q) could be expressed sufficiently and to check recognition by known antibodies, each construct was transfected into HeLa cells and confirmed by Western blot (Appendix 4).

3.9.1 SIK1 knockdown in myeloma cell lines

3.9.1.1 SIK1 knockdown in U266

Combinations of SIK1 siRNA were introduced into U266 using electroporation-based nucleofection (Amaxa®). U266 was used in the first instance as it expressed moderate levels of SIK1, was susceptible to HG-9-91-01 and optimised conditions for transfection were available online.

As seen in Figure 3.38A, transfection efficiency was relatively high at around 68% confirming that the reagent (Kit V) and electroporation program (X-005) were suitable for the application. Although promising, immunoblot analysis revealed that SIK1 band size did not appear to decrease in relation to the negative control showing that protein expression was unaffected by the siRNA.

A

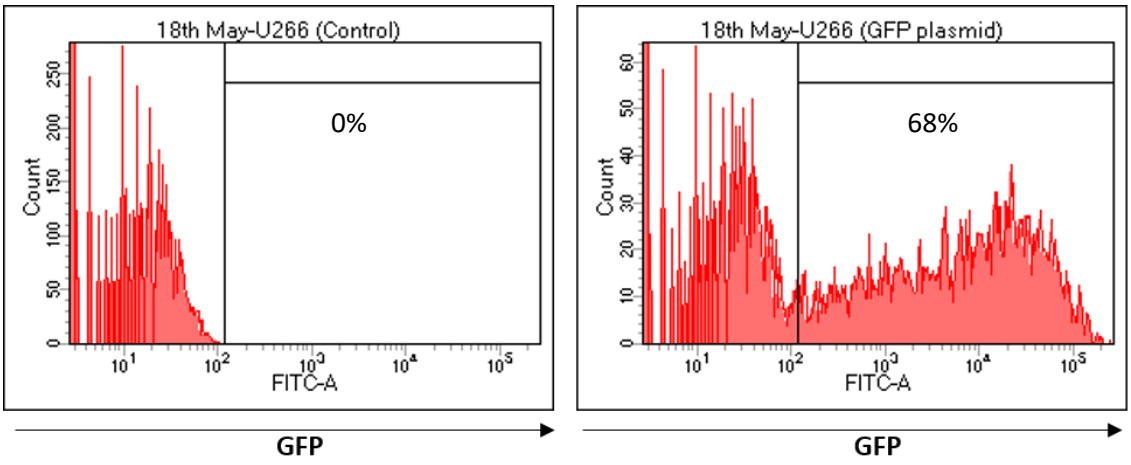

B

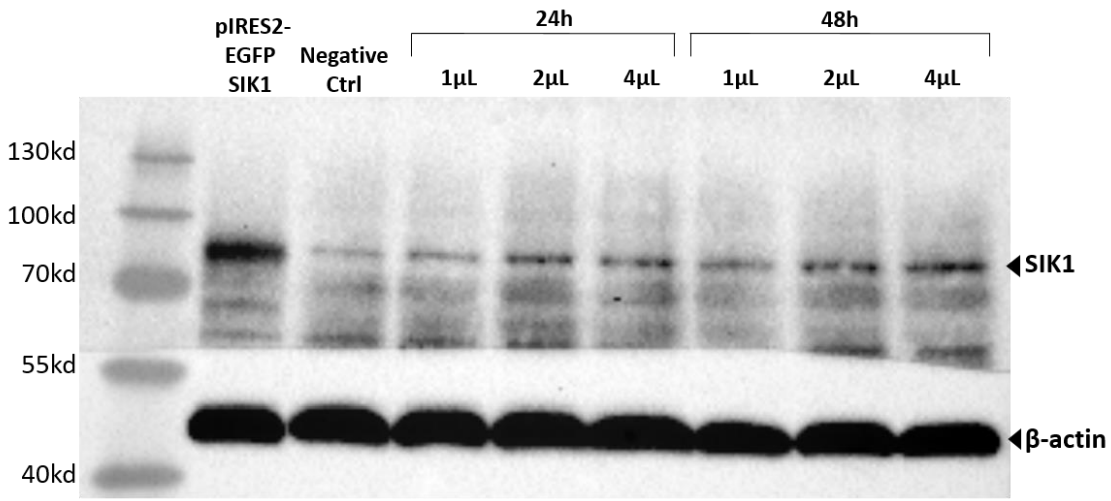

Figure 3.38 Electroporation of U266 with pmaxGFP and SIK1 siRNA. (A) Histogram showing GFP expression in U266 to calculate percentage uptake of the plasmid. (B) Immunoblot showing lysates generated from samples transfected with pIRES2-EGFP-SIK1 (positive control), negative control or increasing amounts of SIK1 siRNA. Time points indicated time in which lysate was taken following nucleofection.

3.9.2 Optimising electroporation conditions in KMS11

Following the inability to knockdown SIK1 in U266, an alternative myeloma cell line was chosen to test (KMS11). As there was no manufacturers protocol available, an optimisation kit was acquired in order to determine which solutions and programs were best for both viability and transfection efficiency.

Following transfection, viability was between 5-50% for the majority of the programs. The 3 best programs were Z-001 (V), X-001 (V) and W-001 (V) with viability reaching around 60%. Interestingly, solution V promoted higher viability than solution L (Figure 3.39). When considering transfection efficiency, most of the programs resulted in low GFP expression of around 1-15%. The programs with the highest efficiencies were W-001 (V), Y-001 (V) and Z-001 (V) reaching up to 20%.

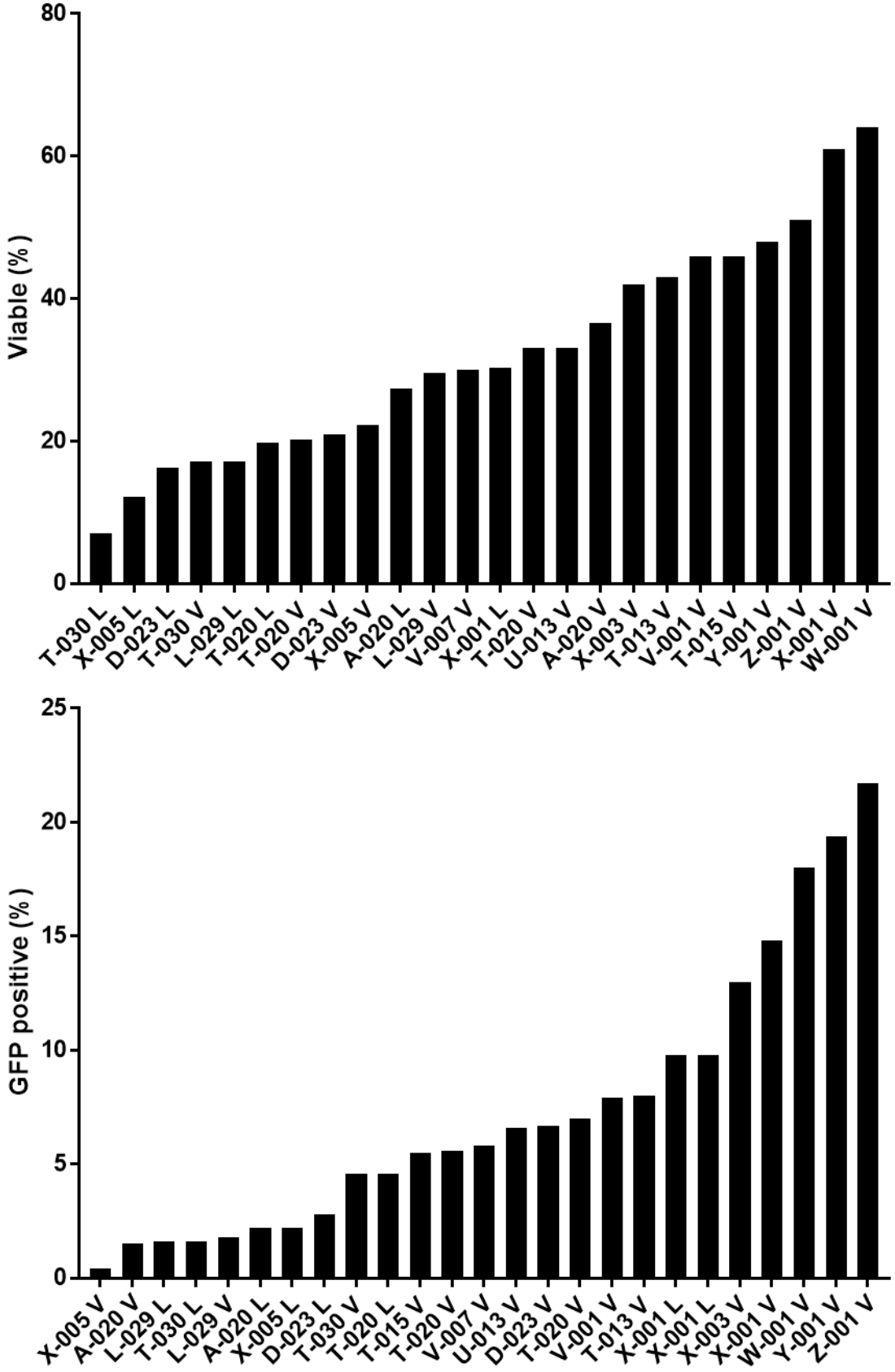

Figure 3.39 Optimising nucleofection™ of pmax-GFP in KMS11. Cells were re-suspended in reagent V or reagent L and then nucleofected with pmax-GFP using the indicated programs (Amaxa Nucleofector™). 24h post-nucleofection, viability and GFP expression was recorded using flow cytometry.

3.9.3 TransIT® optimisation on MM cell lines

As transfection efficiency using nucleofection was quite low, polymeric transfection reagents were acquired from Mirus® including TransIT-Jurkat, TransIT-X2 and TransIT-2020. To determine whether any of these reagents would be suitable for transfecting myeloma cell lines with SIK1 siRNA or SIK1 vectors, transfection efficiency was recorded 24h, 48h and 72h post-transfection with pmaxGFP in KMS11, OPM2, U266 and H929.

In KMS11, TransIT-X2 resulted in the highest efficiency (30%) 72h post-transfection whereas in OPM2, TransIT-Jurkat and TransIT-X2 had similar efficiencies (25-30%). In U266, TransIT-Jurkat performed the best, however overall efficiency was low (5%) and H929 was even lower with a maximum efficiency of 1%. Overall, transfection efficiency was generally better between 48-72h post-transfection. This suggests that TransIT-X2 could be used to transfect KMS11 and OPM2 with SIK1 siRNA, but not U266 or H929 (Figure 3.40).

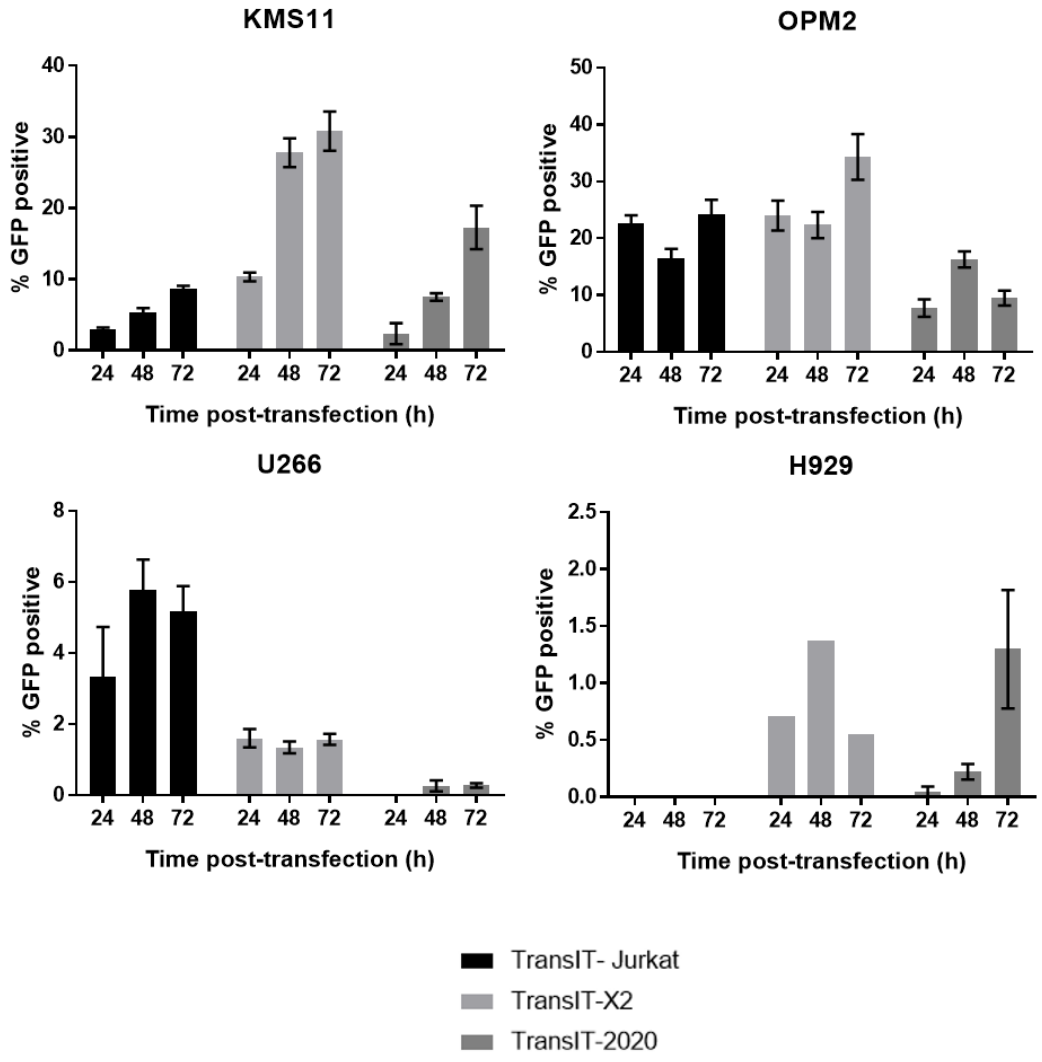

Figure 3.40 Assessing TransIT® transfection reagents on myeloma cell lines. pmax-GFP was transfected into KMS11. OPM2, U266 and H929 using TransIT-Jurkat, TransIT-X2 or TransIT-2020. GFP expression was analysed using flow cytometry at the indicated time points.

3.9.4 Further optimisation of TransIT®-X2

To try and further improve transfection efficiency in KMS11 and OPM2, the conditions from the previous experiment were altered slightly to include an extra wash after the cells had been exposed to the reagent for 24h, a spin following addition of the reagent (20 minutes x 340 x g) and twice the amount of reagent. Overall, GFP expression increased over the 72h period across the majority of conditions. In OPM2, the extra wash appeared to increase GFP expression by around 7% at 72h post-transfection, whereas in KMS11 differences were negligible. Due to time constraints, it was decided that further transfections would predominantly focus on primary cells.

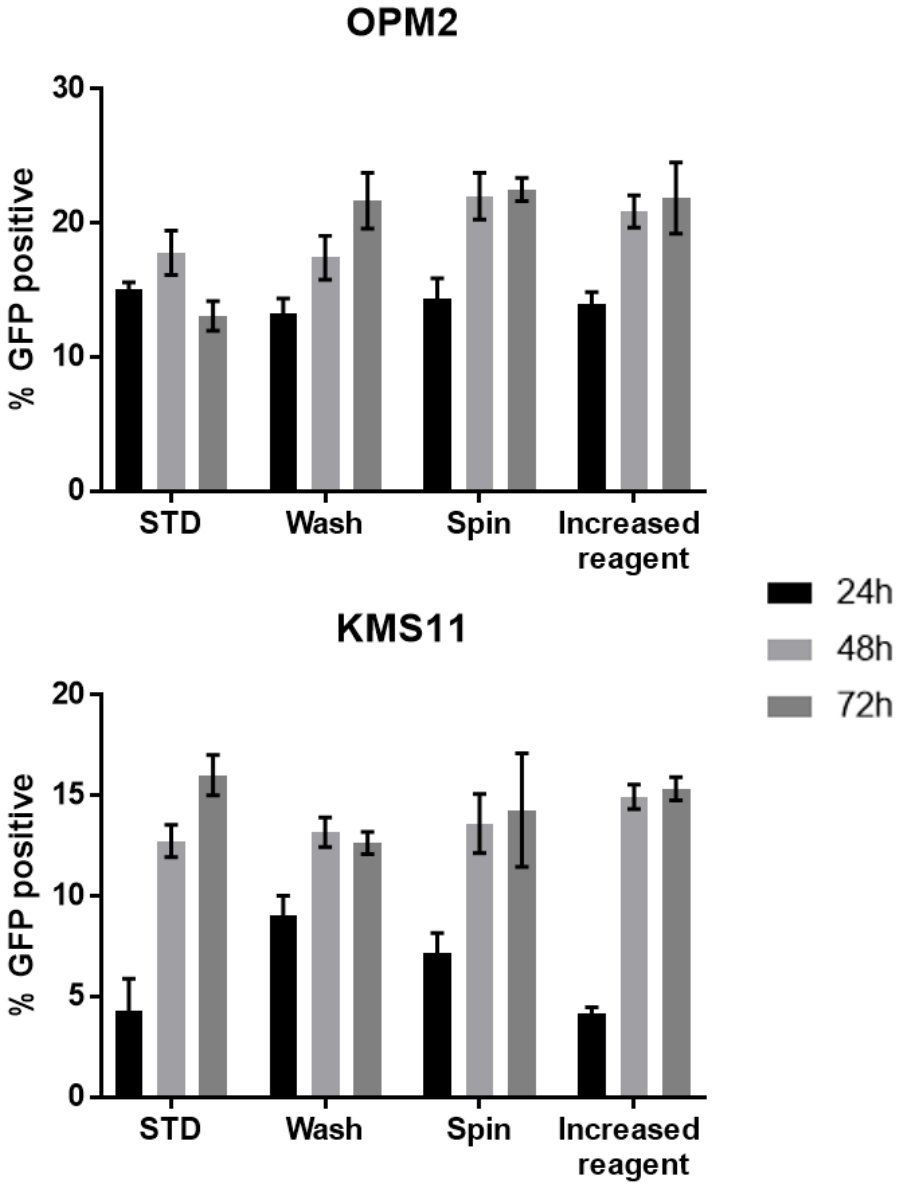

Figure 3.41 Optimising transfection of pmax-GFP in OPM2 and KMS11. Using TransIT-X2, cells were transfected with pmax-GFP using various conditions (wash, spin, increased reagent) and compared against the standard protocol. GFP expression was recorded using flow cytometry.

3.9.5 Primary cells

Historically, primary lymphocytes have been difficult to manipulate as transient gene delivery systems such as electroporation and lipofection can be detrimental to cell survival. Following the development of Nucleofector® technology, 50-70% transfection efficiency in freshly isolated B-cells has been demonstrated without compromising viability (Seiffert *et al.*, 2007). To assess the transfection efficiency of primary differentiating B-cells within the in vitro system, the Ingenio® electroporation kit (Mirus) was obtained which is described as highly efficient in hard-to-transfect cells. Furthermore, it can be used in combination with the Amaxa® Nucleofector® instrument.

Activated B-cells were transfected with a small vector (pmaxGFP) as this would indicate if it was possible to transfect with siRNA. It was also important to determine whether large SIK1 vectors (pIRES2-EGFP SIK1) could be introduced to examine different aspects of SIK regulation. 48h post-transfection, there was relatively high GFP expression (25%) in cells transfected with the small vector and this was still detectable at 120h. Alternatively, transfection efficiency with the large vector was poor and GFP expression was less than 2%. Furthermore, after 120h there was no detectable GFP expression (Figure 3.42). This suggests that knockdowns would be appropriate using these parameters, however further optimisation would be required to enable transfection of the various SIK1 vectors.

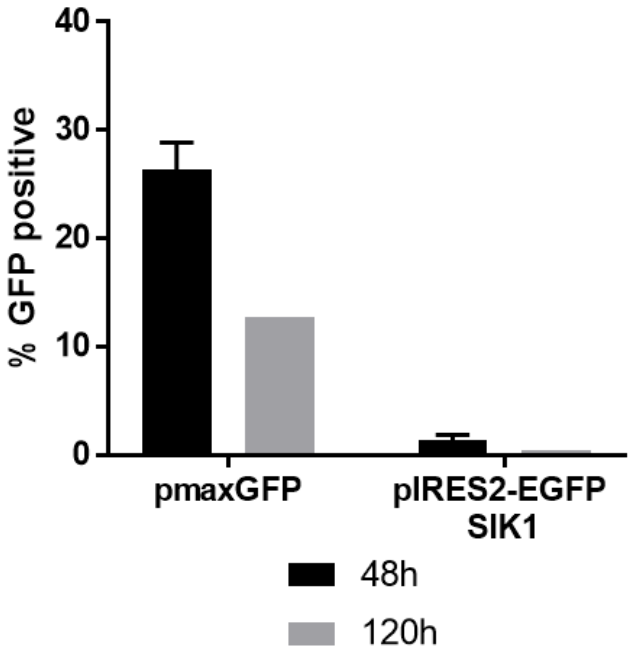

Figure 3.42 Testing Nucleofection™ on day 1 primary cells using Mirus Ingenio®. 6x10^6 cells per condition were transfected with pmaxGFP (2µg) or pIRES2-EGFP SIK1 (10µg). 48h and 120h post-nucleofection™, GFP positive cells were identified using flow cytometry.

As B-cells undergo increasing rounds of cell division following activation, the next step was to compare efficiency following transfection on day 1, day 2 and a double transfection on both day 1 and 2. Cells transfected on day 1 were 30% positive for GFP expression which increased in cells transfected on day 2 to 47.5%. Furthermore, cells transfected on day 1 and day 2 demonstrated 66% GFP expression on day 6 (Figure 3.43). This is useful because it shows that both the method of transfection is suitable for primary B-cells and that the vector is still detectable 96h post-transfection.

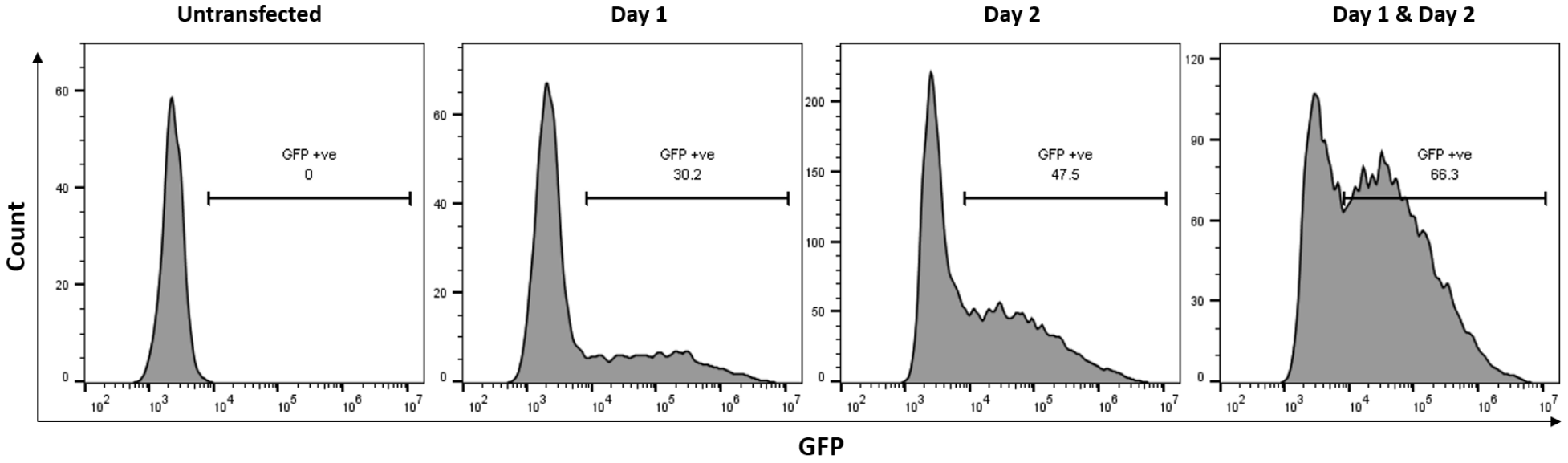

Figure 3.43 Optimising pmaxGFP uptake in differentiating human B-cells using Mirus Ingenio®. Freshly isolated B-cells from human donors were cultured with CD40-L, R848, IL-2 and IL-21. Cells were transfected at the indicated time points with pmaxGFP (2µg). On day 6, cells were stained with 7-AAD and GFP expression was assessed using flow cytometry.

As further evidence, co-staining of CD38 (a plasmablast marker) and GFP showed that $CD38^+$ cells transfected on day 2 were 64.4% GFP positive on day 6 and this increased to 80% when cells were transfected on both day 1 and 2 (Figure 3.44). Overall, this provides a promising method for the knockdown of SIK1 in primary differentiating B-cells.

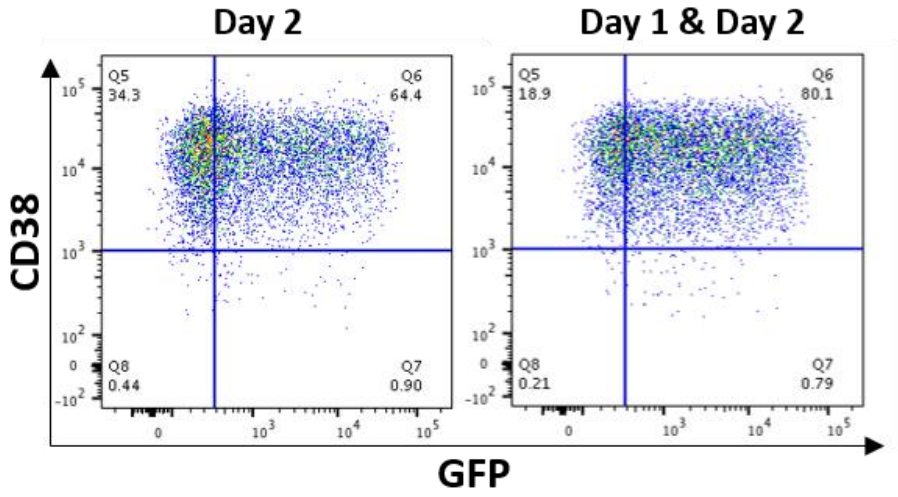

Figure 3.44 Assessing co-expression of CD38 and GFP. Freshly isolated B-cells from human donors were cultured with CD40-L, R848, IL-2 and IL-21. Cells were transfected at the indicated time points with pmaxGFP (2µg). On day 6, cells were stained with an antibody against CD38. GFP expression was assessed using flow cytometry.

3.10 Discussion

The work presented in this chapter originated from the identification of *SIK1* as a hub gene during the transition of a plasmablast to a plasma cell. Although this suggested SIK1 was likely to be the dominant isoform, consideration was also given to SIK2 and SIK3 as various work into SIK signalling has demonstrated redundancy between isoforms (Abend *et al.*, 2017; Darling *et al.*, 2017; Sall *et al.*, 2017).

Initial analysis of *SIK* transcripts and protein during B-cell differentiation revealed that cells expressed similar levels of each isoform during early time-points, however preferential expression of *SIK1* was evident as cells approached terminal differentiation. This is consistent with an increase in SIK protein expression seen following the differentiation of peripheral blood monocytes into macrophages or dendritic cells (Lombardi et al., 2016). Whilst these results provide further indication of a role for SIKs, discrepancies were apparent between mRNA and protein expression limiting the overall conclusion about isoform involvement. To overcome this, an in vitro kinase assay should be performed to determine SIK enzymatic activity as seen in work by Darling and colleagues (Darling et al., 2016). In combination with the expression data, this would hopefully confirm isoform contribution to overall activity across the differentiating cells.

Experiments using small-molecule SIK inhibitors such as HG-9-91-01, KIN112 and ARN-3236 have so far played a fundamental role in revealing SIK function in cell types such as macrophages, adipocytes and hepatocytes (MacKenzie *et al.*, 2013b; Henriksson *et al.*, 2015; Patel *et al.*, 2014), however this is the first study to characterize the effect in both primary differentiating B-cells and myeloma cell lines. Freshly isolated B-cells were unresponsive to SIK inhibition, correlating with the lack of SIK1, 2 or 3 protein expression at day 0. In contrast, activation with either BCR or TLR stimuli caused cells to become highly sensitive and this was apparent for activated B-cells, plasmablasts and plasma cells. Consequently, this data strongly suggests that cells depend on SIK kinase activity, however as HG-9-91-01 and YKL-05-099 inhibit SIK1, SIK2 and SIK3, it is not possible to conclude any isoform-specific effects.

Unexpectedly, inhibiting SIKs in cells which represent different stages of differentiation such as activated B-cells, plasmablasts and plasma cells highlighted potential differences in SIK regulation. For example, activated B-cells did not proliferate in line with control cells suggesting that SIKs may regulate growth and proliferation during early differentiation. Activated B-cells also undergo class switch recombination in the germinal centre reaction and during this process double strand breaks occur (Stavnezer, Guikema and Schrader, 2008). Sherman and colleagues demonstrated that

exogenous and intrinsic AID-induced DNA strand breaks activate ATM, which signals through an LKB1 intermediate to inactivate CRTC2. Furthermore, CRTC2 inactivation represses a genetic program controlling GC B cell proliferation, self-renewal, and differentiation (Sherman *et al.*, 2010). This highlights how DNA damage response signalling can promote B cell differentiation in response to genotoxic stress and gives rise to the idea that SIKs may also regulate CSR through CRTC2.

SIK inhibition in activated B-cells caused an increase in the percentage of $CD27^+$ $CD38^+$ cells indicative of accelerated differentiation. In contrast, plasmablasts displayed an increase in the percentage of cells expressing $CD19^+CD20^+$ which is characteristic of a B-cell phenotype and could suggest that cells which are slower to differentiate preferentially survive. Although SIK inhibition resulted in a decrease in the percentage of cells expressing $CD27^+$ and $CD38^+$ in plasmablasts, those that did express the markers demonstrated higher expression, again indicative of enhanced differentiation. Although not conclusive, this suggests that the SIKs are able to regulate aspects of differentiation. Furthermore, a large reduction in viability suggests that SIKs are also responsible for regulating survival pathways. For example, a hallmark of short/long-lived plasma cells is the ability to secrete immunoglobulin which puts differentiating cells under large amounts of metabolic stress (Bayles and Milcarek, 2014). Therefore it seems plausible that the SIKs may control various metabolic pathways. Collectively, this highlights the complex nature of SIK regulation in differentiating B-cells.

Although cells were highly sensitive across numerous inhibitor experiments, a small percentage of cells continuously remained (1-10%). This raises a key question regarding the ability of these cells to overcome inhibition of SIK kinase activity. It is plausible that the small-molecule inhibitors are saturated at the concentrations tested and therefore it would be of interest to determine whether repeated inhibitor exposure or increased concentrations could eliminate these small populations. Another possibility is that the cells do not homogenously express SIK proteins at the defined stages of differentiation. For example, there may be subsets of cells that have down-modulated SIK and are therefore relatively resistant to SIK kinase inhibition.

Remarkably, this was one of the first pieces of work to report an association between SIK activity and cell survival until Tarumoto and colleagues published work in 2018 showing AML cells were sensitive to on-target chemical inhibition of SIK activity (Tarumoto *et al.*, 2018). Prior to the work by Tarumoto, it seemed necessary to confirm the SIK inhibitor HG-9-91-01 was working as expected in a well characterised cell type, such as monocytes and macrophages where cell death had not been described. Although there is limited data available regarding viability in monocytes, Lombardi and colleagues assessed the effect of SIK inhibition in mouse RAW264.7 cells and showed no signs of

cellular toxicity up to a concentration of 10μM (Lombardi *et al.*, 2016). To confirm these results in the host lab, HG-9-91-01 was added to 3 cell lines as well as primary monocytes. U937 and RAW264.7 were sensitive to AMPK inhibition but not SIK inhibition, whereas primary cells were unaffected by both. Surprisingly, THP-1 displayed concentration-dependent sensitivity to SIK inhibition. The differences observed here may be explained by previous monocyte experiments utilising a short exposure time of around 1-2 hours (Clark et al., 2012) which may not be sufficient to induce effects on cell survival.

After demonstrating that differentiating B-cells rely on SIK kinase activity, it was proposed that SIKs may be a promising therapeutic target in the treatment of diseases such as multiple myeloma. To test this theory, inhibition experiments were carried out on myeloma cell lines with a variety of underlying genetic abnormalities. Responses varied, however OPM2 and KMS11 were highly sensitive, reducing viability by over 90% and RPMI8226 and H929 were more resistant to inhibition reducing viability by around 50-75% at the same concentration. Attempts to identify what could be responsible for these differences included sequencing of the *SIK1* kinase domain and evaluation of SIK1-3 protein expression, however these provided no additional insight. To extend on this, further work would include the generation of a HG-9-91-01 resistant cell line using a drug-training technique, to hopefully identify underlying differences between sensitivity and resistance within the same cell line.

Although cell lines provide a useful tool to study cell biology, multiple myeloma develops primarily inside the bone marrow microenvironment which confers pro-survival signals and drug resistance. Interestingly, plasma cells from MGUS and myeloma patient samples expressed high levels of *SIK1* mRNA and intermediate levels of *SIK2* in relation to a control sample. To determine whether myeloma cells within this environment would change sensitivity to SIK inhibition, it would be of interest to test the inhibitors on ex vivo human myeloma cells within 3D cultures that reproduce myeloma–bone marrow interactions (Belloni *et al.*, 2018). Alternatively, a xenograft model of myeloma (Lwin, Edwards and Silbermann, 2016) would allow for the assessment of tumour burden following treatment with the in vivo inhibitor YKL-05-099.

When considering SIK inhibitors as therapeutic compounds, it is important to consider pharmacodynamic properties. In primary cells and myeloma cell lines, SIK inhibitors acted in both a concentration and time-dependent manner, with HG-9-91-01 achieving a similar standard of response to bortezomib in primary cells. Although these properties are representative of a promising compound, it is clear that HG-9-91-01 and YKL-05-099 as well as other inhibitors not used in this work represent early efforts in the development of small molecule SIK inhibitors for

therapeutic use. As further research emerges about the mechanism of these kinases, it is plausible that more specific and potent inhibitors will become available.

This chapter relies heavily on conclusions drawn from inhibition experiments, however as previously described 'off-target effects' could affect interpretation of these results. In an attempt to rule these out, HG-9-91-01-resistant vectors were transfected into HeLa cells, however due to this type of cell exhibiting resistance to HG-9-91-01, this avenue of research was not productive. To overcome this, the experiment should be repeated in an alternative cell line sensitive to HG-9-91-01. Furthermore, the data obtained using HG-9-91-01 and myeloma cell lines appeared to be replicated by the AMPK-related kinase inhibitor MRT19965. Both compounds are potent SIK inhibitors but have different off target effects. For example, MRT19965 does not inhibit protein tyrosine kinases but inhibits nearly all members of the AMPK subfamily of protein kinases (Clark *et al.*, 2012). Although crude, the theory is that if the two compounds have similar effects on cells, this would be suggestive of an involvement of one or more SIK isoforms. Alternatively, if the results do not match then it is likely the result is a consequence of an off-target effect. To extend on this further, compounds which target BTK and Src family kinases were tested on myeloma cell lines and primary plasmablasts. As a result of this, it was apparent that BTK inhibition had no effect on cell survival and therefore it could be considered that off-target BTK inhibition of HG-9-91-01 does not contribute to the observed effects. Alternatively, Src inhibition with dasatinib resulted in a decrease in cell survival. Initially this seemed surprising, however it soon became apparent that this effect was not an artefact of HG-9-91-01 since the Src inhibitor dasatinib has been shown to bind to SIK2 in vitro (Miranda *et al.*, 2016). Additionally, salt-inducible kinases have been shown to be major targets of additional protein tyrosine kinase inhibitors such as bosutinib (Ozanne, Prescott and Clark, 2015). This cross-over between inhibitors therefore makes it difficult to rule out loss of Src activity as a result of using HG-9-91-01.

The most appropriate way to overcome off-target effects is through use of SIK knockdowns, particularly SIK1 as this will reveal if specific loss leads to similar effects on viability, proliferation, growth and differentiation. Initial attempts were made in myeloma cell lines, however it was deemed more appropriate to continue in primary human cells. Optimisation experiments revealed that a double transfection at day 1 and 2 achieved the highest efficiency with cells still expressing GFP 96-hours later, therefore further work will include a SIK1 knockdown in primary cells and subsequent gene profiling.

In conclusion, this chapter provides evidence that SIKs are important and may regulate growth, proliferation, differentiation and survival in differentiating human B-cells. In addition, the results

provide novel insight that the SIKs may targetable in diseases such as, but not limited to multiple myeloma. With the potential to regulate a wide variety of functions, the next chapter will focus on downstream substrates of the SIKs.

Chapter 4 - Downstream analysis of potential SIK substrates and impact on gene expression profile

To fully delineate the role of SIKs and their contribution to the survival and differentiation of B-cells, the focus was shifted onto downstream substrates. SIK isoforms have predominantly been shown to regulate cellular gene expression by phosphorylating transcriptional regulators such as CREB-regulated transcription co-activators (CRTCs 1, 2 and 3) (Altarejos and Montminy, 2011) and class IIa histone deacetylases (HDACs 4, 5 7, and 9) (Di Giorgio and Brancolini, 2016)). Phosphorylation by SIKs results in cytoplasmic localisation due to an interaction with 14-3-3 adapter proteins (Bittinger *et al.*, 2004; Jansson *et al.*, 2008; Screaton *et al.*, 2004). Following dephosphorylation in response to SIK inhibition or cAMP signalling, substrates translocate to the nucleus where they modulate gene expression by associating with transcription factors or modifying chromatin.

In addition to CRTCs and HDACs, additional tissue-specific SIK substrates have also been identified. For example, in epithelial cells SIK1 has been identified as a regulator of p53-dependent anoikis and metastatic spread (Cheng *et al.*, 2009) and in hepatocytes phosphorylation of SMRT by SIK1 may modulate Wnt/β-catenin signalling, contributing to the initiation and progression of hepatocellular carcinoma (Qu *et al.*, 2016). Furthermore, complemented by an adipocyte-rich microenvironment, activated SIK2 plays a dual role in augmenting AMPK-induced phosphorylation of acetyl-CoA carboxylase and in activating the PI3K-AKT pathway through p85α-S154 phosphorylation, facilitating ovarian cancer cell proliferation and metabolism (Miranda *et al.*, 2016).

With this in mind, this chapter will consider previously described substrates such as CRTCs and class II HDACs to determine whether such signalling pathways are responsible for regulating viability, proliferative capacity and differentiation during the process of terminal differentiation. Similar pathways may be equally operative in multiple myeloma cells where continuous growth is coupled with sustained immunoglobulin production, thus generating extra metabolic requirements. As a result, myeloma cell lines will be assessed too. The final section of this chapter will utilise gene expression analysis (RNA-sequencing) following SIK inhibition in activated B-cells, plasmablasts and plasma cells in an attempt to identify novel signalling pathways connected with the process of terminal differentiation.

4.1 SIK expression following SIK inhibition

Although work in this chapter will focus primarily on downstream substrates, it was essential to determine whether loss of SIK kinase activity could affect SIK1, 2 or 3 protein expression. Recent work demonstrated that HG-9-91-01 treatment does not impact endogenous SIK2 expression in hepatocytes (Patel *et al.*, 2014) however it was still necessary to determine if this was consistent in both primary plasmablasts and myeloma cell lines for SIK1, 2 and 3. Work presented in chapter 3 identified that a 24 hour exposure to HG-9-91-01 was sufficient to perturb cell viability. In addition to this, Patel and colleagues revealed that changes in CRTC2 dephosphorylation could be observed as soon as 4 hours post-inhibition (Patel *et al.*, 2014). With this in mind, lysates were taken at two different time points (6h and 24h) to see if any changes in SIK expression could be observed.

Interestingly, Western blot analysis revealed a decrease in SIK2 expression (upper portion of the band) after both 6 hour and 24 hour incubation with HG-9-91-01. There also a slight decrease in SIK3 after 24 hours (Figure 4.1). In contrast, SIK1 expression was unaffected at both time points. Following a 6 hour incubation in the myeloma cell lines KMS11, OPM2, RPMI8226 and H929, SIK1 expression did not change. There was a slight decrease in SIK2 expression in KMS11 and H929 and a decrease in SIK3 band intensity in KMS11, OPM2 and H929. Although unexpected, a similar result was observed in macrophages differentiated from peripheral blood monocytes, however these were not shown to be significant (Lombardi *et al.*, 2016).

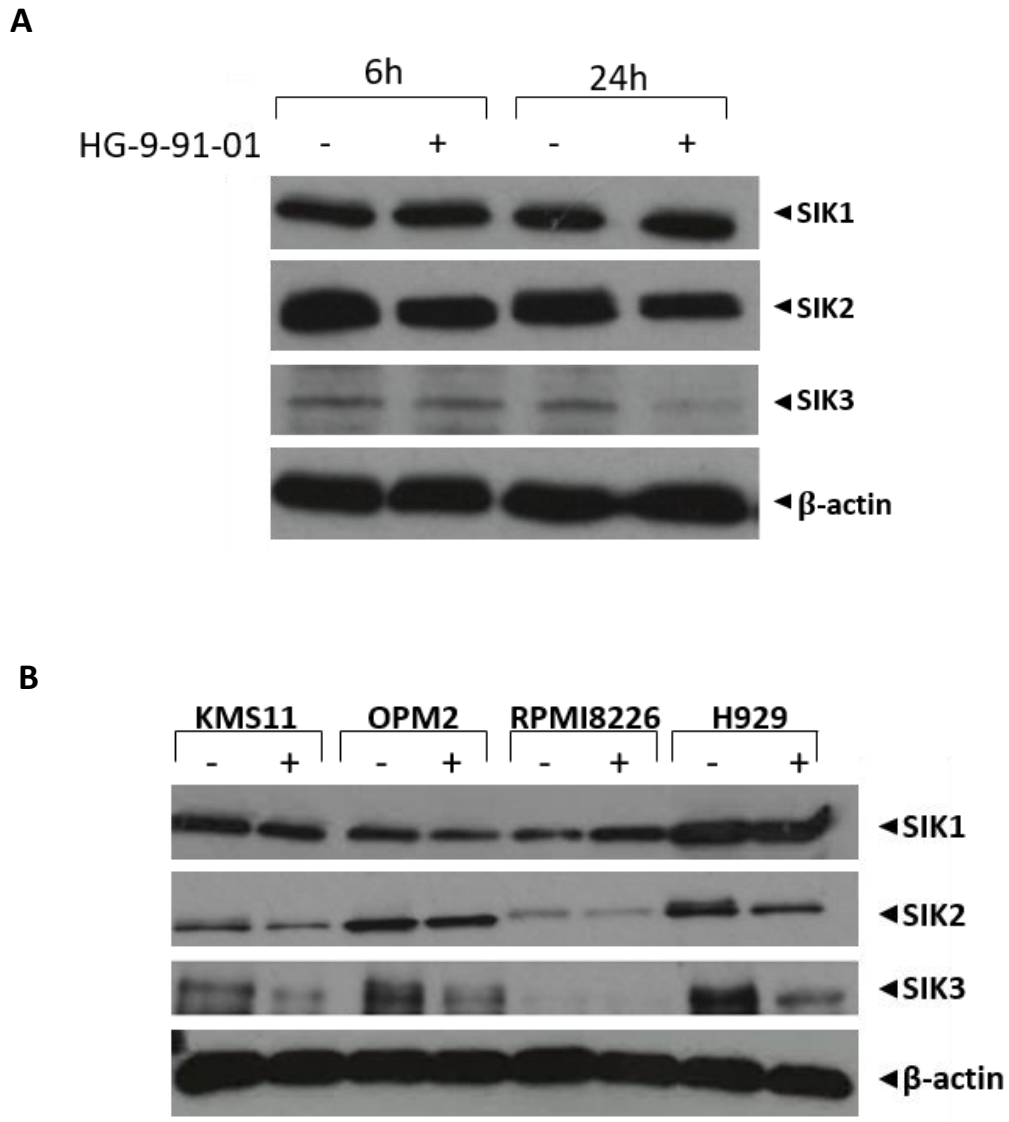

Figure 4.1 Endogenous expression of SIKs following SIK inhibition. (A) Day 6 plasmablasts were incubated with DMSO or HG-9-91-01 (1μM) for 6/24h in addition to IL-6, IL-21, APRIL, GSI, lipids and amino acids. (B) KMS11, OPM2, RPMI8226 and H929 were incubated with DMSO or HG-9-91-01 (2μM) for 6 hours. Protein samples were taken, loaded on to a 10% gel and transferred to a nitrocellulose membrane. Membranes were probed with antibodies for SIK1, SIK2 and SIK3. β-actin was used as a loading control.

4.2 CRTCs

Phosphorylation-dependent transcriptional activators such as CRTCs provide a rapid but reversible mechanism by which extracellular signals regulate gene expression. In response to various stimuli, CRTCs exert their action through binding to the bZIP (basic leucine zipper domain) domain of CREB (and other bZIP transcription factors) and driving gene expression by recruiting TAFII130 and basal transcriptional machinery (Altarejos and Montminy, 2011; Ravnskjaer *et al.*, 2007).

The CRTC family consists of 3 members; CRTC1, CRTC2 and CRTC3 which have been shown to regulate gene expression in a wide variety of cell types. For example, intracellular cAMP prevents the rapid re-phosphorylation of CRTC1 by inactivating SIK and/or AMP kinases, which in turn prolongs CRTC1 nuclear accumulation. This dynamically informs the nucleus about synaptic activity during neuronal signalling (Ch'ng *et al.*, 2012). Alternatively in macrophages, CRTC3 has been shown to play a role in the elevation of IL-10 production following the loss of SIK kinase activity (Clark *et al.*, 2012). Interestingly, CRTC2 is the only member to have been implicated in B-cell differentiation with work by Sherman and colleagues revealing that physiologic CRTC2 inactivation occurs during class switch recombination as a consequence of AID generated DNA double-strand breaks. Further to this, CRTC2 inactivation is necessary for the repression of the GC B-cell program, silencing genes such as *AICDA, MYC, MTA3, CDK6, BACH2, TCF3, SMAD6, SMARCA2, SMARCA4,* and *TCL1* (Sherman *et al.,* 2010*).* This provides evidence for a role consistent with terminal differentiation, and therefore CRTC2 will be assessed in both primary differentiating cells and myeloma cell lines. It is important to note that SIKs phosphorylate CRTC2 at various sites including S70, S171, and S275 (Sonntag *et al.*, 2017) and as a result, SIK inhibition causes increased electrophoretic mobility on SDS-PAGE, indicative of dephosphorylation at these sites (Henriksson *et al.*, 2015; Patel *et al.*, 2014).

4.2.1 CRTC2 expression in differentiating B-cells

To gain insight into CRTC2 expression, samples were taken at various time-points during the differentiation. Although no β-actin was used to verify equal loading, the expression pattern of CRTC2 across the in vitro differentiation provided interesting results. In both donors, CRTC2 could be detected quite strongly between day 1 and 6. On days 8 and 10 band intensity decreased, however this is likely due to a loss of total protein which could be a consequence of declining cell numbers at this time point during the in vitro differentiation (Figure 4.2). On day 13, a band appeared at ~37kd in D1019. This could be indicative of a plasma cell specific isoform however there weren't sufficient live cells taken from D1919 at day 13 to confirm this finding. Moreover, there appeared to be a doublet most prominently observed at days 1 and 2 that was lost on day 3 and regained to some extent on day 6, consistent with phosphorylated (upper band) and non-phosphorylated forms. The transient loss of phosphorylated CRTC2 at day 3 would fit with the reported sequential requirement for LKB1 and CRTC2 during B-cell activation and terminal differentiation (Sherman *et al.*, 2010).

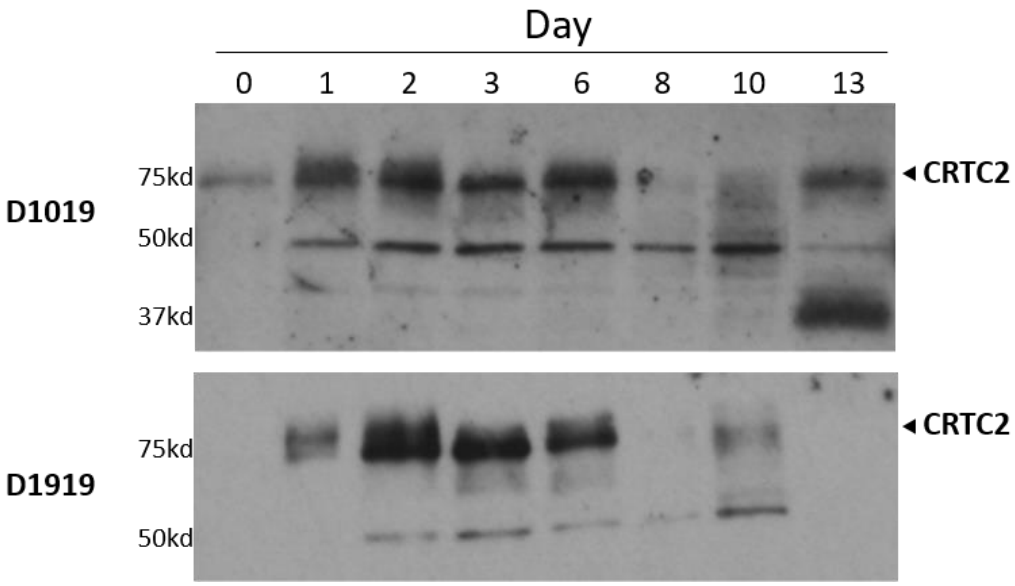

Figure 4.2 Endogenous expression of CRTC2 in differentiating B-cells. Protein samples were taken at the indicated time points, loaded on to a 10% gel and transferred to a nitrocellulose membrane. Membranes were probed with an antibody for CRTC2.

4.2.2 CRTC2 phosphorylation

With Figure 4.2 identifying substantial CRTC2 expression in doublet form in day 6 plasmablasts, analysis of CRTC2 mobility was carried out at this time-point. Following a 6-hour incubation with HG-9-91-01, robust CRTC2 dephosphorylation was apparent (as judged by band shift) in both donors (Figure 4.3). In myeloma cell lines, the higher mobility form was detected in KMS11, OPM2 and H929 and was more pronounced than in the primary cells. In RPMI8226 expression of CRTC2 was less evident and cells treated with DMSO appeared to lack phosphorylation. Following SIK inhibition, CRTC2 expression was undetectable.

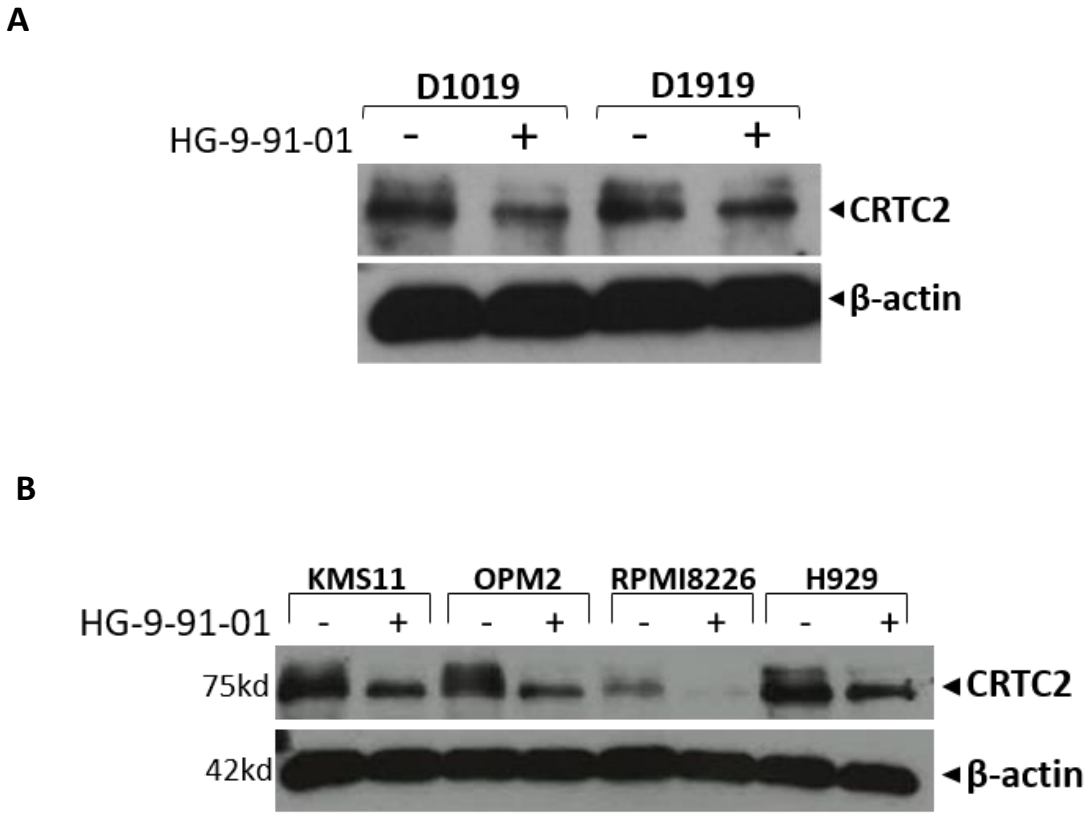

Figure 4.3 Assessment of CRTC2 dephosphorylation following SIK inhibition. (A) Day 6 plasmablasts were incubated with DMSO or HG-9-91-01 (1μM) for 6/24h in addition to IL-6, IL-21, APRIL, GSI, lipids and amino acids. (B) KMS11, OPM2, RPMI8226 and H929 were incubated with DMSO or HG-9-91-01 (2μM) for 6 hours. Protein samples were taken, loaded on to a 10% gel and transferred to a nitrocellulose membrane. Membranes were probed with an antibody for CRTC2. β-actin was used as a loading control.

4.2.3 CRTC2 localisation

As an extension to CRTC phosphorylation assessment, various groups have demonstrated subsequent nuclear accumulation using immunohistochemistry. For example, in bone-marrow derived macrophages dephosphorylation of the SIK substrate CRTC3 at Ser162 and Ser370 causes translocation to the nucleus where it can promote CREB-dependent gene transcription (Ozanne, Prescott and Clark, 2015).

To assess CRTC2 localisation in myeloma cell lines, cells were incubated with HG-9-91-01 for 6h and subjected to nuclear and cytoplasmic fractionation. Interestingly, the results varied between the cell lines. For example, OPM2 was the only cell line to confirm recent findings with DMSO treated cells displaying mainly cytoplasmic CRTC2 (Figure 4.4). Following SIK inhibition, this decreased vastly and there was a slight increase in nuclear CRTC2. KMS11 displayed a decrease in cytoplasmic CRTC2 following SIK inhibition, but also a decrease in nuclear CRTC2. Finally, RPMI8226 and H929 displayed a decrease in cytoplasmic CRTC2 following SIK inhibition, but no changes in nuclear CRTC2.

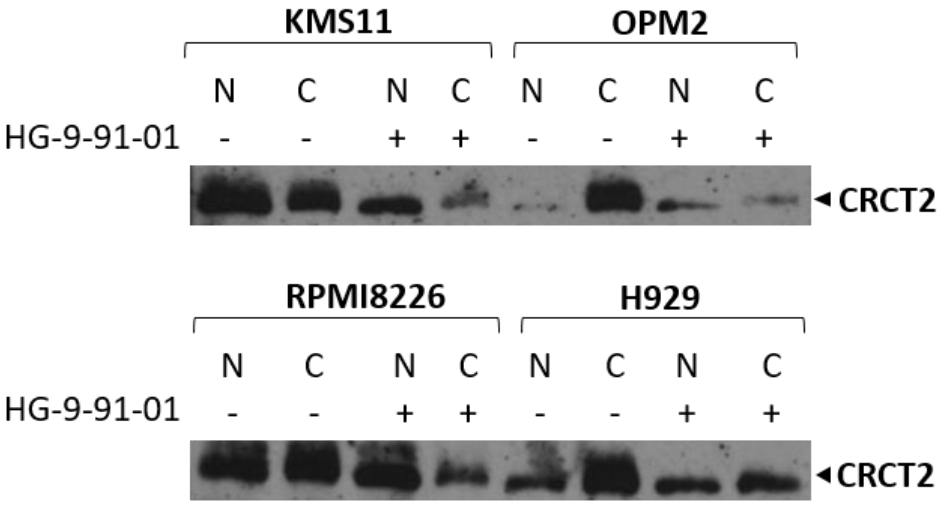

Figure 4.4 Nuclear and cytoplasmic expression of CRTC2 following SIK inhibition in myeloma cell lines. KMS11, OPM2, RPMI8226 and H929 were incubated with DMSO or HG-9-91-01 (2μM) for 6 hours. Following nuclear and cytoplasmic extraction, samples were loaded on to a 10% gel and transferred to a nitrocellulose membrane. Membranes were probed with an antibody for CRTC2.

4.3 HDACs

Histone deacetylases (HDACs) are key epigenetic regulators that mediate dynamic changes in the acetylation of histones at lysine residues. Additionally, many non-histone proteins can also be acetylated and reversible acetylation affects functional properties including interaction, localisation, enzymatic ability and stability (Ellmeier and Seiser, 2018). Class II HDACs (HDAC 4, 5, 6 and 7) have been well described as substrates of SIKs. For example, pharmacologic inhibition of SIKs with HG-9-91-01 directs HDAC4 to the nucleus in a dose-dependent manner and inhibits the calcification process in vascular smooth muscle cells (Abend *et al.*, 2017). HDAC4 has various phosphorylation sites including S246, S467 and S632, and therefore it is conceivable that SIK inhibition may cause increased electrophoretic mobility on SDS-PAGE in a manner analogous to CRTCs. To establish whether class IIa HDACs could be responsible for mediating SIK regulation, HDAC4 expression was evaluated in primary plasmablasts and myeloma cell lines.

4.3.1 HDAC4 expression

In plasmablasts, SIK inhibition resulted in a slight decrease of an upper band after 6h, suggestive of dephosphorylation (Figure 4.5A). More surprisingly, 24h post-inhibition there was vast decrease in intensity of both the upper and lower bands possibly indicative of total HDAC4 degradation. In myeloma cell lines, HDAC4 was expressed at a substantial amount in KMS11, OPM2 and H929 but not RPMI8226. Following SIK inhibition it could be argued that there was a small decrease in HDAC4 band intensity, but interestingly the upper band observed in primary cells was not present (Figure 4.5B).

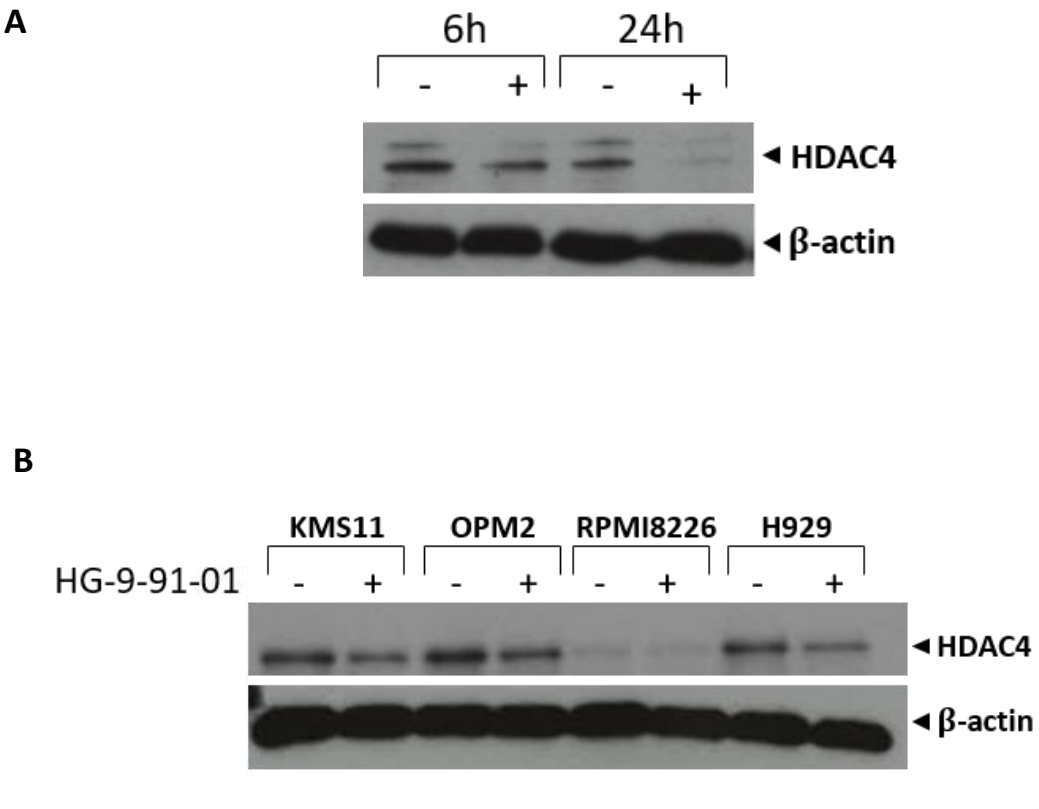

Figure 4.5 Expression of HDAC4 following SIK inhibition. (A) Day 6 plasmablasts were incubated with DMSO or HG-9-91-01 (1μM) for 6/24h in addition to IL-6, IL-21, APRIL, GSI, lipids and amino acids. (B) KMS11, OPM2, RPMI8226 and H929 were incubated with DMSO or HG-9-91-01 (2μM) for 6 hours. Protein samples were taken, loaded on to a 10% gel and transferred to a nitrocellulose membrane. Membranes were probed with an antibody for HDAC4. β-actin was used as a loading control.

4.3.2 Class II HDAC expression in differentiating B-cells

To broaden the investigation into HDAC involvement, a class II HDAC sampler kit was obtained and expression analysis was extended to activated B-cells and plasma cells as well as plasmablasts. Following a 24 hour incubation, there was no difference in HDAC4, 5, 6 or 7 expression in activated B-cells. As cells approached terminal differentiation, this changed and detectable levels of HDAC5, 6, and 7 decreased following SIK inhibition (Figure 4.6). This slightly contradicts Figure 4.5 which showed a decrease in total HDAC4 at this time-point, however this is most likely a consequence of using different antibodies across the 2 experiments. In plasma cells, inhibition caused a total loss of HDAC4, a large decrease in HDAC6 and HDAC7 and a slight decrease in HDAC5 expression.

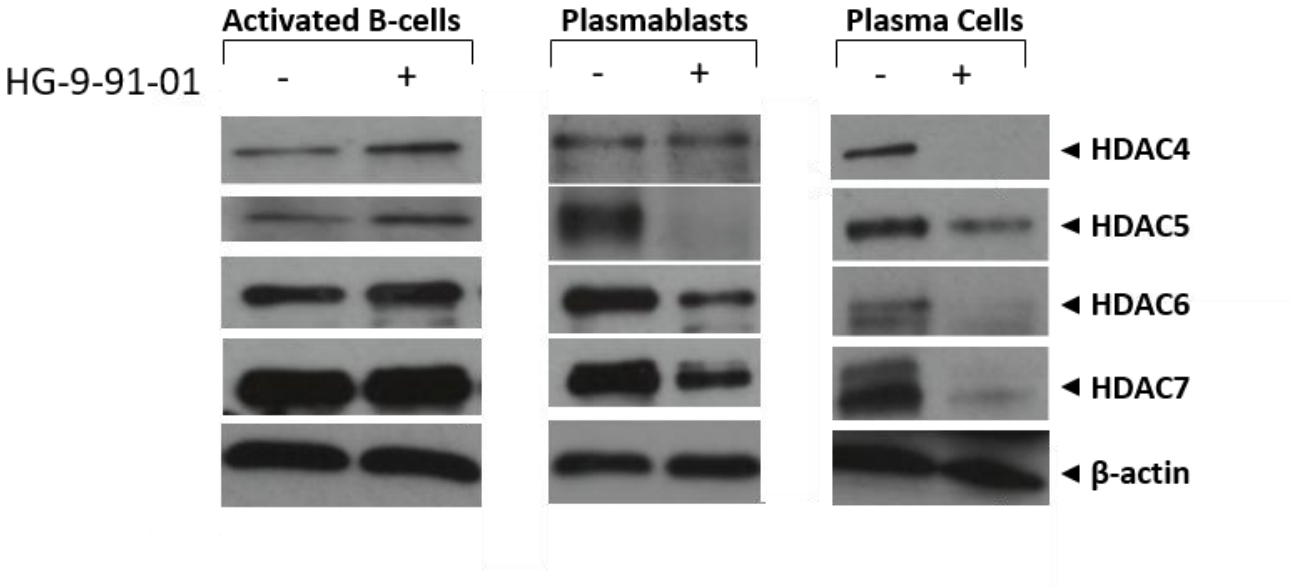

Figure 4.6 Expression of class II HDACs in differentiating B-cells following SIK inhibition. Activated B-cells, plasmablasts and plasma cells were incubated with DMSO or HG-9-91-01 (1μM) in addition to the respective cytokines and growth factors for 24 hours. Protein samples were taken, loaded on to a 10% gel and transferred to a nitrocellulose membrane. Membranes were probed with antibodies for HDAC4, HDAC5, HDAC6 and HDAC7. β-actin was used as a loading control. Results are representative of 2 samples.

4.4 MEF2

Class II HDACs function as co-repressors of different transcription factors, most notably members of the myocyte enhancer factor 2 (MEF2) family including MEF2A, -B, -C and –D. Their main role is to regulate a variety of MEF2-dependent physiological processes including development of skeletal muscle, bone, and the vascular system as well as fine tuning cell differentiation, growth and survival (Clocchiatti *et al.*, 2015; Haberland, Montgomery and Olson, 2009).

The MEF2 family has been implicated in various aspects of B-cell biology with conditional deletion of *Mef2b* in mice leading to a reduction in GC formation (Brescia *et al.*, 2018). In addition, there has recently been reports of a SIK-HDAC-MEF2 signalling module downstream from LKB1. In the mouse skeletal muscle cell line C2C12, SIK2 activates MEF2-dependent transcription and relieves repression of myogenesis by the HDACs (Walkinshaw *et al.*, 2013). Furthermore, an essential role for LKB1 and SIKs in the maintenance of MEF2C function in acute myeloid leukaemia has also been described (Tarumoto *et al.*, 2018). It was therefore of interest to assess MEF2 protein expression following SIK inhibition.

Following treatment, there was a decrease in the detectable levels of MEF2 after both 6h and 24h comparable with the loss of class II HDACs after 24h (Figure 4.7). In myeloma cell lines, there was a considerable amount of non-specific binding, however it seemed that H929 was the only cell line with detectable levels of MEF2 at the expected band size of around 64kd. Consequently, it was difficult to conclude the effect of SIK inhibition on MEF2 expression although there seemed to be no differences in expression levels.

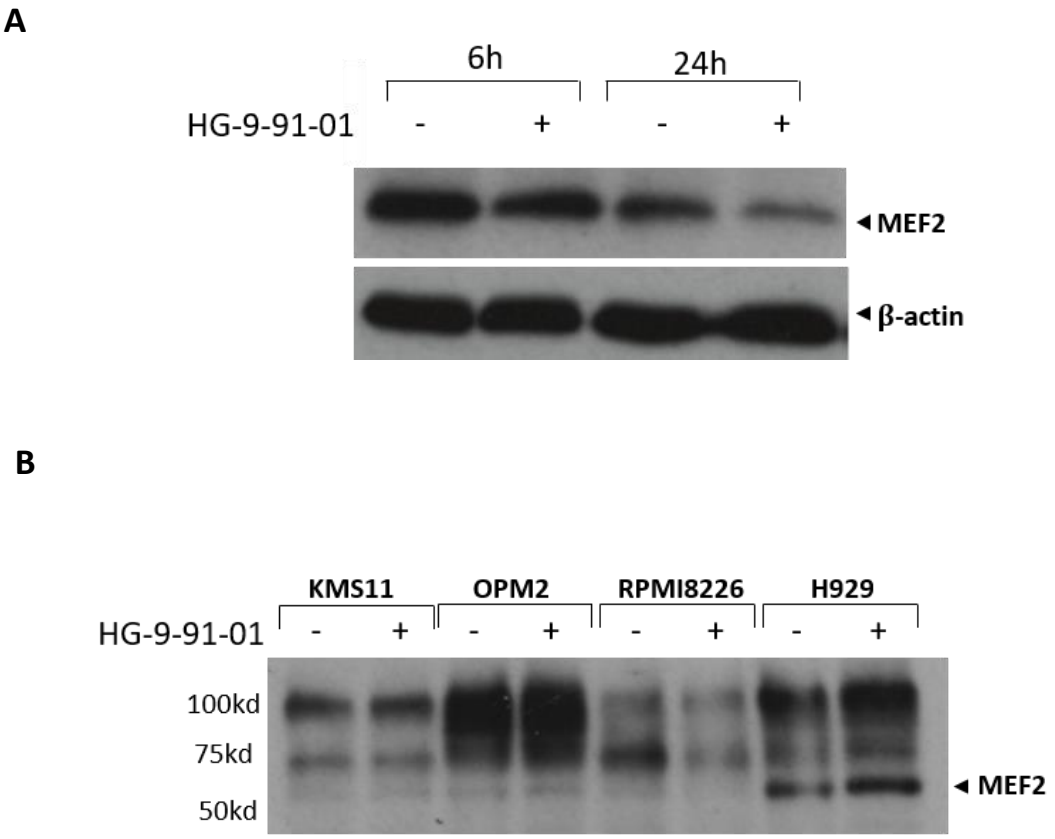

Figure 4.7 Expression of MEF2 following SIK inhibition. (A) Day 6 plasmablasts were incubated with DMSO or HG-9-91-01 (1μM) for 6/24h in addition to IL-6, IL-21, APRIL, GSI, lipids and amino acids. (B) KMS11, OPM2, RPMI8226 and H929 were incubated with DMSO or HG-9-91-01 (2μM) for 6 hours. Protein samples were taken, loaded on to a 10% gel and transferred to a nitrocellulose membrane. Membranes were probed with a pan-antibody for MEF2 family members. β-actin was used as a loading control.

4.5 IRF4

The transcription factor interferon regulatory factor 4 (IRF4) has been extensively characterised and as a result has been shown to control important events during both B-cell development and maturation. For example, GC formation is severely impaired in mice with a conditional *Irf4* deletion resulting in an absence of post-germinal centre plasma cells (Klein *et al.*, 2006) whereas mature plasma cells and multiple myeloma require IRF4 expression for survival (Tellier *et al.*, 2016b; Shaffer *et al.*, 2008). This highlights IRF4 as a crucial 'switch' in the generation and maintenance of functionally competent plasma cells.

SIK has been shown to negatively regulate *MITF*, a regulator of pigment gene expression through its activity on CRTC and CREB (Mujahid *et al.*, 2017). Furthermore, *IRF4* was identified as a novel MITF target gene in melanocytes (Hoek *et al.*, 2008). It is therefore conceivable that IRF4 may be affected by SIK inhibition as a consequence of *MITF* regulation. In plasmablasts, SIK inhibition resulted in no difference in IRF4 expression. In myeloma cell lines, IRF4 expression was diminished to some extent, most noticeably in the KMS11 cell line (Figure 4.8).

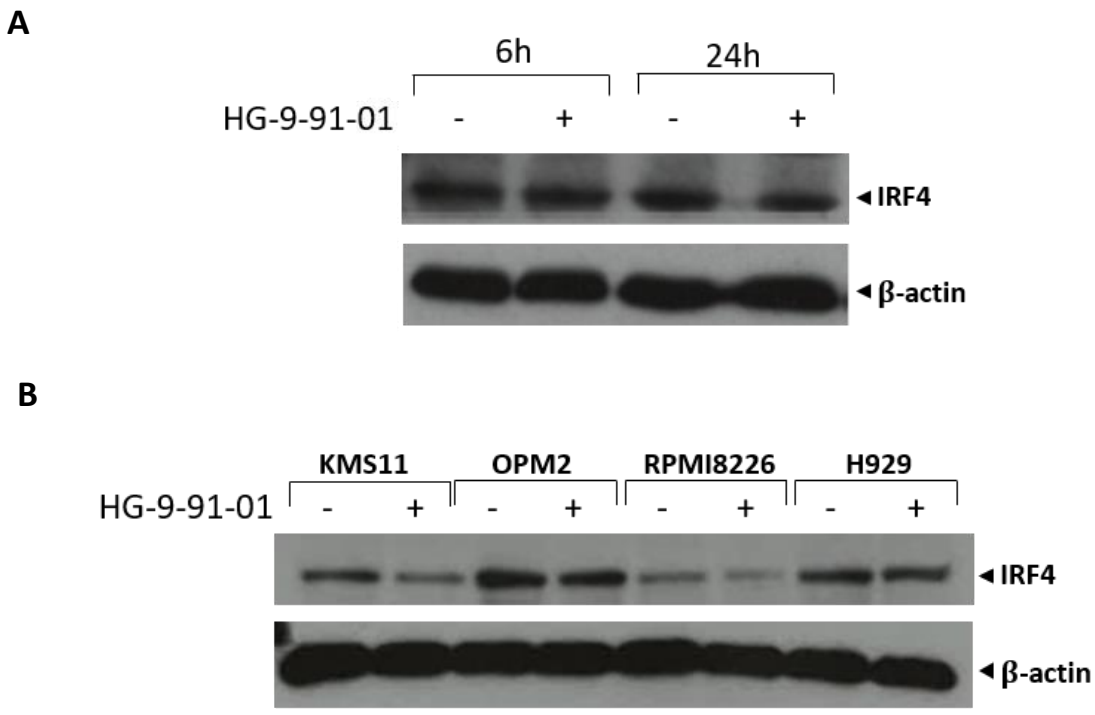

Figure 4.8 Expression of IRF4 following SIK inhibition. (A) Day 6 plasmablasts were incubated with DMSO or HG-9-91-01 (1µM) for 6/24h in addition to IL-6, IL-21, APRIL, GSI, lipids and amino acids. (B) KMS11, OPM2, RPMI8226 and H929 were incubated with DMSO or HG-9-91-01 (2µM) for 6 hours. Protein samples were taken, loaded on to a 10% gel and transferred to a nitrocellulose membrane. Membranes were probed with an antibody for IRF4. β-actin was used as a loading control.

4.6 Gene expression analysis

Given the convincing alterations in class II HDAC expression levels following SIK inhibition there seemed a high probability that this would be matched by equally compelling changes in downstream gene expression. Therefore, an assessment of the transcriptome using RNA-sequencing was carried out in an attempt to further understand SIK-mediated regulation during different stages of terminal differentiation. Following bioinformatic analysis of the data, heat maps and Venn-diagrams were created in order to visualise differential gene expression as well as identify genes both unique and overlapping across the different cell types (activated B-cell, plasmablast and plasma cell) following SIK inhibition.

It was evident from the heat map that SIK inhibition convincingly orchestrated distinct changes in gene expression across differentiating cells (Figure 4.9A). Venn-diagram analysis revealed 37 common upregulated genes and 13 common downregulated genes across the 3 different cell types (Figure 4.9B). Interestingly, the highest degree of overlap occurred between plasmablasts and plasma cells (59 higher and 44 lower).

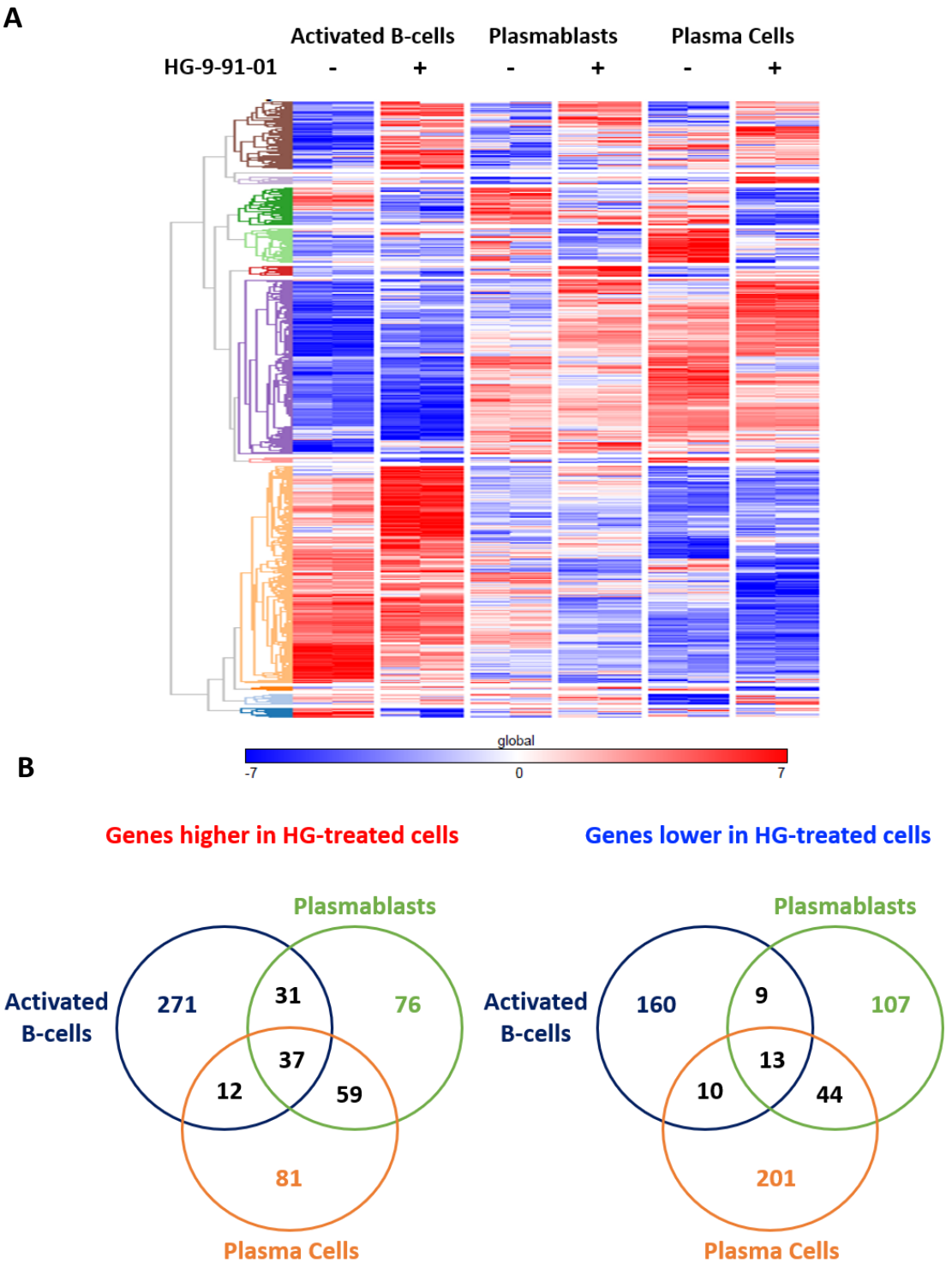

Figure 4.9 Gene expression comparisons. Activated B-cells (D3), plasmablasts (D6) and plasma cells (D13) were treated with DMSO or HG-9-91-01 (1µM) for 24 hours and assessed for changes in gene expression by RNA-seq. (A) Hierarchically clustered heat map of differentially expressed genes. Log_2 FPKM expression values of genes are shown. (B) Venn diagrams showing both overlaps and differences between genes that were significantly up- and downregulated in the indicated cell types.

4.6.1 Gene ontology

Using the database for annotation, visualization and integrated discovery (DAVID), functional annotation was carried out on the differentially expressed gene sets displayed in Figure 4.9. Ontology terms were derived from KEGG pathways and are listed in the tables below along with the contributing differentially expressed genes.

4.6.1.1 Activated B-cells

In activated B-cells, ontology analysis revealed downregulation of genes associated with purine/ pyrimidine metabolism and ribosome biogenesis (Table 4.1). Alternatively, there was upregulation of genes associated with BCR and TLR signalling, as well as an anti-viral response and cell adhesion. Of interest, the MAPK pathway including *MAPK8 (JNK1)*, *MAP2K3 (MEK3)*, MAP2K6 *(MEK6)*, *MAPK1 (ERK1)* contributed to the majority of upregulated ontology terms.

Table 4.1 Ontology terms derived from KEGG pathway analysis of activated B-cells

Up	Down
TLR signalling (*FOS, IKBKE, MAPK1, MAPK8, MAP2K3, MAP2K6, PIK3R3*) **BCR signalling** (*FOS, MALT1, CARD11, DAPP1, MAPK1, PIK3R3*) **Anti-viral response** (*OAS3, PYCARD, CASP9, EIF2AK4, FURIN, HNRNPUL1, IKBKE, MAPK1, MAPK8, MAP2K3, MAP2K6, NUP98, PIK3R3, SOCS3, TMPRSS13, TNFSF10*) **ErbB signalling pathway** *(CBLB, NCK2, SHC4, SRC, AREG, CAMK2G, HBEGF, MAPK1, MAPK8, PIK3R3)* **Cell adhesion** (*CD99, F11RM, CDH1, CDH3, CTLA4, ITGB2, MPZ, PDCD1LG2, SELL*)	**Purine/Pyrimidine metabolism** (*CTPS1, POLR1B, POLR1C, POLR3D, POLR3E, PNPT1, PNP, ADA, IMPDH2*) **Ribosome biogenesis** (*GNL3, RCL1, SBDS, UTP14A, WDR3, WDR36, WDR43, NOL6, RPP25*)

To determine whether any core B-cell/ASC factors were specifically affected by SIK inhibition, fold changes were examined. There was a greater than 1.4-fold decrease in the B-cell regulators *SPIB*, *HHEX*, *ABLIM1, SOX2, BACH2, AICDA, MEF2B* and *CCND2* (Figure 4.10A). There was also a profound decrease (6 fold) in the ASC regulator *TNFRSF17* which encodes for BCMA (Figure 4.10B).

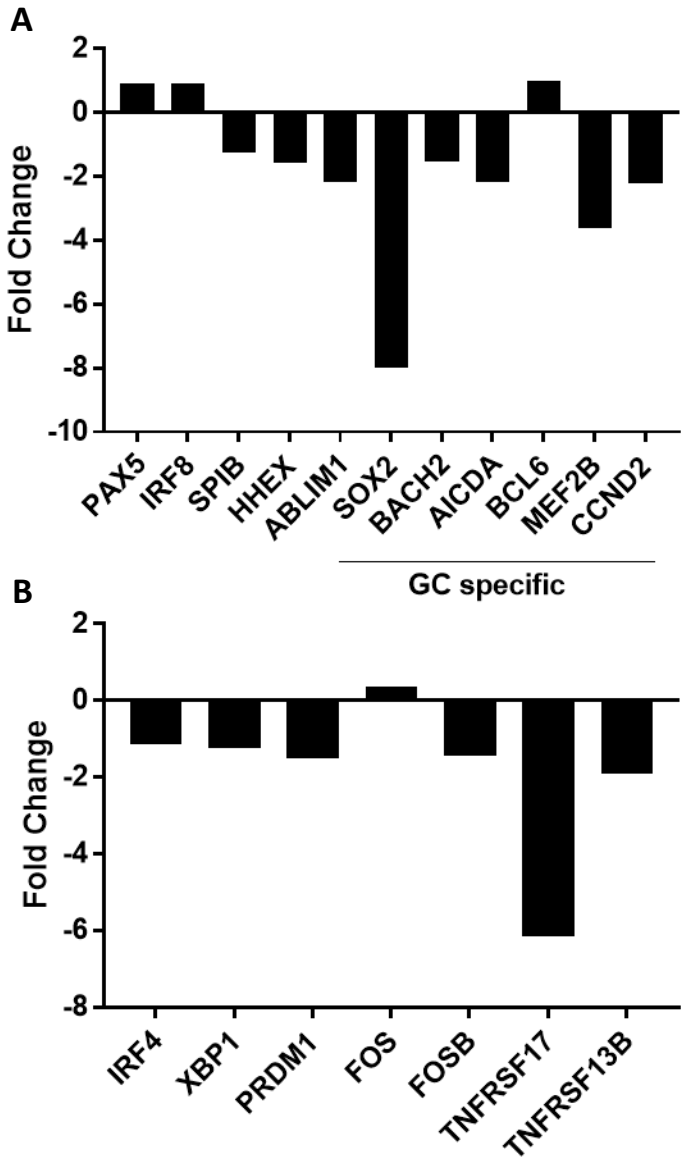

Figure 4.10 Fold change of critical regulators following SIK inhibition in activated B-cells. Cells were treated with DMSO or HG-9-91-01 (1µM) for 24 hours and RNA-Seq was performed. Data is derived from 2 human donors.

4.6.1.2 Plasmablasts

Analysis of plasmablasts identified unique gene sets and ontology terms compared with activated B-cells, however there was upregulation of cell adhesion markers at both time-points. There was also upregulation of genes associated with lysosome formation (Table 4.2). Alternatively, there was downregulation of genes associated with glycolysis, PI3K-AKT signalling, NF-κB signalling and cytokine-cytokine receptor interaction.

Table 4.2 Ontology terms derived from KEGG pathway analysis of plasmablasts

Up	Down
Cell adhesion *(CD274, CD86, F11R, CDH1, CLDN14, CTLA4, ITGA6, ITGA8, ITGB8, MPZ, PECAM1, SELL, SDC1*)	**Glycolysis** *(ALDOA, ALDOC, ENO1, ENO2, GPI, GAPDH, PFKP, PKM, TPI1)*
Lysosome formation *(GM2A, GNPTG, ASAH1, ACP5, CTSC, CTSO, CTSS, GNS, HEXB)*	**PI3K-AKT Signalling** *(CD19, GNG3, SOS2, CREB1, COL24A1, FGF11, INSR, ITGA3, ITGA4, ITGB4, IL2RG, LPAR5, PIK3CD, PTK2, SGK1, TP53, VEGFA)*
	NF-κB signalling *(ERC1, NFKBIA, TRAF2, TRAF5, LTA, LTB, NFKB2, TNF)*
	Cytokine-cytokine receptor interaction *(CCR1, CCR2, CCR5, TNFRSF13B, TNFRSF17, IFNGR1, IL2R, IL4R, TNFSF13, TNF)*

Although plasmablasts are in the process of switching off the B-cell programme, it was of interest to evaluate both B-cell and ASC regulators to determine if SIK inhibition affected genes associated with this transition. Notably, there was a profound decrease (2-6 fold) in *IRF8, SPIB, HHEX, BACH2, AICDA* and *BCL6*. At this time-point, there was a decreased effect on *MEF2B* and CCND2 expression. Once again, there was a profound decrease in both *TNFRSF17* (6 fold) and *TNFRSF13B* (3 fold) which encodes for TACI.

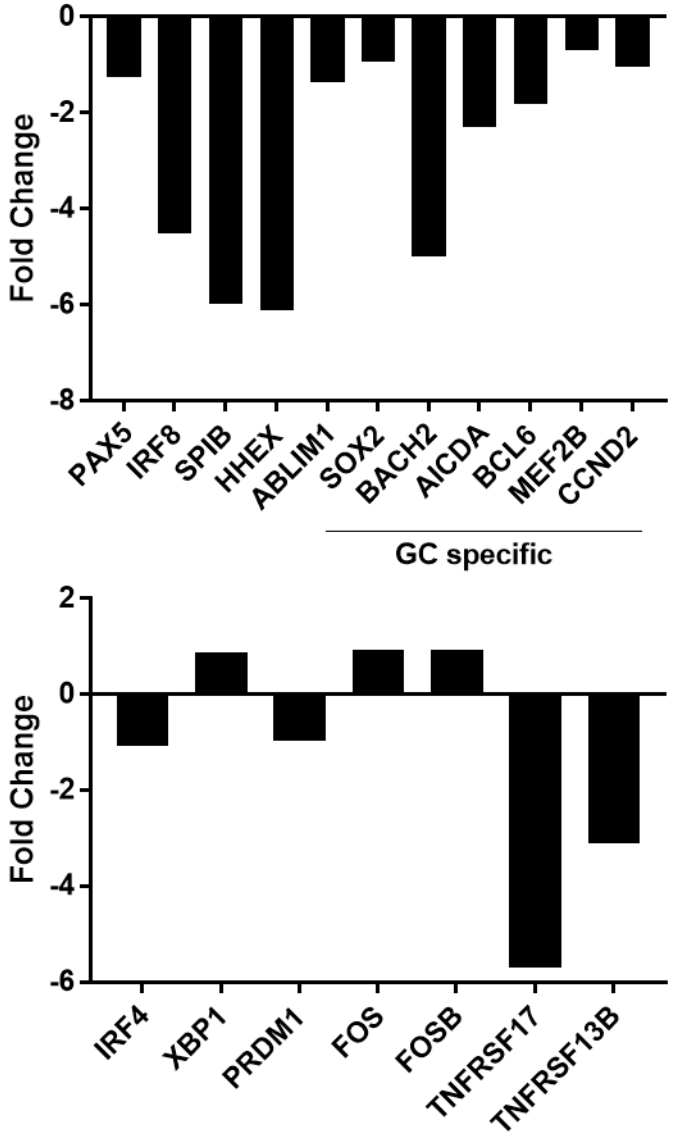

Figure 4.11 Fold change of critical regulators following SIK inhibition in plasmablasts. Cells were treated with DMSO or HG-9-91-01 (1µM) for 24 hours and RNA-Seq was performed. Data is derived from 2 human donors.

4.6.1.3 Plasma Cells

The final stages of terminal differentiation are characterised by cell cycle exit, high levels of immunoglobulin secretion and complete repression of the B-cell gene expression programme. As seen in plasmablasts, plasma cells displayed downregulation of numerous glycolytic enzymes as well as genes associated with PI3K-AKT signalling and NF-κB signalling (Table 4.3). There was also downregulation of genes involved in the unfolded protein response (UPR) such as *XBP1*, *ATF6* and *EIF2AK3*. Alternatively, upregulation of genes associated with lysosome formation was evident as seen in plasmablasts as well as regulation of the actin cytoskeleton.

Table 4.3 Ontology terms derived from KEGG pathway analysis of plasma cells

Up	Down
Lysosome formation *(CD68, ACP5, CTSC, GLA, HEXB, TPP1)* **Regulation of actin cytoskeleton** *(BAIAP2, IQGAP2, IQGAP3, ACTB, ACTG1, ITGB3, ITGB8, MYL12A, PIP4K2A, PIP4K2C, PPP1R12B)*	**Glycolysis** *(ALDOA, ALDOC, ENO1, GPI, GAPDH, HK2, LDHA, PCK2, PFKP, PGK1, PGAM1, PKM, TPI1)* **PI3K-AKT signalling** *(MCL1, CD19, PHLPP1, CREB3L2, COL24A1, CCND2, CCNE1, CCNE2, CDKN1B, FGF11, FLT1, HGF, IRS1, INSR, IL2RG, PCK2, SGK1, MYC*) **NF-κB signalling** *(BCL10, BLNK, CCL4L2, CCL4, CLFAR, CD40, ERC1, RELB, TNFAIP3, TRAF2, BIRC3*) **Protein processing in ER** *(EDEM1, NGLY1, SEC24A, TRAF2, XPB1, ATF6, EIF2AK3, MAP3K5, PDIA4, TXNDC5, UBE2D2, UBE2J1)*

As would be expected at this time-point, the overall effect on B-cell factors was smaller than in plasmablasts, however there was a pronounced decrease in *ABLIM1* (3 fold) *and BACH2* (2 fold). There was also a decrease in the all of the ASC factors examined including *IRF4, XBP1, PRDM1, FOS, FOSB*, *TNFRSF17* and TNFRSF13B.

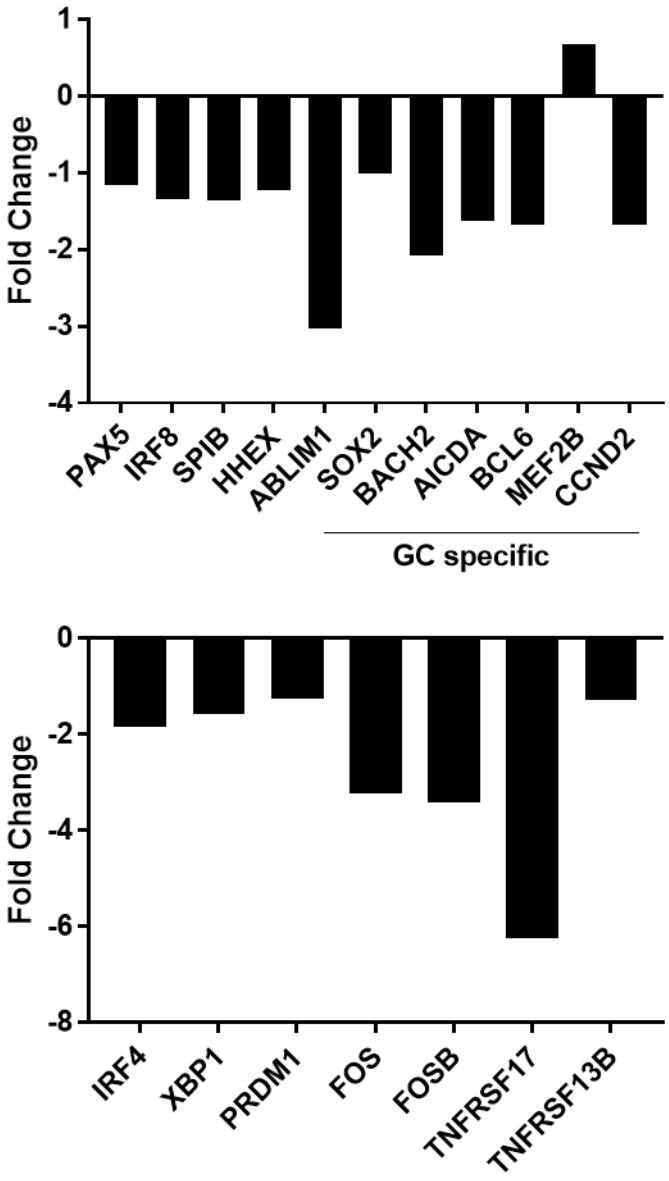

Figure 4.12 Fold change of critical regulators following SIK inhibition in plasma cells. Cells were treated with DMSO or HG-9-91-01 (1µM) for 24 hours and RNA-Seq was performed. Data is derived from 2 human donors.

Because of the energy and nutrients needed to secrete large amounts of glycosylated antibody molecules, metabolic demands in plasma cells are high (Aronov and Tirosh, 2016). Plasma cells import and utilize glucose and glycolysis as a source of mitochondrial respiration to enhance survival and support immunoglobulin production (Corcoran and Nutt, 2016). Interestingly, the expression of numerous genes involved in both glucose transport and glycolysis were downregulated in both plasmablasts (9 genes) and plasma cells (13 genes) after just 24h SIK inhibition (Figure 4.13).

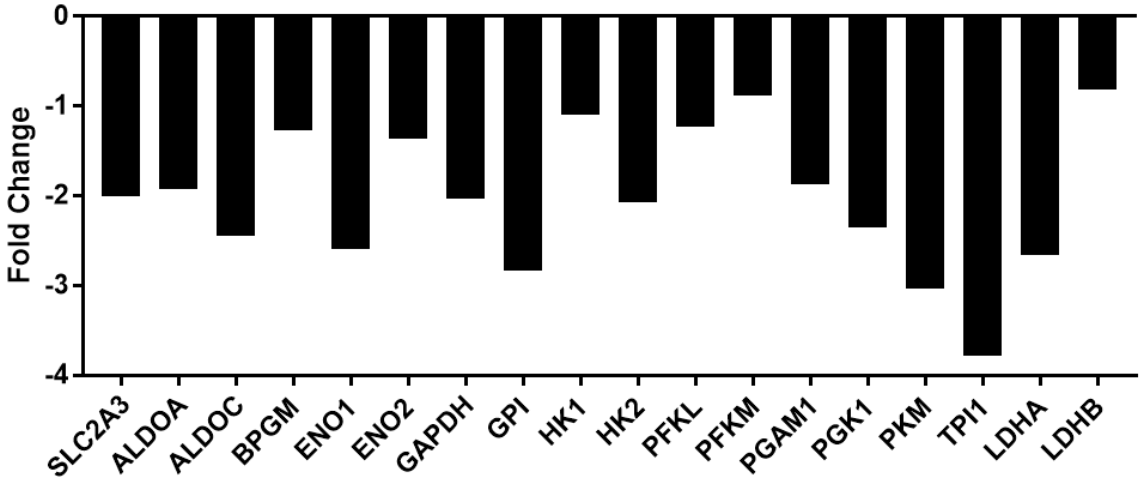

Figure 4.13 Fold change of genes involved in glycolysis following SIK inhibition. Plasmablasts and plasma cells were treated with DMSO or HG-9-91-01 (1µM) for 24 hours and RNA-Seq was performed. Data is derived from 2 human donors.

4.7 Discussion

This chapter has provided insight into likely downstream substrates of the SIKs in differentiating B-cells as well as revealing potential mechanisms that may account for the observed effects on proliferation, differentiation and apoptosis. Firstly, SIK inhibition resulted in a surprising decrease in SIK2/3 expression but not SIK1 in both primary cells and myeloma cell lines. In other settings, SIK1 protein stability has been linked to direct association with an E3-ubiquitin ligase (Qu and Qu, 2017) and regulation by PKA activity (Stewart *et al.*, 2013b). However, there has been no previous association between the loss of SIK kinase activity and a decrease in SIK protein expression.

Initial experiments focused on the CREB-regulated transcription coactivator (CRTC2) since previous work reported a link between CRTC2 inactivation and terminal differentiation of GC B-cells. Although CRTC2 de-phosphorylation was visible in both primary cells and myeloma cell lines confirming loss of SIK kinase activity, fractionation of cell lines revealed varying results. OPM2 was the only cell line that supported previous findings regarding nuclear accumulation, whereas KMS11, RPMI8226 and H929 displayed a decrease in cytoplasmic expression but varying nuclear expression. Although a 6-hour treatment with HG-9-91-01 could be too soon to observe final changes in localisation, these results seem to suggest that SIK inhibition causes cytoplasmic degradation of CRTC2 rather than nuclear translocation. Since the known roles for CRTCs in regulating transcription and alternative splicing (Altarejos and Montminy, 2011) require nuclear localisation, it seems likely that CRTC2 may not be the main driver of SIK regulation in differentiating B-cells. Furthermore, cell lines both sensitive and resistant to SIK inhibition displayed similar levels of CRTC2 dephosphorylation providing further evidence that an alternative downstream substrate may confer sensitivity.

The large number of studies into the LKB1-SIKs-class II HDAC axis have established nuclear/cytoplasmic shuttling as a means of influencing class II HDAC activity. By a simple process, it is possible to reset the transcriptional landscape of cells through induction and repression of numerous target genes (Di Giorgio and Brancolini, 2016). As class II HDACs mainly exert their function in the nucleus, cytoplasmic accumulation is generally considered as a negative regulation. This can be seen in cardiac cells, in which class II HDACs accumulate in the cytoplasm during cell differentiation (Clocchiatti *et al.*, 2013; Backs *et al.*, 2006). Preliminary investigation into total HDAC4 expression in plasmablasts revealed surprising results with a near complete loss of detectable protein after 24 hours. This result prompted further research into other class II HDACs as well as additional time-points. In activated B-cells, HDAC expression levels did not change following SIK inhibition, however there was a decrease/loss of total HDACs (4, 5, 6 and 7) in both

plasmablasts and plasma cells. This appears to be a novel finding since there has been no reported loss of total protein following SIK inhibition, compared with SIK mediated class II HDAC relocalisation which has been reported on numerous occasions (Wang *et al.*, 2011; Mihaylova *et al.*, 2011; Luan *et al.*, 2014). Although loss of protein has not been described in response to SIK inhibition, the ubiquitin-proteasome system (UPS) is known to affect class II HDAC levels. Previous reports have shown that class II HDACs can be degraded in both the cytoplasm (Li *et al.*, 2004) and nucleus (Potthoff *et al.*, 2007) following ubiquitination and therefore it is possible that ubiquitin mediated degradation of class II HDACs occurs following SIK inhibition in both plasmablasts and plasma cells. To investigate this further, it will be important to establish localisation of the class II HDACs in differentiating B-cells as well as post-SIK inhibition. Furthermore, experiments using the proteasome inhibition MG-132 would also be useful to confirm whether ubiquitination accounts for total loss of HDAC protein. Collectively, this data provides strong evidence that class II HDACs could be responsible for mediating SIK function through the repression of both histone or protein de-acetylation. It also supports the idea that SIKs regulate distinct pathways as cells progress through the stages of differentiation as was previously observed for macrophages (Darling *et al.*, 2017).

To extend these findings and probe downstream of HDACs, MEF2 expression levels were also examined. Interestingly, levels of detectable MEF2 decreased after 24h SIK inhibition in a similar manner to the class II HDACs, providing the first indication that the SIK-HDAC-MEF2 axis may be essential to various aspects of B-cell differentiation.

4.7.1 Activated B-cells

Gene ontology analysis revealed potential novel mechanisms of SIK regulation at various time points of B-cell differentiation. In response to antigen stimulation, BCR and TLR engagement induce mediators such as ERK, JNK and p38 which form part of the MAPK signalling pathway (Guo and Rothstein, 2005; Peroval *et al.*, 2013). Following SIK inhibition in activated B-cells, there was considerable upregulation of various MAPK signalling intermediates which contributed to BCR and TLR signalling ontology as well as an anti-viral response. In chapter 1, it seemed plausible that treating activated B-cells with HG-9-91-01 affected proliferative capacity rather than inducing apoptosis since cell number did not alter from the seeding density at day 3, however it is also possible that cells could have proliferated and then undergone apoptosis. Examination of MAPK signalling has revealed that transient activation of ERK leads to cell proliferation, whereas sustained activation results in cell differentiation (Marshall, 1995). More recently, work carried out in the yeast *Saccharomyces cerevisiae has shown that* exposure to mating pheromone activates a

prototypic MAPK cascade and triggers a dose-dependent differentiation response. For example, a high pheromone dose induces growth arrest and budding, whereas lower pheromone doses elicit elongated cell growth (Li *et al.*, 2017). In mice, ERKs have been shown to be essential for the differentiation of B-cells into plasma cells and induce the expression of *Prdm1*, which encodes Blimp-1, a transcriptional repressor and "master regulator" of plasma cell differentiation (Yasuda *et al.*, 2011). This provides inter-species evidence that sustained MAPK activation can encourage differentiation over growth and may explain why activated B-cells fail to proliferate but maintain a relatively normal, if not slightly accelerated phenotype at day 6 following SIK inhibition.

Furthermore, there was downregulation of both purine/pyrimidine metabolism and ribosome biogenesis. It has been demonstrated that mTORC1 fails to induce ribosome biogenesis when nucleotides are limiting (specifically purines), highlighting the ability to tightly coordinate nutrient availability with the synthesis of macromolecules such as protein and nucleic acids (Hoxhaj *et al.*, 2017). It is therefore plausible that activated B-cells which face high metabolic demands shut down key processes such as these following SIK inhibition in an attempt to try and preserve cellular homeostasis and maintain integrity. Taken together, this could account for the decrease in proliferative capacity observed in chapter 3.

Assessment of B-cell specific genes revealed a decrease in *HHEX* and *ABLIM1* which were recently recognised as B-cell factors in a cluster with *Pax5* and *Spib* (Shi *et al.*, 2015). *Ablim1* is mainly known for its role in cell adhesion and migration whereas *Hhex* has been shown as essential for early B-cell development (Narahara *et al.*, 2018; Goodings *et al.*, 2015), however little is known about these factors regarding B-cell differentiation. GC specific genes were also downregulated including *SOX2, AICDA, MEF2B* and *CCND2*. Whilst *AICDA* is essential for both CSR and SHM, *SOX2* has been shown to specifically regulate AID expression in class-switched B cells to suppress genomic instability associated with CSR (DiMenna *et al.*, 2017; Xu *et al.*, 2007). Furthermore, expression of *MEF2B* (but not *2A, 2C or 2D*) decreased significantly in activated B-cells and Western blot analysis revealed a decrease in protein expression of MEF2 in plasmablasts. *Mef2b* has been shown to be essential for GC formation with roles in cell proliferation, apoptosis, GC confinement, and differentiation (Zan and Casali, 2013; Brescia *et al.*, 2018). Finally, there was a decrease in *CCND2* consistent with an inability to proliferate. Collectively, these results suggest that SIKs could be responsible for regulating events occurring in the germinal centre reaction due to the broad impact on gene expression.

4.7.2 Plasmablasts and plasma cells

Following SIK inhibition in plasmablasts, there was a decrease in the B-cell factors *IRF8, SPIB, HHEX, BACH2, AICDA* and *BCL6* as well as a decrease in the ASC factors *TNFRSF17* (BCMA) and *TNFRSF13B* (TACI) as seen in activated B-cells. As cells at this time-point are in the process of naturally turning off the B-cell programme, it was of interest to see enhanced downregulation of such genes. Whereas IRF8 is known for its role in GC formation, the Ets factor SPIB has been shown to maintain GC B-cells through direct repression of the major plasma cell factors BLIMP-1 and XBP-1 (Lee *et al.*, 2006; Schmidlin *et al.*, 2008). BACH2 is known for sustaining high levels of BCR-induced proliferation, survival, and cell cycle progression (Miura *et al.*, 2018) and BCL6 suppresses BLIMP-1 expression through direct binding to the *IRF4* gene, as well as promoting the expression of MITF, a known suppressor of *IRF4* (Alinikula *et al.*, 2011). As the downregulated genes are known to directly target factors involved in terminal differentiation such as BLIMP-1 and XBP-1, it is conceivable that the SIKs may regulate differentiation at this time-point.

In plasma cells, there was a decrease in the B-cell factors *ABLIM1, BCL6 and CCND2*, as well as a decrease in numerous ASC factors including *IRF4, XBP1, PRDM1, FOS, FOSB, TNFRSF17 (*BCMA*)* and *TNFRSF13B (*TACI*).* IRF4 expression markedly increases as cells differentiate and is essential for ASC development (Sciammas *et al.*, 2006). *PRMD1* which encodes for BLIMP-1 regulates components of the unfolded protein response (UPR), including XBP-1 and ATF6, enabling secretion of antibody and XBP-1 coordinates diverse changes in cellular structure and function resulting in the characteristic phenotype of professional secretory cells (Shaffer *et al.*, 2004; Tellier *et al.*, 2016b). Furthermore, BCMA has been implicated in the survival of long-lived bone marrow plasma cells (Yang *et al.*, 2005; O'Connor *et al.*, 2004) and TACI signalling in response to multimeric BAFF and APRIL regulates isotype switching (Mackay and Schneider, 2008; Castigli *et al.*, 2005). These represent hallmark genes involved in terminal differentiation and downregulation suggests that SIKs may be crucial for both the final stages of differentiation and survival, in a manner similar to plasmablasts. Overall there were differences in the expression of B-cell and plasma cell related genes, however it is important to note that cells which survive at each stage appear to have a relatively normal phenotype, so the core differentiation factors may not be as critical as other pathways during SIK inhibition.

Ontology analysis of plasmablasts and plasma cells revealed downregulation of genes associated with PI3K-AKT signalling, NF-κB signalling, cytokine-cytokine receptor interaction and glycolysis. PI3K activation is tightly controlled by receptor tyrosine kinases (RTKs) in response to growth factors. Recruitment of Akt to the plasma membrane and subsequent activation then leads to substrate-

specific phosphorylation events and the regulation of cellular functions including metabolism, growth, proliferation, survival and apoptosis (Hemmings and Restuccia, 2012).

During B-cell development and differentiation, B-cells exhibit distinct biosynthetic requirements and must be able to tightly regulate metabolic activity in regards to nutrient availability. In particular, the PI3K signalling network has been implicated in regulating nutrient acquisition, utilization and biosynthesis, thus integrating receptor mediated signalling with cell metabolism (Jellusova and Rickert, 2016). In both plasmablasts and plasma cells, there was downregulation of numerous genes involved in PI3K-AKT signalling (highlighted in blue in Figure 4.14) relating to cell survival, cell cycle progression and metabolism. As cells approach terminal differentiation, the focus switches from proliferation to secretion and so it is possible that SIKs regulate PI3K signalling to adjust to the increasing metabolic demands of the cell. Of interest, the HDAC-MEF2 axis has been shown to be directly influenced by the PI3K/AKT pathway. Furthermore, blocking the PI3K/AKT pathway and impeding the interaction between MEF2 and class II HDACs resulted in the additive suppression of cell proliferation (Di Giorgio *et al.*, 2013). This provides evidence for MEF2 as a converging hub downstream of class II HDACs and the PI3K/AKT pathway and may account for the observed effects following SIK inhibition.

As highlighted in Figure 4.14, there was also downregulation of *MCL1* which has shown to be essential for plasma cell survival *in vivo* (Peperzak *et al.*, 2013). Furthermore, Peperzak and colleagues demonstrated that the receptor BCMA was needed to establish high expression of Mcl-1 in bone marrow but not splenic plasma cells suggesting the spleen must contain factors that can substitute for BCMA signalling to induce Mcl-1. With this in mind, downregulation of *MCL1* may contribute to the observed decrease in cell survival in combination with the loss of BCMA (TNFRSF17) which is profoundly downregulated (~6 fold) across activated B-cells, plasmablasts and plasma cells. As myeloma cells critically depend on BCMA in the bone marrow microenvironment, and BCMA downregulation has been shown to strongly decrease myeloma cell viability and colony formation, it is conceivable that SIK inhibition provides a potential treatment strategy to prevent BCMA activation (Tai *et al.*, 2016).

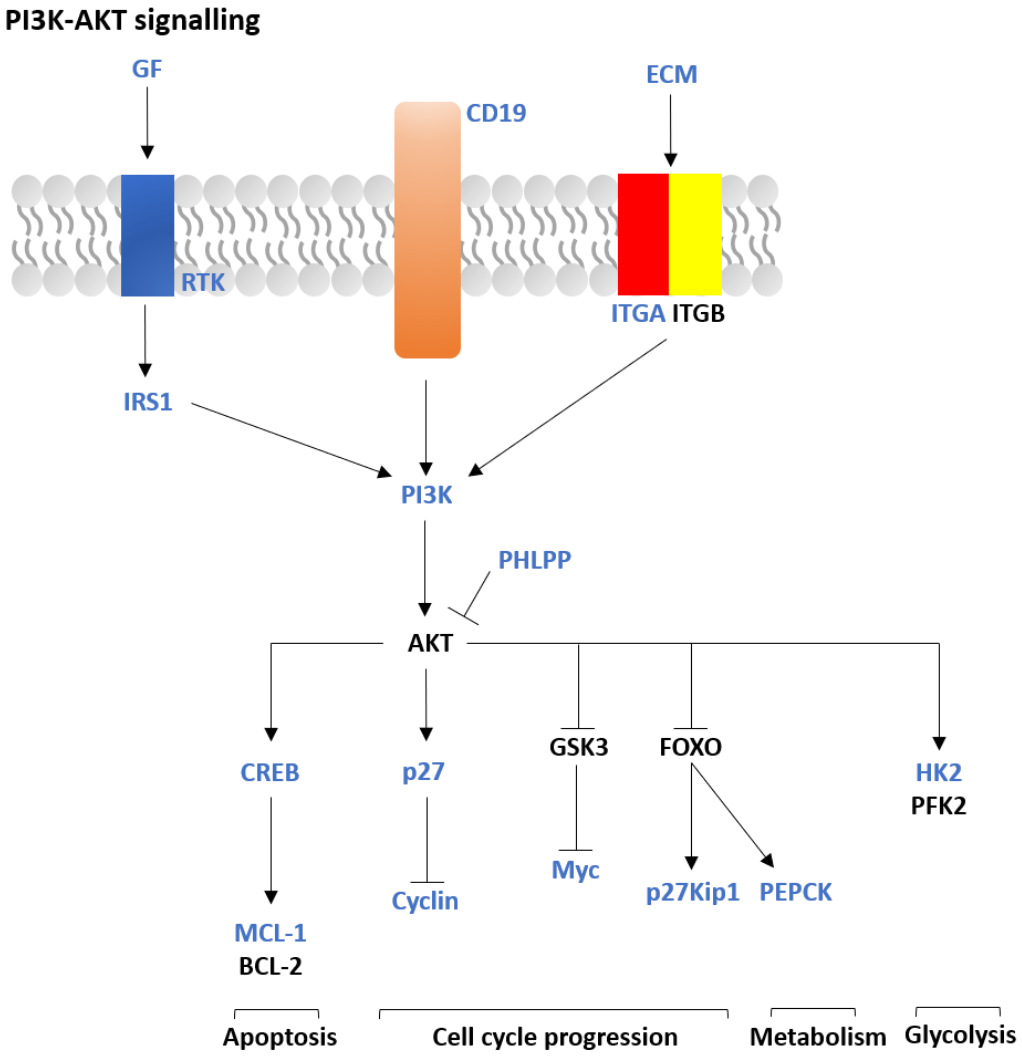

Figure 4.14 Downregulation of genes in PI3K-AKT signalling pathway following SIK inhibition. Genes highlighted in blue are downregulated greater than 0.5 $\log^2$ fold. GF, growth factor; RTK, receptor tyrosine kinase; ECM, extracellular matrix.

As shown in Figure 4.14, PI3K-AKT activation can promote glycolysis to co-ordinate metabolism (Jellusova and Rickert, 2016; Hu *et al.*, 2016). After just 24h inhibition of the SIKs, there was a dramatic decrease in numerous glycolytic genes suggesting profound metabolic collapse (Figure 4.15). Notably, the affected genes are targets of both HIF1α and ATF4 which were identified as part of gene signature enrichment analysis following SIK inhibition. Although the gene expression levels of *HIF1α* and *ATF4* were unaffected by SIK inhibition, HDACs have been shown to directly interact with both ATF4 and HIF-1α to regulate both transcription factor activity and stabilisation (Kikuchi *et al.*, 2015; Kim *et al.*, 2007) and therefore could account for a further mechanism of regulation.

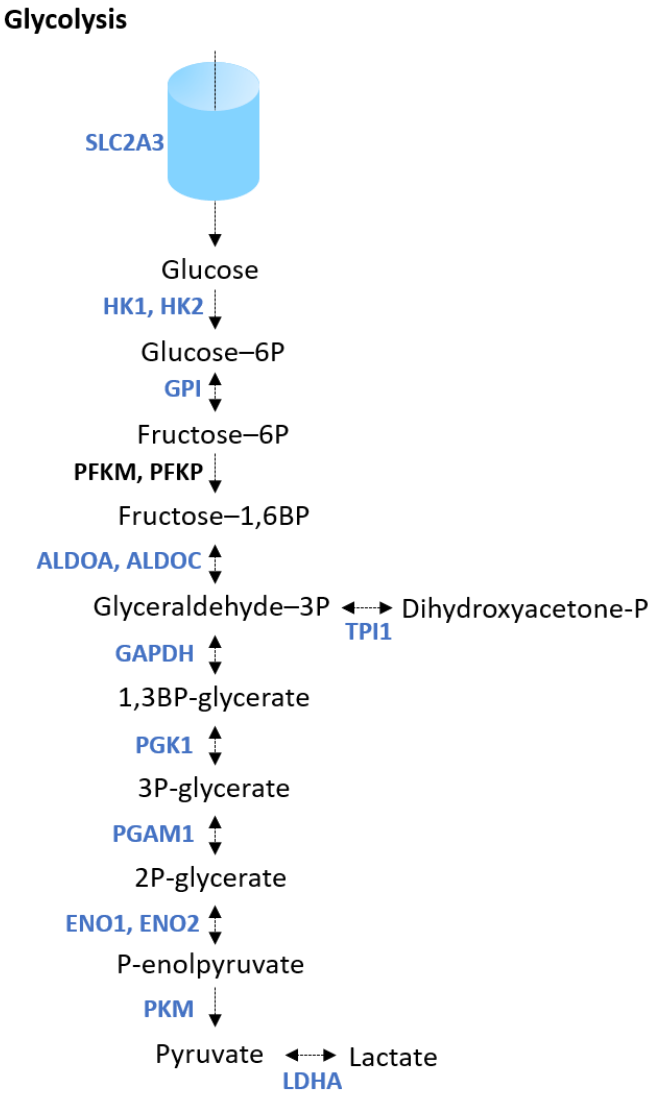

Figure 4.15 Downregulation of genes involved in glycolysis in plasma cells following SIK inhibition. Genes highlighted in blue are downregulated greater than 0.5 $\log^2$ fold.

In both plasmablasts and plasma cells, there was also upregulation of genes involved in endocytosis and lysozyme formation potentially suggesting an attempt at nutrient uptake and recovery (Figure 4.16), similar to what has been demonstrated in *K-Ras* mutant pancreatic ductal carcinoma cells that utilise micropinocytosis to survive amino acid deprivation (Commisso *et al.*, 2013; Davidson *et al.*, 2017) (Figure 4.16). In plasma cells, downregulation of genes including *XBP1, ATF6* and *EIF2AK3* contributed to the signature term 'protein processing in the ER'. ER stress occurs following the accumulation of unfolded/misfolded proteins, thus activating the unfolded protein response (UPR). As a result, splicing of XBP1 to XBP1s by IRE1a, cleavage of ATF6a into an active transcription factor, and phosphorylation of Eif2a by EIF2AK3/PERK ensues in an effort to restore normal function (Ron and Walter, 2007).

Moreover, it has been documented that aggresomes represent a pathway for the catabolism of misfolded proteins and develop when production of misfolded ubiquitinated proteins exceeds the capacity of proteasomes to degrade them (Catley *et al.*, 2006). It is therefore possible that SIK inhibition damages the UPR, leading to the accumulation of ubiquitinated proteins which get shuttled towards the lysosomal pathway in an effort to be degraded. As the bulk of the population does not survive, it is plausible that this process is not sufficient, however conditions of prolonged ER stress can also result in the UPR to commit the cell to a pathway of apoptosis.

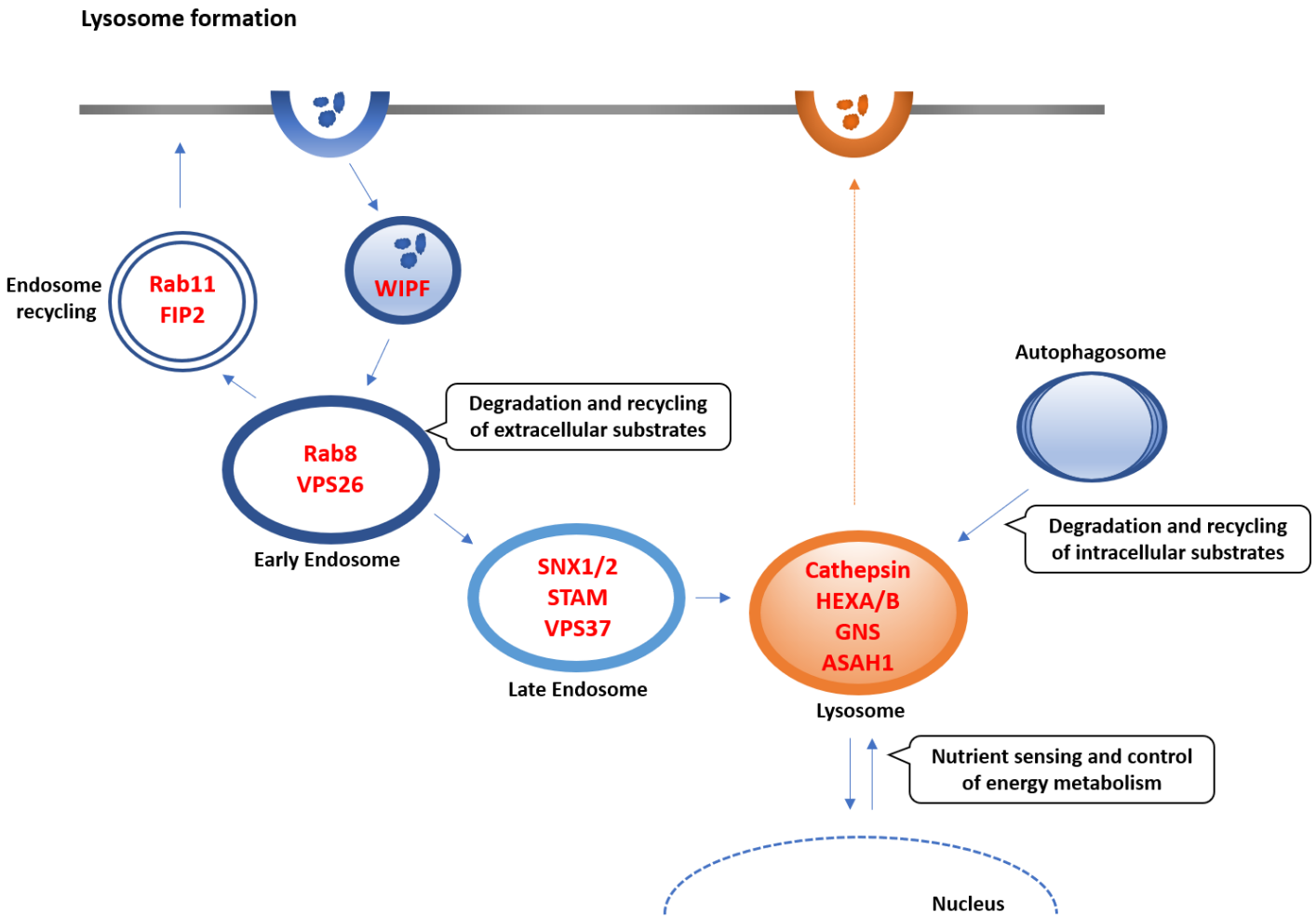

Figure 4.16 Upregulation of genes involved in endocytosis and lysozyme formation following SIK inhibition. Genes highlighted in red are upregulated greater than 0.5 $\log^2$ fold.

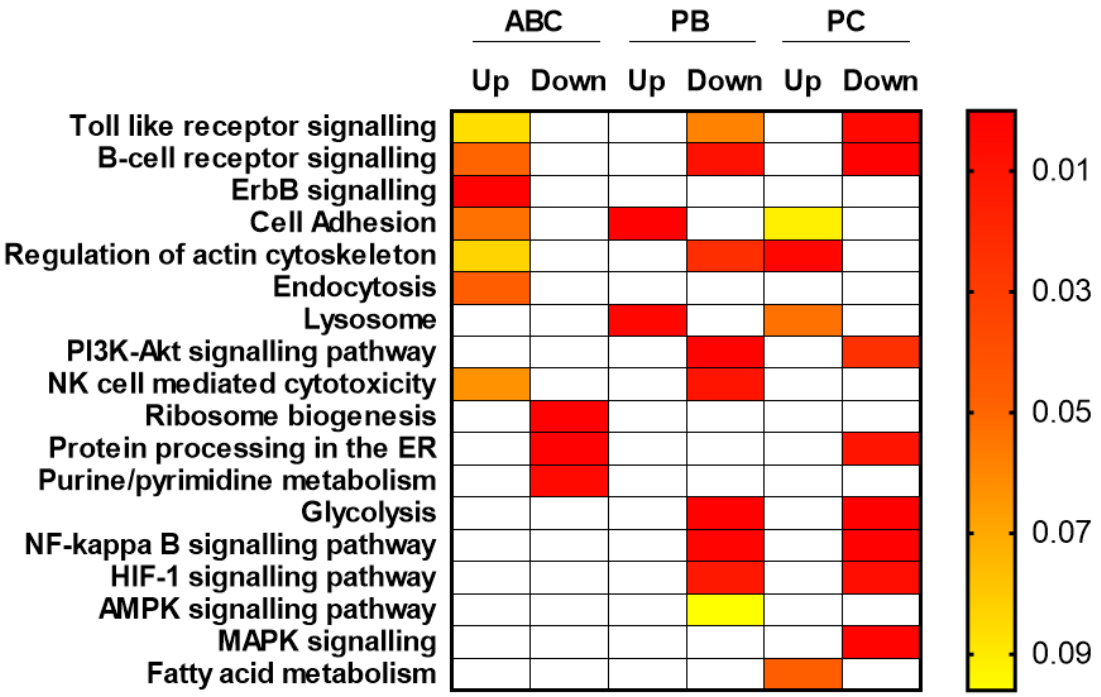

Figure 4.17 Heat map of gene ontology enrichment analysis following SIK inhibition. Summary of up and down-regulated genes involved in numerous biological pathways. ABC, activated B-cell; PB, plasmablast; PC, plasma cell. (p-value <0.05)

In conclusion, this chapter provides an understanding of the pathways influenced by loss of SIK kinase activity (Figure 4.17) and demonstrates several functions that are predominantly regulated by the SIKs including growth and proliferation in activated B-cells, differentiation and survival in plasmablasts as well as secretion and glycolysis in plasma cells. Overall, this highlights that the convergence of various pathways is crucial to the development of a long-lived, productive immune response, although a consistent theme emerged during gene expression analysis highlighting dramatic changes in genes related to metabolic fitness. Furthermore, it is clear from Western analysis that SIKs can regulate class II HDAC expression levels suggesting a potential signalling axis downstream of the SIKs. However, there was no effect on class II HDAC expression in activated B-cells and gene expression generally differed between activated B-cells and ASCs indicative of different downstream mechanisms. This highlights the complex and time-dependent nature of SIK mediated regulation.

Chapter 5 - In vitro generation of murine plasma cells

There are many variations of murine in vitro ASC generation, but the most commonly described technique uses the toll-like receptor 4 (TLR4) agonist, bacterial lipopolysaccharide (LPS). To enhance B-cell activation, T-cell help can be included in the form of co-stimulatory proteins (CD40-L) and cytokines (IL-4). Although conditions such as these are effective at producing plasmablasts, they fail to terminally differentiate into plasma cells and therefore survival is short-lived (Shi *et al.*, 2015). This inability to generate long-lived plasma cells means that studies of normal murine plasma cell biology are limited in an in vitro setting.

To address this issue, a review of both past and present techniques was carried out to identify a set of promising conditions. This led to the adaptation of two model systems used for both human (Cocco *et al*, 2015) and murine (Ozcan *et al,* 2010) B-cell differentiation. Following additional optimisation, two mechanisms of plasma cell generation using TLR and B-cell receptor (BCR) signalling was achieved. The plasma cells generated in each condition were then validated to ensure characteristics such as quiescence and phenotypic markers along with gene expression profile were consistent with in vivo murine plasma cells.

The overall aim of this project is to identify the role of SIKs in terminal B-cell differentiation. This platform provides a resource to sequentially explore each stage of murine plasma cell differentiation and therefore will be used to study the effect of SIK activity on B-cell differentiation in a controlled, cell-autonomous fashion.

5.1 Phenotypic changes in maturing B-cells

ASCs generated in culture typically express the ASC marker CD138 and maintain the B-cell marker B220 (Steinman *et al.*, 1978), however fail to terminally differentiate into plasma cells characterised by loss of the B220 marker and exit from cell cycle. This end point is represented in Figure 5.1 by the red-dashed line.

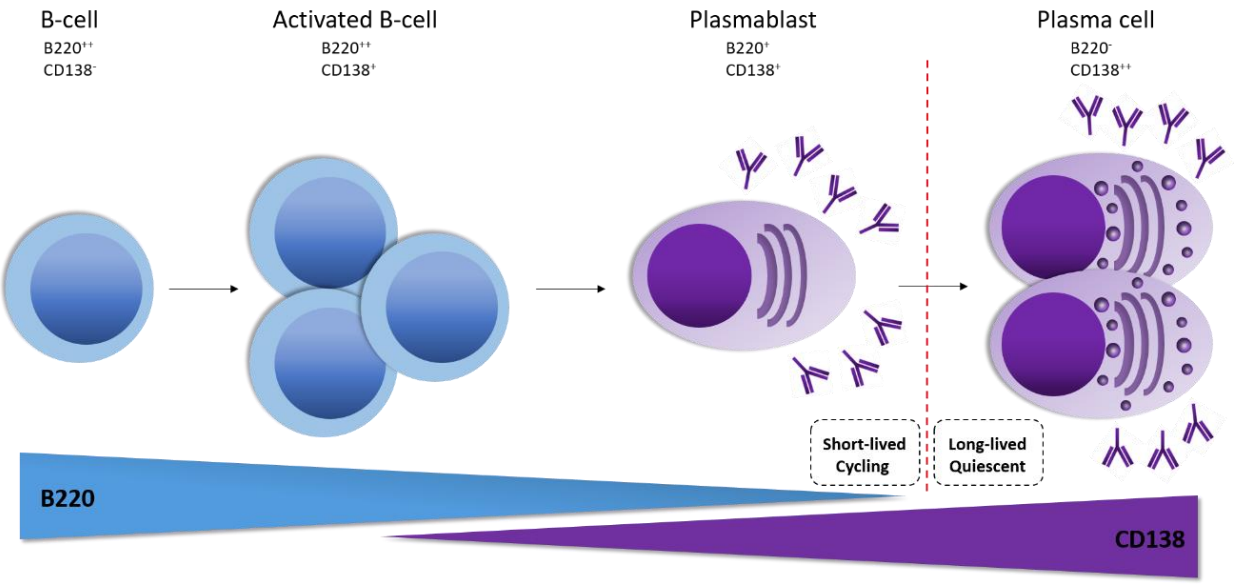

Figure 5.1 Schematic diagram of ASCs generated in vitro. (Adapted from Nutt et al., 2015)

5.2 Comparison of CD40-L stimuli on B-cell activation

Research on B-cells has shown that CD40 engagement is required for numerous processes including antigen presentation, germinal centre formation, isotype switching and affinity maturation and is therefore essential to the generation of long-lived plasma cells (Foy, Durie and Noelle, 1994). To determine the best origin of CD40-stimulus, the effect of both soluble CD40-L and cell-bound CD40-L expressed by irradiated murine fibroblasts on B-cell activation was assessed.

In each condition, there was a small population of non-B-cells ($B220^-$) present at day 1 that did not persist in culture. 24h-post isolation, unstimulated B-cells demonstrated upregulation of CD138 (characteristic of a plasmablast) however by day 6 this population of cells had disappeared. Soluble CD40-L appeared to decrease the percentage of cells expressing $B220^+CD138^+$ at day 1, although by day 6 the overall population looked similar to unstimulated cells. In contrast, cell-bound CD40-L promoted a heterogeneous population of cells as well as a population of $B220^+$ $CD138^+$ cells still present at day 6 (Figure 5.2A).

Cell counts showed that cells survived better following stimulation with cell-bound CD40-L, although cell number decreased in all conditions between day 1 and 6 in culture (Figure 5.2B). As a result, cell-bound CD40-L was used throughout the following experiments.

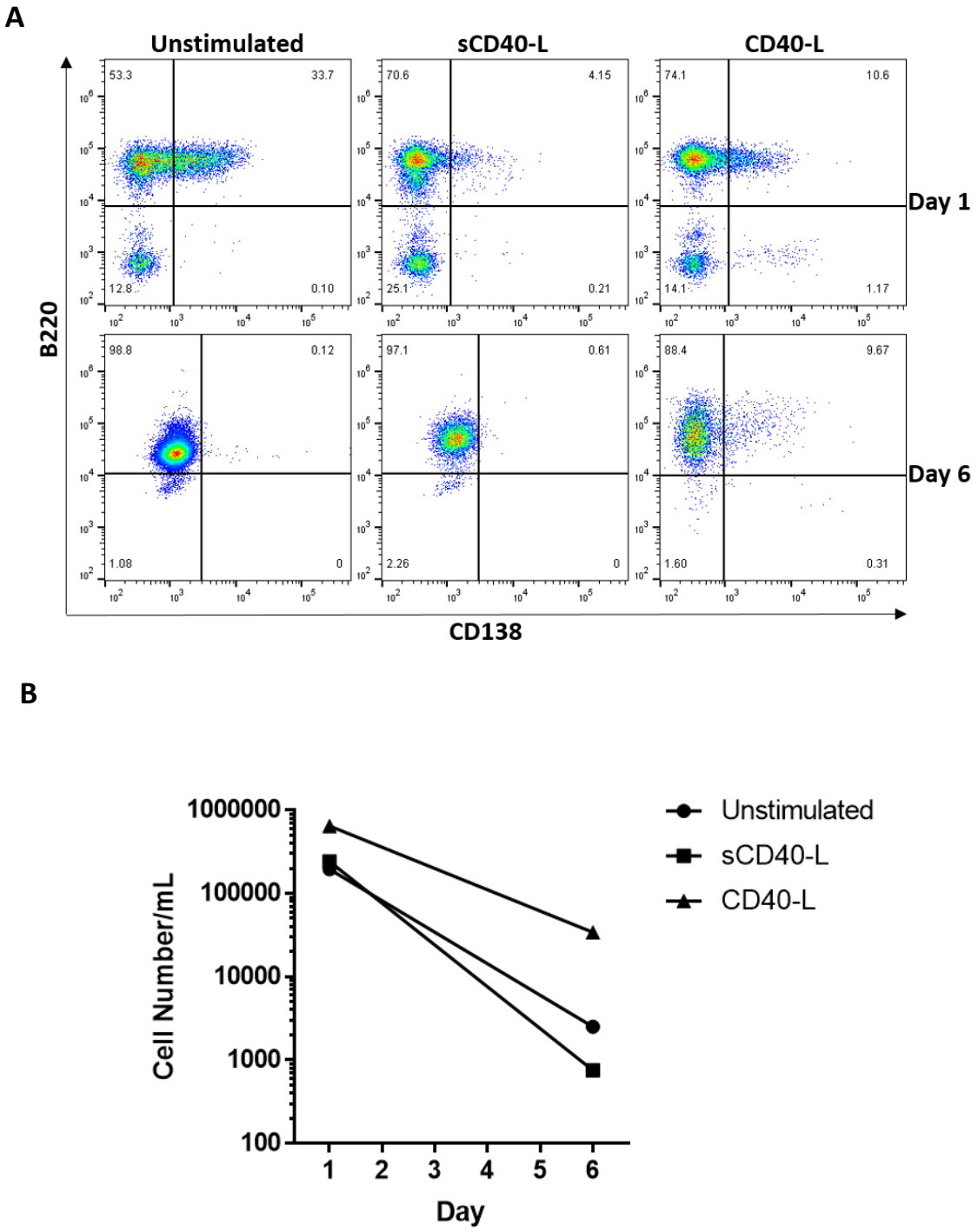

Figure 5.2 Assessing the impact of different forms of CD40-L on B-cell activation. (A) Total B-cells isolated using the pan B-cell isolation kit II were re-suspended in IMDM complete media with either no CD40-L, soluble CD40-L (sCD40-L) or cell-bound CD40-L (CD40-L). On day 1 and 6, cells were phenotyped using antibodies to B220 and CD138. (B) Cell number was recorded using cell counting slides (TC-10 Automated Cell Counter, BioRad).

5.3 Evaluating current methods of generating ASCs

With a source of CD40-L suitable for B-cell activation in place, the next stage was to assess the impact of commonly used cytokines and co-stimulatory proteins on ASC generation including LPS (TLR4 agonist), CpG (TLR9 agonist), $F(ab')_2$ anti-IgM/IgG (BCR) and CD40-L (CD40).

All stimuli were able to generate plasmablasts ($B220^+$ $CD138^+$) between day 2 and 5, however the distribution of both surface markers varied. On day 5, the TLR agonists LPS and CpG resulted in phenotypes consistently associated with being a plasmablast. Alternatively, CD40-L in addition to LPS or $F(ab')_2$ anti-IgM/IgG and IL-4 promoted B220 downregulation and low/intermediate CD138 expression. CD40-L and IL-21 led to two discrete populations at day 2 which resulted in a convincing population of $B220^-$ $CD138^+$ plasma cells by day 5 (Figure 5.3A).

Cell counts revealed that CD40-L/LPS and CD40-L/$F(ab')_2$ anti-IgM/IgG and IL-4 were the only conditions capable of promoting proliferation between day 2 and 5 (Figure 5.3B). Although CD40-L and IL-21 promoted plasma cell generation, the number of these at day 5 was extremely low.

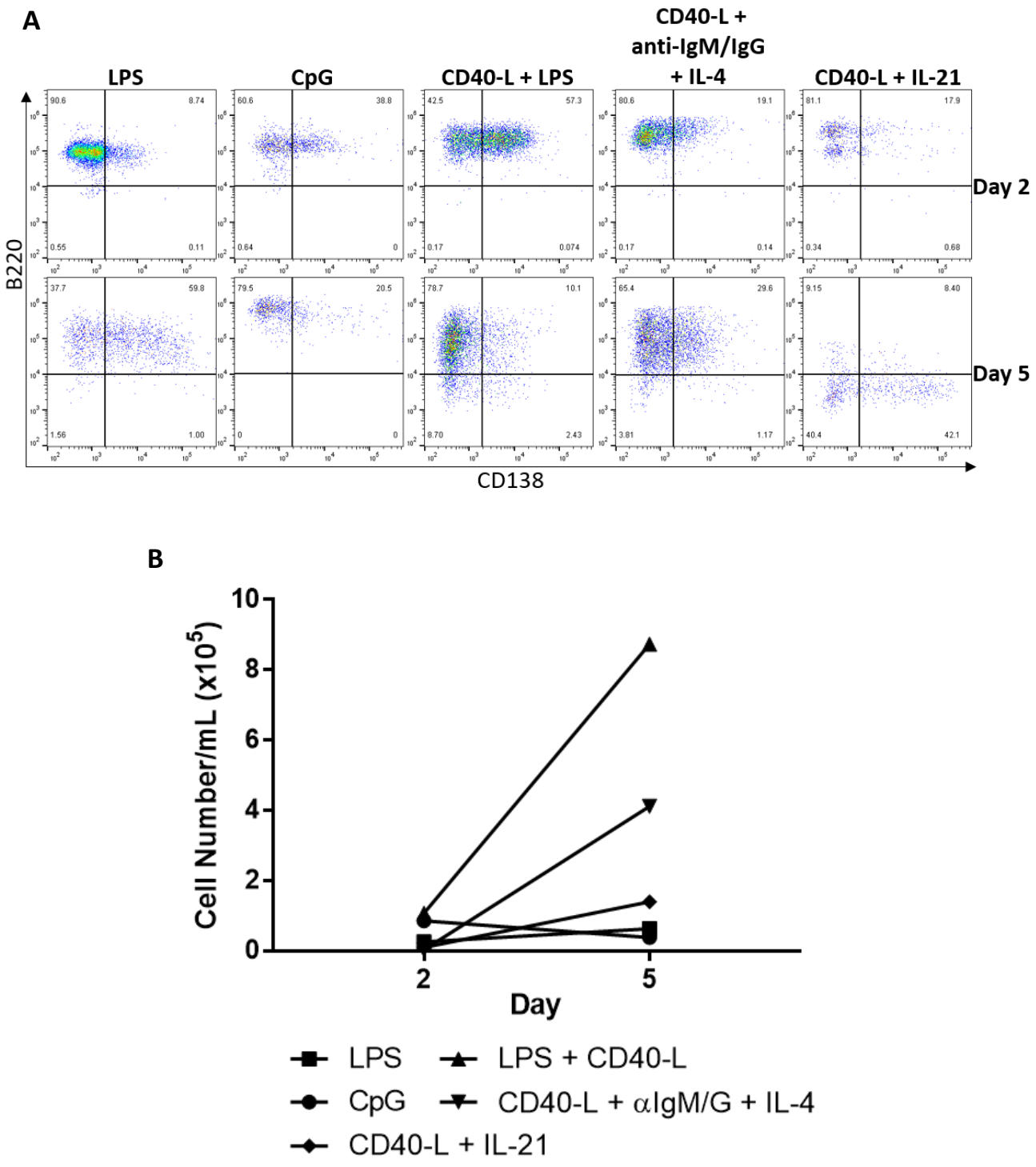

Figure 5.3 Evaluating the effect of cytokines and co-stimulatory proteins on B-cell differentiation. Total B-cells isolated using the pan B-cell isolation kit II were re-suspended in conditions including LPS, CpG, CD40-L + LPS, CD40-L + F(ab')$_2$ anti-IgM/IgG + IL-4 and CD40-L + IL-21 for 5 days. On day 2 and 5, cells were (A) phenotyped using antibodies to B220 and CD138 and (B) cell number was recorded using cell counting slides (TC-10 Automated Cell Counter, BioRad).

5.4 Adaptation of current B-cell differentiation models

To encourage cell differentiation past the plasmablast stage, alternative combinations of cytokines were tested. The first combination was based on a model of human plasma cell differentiation shown to promote the long-term culture of plasma cells (Cocco *et al.*, 2012). In this system, cells are initially cultured with CD40-L, $F(ab')_2$ anti-IgM/IgG, IL-21 and IL-2. On day 3, cells are removed from CD40-L expressing fibroblasts and re-suspended in IL-21 and IL-2. From day 6 the activated human B-cells are exposed to IL-6, IFNα, lipids and amino acids in the presence of a stromal support layer to promote terminal differentiation and survival. Recent unpublished modifications to the system include the substitution of APRIL and gamma secretase inhibitor (GSI) which promote cell surface retention of the receptor for APRIL (Laurent *et al.*, 2015) in lieu of stromal cells to improve survival. To modify this protocol so that it would be suitable for murine B-cells, cells were cultured with CD40-L, $F(ab')_2$ anti-IgM/IgG, IL-21 and IL-4. Cells were then removed from CD40-L expressing fibroblasts at day 2 and kept in the original cytokines. This adaptation was made after a lab member had previously noticed that murine B-cells appeared to differentiate faster than their human counterpart. At day 4, cells were re-suspended in IL-6, IL-21, APRIL and GSI and re-fed every 3 days.

A large proportion of $B220^+$ $CD138^+$ plasmablasts were present 2 days post-stimulation. By day 4, this population began to disperse due to a slight downregulation of B220. Following re-seeding on day 4, cells significantly downregulated B220 and a small population of $B220^-$ $CD138^+$ cells were visible. By day 9 however these had disappeared, suggesting the conditions promoted differentiation but were not suitable for long-term culture (Figure 5.4).

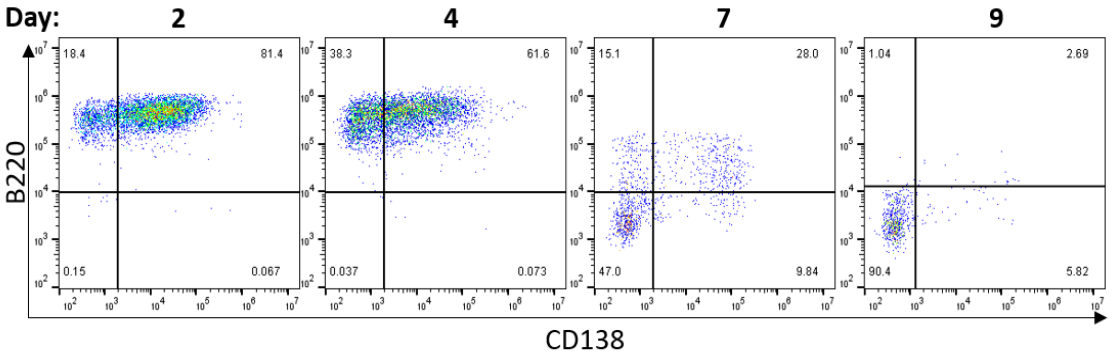

Figure 5.4 Assessing a differentiation system designed for human B-cells. Total B-cells isolated using the pan B-cell isolation kit II were re-suspended in CD40-L, $F(ab')_2$ anti-IgM/IgG, IL-21 and IL-4. On day 2, cells were removed from CD40-L expressing fibroblasts and transferred to a fresh plate. On day 4, cells were re-suspended in IL-6, IL-21, APRIL and GSI. Cells were then re-fed every 2-3 days with IL-6, IL-21, APRIL and GSI. Cells were phenotyped using antibodies to B220 and CD138. Data is representative of 2 individual mice.

A further search of the literature highlighted a promising set of murine conditions in which cells were cultured for 6 days using LPS, APRIL and IL-4 and a population of $CD138^+$ cells, expressing BLIMP-1, IRF4 and the spliced form of XBP-1 were generated (Ozcan *et al.*, 2009). Adaptations to this condition were made at day 0 and included CD40-L and GSI in addition to LPS, APRIL, IL-4. Cells were then removed from CD40-L expressing fibroblasts at day 2 and kept in the original cytokines. Finally, a step was included at day 4 in which the cells were re-suspended in IL-6, APRIL and GSI.

On day 2, the proportion of $B220^+$ $CD138^+$ cells significantly decreased compared with the previous condition suggesting that these cells were undergoing different differentiation kinetics. Following re-seeding, there were two populations present at day 7 – those that still maintained a B-cell phenotype and those that were $B220^-$ $CD138^+$, representative of a plasma cell population. By day 9, the remaining B-cell population disappeared leaving behind the plasma cell population (Figure 5.5).

Combining CD40-L, GSI and IL-6 from the human model and LPS, APRIL and IL-4 from the murine model seemed like a promising approach to generating plasma cells and going forward would form the basis of the model system.

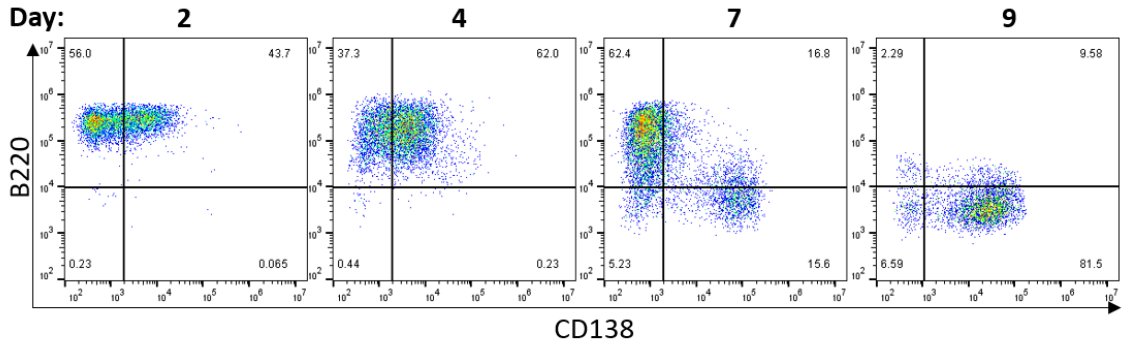

Figure 5.5 Assessing a differentiation system designed for murine B-cells. Total B-cells isolated using the pan B-cell isolation kit II were re-suspended in CD40-L, IL-4, APRIL and GSI. On day 2, cells were removed from CD40-L expressing fibroblasts and transferred to a fresh plate. On day 4, cells were re-suspended in IL-6, APRIL and GSI. Cells were then re-fed every 2-3 days with IL-6, APRIL and GSI. Cells were phenotyped using antibodies to B220 and CD138. Data is representative of 2 individual mice.

5.5 Determining which cytokines are required from day 0

With a working system in place, the next step was to assess which cytokines were absolutely necessary from day 0 to promote plasma cell generation. The full set of cytokines used in Figure 5.5 were compared against conditions which dropped one cytokine out at a time.

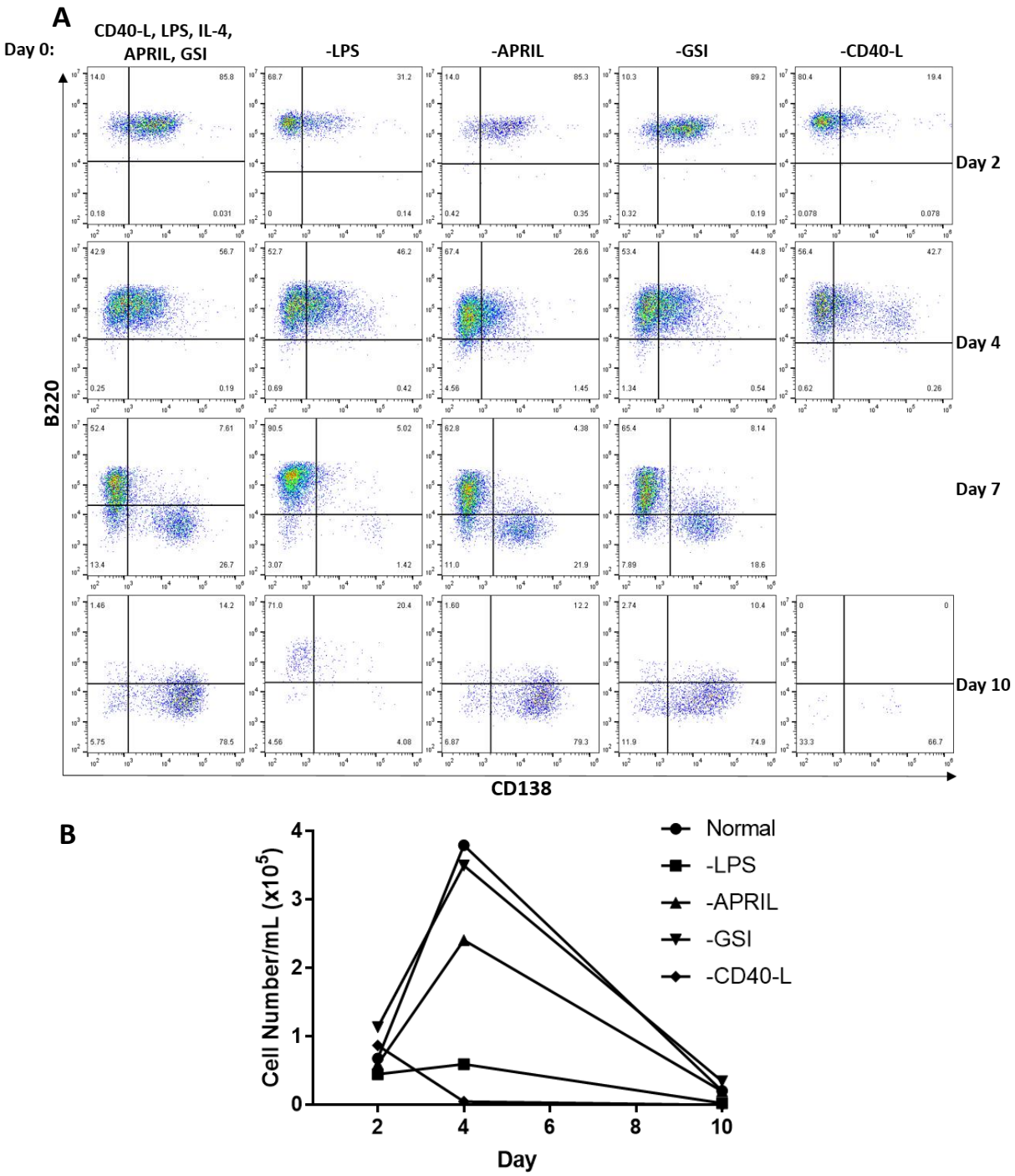

Figure 5.6 The impact of removing each cytokine individually from day 0 on plasma cell generation. (A) Total B-cells isolated using the pan B-cell isolation kit II were re-suspended in CD40-L, LPS, IL-4, APRIL and GSI. Alternative conditions dropped out one cytokine at a time from day 0. On day 2, cells were removed from CD40-L and transferred to a fresh plate. On day 4, cells were re-seeded in IL-6, APRIL and GSI. On day 2, 4, 7 and 10, cells were phenotyped using antibodies to B220 and CD138 and (B) cell number was recorded using cell counting slides (TC-10 Automated Cell Counter, BioRad). Data is representative of 2 individual mice.

Removing LPS alone or CD40-L alone was detrimental to cell proliferation between day 2 and 4 (Figure 5.6B) and as a result there were very few $B220^{-}$ $CD138^{+}$ plasma cells at day 10 (although a small population could be seen at the earlier time points) (Figure 5.6A). Removing APRIL had a minimal effect on phenotype and slightly compromised proliferative capacity whereas removing GSI had no effect on proliferative capacity but resulted in a wider spread of CD138 expression at day 10. These results suggested that CD40-L and LPS in addition to IL-4 are an absolute requirement of long-lived plasma cell generation in vitro.

As removing APRIL and GSI in individual conditions appeared to have little effect on plasma cell generation, the next step was to establish whether removing both at the same time would have any impact. GSI was included to prevent the shedding of the APRIL receptor (Laurent *et al.*, 2015), however its application is likely to have broader effects, that may have some impact on the differentiation process (Thomas *et al.*, 2007). Notably, cells differentiated in a similar manner regardless of whether APRIL and GSI were present. The only observable difference was on day 15, in which there was slight variance in the distribution of CD138. Differences in CD138 expression however, have been observed across multiple experiments suggesting that it is the result of inter-sample variation rather than the effect of removing APRIL and GSI (Figure 5.7).

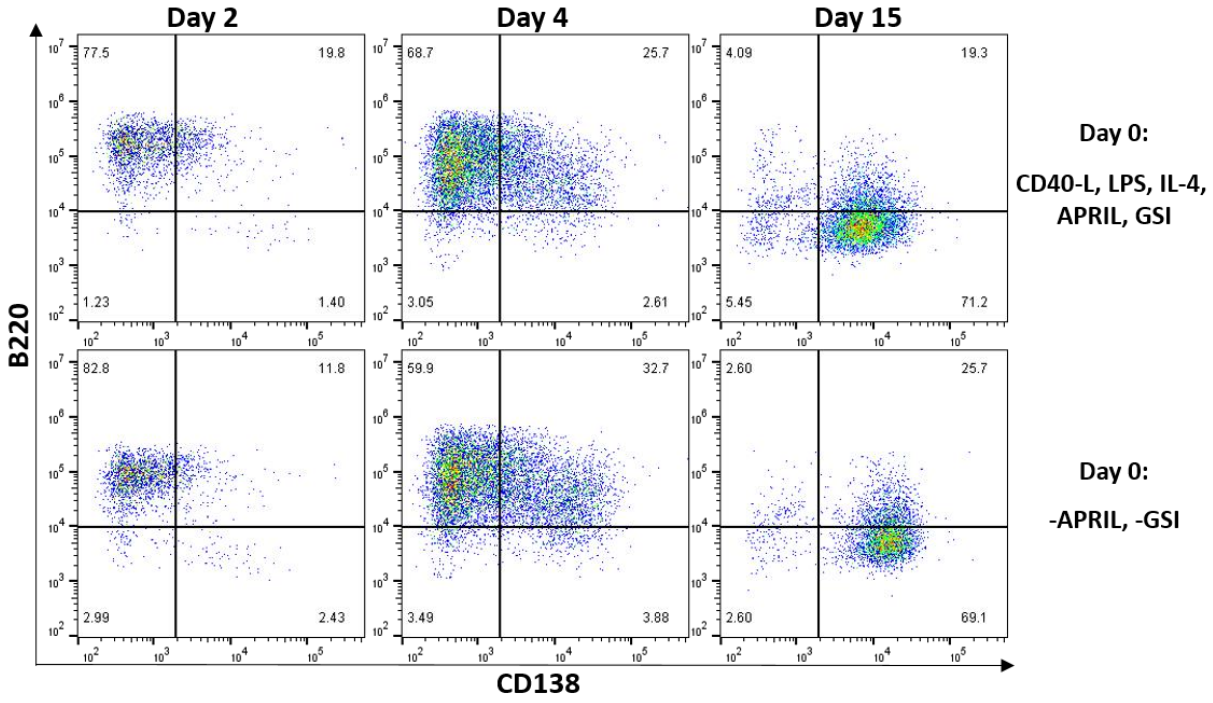

Figure 5.7 The impact of removing both APRIL and GSI from day 0 on plasma cell generation. Total B-cells isolated using the pan B-cell isolation kit II were re-suspended in CD40-L, LPS, IL-4, APRIL and GSI. Alternatively, cells were cultured without both APRIL and GSI from day 0. On day 2, cells were removed from CD40-L and transferred to a fresh plate. On day 4, cells were re-seeded in IL-6, APRIL and GSI. On day 2, 4 and 15 cells were phenotyped using antibodies to B220 and CD138. Data is representative of 2 individual mice.

5.6 Determining which cytokines are required from day 4

After establishing cytokines essential from day 0 (CD40-L, LPS and IL-4), the next step was to determine which were important from day 4 onwards at the point in which re-seeding takes place. As before, the full set of cytokines used at day 4 were compared against conditions which dropped out one cytokine at a time.

Phenotypic profiles were comparable between conditions at both day 7 and 11 (Figure 5.8A), however there were varying effects on cell number (Figure 5.8B). Removing IL-6 resulted in a dramatic reduction in cell number at day 7 and by day 11 the majority of the population had died. Removing APRIL had a small impact on cell number, whereas removing GSI improved cell number quite significantly. This suggests that IL-6 is crucial for long term plasma cell survival in vitro, and although APRIL does not appear to be essential, it does have a positive impact on cell number. Furthermore, as GSI had a negative impact on survival and may be influencing other signalling pathways, a decision was made to remove it from further cultures. Collectively, the data generated in section 5.5 and 5.6 provided the initial conditions of the model system, including CD40-L, LPS and IL-4 from day 0 and IL-6 and APRIL from day 4.

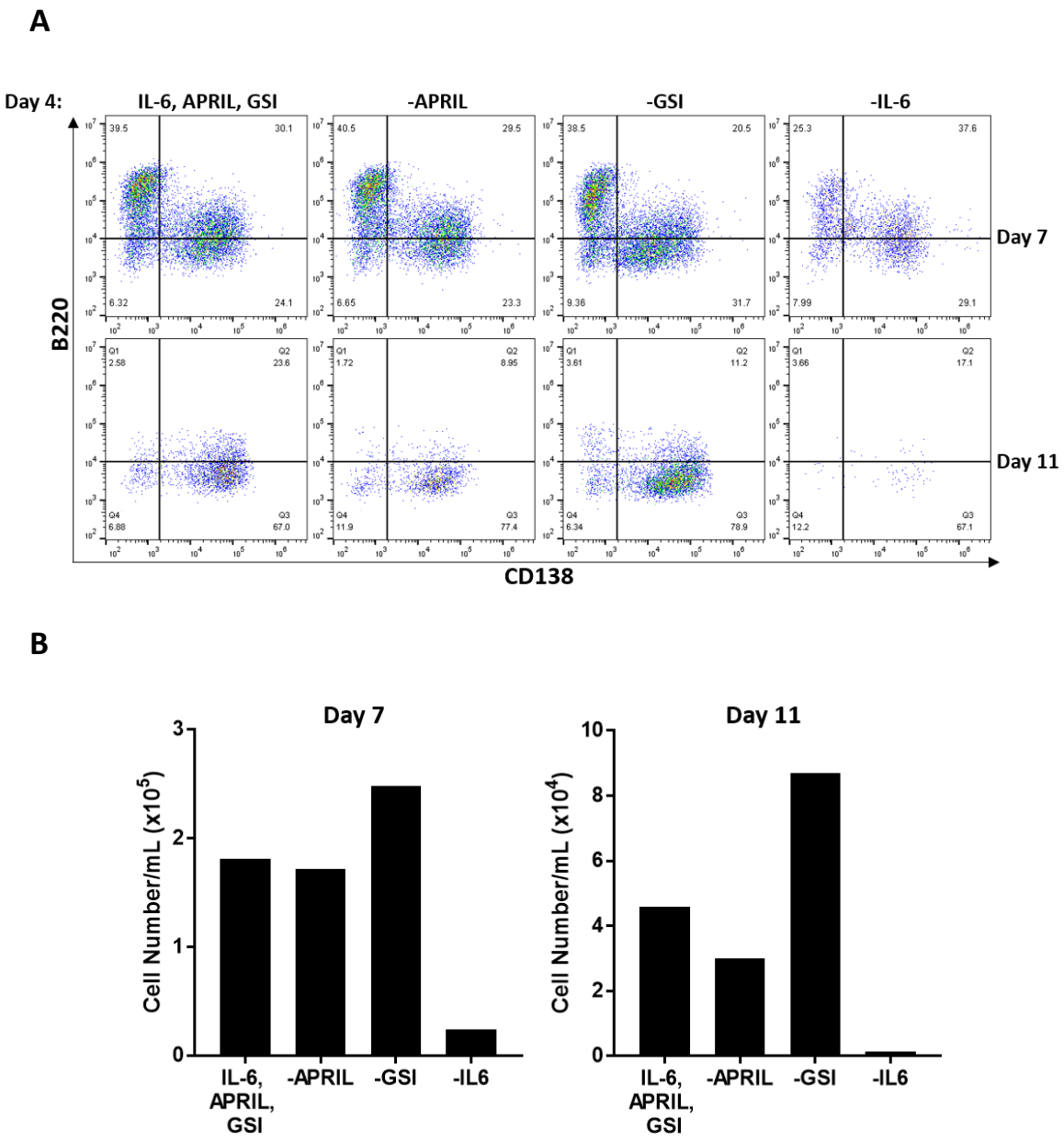

Figure 5.8 The impact of removing each cytokine individually from day 4 on plasma cell generation. (A) Total B-cells isolated using the pan B-cell isolation kit II were re-suspended in CD40-L, LPS and IL-4. On day 2, cells were removed from CD40-L and transferred to a fresh plate. On day 4, cells were re-seeded in various conditions including IL-6/APRIL/GSI, IL-6/GSI, IL-6/APRIL and APRIL/GSI. On day 7 and 11, cells were phenotyped using antibodies to B220 and CD138 and (B) cell number was recorded using cell counting slides (TC-10 Automated Cell Counter, BioRad). Data is representative of 2 individual mice.

5.7 Long term survival

A key feature of a long-lived plasma cell (LLPC) is the ability to survive long term. Typically formed during the germinal centre reaction, LLPCS migrate to bone marrow where they can reside for the lifetime of the host providing long-term immunity (Slifka *et al.*, 1998; Brynjolfsson *et al.*, 2018). Human cultures have demonstrated plasma cell survival past 62 days (Cocco *et al.*, 2012), therefore it was important to determine whether murine plasma cells generated in vitro are capable of surviving for extended periods of time.

On various occasions, cells in culture were still alive between 7 and 15 days post-isolation, however it is plausible that this could have been longer if large amounts of cells had not been sacrificed for phenotypic analysis. A further experiment showed that a population of $B220^{-}$ $CD138^{+}$ plasma cells, as well as a small population of $B220^{-}$ $CD138^{-}$ cells were still present at day 21 in culture (Figure 5.9).

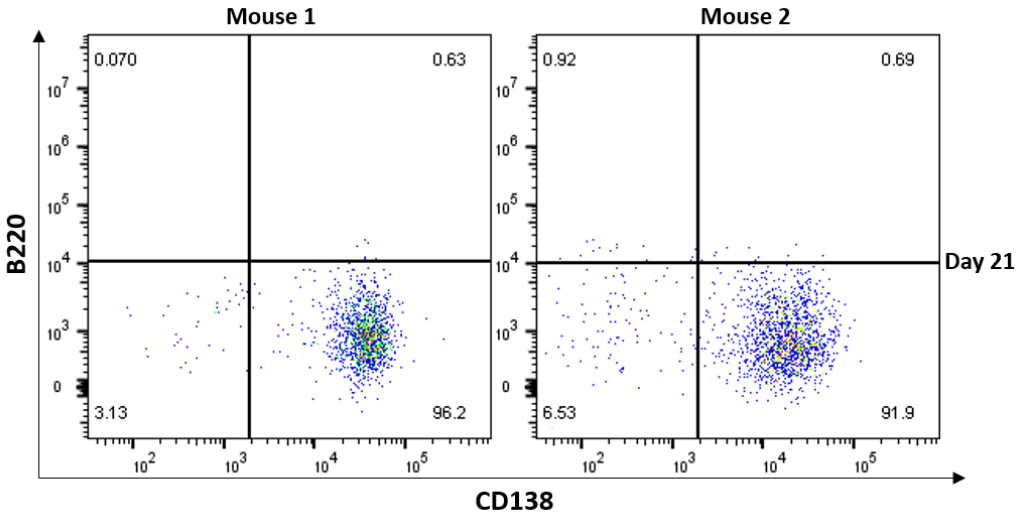

Figure 5.9 Assessing the ability to survive long term. Total B-cells isolated using the pan B-cell isolation kit II were re-suspended in CD40-L, LPS, IL-4. On day 2, cells were removed from CD40-L and transferred to a fresh plate. On day 4, cells were re-seeded in IL-6 and APRIL. On day 21, cells were phenotyped using antibodies to B220 and CD138. Data is representative of 2 individual mice.

5.8 Evaluating marker expression

With established conditions, an overall assessment of marker expression was carried out over a 13 day differentiation. The panel included the APRIL receptors, B-cell maturation antigen (BCMA) and transmembrane activator and CAML interactor (TACI), which have been reported to faithfully identify ASCs in mice (Tellier and Nutt, 2017). Over the time course, downregulation of the B-cell marker B220 mirrored upregulation of the plasma cell marker CD138. In addition, there was slight upregulation of BCMA between day 0 and 4 but this decreased at day 9 onwards. TACI displayed significant upregulation between day 0 and 9, but decreased between day 9 and 13 (Figure 5.10).

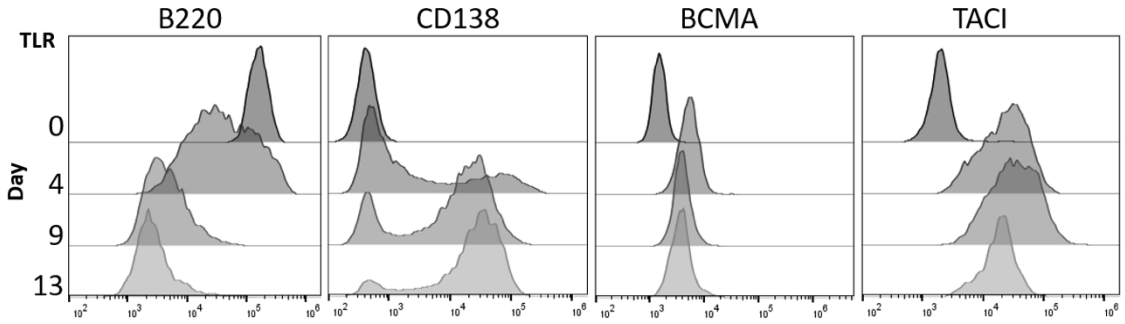

Figure 5.10 Cardinal marker expression in differentiating cells. Total B-cells isolated using the pan B-cell isolation kit II were re-suspended in CD40-L, LPS, IL-4. On day 2, cells were removed from CD40-L and transferred to a fresh plate. On day 4, cells were re-seeded in IL-6 and APRIL. Cells were phenotyped on day 0, 4, 9 and 13 using antibodies to B220, CD138, BCMA and TACI. Data is representative of 2 individual mice.

5.9 Establishing BCR conditions

When BCR stimulation using F(ab')$_2$ anti-IgM/IgG was first tried using the human conditions (Figure 5.4), it didn't appear to support long term plasma cell survival. Following optimisation of the conditions using TLR signalling, the next stage was to re-visit and attempt a system based on BCR signalling. Additional cytokines were incorporated such as IL-5, which has been shown to regulate genes involved in murine B-cell terminal maturation (Horikawa and Takatsu, 2006) and IL-2 which has been identified as a crucial early input in mature B cell fate commitment (Le Gallou *et al.*, 2012) in addition to CD40-L, F(ab')$_2$ anti-IgM/IgG and IL-4.

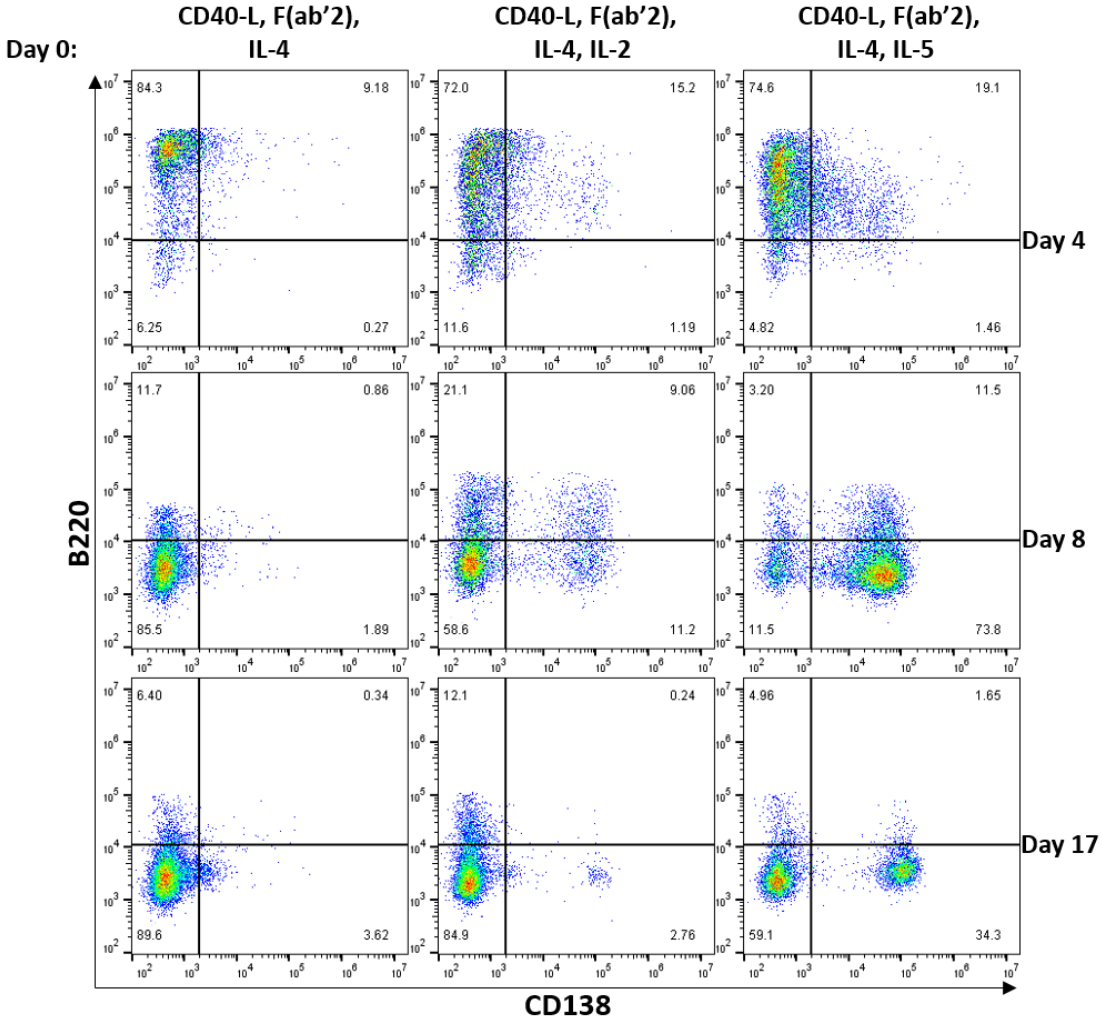

Figure 5.11 The impact of IL-2 and IL-5 on the generation of BCR stimulated plasma cells. Total B-cells isolated using the pan B-cell isolation kit II were re-suspended in CD40-L, F(ab')$_2$ anti-IgM/IgG and IL-4. Alternatively, B-cells were re-suspended in CD40-L, F(ab')$_2$ anti-IgM/IgG and IL-4 plus IL-2 or IL-5. On day 2, cells were removed from CD40-L and transferred to a fresh plate. On day 4, cells were re-seeded in IL-6 and APRIL and re-fed every 3 days. On day 4, 8 and 17, cells were phenotyped using antibodies to B220 and CD138. Data is representative of 2 individual mice.

Substituting F(ab')$_2$ anti-IgM/IgG for LPS without any additional cytokines had a negative impact and as a result, no plasma cells were generated. The addition of IL-2 appeared to improve the percentage of plasma cells to a certain degree (10%), however by the later time point the majority of these had disappeared. IL-5 supported the generation of a substantial population of plasma cells at day 8 (73.8%) that survived for an extended period of time of 17 days (Figure 5.11). In the depicted experiment, cells persisted that were B220$^-$ but did not acquire the cardinal plasma cell marker CD138.. Interestingly, McHeyzer-Williams and colleagues identified a unique and major subtype of antigen-specific memory B-cells (B220$^-$ CD138$^-$) that are distinct from antibody secreting B-cells (B220$^{+/-}$ CD138$^+$) in both the spleen and bone marrow (McHeyzer-Williams, Cool and McHeyzer-Williams, 2000). Furthermore, the B220$^-$CD138$^-$ population initially develops in the primary response, undergoing mutation and affinity-driven selection in the GC, and persists as a major component of the post-GC memory B cell compartment (Driver *et al.*, 2001). This population was observed in multiple experiments to different degrees but was not characterised further.

Cell counts supported flow cytometry data and showed that the addition of IL-5 had the greatest impact on cell number at both day 4 and 8, followed by the addition of IL-2 when compared with no additional cytokines (Figure 5.12).

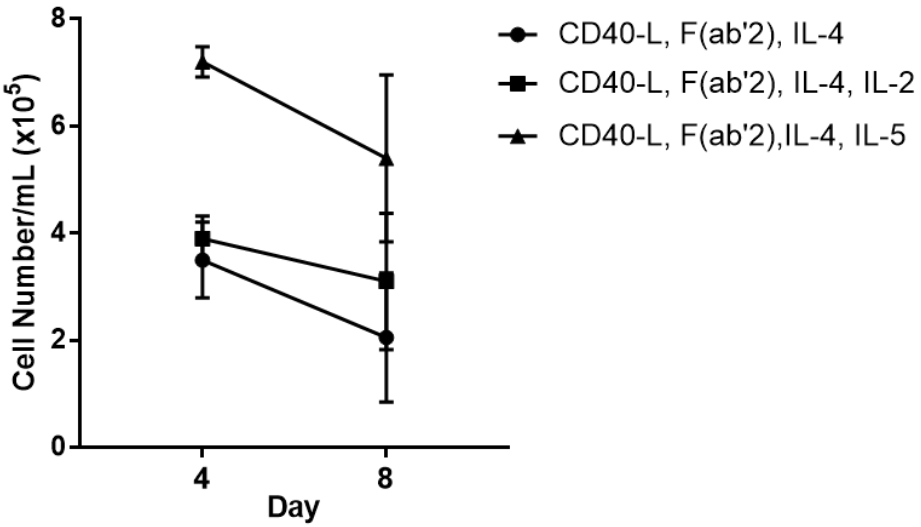

Figure 5.12 The impact of IL-2 and IL-5 on BCR stimulated plasma cell survival. Total B-cells isolated using the pan B-cell isolation kit II were re-suspended in CD40-L, F(ab')$_2$ anti-IgM/IgG and IL-4. Alternatively, B-cells were re-suspended in CD40-L, F(ab')$_2$ anti-IgM/IgG and IL-4 plus IL-2 or IL-5. On day 2, cells were removed from CD40-L and transferred to a fresh plate. On day 4, cells were re-seeded in IL-6 and APRIL and re-fed every 3 days. On days 4 and 8, cell number was recorded using cell counting slides (TC-10 Automated Cell Counter, BioRad). Data is representative of 2 individual mice.

5.10 Addition of growth factors

Plasma cells have high metabolic demands due to their role in antibody synthesis, folding and secretion (Lam and Bhattacharya, 2018). With this in mind, growth factors (lipids and amino acids) were added to the culture at day 4 along with IL-6 and APRIL in an attempt to improve cell survival. Overall, the addition of lipids and amino acids in both TLR and BCR stimulating conditions appeared beneficial with improved cell survival at day 7 (Figure 5.13A) and little effect on phenotype (Figure 5.13B).

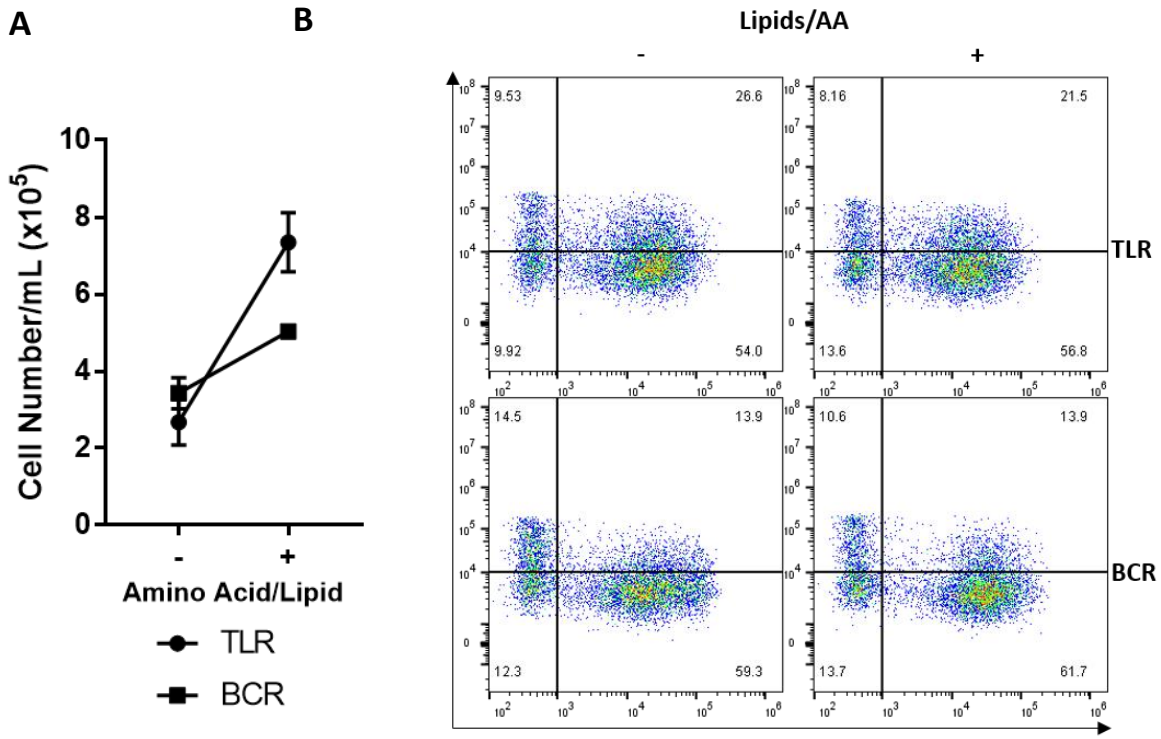

Figure 5.13 The impact of growth factors on plasma cell phenotype and survival. Total B-cells isolated using the pan B-cell isolation kit II were CD40-L, LPS, IL-4, and IL-5 (TLR) or CD40-L, F(ab')$_2$ anti-IgM/IgG, IL-4 and IL-5 (BCR). On day 2, cells were removed from CD40-L and transferred to a fresh plate. On day 4, cells were re-seeded in IL-6 and APRIL with (+) or without (-) growth factors (lipids and amino acids). On day 7 cell number was recorded using cell counting slides (TC-10 Automated Cell Counter, BioRad) and cells were phenotyped using antibodies to B220 and CD138. Data is representative of 2 individual mice.

5.11 Comparison of TLR and BCR conditions

5.11.1 Phenotype

Once TLR and BCR stimulating conditions had been optimised across separate experiments, a direct comparison of the two systems was performed. On day 4, populations appeared similar to one another although there was a decreased percentage of cells expressing $B220^{+}CD138^{+}$ following BCR stimulation. On day 8 overall populations were still comparable, however cells stimulated with BCR conditions appeared as a more discrete population with slightly higher CD138 expression. By day 13, cells generated using TLR stimuli were more discrete but still demonstrated much lower CD138 expression than BCR stimulated cells (Figure 5.14).

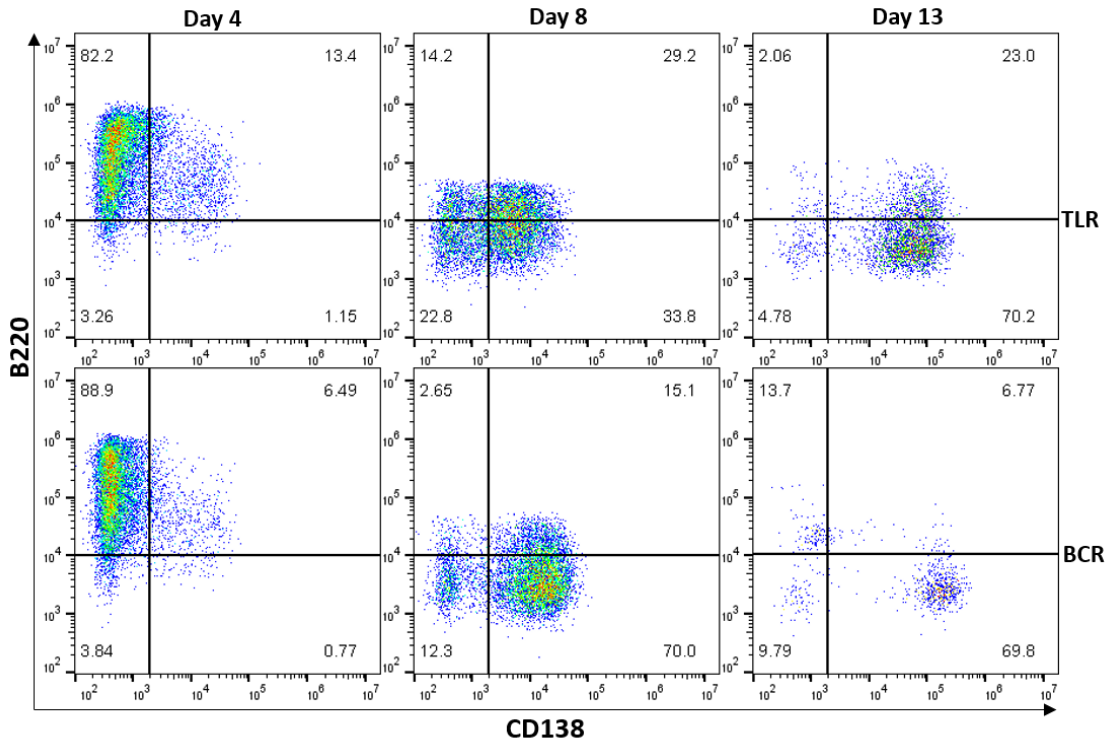

Figure 5.14 Comparing TLR and BCR stimulation. Total B-cells isolated using the EasySep™ mouse B-cell isolation kit were re-suspended in CD40-L, LPS, IL-4, and IL-5 (TLR) or CD40-L, $F(ab')_2$ anti-IgM/IgG, IL-4 and IL-5 (BCR). On day 2, cells were removed from CD40-L and transferred to a fresh plate. On day 4, cells were re-seeded in IL-6, APRIL, lipids and amino acids and re-fed every 3 days. Cells were phenotyped using antibodies to B220 and CD138. Data is representative of 3 individual mice.

5.11.2 Cell number

Cell counts revealed that a high degree of proliferation occurred between day 2 and 4 using TLR stimuli, which was dramatically reduced in cells generated using BCR conditions. Following the proliferative phase, cell number decreased. By day 13, cell number was comparable in both conditions (Figure 5.15).

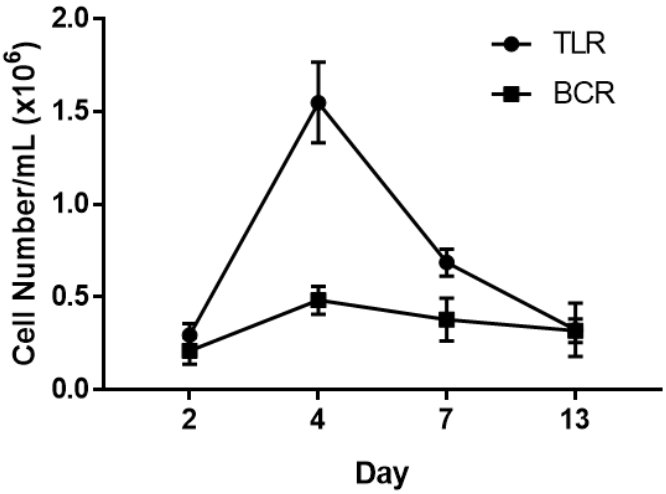

Figure 5.15 The impact of TLR and BCR stimulated B-cells on cell number. Total B-cells isolated using the EasySep™ mouse B-cell isolation kit were cultured using TLR or BCR conditions. Cell number was recorded throughout the differentiation using cell counting slides (TC-10 Automated Cell Counter, BioRad). Results are displayed as the mean ± SD for 3 individual mice.

5.11.3 Growth characteristics

Images of cells taken at day 4 also revealed key differences in growth characteristics. For example, TLR stimulated cells appeared to grow in monolayers whereas BCR stimulated cells grew as dense cell clusters (Figure 5.16).

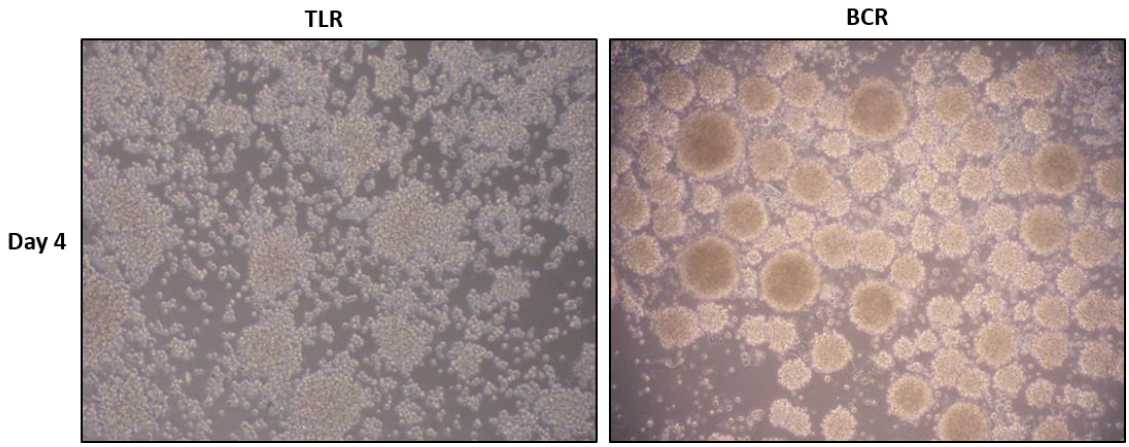

Figure 5.16 The impact of TLR and BCR stimulated B-cells on growth characteristics. Total B-cells were isolated using the EasySep™ mouse B-cell isolation kit and cultured using TLR or BCR conditions. Images were taken on day 4 using a microscope (Olympus CKX41), magnification 20X.

5.12 Influence of medium on cell survival

Due to the high amount of metabolic stress that plasma cell differentiation exerts on cells, IMDM was used as the medium of choice (in line with human cultures) due to its rich formulation. Interestingly, the majority of murine B-cell culture systems report using either RPMI-1640 (Liebig *et al.*, 2010) or DMEM medium (Pellegrini *et al.*, 2007). To evaluate the effect that medium choice can have on differentiating murine B-cells, cells were cultured in either IMDM or DMEM and both phenotype and cell number was recorded.

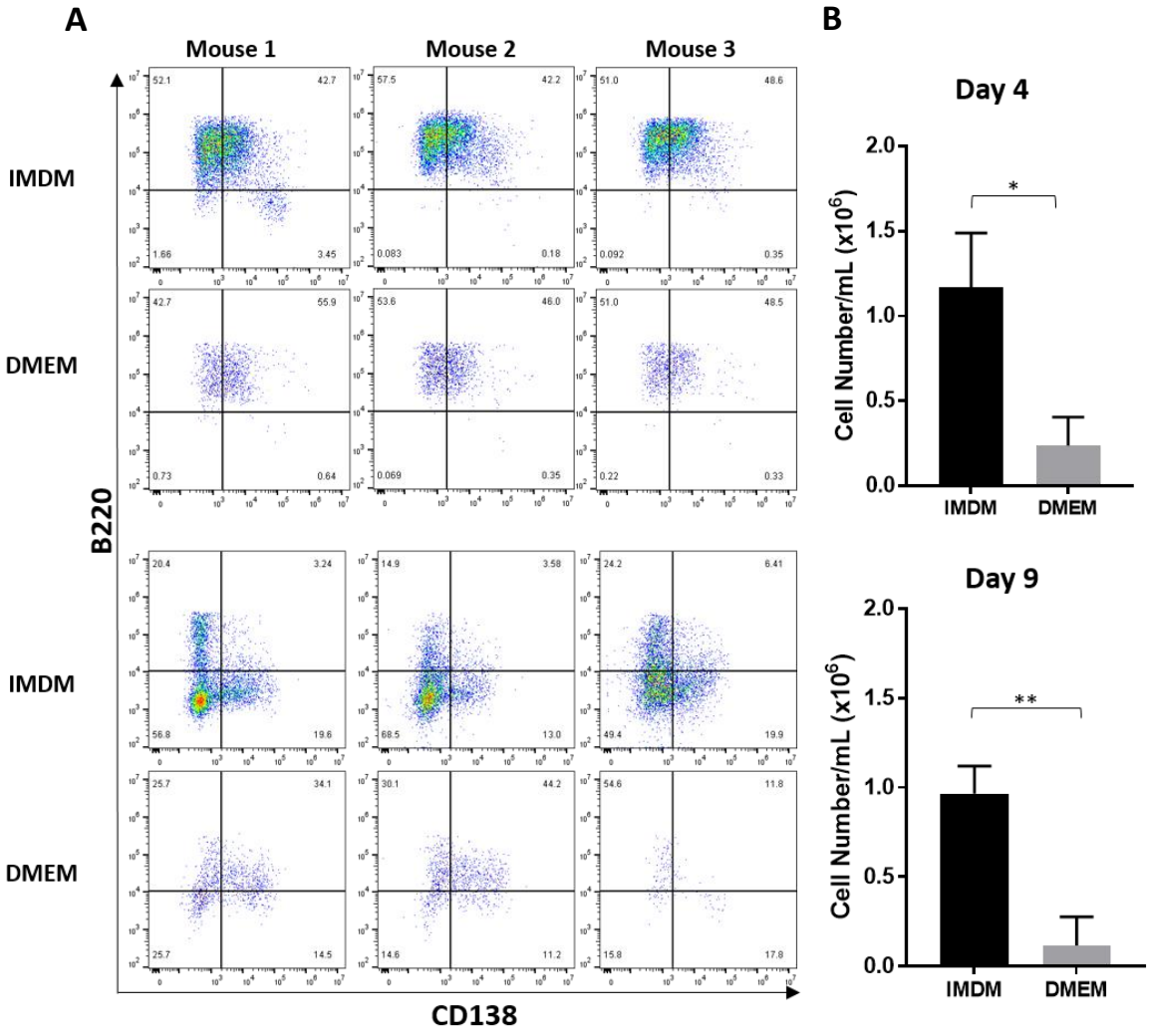

Figure 5.17 The impact of medium choice on murine B-cell differentiation. (A) Total B-cells isolated using the pan B-cell isolation kit II were cultured using TLR conditions in either IMDM or DMEM. On day 2, cells were removed from the CD40-L fibroblast layer and transferred to a fresh plate. On day 4, cells were re-suspended in IL-6 and APRIL in either IMDM or DMEM. On day 4 and 9, cells were phenotyped using antibodies to B220 and CD138 and (B) counted using cell counting slides (TC-10 Automated Cell Counter, BioRad). Results are representative of 3 individual mice.

On day 4 medium choice did not appear to affect phenotype, however on day 9 cells cultured in DMEM did not downregulate B220 as much as those cultured in IMDM (Figure 5.17A). The most striking difference at both time points was a decrease in cell number (around 75%) when cultured in DMEM (Figure 5.17B).

5.13 Evaluating proliferative capacity

The key difference between a plasmablast and plasma cell is the cessation of cell cycle (Oracki *et al.*, 2010). With this in mind, it was important to assess proliferative capacity during both models in vitro differentiation. Cells were loaded with CFSE (Carboxyfluorescein succinimidyl ester) at different time points and division-tracking profiles were generated.

Upon exposure to the stimuli, freshly isolated B-cells initiated extensive proliferation and as a result the dilution of CFSE reached the limit of the assay range by day 4. This was the case for cells stimulated in both TLR and BCR conditions (Figure 5.18).

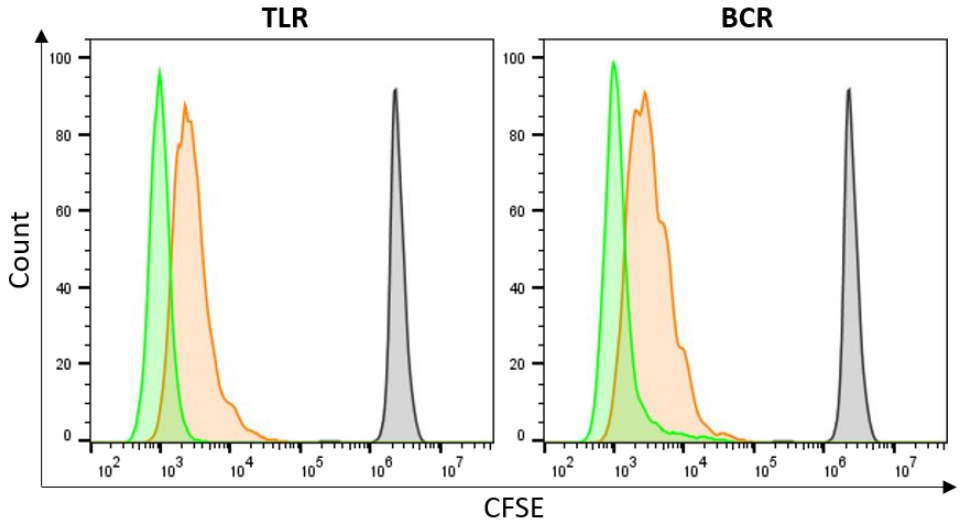

Figure 5.18 Evaluation of proliferative capacity between day 0 and 4. Total B-cells isolated using the EasySep™ mouse B-cell isolation kit were stained with CFSE. Cells were then re-suspended in CD40-L, LPS, IL-4 and IL-5 (TLR)) or CD40-L, F(ab')$_2$ anti-IgM/IgG, IL-4 and IL-5 (BCR). On day 2, cells were removed from CD40-L and transferred to a fresh plate. On day 4, cells were analysed using flow cytometry (CFSE). Histograms show initial loading control (*Grey*), day 4 (*Orange*) and negative control (*Green*).

In a further experiment, cells were loaded at day 4 following re-seeding in IL-6, APRIL, lipids and amino acids and tracked over the course of 3 days. Between day 5 and 6, significant dilution of CFSE occurred, however between day 6 and 7 this decreased suggesting that proliferative capacity begins to decline at day 6. Moreover, the degree of CSFE dilution seemed to suggest that BCR activation triggered a faster rate of proliferation than TLR stimulation although differences were minimal (Figure 5.19).

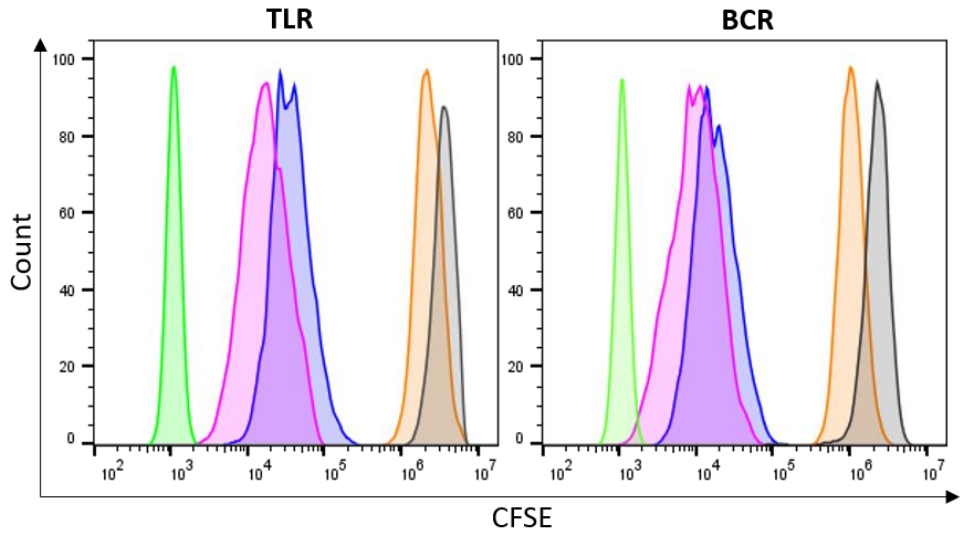

Figure 5.19 Evaluation of proliferative capacity between day 4 and 7. Total B-cells isolated using the EasySep™ mouse B-cell isolation kit were re-suspended in CD40-L, LPS, IL-4 and IL-5 (TLR) or CD40-L, $F(ab')_2$ anti-IgM/IgG, IL-4 and IL-5 (BCR). On day 2, cells were removed from CD40-L and transferred to a fresh plate. On day 4, cells were stained with CFSE, washed and re-suspended in IL-6, APRIL, lipids and amino acids. On subsequent days cells were analysed using flow cytometry (CFSE). Initial loading control (*Grey*), day 5 (*Orange*), day 6 (*Blue*), day 7 (*Pink*), negative control (*Green*).

As Figure 5.19 seemed to suggest that cells were beginning to slow down proliferation, indicative of an upcoming exit from cell cycle, a final experiment was conducted to assess proliferation at a later time point (day 8 onwards). Following loading with CFSE, no further dilution occurred suggesting that cells lose proliferative capacity at around day 8 (Figure 5.20).

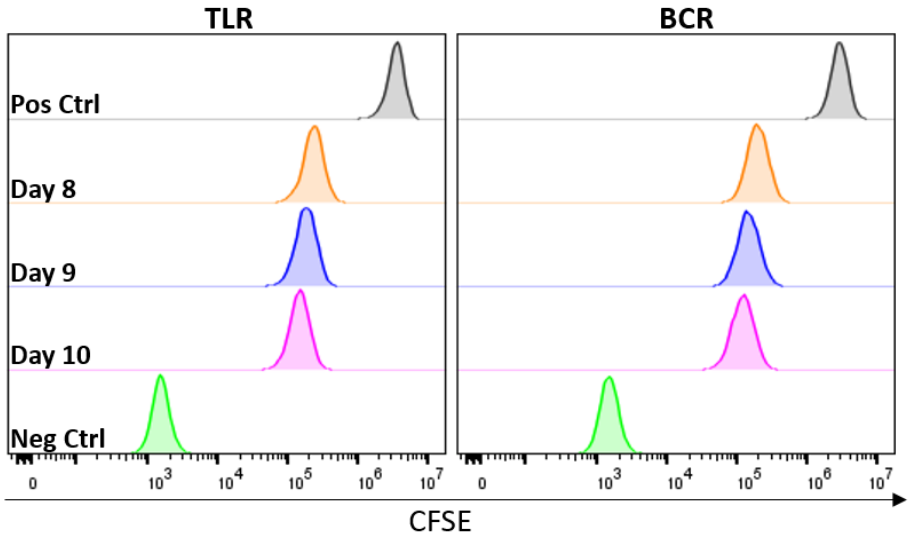

Figure 5.20 Evaluation of proliferative capacity after day 8. Total B-cells isolated using the EasySep™ mouse B-cell isolation kit were re-suspended in CD40-L, LPS, IL-4 and IL-5 (TLR) or CD40-L, $F(ab')_2$ anti-IgM/IgG, IL-4 and IL-5 (BCR). On day 2, cells were removed from CD40-L and transferred to a fresh plate. On day 4, cells were re-suspended in IL-6, APRIL, lipids and amino acids. Cells were stained with CFSE at day 8, and re-suspended in day 4 conditions. On subsequent days cells were analysed using flow cytometry (CFSE). Initial loading control (*grey*), day 9 (*orange*), day 10 (*blue*), day 11 (*pink*), negative control (*green*).

As additional evidence to support cessation of cycling, phenotypic profiles were analysed in conjunction with CFSE over a 4 day time-course. Between day 7 and 8, there was a change in CD138 distribution to form a discrete plasma cell population. After this, phenotype remained stable suggesting that establishment of the plasma cell population and cell cycle exit occur concurrently (Figure 5.21).

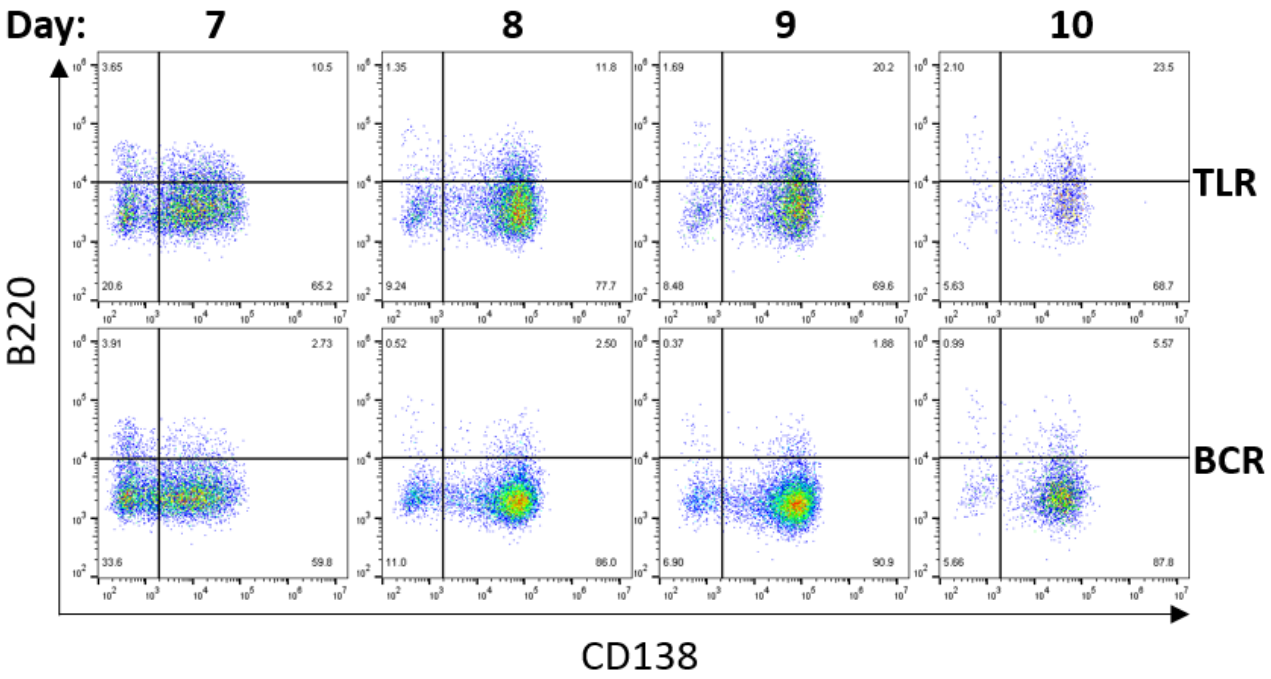

Figure 5.21 Phenotypic characterisation of differentiating B-cells. Total B-cells isolated using EasySep™ mouse B-cell isolation kit were re-suspended in CD40-L, LPS, IL-4 and IL-5 (TLR) or CD40-L, $F(ab')_2$ anti-IgM/IgG, IL-4 and IL-5 (BCR). On day 2, cells were removed from CD40-L and transferred to a fresh plate. On day 4, cells were re-suspended in IL-6, APRIL, lipids and amino acids. Cells were stained with antibodies to B220 and CD138 and analysed using flow cytometry on day 7, 8, 9 and 10.

5.14 Blimp-1 expression

Blimp-1 is a transcriptional repressor able to drive the terminal differentiation of B cells into Ig-secreting plasma cells (Shapiro-Shelef *et al.*, 2003). To confirm Blimp-1 upregulation during culture, *Blimp-1* Venus reporter mice were used (Ohinata *et al.*, 2008). Isolated B-cells were cultured in both TLR and BCR conditions and Blimp-1 expression was tracked over the course of 13 days using flow cytometry.

Blimp-1 expression increased significantly between day 4 and day 7/day 9 consistent with the generation of a $B220^{-}$ $CD138^{+}$ plasma cell population. Interestingly between day 9 and 13, Blimp-1 expression decreased slightly across both samples and conditions (Figure 5.22).

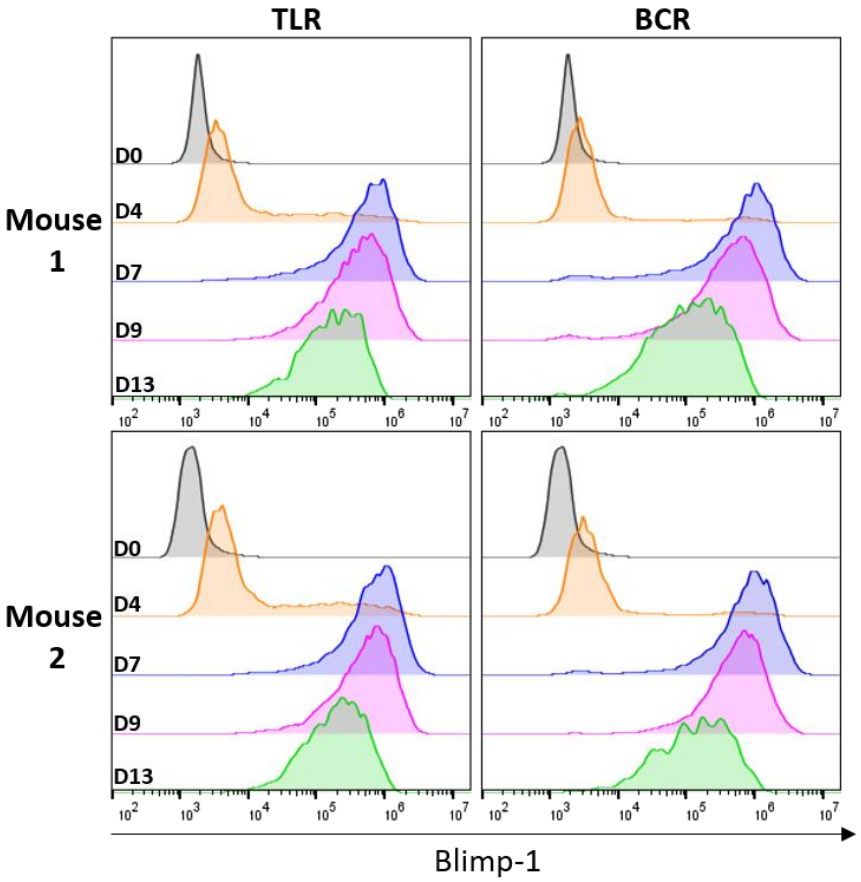

Figure 5.22 Evaluation of Blimp-1 expression during B-cell differentiation. Total B-cells isolated using the EasySep™ mouse B-cell isolation kit were re-suspended in CD40-L, LPS, IL-4 and IL-5 (TLR) or CD40-L, $F(ab')_2$ anti-IgM/IgG, IL-4 and IL-5 (BCR). On day 2, cells were removed from CD40-L and transferred to a fresh plate. On day 4, cells were re-suspended in IL-6, APRIL, lipids and amino acids. Cells generated using both TLR and BCR conditions were analysed using flow cytometry on day 0 (*Grey*), day 4 (*Orange*), day 7 (*Blue*), day 9 (*Pink*) and day 13 (*Green*) for Blimp-1 expression.

5.15 Immunoglobulin secretion

As plasma cells have the functional ability to secrete immunoglobulin, it was also important to determine whether phenotypically maturing cells could both secrete and class switch. Supernatants were collected at day 4, 7 and 11 and analysed using an ELISA.

At day 4, levels of immunoglobulin secretion were low as would be expected. TLR conditions promoted a small degree of IgM secretion and even less IgG, whereas BCR conditions resulted in barely detectable levels of both IgM and IgG. At day 7, both TLR and BCR conditions promoted high levels of IgM-secreting cells and lower levels of IgG. At day 10, TLR conditions promoted even higher levels of IgM whereas BCR conditions produced similar amounts to day 7. IgG increased in both conditions between day 7 and 10 but still remained low (Figure 5.23).

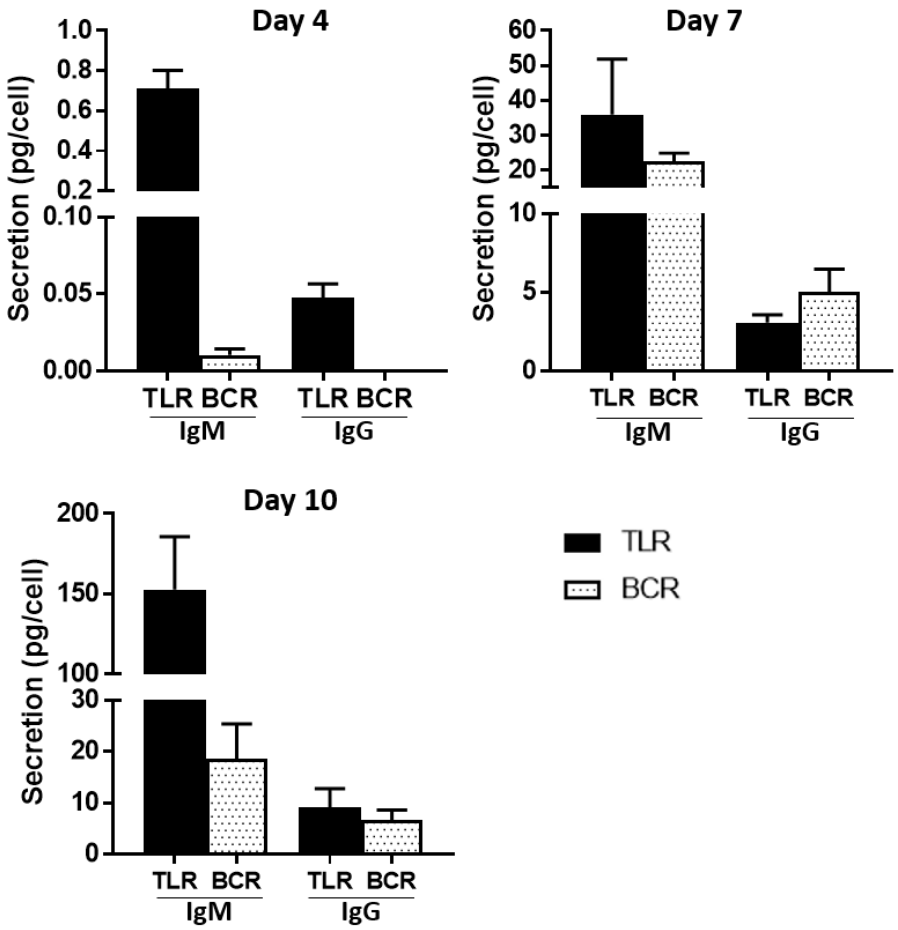

Figure 5.23 Quantification of IgM and IgG secretion. Total B-cells isolated using the EasySep™ mouse B-cell isolation kit were re-suspended in CD40-L, LPS, IL-4 and IL-5 (TLR) or CD40-L, $F(ab')_2$ anti-IgM/IgG, IL-4 and IL-5 (BCR). On day 2, cells were removed from CD40-L and transferred to a fresh plate. On day 4, cells were re-suspended in IL-6, APRIL, lipids and amino acids. Supernatant was collected at day 4, 7 and 10. IgM and IgG concentrations were quantified using an ELISA and normalised using cell counts. Results are representative of 3 individual mice.

5.16 Assessment of 2-NBDG uptake

Lam et al (2018) recently demonstrated that short- and long-lived plasma cells are distinguished by metabolic properties such as nutrient uptake. They reasoned that imported glucose is used both to glycosylate antibodies and to provide spare respiratory capacity, thereby allowing plasma cells to survive long-term. With this in mind, in vitro generated plasma cells were incubated with the fluorescent glucose analogue 2-NBDG for 1 hour and assessed for glucose uptake using flow cytometry.

Results showed that between day 8 and 16 (the period in which plasma cells emerge), 2-NBDG uptake increased in cells stimulated with both TLR and BCR conditions resulting in a bimodal distribution indicative of short- and long-lived populations (Figure 5.24).

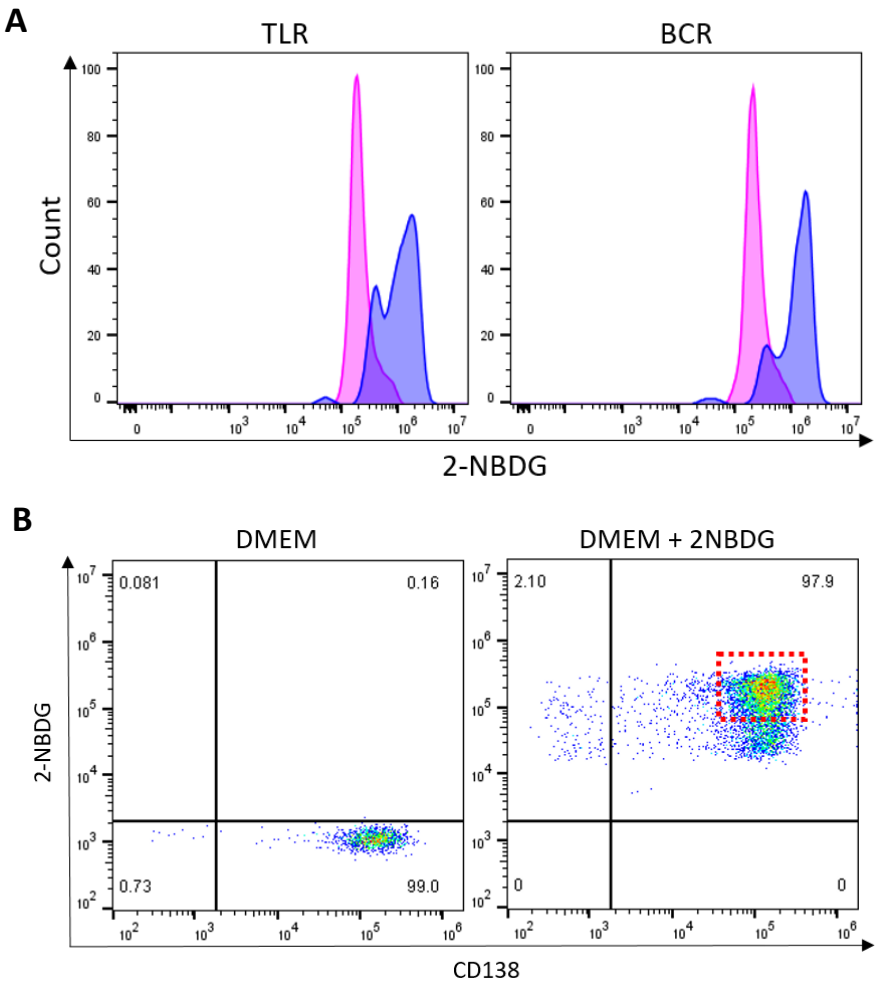

Figure 5.24 Assessing glucose uptake as a determinant of long-term survival. Total B-cells isolated using the EasySep™ mouse B-cell isolation kit were cultured in TLR or BCR conditions. On day 8 and 16, cells were incubated with DMEM and 2-NBDG for 1 hour, stained with CD138 and analysed using flow cytometry. (A) Histogram plot represents 2-NBDG uptake on day 8 (pink) and day 16 (purple). (B) Dot plot represents CD138 expression and 2-NBDG uptake on day 16 in BCR stimulated cells. The $CD138^{+}$ cells demonstrating increased capacity for 2-NBDG internalisation are highlighted in red.

5.17 Gene expression analysis

The differentiation of activated B-cells into ASCs requires co-ordinated changes in the expression of many hundreds of genes and the data from Shi et al. convincingly demonstrates that current in vitro protocols fail to generate cells that match bone marrow-derived LLPCs. To provide evidence that the transcriptome of ASCs generated using the BCR and TLR conditions exhibited progressive plasma cell characteristics, gene expression profiling was performed at multiple time points across the system (day 0, 4, 7 and 10).

Although comprehensive bioinformatic analysis is yet to take place, initial gene expression profiling of individual genes appeared to suggest that late time points are indeed plasma cell-like in both BCR and TLR conditions with high expression of genes such as *Irf4, Prdm1 and Xbp1*. Furthermore, plasma cells appeared distinct from the in vitro versions demonstrated by Shi and colleagues and instead displayed a common gene program consistent with bone marrow plasma cells (Shi *et al.*, 2015). Finally, the expression of *Hells* (a marker of proliferation) appeared most prominent at day 4 and decreased as cells approached terminal differentiation, consistent with the exit from cell cycle that accompanies maturation (Figure 5.25).

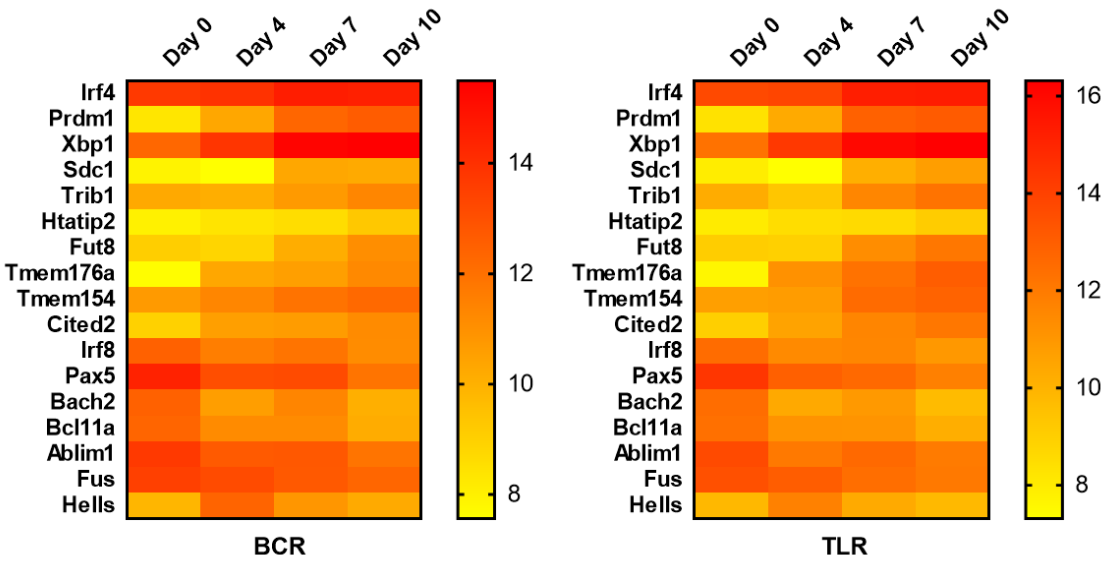

Figure 5.25 Heat map of gene expression during B-cell differentiation. Total B-cells isolated using the EasySep™ mouse B-cell isolation kit were stimulated with BCR or TLR conditions. On day 0, 4 and 7 and 10, RNA was isolated and prepared for sequencing. Log_2 FKPM expression values of genes are shown.

5.17.1 Functional annotation

Hierarchical clustering of differentially expressed genes were used to compare TLR and BCR conditions and to establish recurring general patterns of gene regulation. The biological significance of each cluster was also assessed by analysis of gene ontology (Figure 5.26).

Cluster 1 contained genes strongly induced by TLR stimulation and included typical UPR genes such as *Xbp1* and *Herpud1*, as well as immunoglobulin. Cluster 2 consisted of genes that are more highly repressed by BCR stimulation, the most prominent of which are MHC-encoding genes. Cluster 3 was characterised by genes that were rapidly induced, more strongly by TLR and then declined over time. Cluster 4 was similar to cluster 3 in terms of kinetics, but with BCR providing the dominant effect. This cluster had a prominent cell cycle component, consistent with the early phase of proliferation. Cluster 5 contained BCR induced genes that slowly accumulate and are highly expressed at the final time point. The fact that several key signaling pathways are overrepresented is suggestive that BCR-generated plasma cells may be more receptive to secondary signaling events. Finally, cluster 6 was comprised of genes typifying NK/T cell type responses that are more strongly downregulated by TLR stimulation. Overall, this highlights key differences between ASCs generated using TLR and BCR conditions at the transcriptome level.

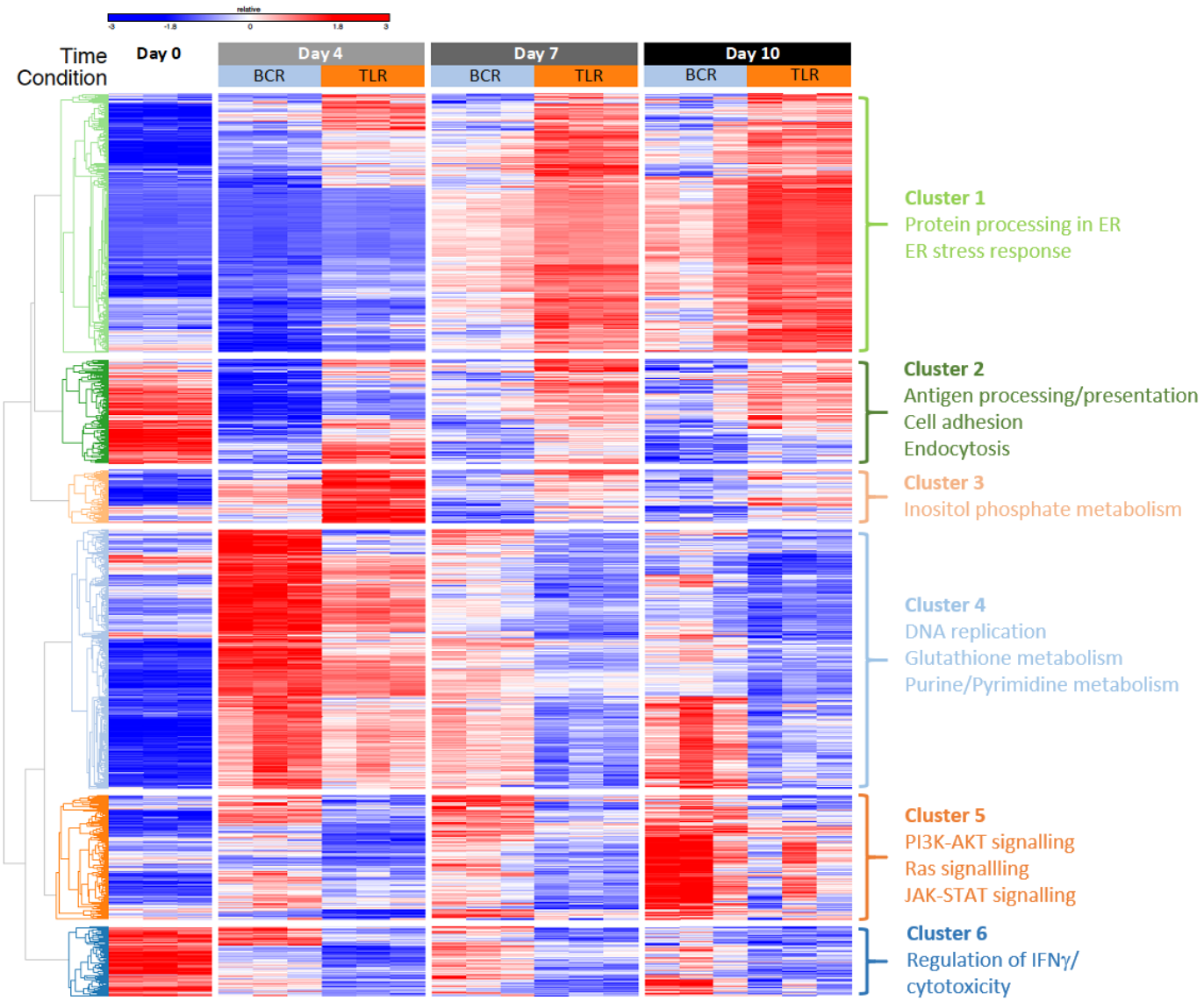

Figure 5.26 Cluster analysis and functional annotation of differentially regulated genes during in vitro B-cell differentiation.

5.17.2 Immunoglobulin genes

As further evidence for class-switch recombination, immunoglobulin heavy chain transcripts were evaluated from day 10 samples. Multiple V, D and J family transcripts were observed indicating that plasma cells undergo polyclonal expansion similar to the human system (Cocco *et al.*, 2012). Additionally, multiple isoforms were expressed. Notably, IgG1 was the most common transcript however IgA and IgE were also evident providing a useful tool for studying class switch recombination conditions (Figure 5.27).

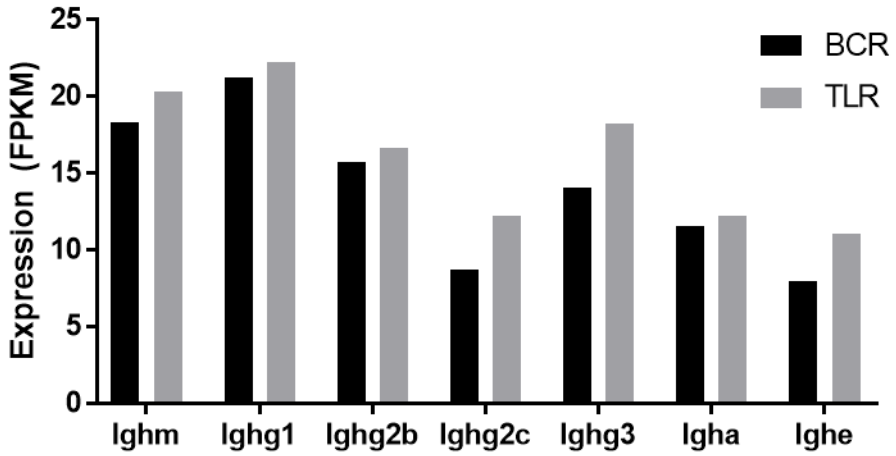

Figure 5.27 Heavy chain transcript analysis. Log_2 FKPM expression values of genes are shown.

5.18 Using the system to address questions about plasma cell biology

With a validated model of murine plasma cell differentiation in place, the next step was to assess the system's applicability to address questions about plasma cell biology using established genetic models. Previous work by Morgan et al. has shown that the mouse *Prdm1* gene has 3 alternative promoter regions (1A, 1B and 1C) which could play important roles in generating regulatory diversity (Figure 5.28).

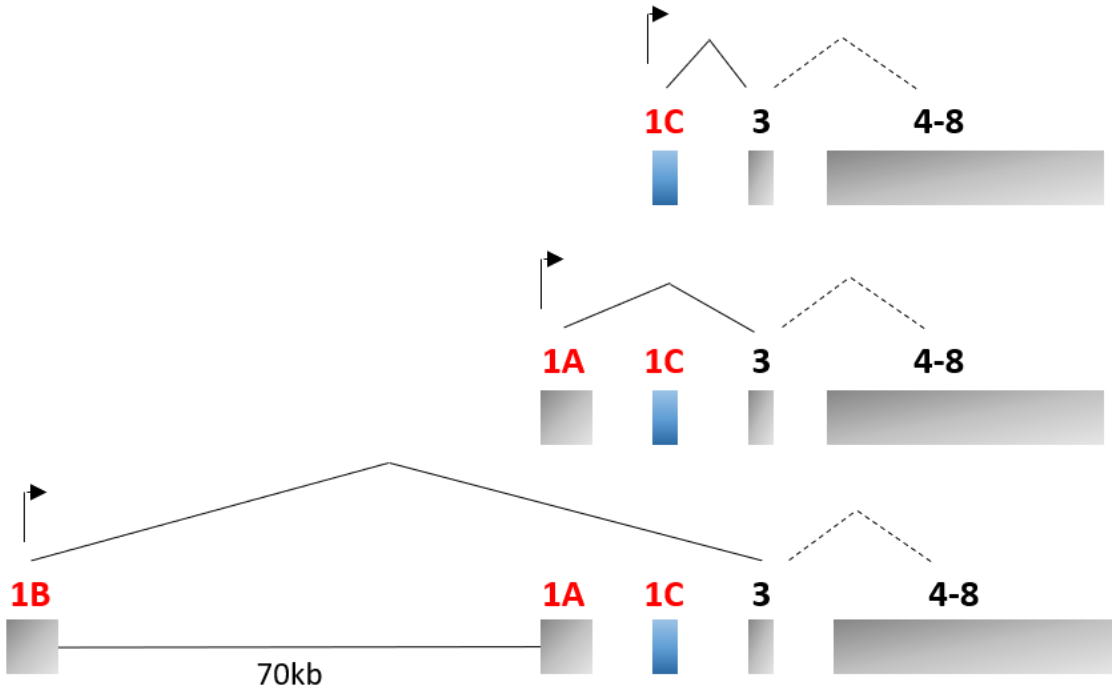

Figure 5.28 Schematic of *Prdm1* alternative promoters. Exons 1 to 3 are depicted with exons 4 to 8 shown in a condensed format. Black arrows indicate transcription start sites. The alternative first exon, exon 1B, and the previously characterised exon 1A both splice directly to exon 3. Transcripts originating from exon 1C retain the intervening intron upstream of exon 3.

Deletion of exon 1A (Δ*ex1A*) leads to the loss of Blimp-1 expression in LPS treated splenocytes in addition to defective IgM secretion (Morgan *et al.*, 2009), leading to the conclusion that exon 1A deletion eliminates Blimp-1 function in the B-cell lineage. Consequently, questions have been raised concerning regulation of *Prdm1* expression by different promoter usage. To investigate this further, the effect of exon 1A deletion on both TLR and BCR generated plasma cells was assessed. B2-cells were isolated from wild type and Δ*ex1A* mice and cultured in LPS alone, TLR or BCR conditions.

5.18.1 Differentiation capacity

When stimulated with LPS, day 4 results appeared to confirm what had been seen by Morgan and colleagues after a 3-day culture, with more of the WT cells displaying a phenotype consistent with differentiation than the Δ*ex1A* cells. However, by day 7 this had changed and a proportion of the Δ*ex1A* cells were characteristically more plasma cell-like than the WT cells (Figure 5.29A). Cell number was also higher in the Δ*ex1A* cells throughout the differentiation (Figure 5.29B).

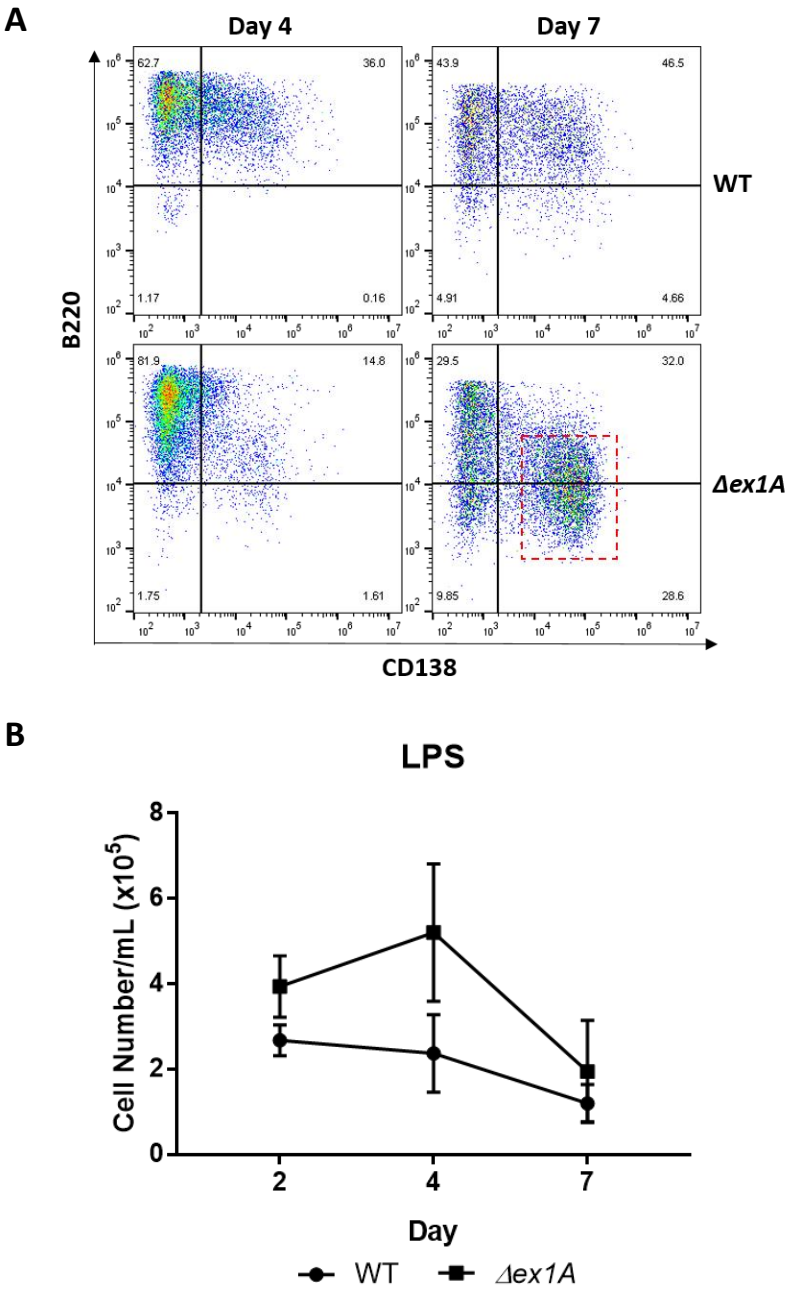

Figure 5.29 Evaluating the impact of Δ*ex1A Prdm1* on B-cell differentiation following stimulation with LPS. (A) Total B-cells isolated using the EasySep™ mouse B-cell isolation kit were stimulated with LPS (5ug/mL). On day 4 and 7, cells were stained with antibodies to B220 and CD138 and analysed using flow cytometry. (B) On day 2, 4 and 7, cells were counted using cell counting slides (TC-10 Automated Cell Counter, BioRad). Dashed red line indicates plasma cell population. Results are displayed as the mean ± SD for 3 individual mice.

Cells were also cultured in TLR and BCR conditions to establish whether plasma cells could be generated in the improved culture system. Under TLR conditions, Δ*ex1A* cells were able to generate plasma cells similar to the WT (Figure 5.30A), although there was a decrease in cell number by day 7 (Figure 5.30B).

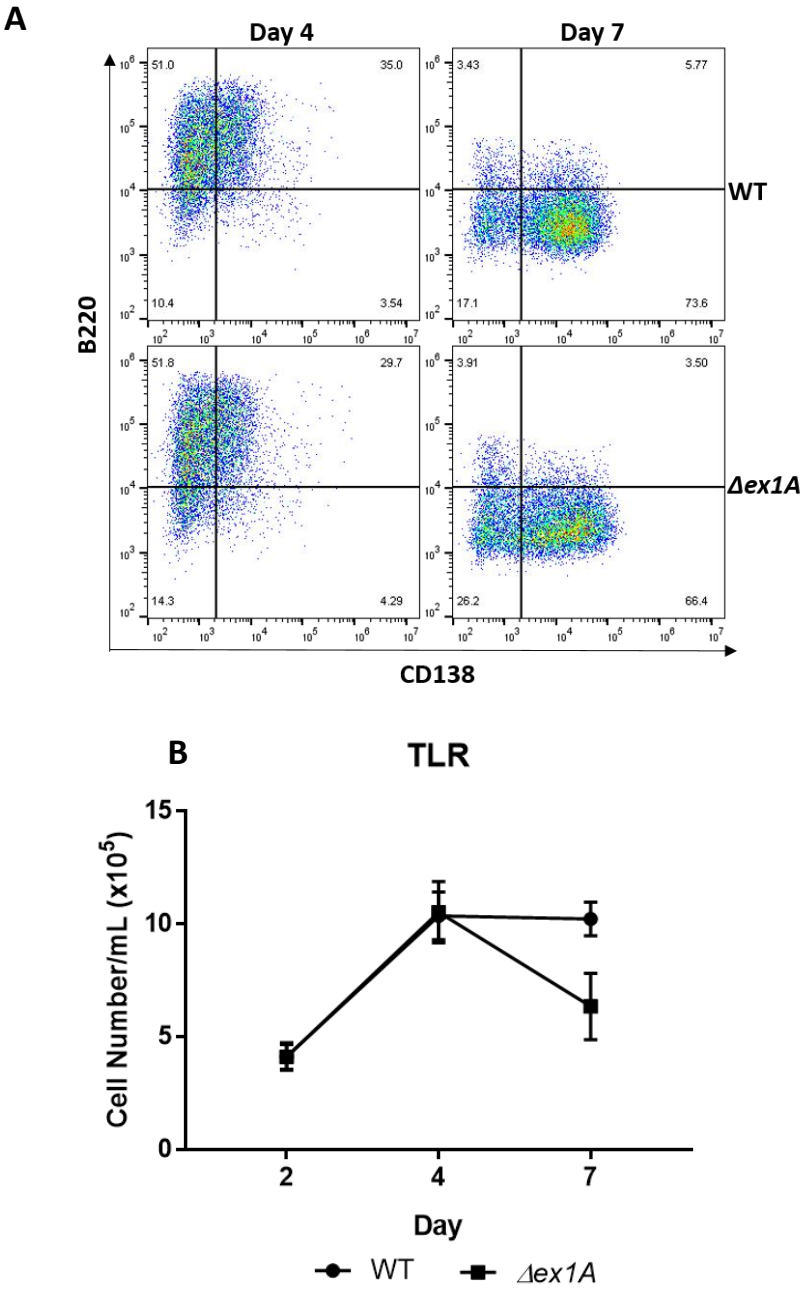

Figure 5.30 Evaluating the impact of Δ*ex1A Prdm1* on B-cell differentiation following stimulation with TLR conditions. (A) Total B-cells isolated using the EasySep™ mouse B-cell isolation kit were stimulated with TLR conditions. On day 4 and 7, cells were stained with antibodies to B220 and CD138 and analysed using flow cytometry. (B) On day 2, 4 and 7, cells were counted using cell counting slides (TC-10 Automated Cell Counter, BioRad). Results are displayed as the mean ± SD for 3 individual mice.

Under BCR conditions, Δ*ex1A* cells failed to generate a substantial plasma cell population by day 7 and the majority of the population was negative for both B220 and CD138 (Figure 5.31A). Cell number was also compromised suggesting that these cells have a reduced proliferative capacity compared with WT cells (Figure 5.31B).

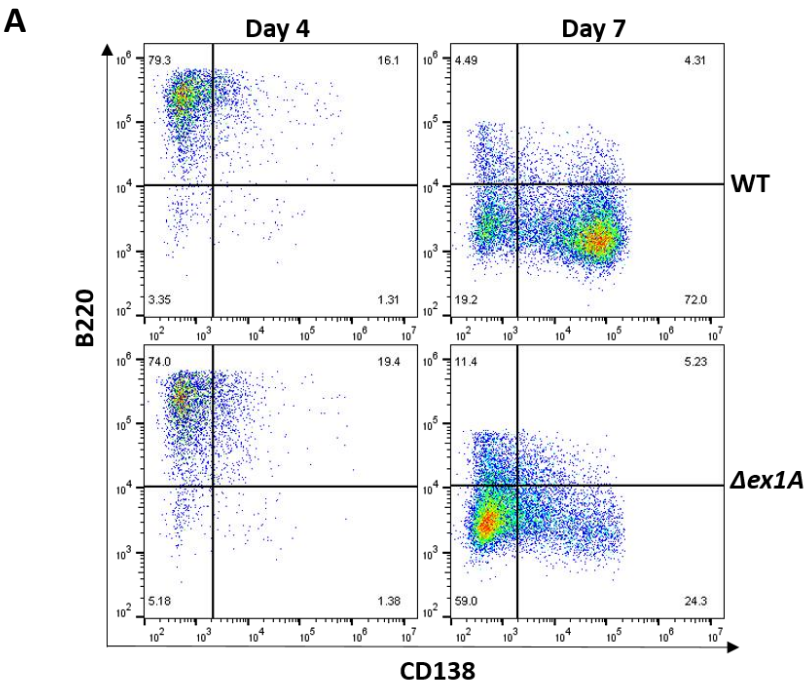

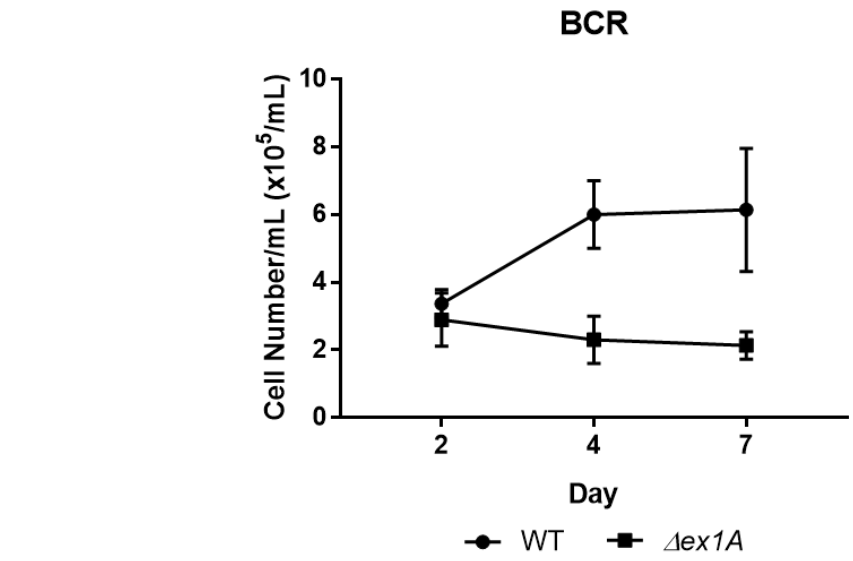

Figure 5.31 Evaluating the impact of Δ*ex1A Prdm1* on B-cell differentiation following stimulation with BCR conditions. Total B-cells isolated using the EasySep™ mouse B-cell isolation kit were stimulated with BCR conditions. On day 4 and 7, cells were stained with antibodies to B220 and CD138 and analysed using flow cytometry. On day 2, 4 and 7, cells were counted using cell counting slides (TC-10 Automated Cell Counter, BioRad). Results are displayed as the mean ± SD for 3 individual mice.

5.18.2 *Prdm1* promoter usage

As cells were able to differentiate under TLR conditions, it seemed plausible that Δ*ex1A* cells could potentially use an alternative *Prdm1* promoter to initiate transcription. BAM files generated from RNA-sequencing (day 4) were analysed using the integrative genomic viewer (Robinson *et al.*, 2011) to compare promoter usage between WT and Δ*ex1A* cells.

Firstly, it was clear that regardless of genotype or stimulating condition, there was a decrease in transcripts originating from exon 1, however this was enhanced in Δ*ex1A* mice (Figure 5.32A). Further IGV analysis of Δ*ex1A* mice showed splice variants upstream of exon 1 which were not present in WT samples (Appendix 5). There also appeared to be transcripts that originated from exon 2, which may represent regulation by the exon 1C promoter. Overall, transcript profiles varied in response to different stimuli conditions, for example BCR stimulating conditions resulted in a greater loss of read depth across all exons compared with TLR stimulation. Finally, there was an abundance of transcripts that originated primarily from exon 4 and evidence of the previously described splice variant Δexon 6(7) (Tunyaplin, Shapiro and Calame, 2000; Morgan *et al.*, 2012; Smith *et al.*, 2010) in both WT and Δ*ex1A* cells (Figure 5.32A and Figure 5.32B). It is important to point out that there have been different versions of exon numbering in previous literature, however the official RefSeq version is used in the figures below where the previous "exon 3" is now annotated as exon 2.

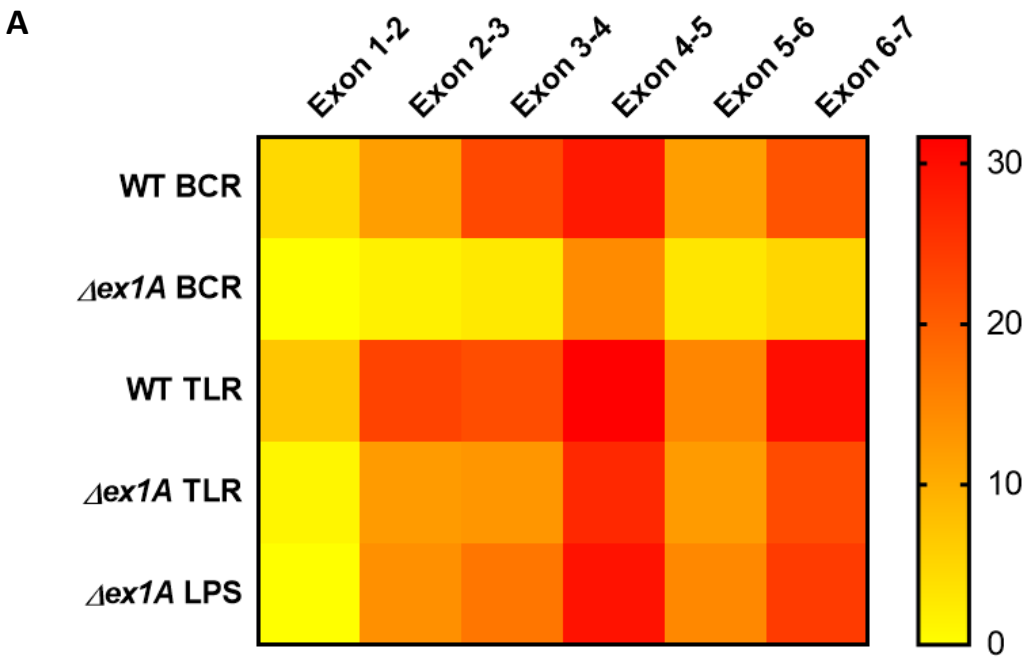

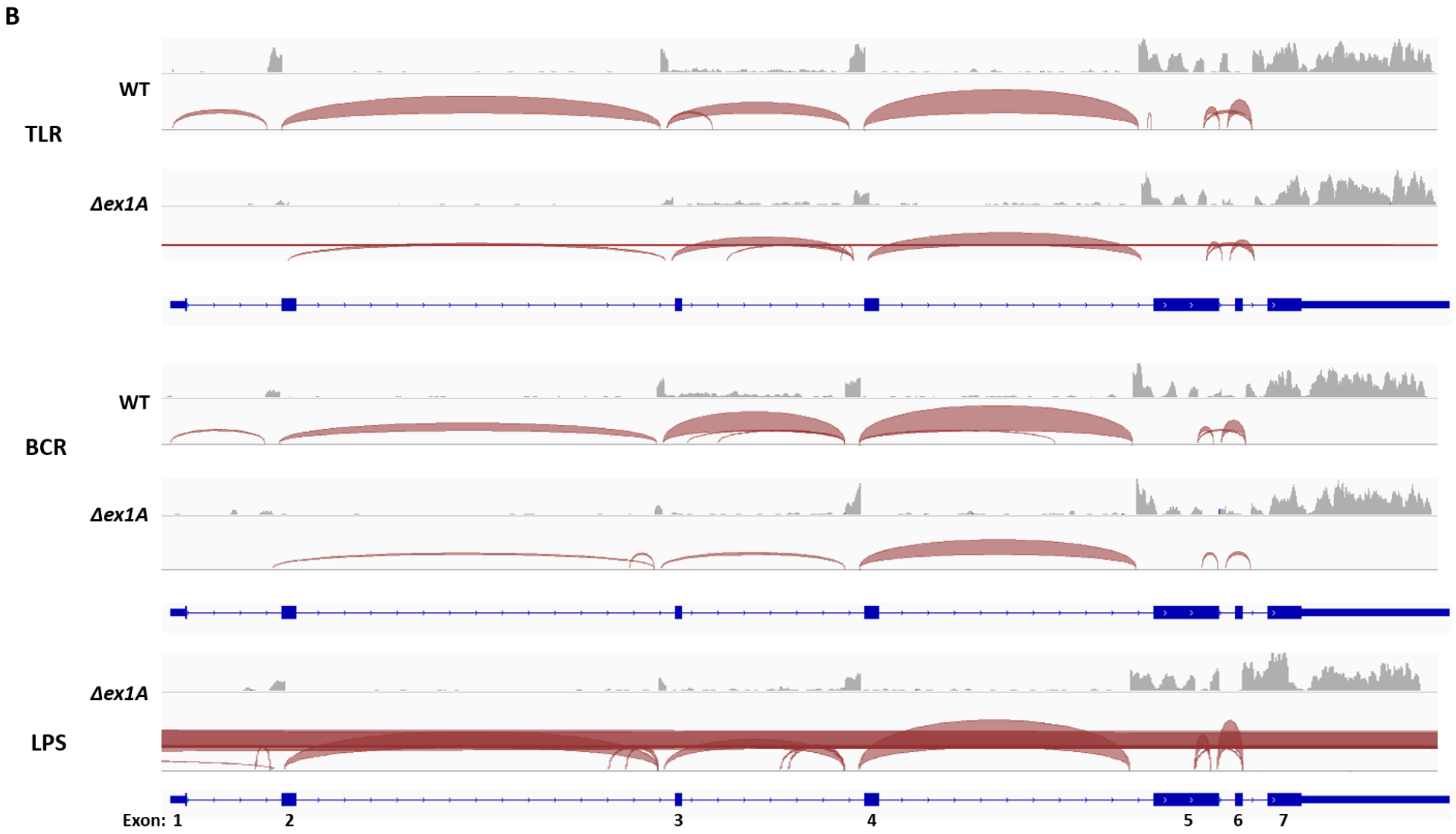

Figure 5.32 *Prdm1* promoter usage during B-cell differentiation. BAM files were extracted from RNA-sequencing and viewed using the integrative genomics viewer (IGV). (A) Read depth was calculated for each exon using 3 individual mice per condition. (B) Tracks were generated for transcript visualisation.

5.18.3 *Prdm1* expression

Deletion of exon 1A also appeared to affect overall expression of *Prdm1*. Δ*ex1A* cells cultured in BCR conditions demonstrated lower expression of *Prdm1* at day 4 in comparison to WT cells, whereas Δ*ex1A* cells cultured in LPS or TLR conditions expressed levels equivalent to the WT (Figure 5.33).

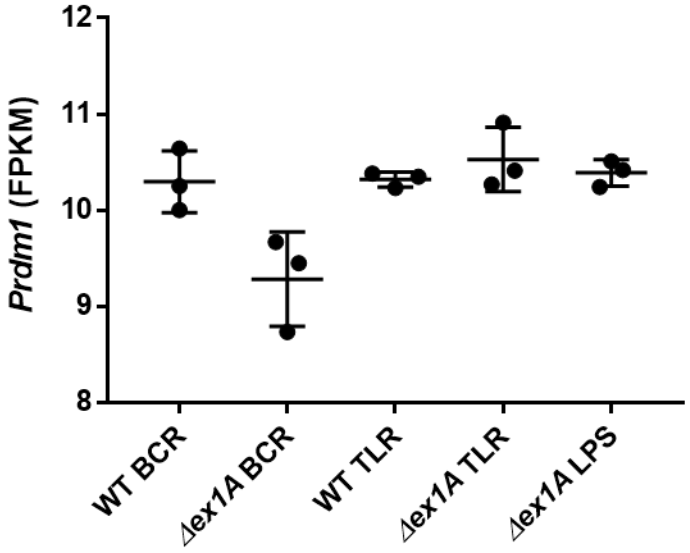

Figure 5.33 *Prdm1* expression on day 4. Log_2 FKPM expression values of genes are shown for 3 individual mice per condition.

5.19 Discussion

Following antigenic encounter, B-cells alter their physiological state and initiate a differentiation process that ultimately produces ASCs. ASC is a broad term that encompasses both short-lived, cycling plasmablasts which occur early in an immune response and long lived and quiescent plasma cells that reside in specialised niches, primarily within the bone marrow (Roth *et al.*, 2014; Tooze, 2013). Over the past 10 years, optimisation of human B-cell differentiation conditions has resulted in the in vitro generation of long-lived plasma cells, capable of surviving in culture for extended periods of time (Jourdan *et al.*, 2014; Cocco *et al.*, 2012; Nguyen *et al.*, 2018; Groves *et al.*, 2018). This has resulted in the ability to sequentially explore and manipulate each stage of both normal and malignant differentiation creating new avenues of research.

At present, a murine counterpart does not appear to exist as various approaches are sufficient at modelling partially differentiated, short-lived plasmablasts, but are unable to terminally differentiate into long-lived plasma cells for sustainable periods. In support of this, work by Shi and colleagues demonstrated that the gene expression profile of in vitro–derived ASCs stimulated using CD40-L, IL-4 and IL-5 for 5 days was as different from fully mature PCs as it was from activated B cells (Shi *et al.*, 2015). This shows that further work is required in order to provide a model system suitable for investigating the full trajectory of murine B-cell differentiation in vitro.

The work displayed in this chapter highlights the steps taken to identify a system suitable for generating long-lived plasma cells through both TLR4 and BCR engagement. The first approach assessed the feasibility of transposing an existing human model of plasma cell differentiation on murine B-cells. The system, which contained CD40-L, $F(ab')_2$ anti-IgM/IgG, IL-21 and IL-4 from day 0 and IL-6, IL-21, APRIL and GSI from day 4 appeared to support plasma cell generation, however by day 9 the majority of these had disappeared. IL-21 is used widely in human B-cell cultures due to its role in B-cell activation and plasma cell differentiation (Kuchen *et al.*, 2007). When tested on murine B-cells in combination with other cytokines and co-stimulatory proteins (Fig 1.3 and Fig 1.4), a population of plasma cells emerged at early time points, however these were not sustained long-term. Interestingly, IL-21 has been shown to differentially influence B-cell fate depending on the signalling context. Ozaki *et al.* demonstrated that IL-21 increased B-cell proliferation induced by anti-IgM, especially in the presence of anti-CD40, however inhibited proliferation induced by anti-IgM plus IL-4 (Ozaki *et al.*, 2004). Furthermore, IL-21 has been shown to act as an immunosuppressive cytokine in certain situations by inducing apoptosis (Wu *et al.*, 2016). This could suggest that the combination of cytokines used within this experiment had a negative impact on cells undergoing differentiation resulting in the inability to survive long term. Alternatively, as plasma cells disappeared 2 days after being generated, it is possible that

IL-21 induces excessive metabolic stress associated with differentiation. IL-21 has been shown to induce the production of all immunoglobulin isotypes in a dose-dependent manner with optimal IgG production-inducing capacity observed at concentrations between 4 and 10 ng/ml cytokine (Pène *et al.*, 2004). With this in mind, it is conceivable that the amount of IL-21 used (50ng/mL) drove excessive proliferation and that titrating the amount may permit plasma cells to emerge and survive. Taken together, this suggests that either the combination of cytokines was not appropriate or regardless of context, IL-21 is not a suitable stimuli for murine plasma cell generation in vitro at the dose tested.

With the first attempt proving unsuccessful, an existing murine model of plasma cell differentiation described by Ozcan and colleagues along with the addition of IL-6 at a later time point was explored. Notably, this generated a substantial population of plasma cells that were still present at the later time point (day 9). Following further optimisation, a robust model system using TLR stimulation was achieved which included cell-bound CD40-L, LPS and IL-4 from day 0 and IL-6, APRIL and GSI from day 4. As BCR and TLR signalling activate distinct downstream pathways, the next step was to develop a system based on BCR activation. The first experiment substituted LPS with $F(ab')_2$ anti-IgM/IgG and interestingly, no plasma cells emerged. To try to overcome this, further T-cell help was included in the form of IL-2 and IL-5. The addition of IL-2 resulted in a small population of $B220^-$ $CD138^+$ cells appearing at day 8 however IL-5 increased this significantly from 2% to 74%. Horikawa and Takatsu demonstrated that IL-5 could induce CD38-stimulated B cells to terminally differentiate to immunoglobulin-secreting cells and class-switched cells while IL-4, a well-known factor for CSR, failed to do so. Following on from this, they identified a set of genes exclusively induced by IL-5 but not IL-4 which included *Prdm1, Aicda* and *J chain* (Horikawa and Takatsu, 2006). This suggests that IL-5 plays a critical regulatory role in genes essential for B-cell terminal maturation.

Once both sets of conditions had been established, validation experiments showed that in vitro generated cells are characteristically similar to in vivo murine plasma cells. For example, phenotypic analysis revealed that downregulation of the pan B-cell marker B220 occurred concurrently with upregulation of the plasma cell markers CD138, TACI and BCMA. Furthermore, the use of a Blimp-1-Venus reporter showed considerable upregulation during differentiation consistent with others who use high Blimp-1 expression to identify plasma cells (Tellier *et al.*, 2016b; Savage *et al.*, 2017). Unexpectedly between day 9 and 13, Blimp-1 expression decreased slightly in both TLR and BCR stimulated cells. A key function of Blimp-1 is to establish the internal cellular structures for the characteristic remodelling of the LLPC cytoplasm for high antibody secretion (Tellier *et al.*, 2016b). With this in mind, there may be a decrease in absolute requirement once roles such as this have been achieved. Interestingly,

others who have used Blimp-1 reporters have demonstrated variation in Blimp-1 expression level. For example, a population of Blimp-1^{INT} cells were present in a resting bone marrow (Kallies *et al.*, 2004). However, with no characterisation and additional gene expression data for this population, no conclusion can be drawn as to whether these are newly emerging plasmablasts or LLPCs. This gives rise to the idea that the lower expression level observed at the later time point may be a consequence of the preferential survival of LLPCs which may typically express lower levels of Blimp-1 than plasmablasts/short-lived plasma cells.

Further validation included assessment of secretory capacity using ELISAs and showed that cells generated in culture had the ability to secrete. Both sets of conditions predominantly promoted IgM secretion, however a small proportion of cells were capable of producing class switched IgG. This could suggest that the cytokines used in these conditions are weak drivers of class switch recombination, however alternative isotypes and IgG subtypes have not yet been investigated. Gene expression analysis confirmed the presence of multiple mRNA transcripts including IgM, IgG, IgA and IgE providing further evidence of CSR. Alternative cytokines have been shown to specifically promote switching to other isotypes, such as TGF-β which promotes IgA (Ehrhardt, Strober and Harriman, 1992) and IFNy which promotes IgG2a (Bossie and Vitetta, 1991). While not explicitly tested, the prediction is that inclusion of other cytokines may allow the generation of different types of immunoglobulin. Furthermore, normalisation showed TLR conditions result in higher concentrations of overall secretion compared with BCR conditions suggesting that LPS is more potent at driving immunoglobulin secretion than $F(ab')_2$ anti-IgM/IgG.

As there is a strong correlation between the concentration of cytokines in culture, the time taken for a cell to divide and the differentiation state of an ASC (Zhou *et al.*, 2018), it was necessary to examine proliferative capacity across the differentiation. After assessing CFSE dilution at various time points, results showed that a high division rate accompanied maturation of murine B-cells to plasmablasts before cessation of proliferation at roughly day 8. Plasma cells were then able to persist in the absence of any additional division and shown to survive for extended periods of time. For example, the majority of cultures displayed between 10-13 days survival, however on another occasion cells were cultured until day 21. This suggests that if given the opportunity these cells could live indefinitely, a characteristic of a long-lived plasma cells.

Gene expression time-course analysis appeared to confirm that cells were indeed plasma cell-like when stimulated with either TLR or BCR conditions. Although numerous differentiation experiments displayed variable kinetics when using either TLR or BCR stimuli, the overall gene expression profile appeared to be similar suggesting that regardless of the pathway taken the end-point in both conditions are comparable. Furthermore, plasma cells displayed a common gene program consistent with bone marrow plasma cells described by Shi and colleagues, and

taken together with additional validation experiments provides the first long-term model of in vitro plasma cell differentiation (Shi *et al.*, 2015).

Perhaps the most surprising result is the observed effect of medium choice on B-cell survival. As the majority of murine B-cell culture systems use DMEM (Liebig *et al.*, 2010) or RPMI-1640 (Pellegrini *et al.*, 2007) these results could partially explain the lack of a robust model for differentiating long-lived murine plasma cells in vitro until now. IMDM is a highly enriched medium compared with DMEM and RPMI-1640 and contains more glucose, selenium and additional amino acids and vitamins. Because of this, it is better equipped to support metabolically active cells experiencing large amounts of proliferation and secretion.

Whilst trying to investigate the requirement of exon 1A for Blimp-1 expression, it became clear that Δ*ex1A* cells stimulated with LPS were able to differentiate into plasma cells. This was also the case for cells differentiated using TLR conditions, however cells cultured in BCR conditions were unable to upregulate CD138 resulting in a population of $B220^{-}$ $CD138^{-}$ cells. Furthermore, Δ*ex1A* cells cultured in BCR conditions lacked transcripts corresponding to the regulatory region of Blimp-1 and exhibited lower *Prdm1* expression compared to both WT cells and Δ*ex1A* cells cultured in both LPS and TLR conditions. As the two conditions differ only in the type of receptor engagement (i.e. BCR crosslinking or TLR4 binding) and LPS stimulated cells acted in a similar manner to TLR conditions without co-stimulation of CD40 and additional cytokines (IL-4 and IL-5), it is plausible that TLR4 signalling overcomes the loss of exon 1A to maintain *Prdm1* and Blimp-1 expression, therefore supporting differentiation. In previous work, Morgan and colleagues established the presence of NF-κB sites upstream of the exon 1A promoter which were essential for *Prdm1* induction and plasma cell differentiation. In agreement with this finding, stimulated B-cells isolated from mice lacking RelA, a subunit of NF-κB, in the B-cell lineage have a severely reduced number of plasmablasts as well as dramatically impaired induction of Blimp-1 (Heise *et al.*, 2014). Collectively, this supports the idea that TLR4 signalling may use alternative binding sites to create new regulatory regions on *Prdm1* thus promoting differentiation. In contrast, the combination of Δ*ex1A* and BCR signalling eliminates essential signals required for *Prdm1* activation.

The ability of Δ*ex1A* B-cells to generate ASCs in response to LPS are contrary to the results published by Morgan and colleagues (Morgan *et al.*, 2009). However, their evaluation was conducted on total splenocytes stimulated for 3 days and may therefore have failed to detect low levels of Blimp-1 generated at this time point. It is also worth noting that when bone marrow derived dendritic cells from exon 1A deficient mice were stimulated with LPS, the cells still produced Blimp-1 protein, albeit at a reduced level. The authors identified substantial expression of *Prdm1* transcripts originating from at least one other promoter (exon 1C) in these

mice, and therefore the results presented here promote the idea that the B-cell lineage is capable of using alternative promoters in different contexts.

To explore this further it was important to assess *Prdm1* promoter usage. Visualisation of transcripts showed that deleting exon 1A resulted in a splice variant which appeared to originate upstream of exon 1 as well as transcripts that started from exon 2. In addition, analysis of read depth showed that transcripts originating from exon 1 were low in both WT and Δ*ex1A* mice. This could suggest that Δ*ex1A* cells use exon 1B (located upstream of Exon 1A), similar to bone marrow dendritic cells (BMDCs) which display elevated expression of exon 1B transcripts following deletion of exon 1A or use the alternative exon 1C promoter which is active in LPS-activated splenocytes and a murine plasmacytoma line (Morgan *et al.*, 2009).

In contrast, WT and Δ*ex1A* cells displayed transcripts that originated largely from exon 4 and may represent a previously described transcript that generates a functional protein lacking the PR domain. Gyory and colleagues were the first to describe this novel mRNA species of the *PRDM1* gene, *PRDM1-β* in myeloma cell lines (Gyory *et al.*, 2003). The group subsequently found PRDM1-β in non-transformed human NK cells (Smith *et al.*, 2010). Interestingly, *PRDM1-β* mRNA was present at ~20-fold higher levels than *PRDM1-α* in NK cells and shown to be transcribed from an alternate promoter, using a distinct transcriptional start site present in the third intron of the full-length protein (Figure 5.34). Overall, the resulting protein has a disrupted PR domain and its repressive activity is dampened relative to PRDM1-α (Smith *et al.*, 2010).

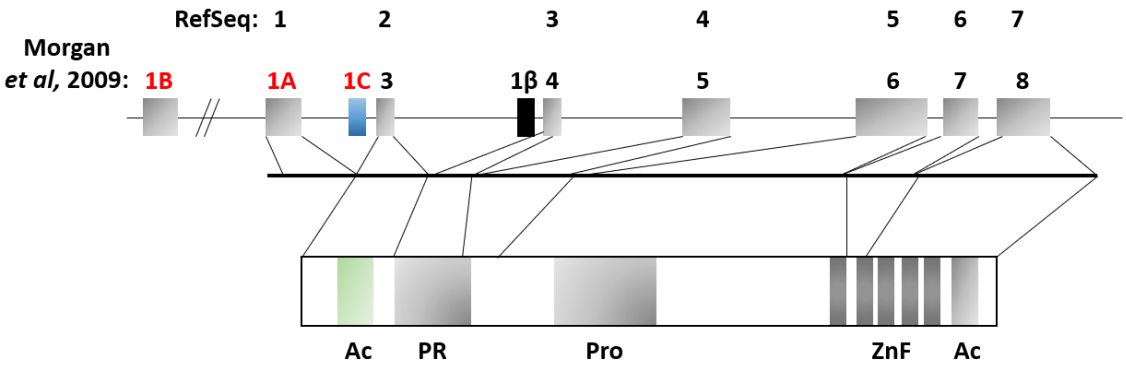

Figure 5.34 Schematic representation of the genomic structure of *Prdm1*. Numbered boxes represent the exons as reported by RefSeq and Morgan *et al.* 2009 and the protein regions encoded are displayed below.

Furthermore, PRDM1-β is structurally similar to the oncogenic form of other members of the positive regulatory domain (PRDM) gene family such as PRDM2 (Sorrentino *et al.*, 2018).

Although PRDM1-β has been shown to be expressed at much lower levels than the full-length form in myeloma cell lines (Gyory *et al.*, 2003; Ocana *et al.*, 2006), PR-negative domain versions of other PRDM family members are typically present at much higher levels in cancer cells (Abbondanza *et al.*, 2012; Jiang and Huang, 2000). In the example of PRDM2, the two isoforms have fundamentally different effects on proliferation with the full-length protein acting in an inhibitory capacity (He *et al.*, 1998) whilst the truncated version is capable of promoting cell growth (Rossi *et al.*, 2004). Therefore, a clear understanding of the functional differences between isoforms will be critical in deciphering a role during oncogenesis and other normal physiological processes. If confirmed, the data presented here would be the first piece of work to describe *Prdm1-β* in the context of murine cells and would expand the scope for BLIMP-1 function.

In addition to PRDM1-α and PRMD1-β, Blimp-1 mRNA lacking exon 6 (RefSeq numbering) was also consistently observed in NK cells. This isoform is generated via splicing to exclude exon 6 and disrupts three crucial zinc fingers necessary for DNA interaction (Smith *et al.*, 2010). An analogous splice variant (Δexon7; Morgan *et al.* numbering) was also described in naive $CD19^{+}$ murine B-cells although it was present at low levels. In addition, Blimp-1 expression and LPS-induced differentiation was supressed following the overexpression of Blimp-1Δexon7 (Schmidt *et al.*, 2008). In agreement with the above findings, read depth analysis highlighted that transcripts containing exon 5-6 were reduced in both WT and Δ*ex1A* cells, which is likely a consequence of the splicing observed between exon 5-7 (Δexon6) evident from the *Prdm1* tracks. Collectively, this data provides indication that murine B-cells express numerous *Prdm1* isoforms analogous to previous findings and therefore detection and characterisation of each isoform will be an important area of future investigation.

In conclusion, the validated models developed within this chapter provide a foundation to systematically explore the terminal stages of murine B-cell differentiation and make use of genetic models to probe the role of individual molecules in a cell-autonomous manner.

Chapter 6 - SIK kinase inactive mice

To extend on the work carried out on human samples and in an effort to determine whether individual SIK isoforms are associated with specific functions during terminal differentiation, mice with catalytically inactive SIKs were utilised. Generation of these mice was achieved by introducing a kinase dead knock-in which permits the assembly of endogenous protein complexes, rather than using the knock-out approach which can significantly alter binding capability due to the loss of all domains (Pauls *et al.*, 2013).

To ascertain whether SIKs had any impact on murine immune cell populations, spleen and bone marrow samples were harvested from wild type and SIK KI mice at both steady state and post-immunisation and subjected to flow analysis. Immunoglobulin titres from serum as well as in vitro cultures were also evaluated as a measure of ASC functionality.

6.1 Generation of kinase inactive (KI) mice

To generate full body knock-in mice of SIK1, SIK2 and SIK3 on a C57BL/6 background, wild type protein was replaced with a catalytically inactive mutant using gene targeting (Darling *et al.*, 2017). The threonine residue which resides in the activation loop of the SIKs was selected as the mutation site, as phosphorylation of this residue by LKB1 is essential for SIK catalytic activity (Lizcano *et al.*, 2004). Homozygous SIK1 and SIK2 KI animals were viable and fertile looking indistinguishable from WT littermates under standard housing conditions, whereas homozygous SIK3 KI animals were present at sub-Mendelian ratios and smaller than their WT littermates due to potential skeletal defects (Darling *et al.*, 2017). With this in mind, the decision was made to concentrate on the following animals including SIK1-T182A, SIK2-T175A and SIK1-T182A/SIK2-T175A which will be referred to as SIK1, SIK2 and SIK1/2 KI mice throughout this work.

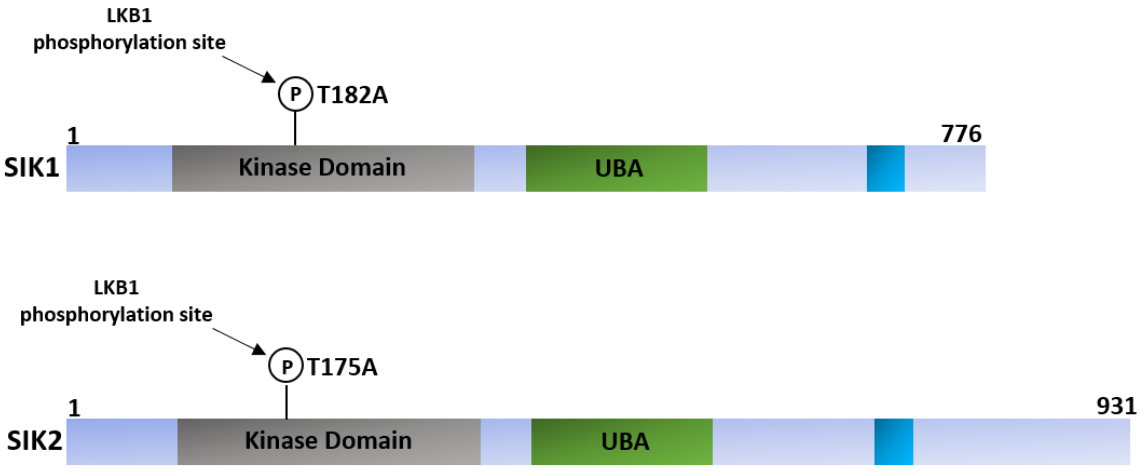

Figure 6.1 Diagrammatic representation of SIK KI mice. SIK1 and SIK2 mutation sites involved in the generation of KI mice.

6.2 Steady state

6.2.1 Analysis of spleen size

Following acquisition of the splenic tissue, a visual observation was made to see if there were any striking differences between littermate control WT and SIK KI mice. As seen in Figure 6.2, WT mice had the most consistently sized spleens, whereas SIK1 and SIK1/2 KI mice demonstrated greater variation. Overall, it was concluded that no prominent differences were visible between genotypes at steady state.

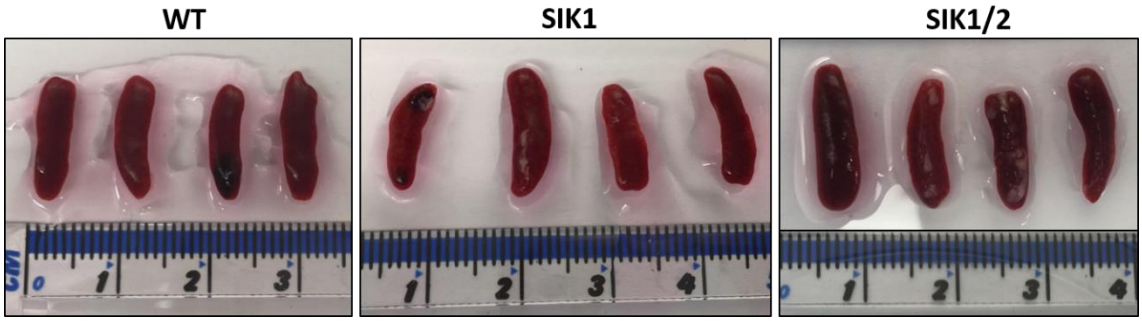

Figure 6.2 Assessing the impact of catalytically inactive SIKs on spleen size. Tissue samples were harvested from both WT and SIK KI mice and evaluated for size.

6.2.2 Phenotypical analysis of splenic PBMCs

LKB1 has recently been shown to regulate numerous metabolic pathways in Tregs independently of AMPK, relying instead on MARK and SIK kinases as downstream metabolic effectors (He *et al.*, 2017). In addition to B-cells, it is therefore it is plausible that SIKs may be important across other elements of the adaptive immune system/response. With this in mind, initial staining panels consisted of a basic assessment of both B- ($B220^+$) and T-cell ($CD3^+CD4^+$ or $CD3^+CD8^+$) populations in the spleen. Flow analysis revealed negligible differences in total B-cells and plasmablasts ($B220^+CD138^+$) across WT and SIK KI mice, however there was a significant decrease in the percentage of plasma cells ($B220^-CD138^+$) in SIK1 KI mice. There were also minimal differences in T-cell populations across the four genotypes.

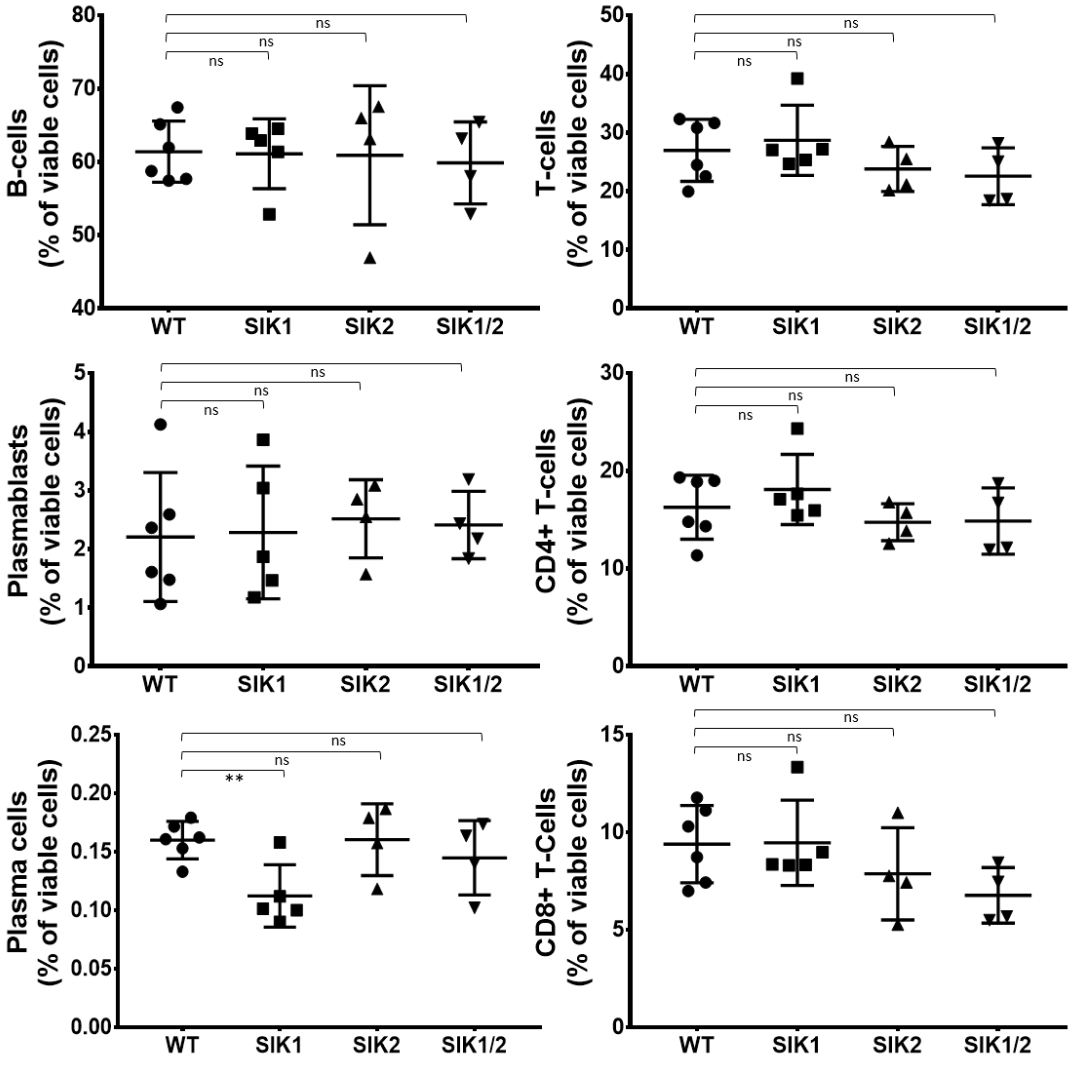

Figure 6.3 Phenotypic analysis of PBMCs in the spleen. Tissues were extracted and homogenised to obtain single cell suspensions. Cells were stained using antibodies against B220, CD138, CD3ε, CD4 and CD8 and analysed using flow cytometry. WT n=6, SIK1 n=5, SIK2 n=4, SIK1/2 n=4. Significance was calculated using a student's t-test (* = $p<0.05$; **=$p<0.01$).

6.2.3 Phenotypical analysis of early B-cell development in the bone marrow

To determine whether loss of SIK kinase activity had any effect on early development, the percentage of B-cell progenitors (Hardy *et al.*, 1991) in the bone marrow were measured as well as mature plasmablasts and plasma cells. Analysis of Hardy fractions A-C ($CD43^+$ $Ly51^-$), D (IgM^- IgD^-), E (IgM^+ IgD^-) and F (IgM^+ IgD^+) demonstrated sample variability across the four different genotypes and therefore no significant differences were observed. There was a higher overall percentage of Fraction D (small pre-B) in SIK2 KI mice, however this was non-significant. There was also sample variation in both plasmablasts and plasma cells resulting in no significant differences between WT and SIK KI mice.

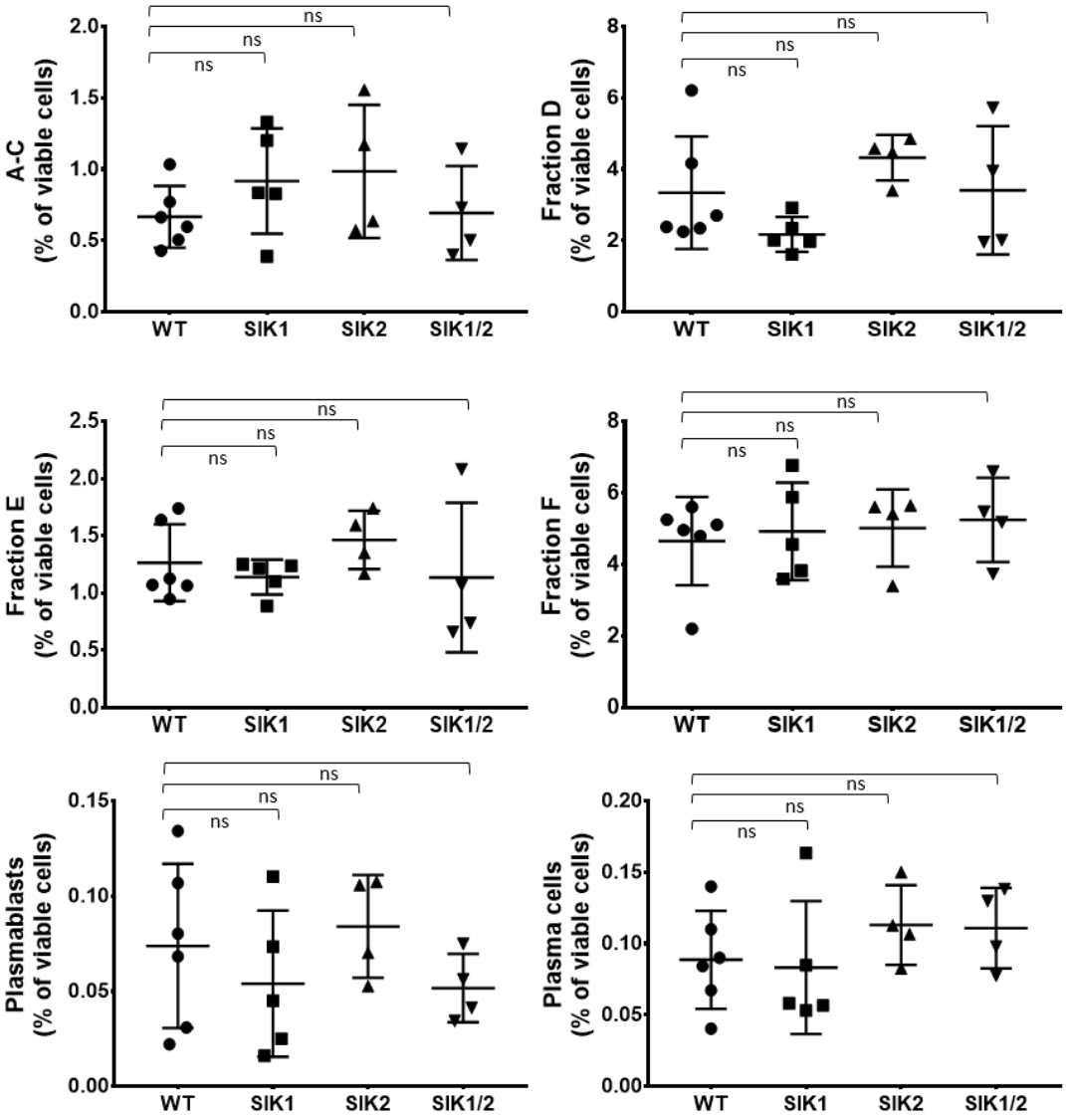

Figure 6.4 Phenotypic analysis of early B-cell populations in the bone marrow. Tissues were extracted and homogenised to obtain single cell suspensions. Cells were stained using antibodies against B220, CD138, Ly51, CD43, IgM and IgD and analysed using flow cytometry. WT n=6, SIK1 n=5, SIK2 n=4, SIK1/2 n=4. Significance was calculated using a student's t-test (* = $p<0.05$; **=$p<0.01$)

6.2.4 Phenotypical analysis of mature splenic B-cell populations

In mice, immature B-cells emerge in the bone marrow and either mature further at this site or in the periphery. Cells that proceed to the spleen to mature are known as 'transitional' B-cells and contribute to a small percentage of the overall B-cell population (Su and Rawlings, 2002). Constituting the majority of splenic B-cells are marginal zone (MZ) B-cells that can be induced to differentiate into short-lived plasma cells in the absence of BCR ligation and follicular (FoB) B-cells which migrate repeatedly through the blood and lymph to B cell areas. In the spleen, FoBs reside in the follicular niche and mediate T-dependent immune responses to protein antigens (Allman and Pillai, 2008). To determine whether loss of SIK kinase activity impairs B-cell maturation in the spleen, B-cell subsets were enumerated in both WT and SIK KI mice.

Although not significant, there was a convincing decrease in the percentage of follicular B-cells ($CD21^+$ $CD23^+$ IgD^+), marginal zone precursors (IgM^+ $CD21^+$ $CD23^+$) and to a lesser extent marginal zone B-cells (IgM^+ $CD21^+$ $CD23^-$) in SIK1/2 KI mice. Alternatively, there was a significant increase in non B-cells ($B220^-$ $CD138^-$). SIK2 KI mice displayed a decrease in marginal zone precursors and marginal zone B-cells, however these were all non-significant. Overall, SIK1 KI mice had B-cell populations most comparable to WT apart from plasma cells in which there was a significant decrease. In contrast, plasma cells populations were normal in SIK2 and SIK1/2 KI mice (Figure 6.5).

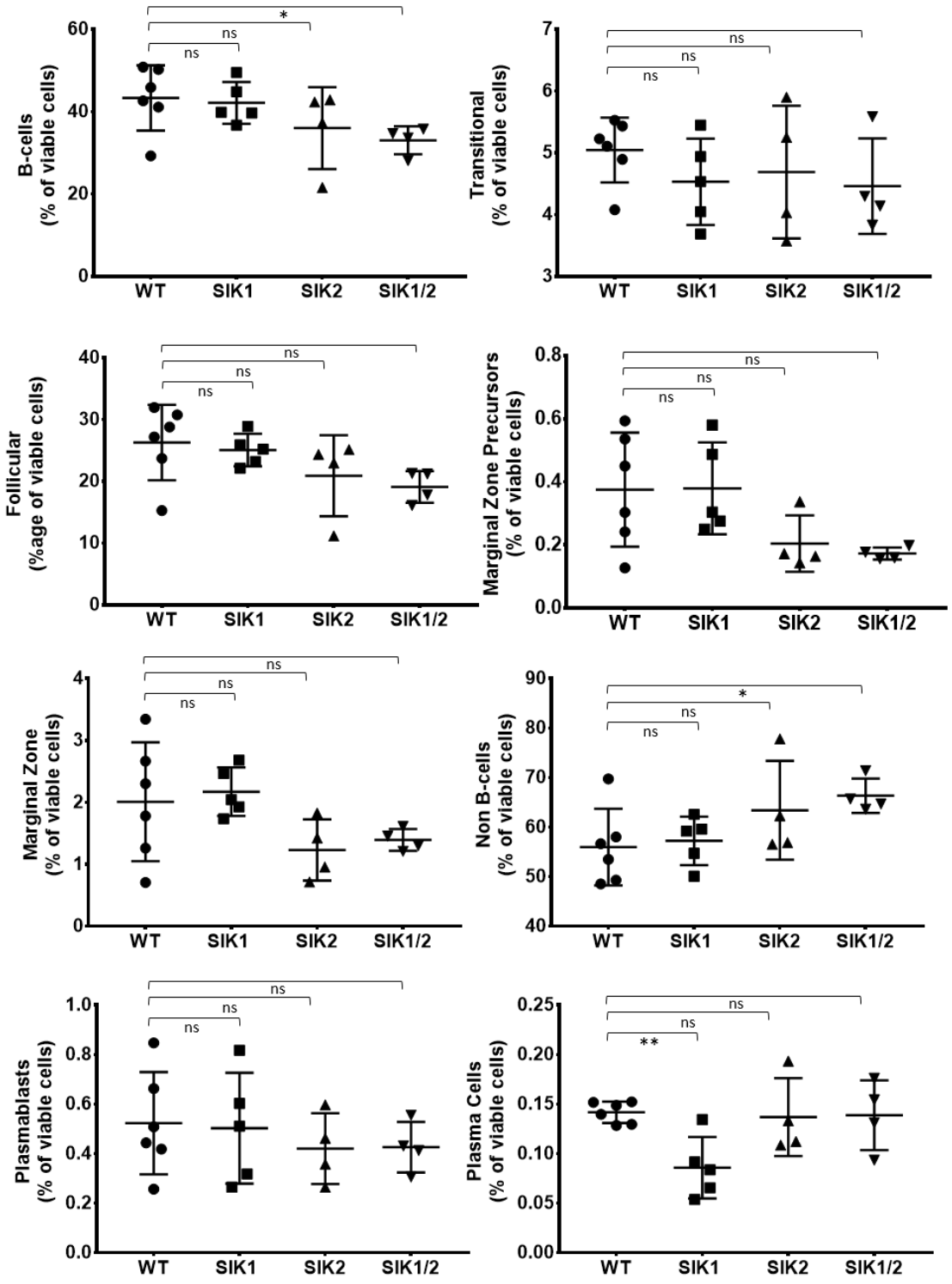

Figure 6.5 Phenotypic analysis of B-cell subsets in the spleen. Tissues were extracted and homogenised to obtain single cell suspensions. Cells were stained using antibodies against B220, CD138, CD21, CD23, IgM and IgD and analysed using flow cytometry. WT n=6, SIK1 n=5, SIK2 n=4, SIK1/2 n=4. Significance was calculated using a student's t-test (* = $p<0.05$; **=$p<0.01$).

6.2.5 Immunoglobulin titres

Although B-cell maturation in the periphery appeared to be largely normal, the reduction in splenic plasma cells in the SIK1 KI mice suggested that the process of terminal differentiation may be affected. The next stage was therefore to assess whether the reduction in cell number was linked to alterations in immunoglobulin production. In order to do this, IgM and IgG titres were measured using ELISAs from serum samples.

Although not significant, both SIK1 and SIK1/2 KI mice demonstrated slightly lower concentrations of IgM compared with WT mice. Unexpectedly, SIK1 KI mice also had elevated concentrations of IgG, whereas SIK2 and SIK1/2 KI mice displayed concentrations at the lower end.

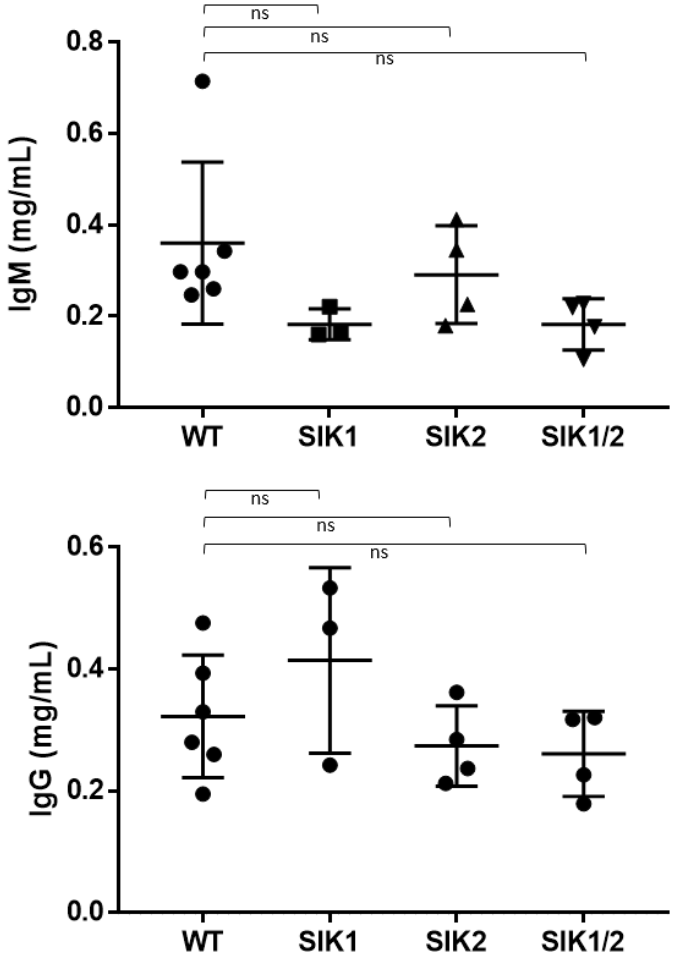

Figure 6.6 The impact of SIK kinase inactivity on immunoglobulin concentration. Serum was extracted from whole blood and diluted to the appropriate concentration. IgM and IgG concentrations were quantified using an ELISA. Significance was calculated using a student's t-test (* = $p<0.05$; **=$p<0.01$).

6.3 In vitro differentiation

Although steady state analysis provided some initial insight into the effects of SIK kinase activity on immune cell populations, the next stage was to utilise the in vitro differentiation protocol generated in chapter 5 to assess the effect of SIK kinase inactivity on B-cell differentiation. Splenic B-cells from SIK KI mice were differentiated in vitro using both BCR and TLR stimuli in order to establish whether ASCs could be generated in a cell-intrinsic manner.

6.3.1 TLR signalling

B-cells isolated from the spleens of WT, SIK1 KI and SIK1/2 KI mice were differentiated using TLR stimuli. On day 4, there were no striking differences in phenotype between the samples, however by day 8 there was a decrease in the percentage of $B220^{-}CD138^{+}$ plasma cells generated from SIK1/2 KI mice. This was consistent on day 10 and there was also an increase in the percentage of $B220^{+}CD138^{-}$ and $B220^{-}CD138^{-}$ cells, suggestive of a delay or defect in differentiation.

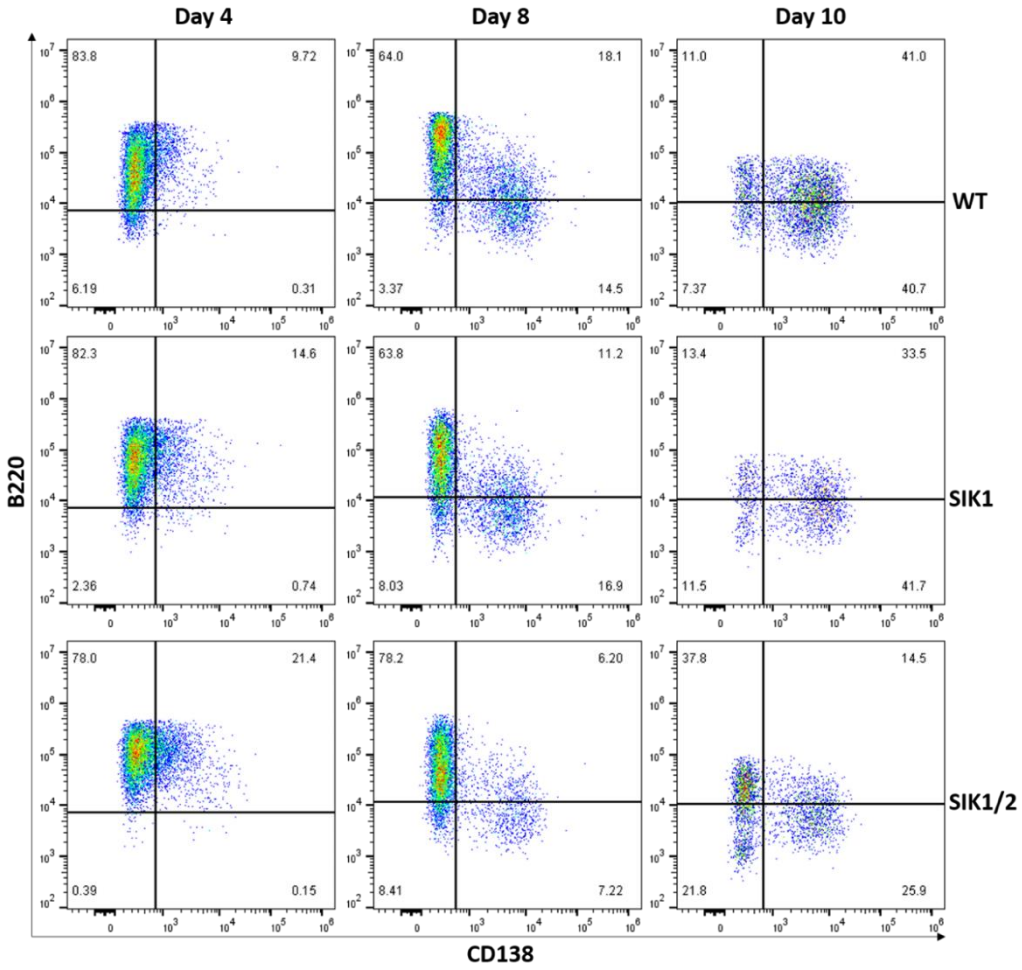

Figure 6.7 The impact of SIK kinase inactivity on B-cell differentiation (TLR). Total B-cells isolated using the pan B-cell isolation kit II were re-suspended in CD40-L, LPS, and IL-4. On day 2, cells were removed from CD40-L and transferred to a fresh plate. On day 4, cells were re-suspended in IL-6, APRIL and GSI and re-fed every 3 days. On day 4, 8 and 10, cells were stained with antibodies against B220 and CD138 and analysed using flow cytometry. Data is representative of 2 individual mice per genotype.

6.3.2 BCR signalling

B-cells isolated from the spleens of WT, SIK1 KI, SIK2 KI and SIK1/2 KI mice were differentiated using BCR stimuli. Phenotypic analysis revealed minor differences across the differentiation, however there was a slight decrease in $B220^{+}CD138^{+}$ cells at day 4 and a broader spread of CD138 expression at day 7 in SIK2 KI mice.

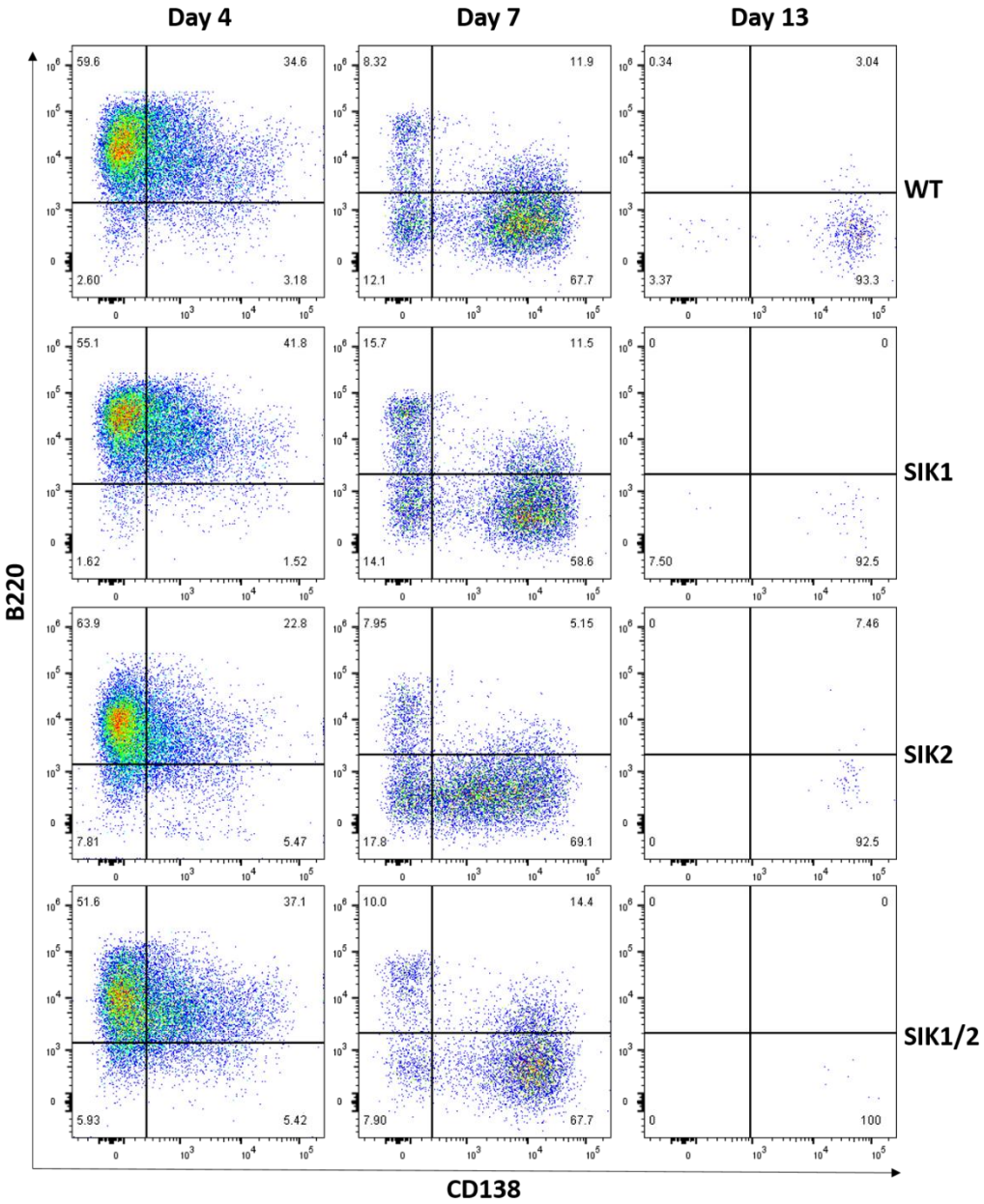

Figure 6.8 The impact of loss of SIK kinase activity on B-cell differentiation (BCR). Total B-cells isolated using the EasySep™ mouse B-cell isolation kit were re-suspended in CD40-L, F(ab'2) anti-IgM/IgG, IL-4 and IL-5. On day 2, cells were removed from CD40-L and transferred to a fresh plate. On day 4, cells were re-suspended in IL-6 and APRIL and re-fed every 3 days. On day 4, 7 and 13, cells were stained with antibodies against B220 and CD138 and analysed using flow cytometry. Data is representative of 3 individual mice per genotype.

6.3.3 Cell number

From data shown in chapter 5, it is evident that murine B-cell proliferation usually occurs between day 2 and 4. Proliferation then slows down until it eventually stops and as a consequence cell number begins to decline. Although cell counts for day 2 weren't taken, it is clear from Figure 6.9 that cells from WT, SIK1 KI and SIK1/2 KI mice decrease between day 4 and day 13 as would be expected. Unusually, cells from SIK2 KI mice appeared to proliferate between day 4 and 7. Most notably, day 13 cell counts from all SIK KI mice were lower in comparison to the WT.

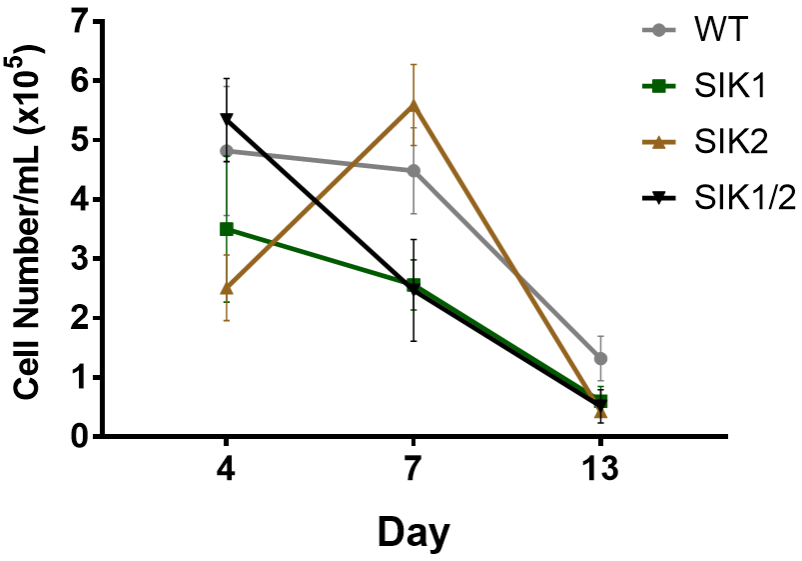

Figure 6.9 The impact of loss of SIK kinase activity on cell number. Total B-cells isolated using the EasySep™ mouse B-cell isolation kit were re-suspended in CD40-L, F(ab'2) anti-IgM/IgG, IL-4 and IL-5. On day 2, cells were removed from CD40-L and transferred to a fresh plate. On day 4, cells were re-suspended in IL-6 and APRIL and re-fed every 3 days. On day 4, 7 and 13, cells were counted using cell counting slides (TC-10 Automated Cell Counter, BioRad). Results are expressed as the mean ± SD and are representative of 3 individual mice.

6.3.4 Immunoglobulin titres

During in vitro culture, supernatants were taken to assess immunoglobulin titres of differentiating cells. Although this was only performed on 2 samples making the results difficult to conclude, the data appeared to suggest that at both day 7 and 11, SIK1 KI mice secrete lower levels of IgM whereas SIK1/2 KI mice secrete amounts more comparable with WT mice. IgG appeared to be consistently elevated in SIK1 KI mice compared with the WT, whereas in SIK1/2 KI mice IgG was similar to WT at day 7 but much higher in 1 sample at day 11 (Figure 6.10).

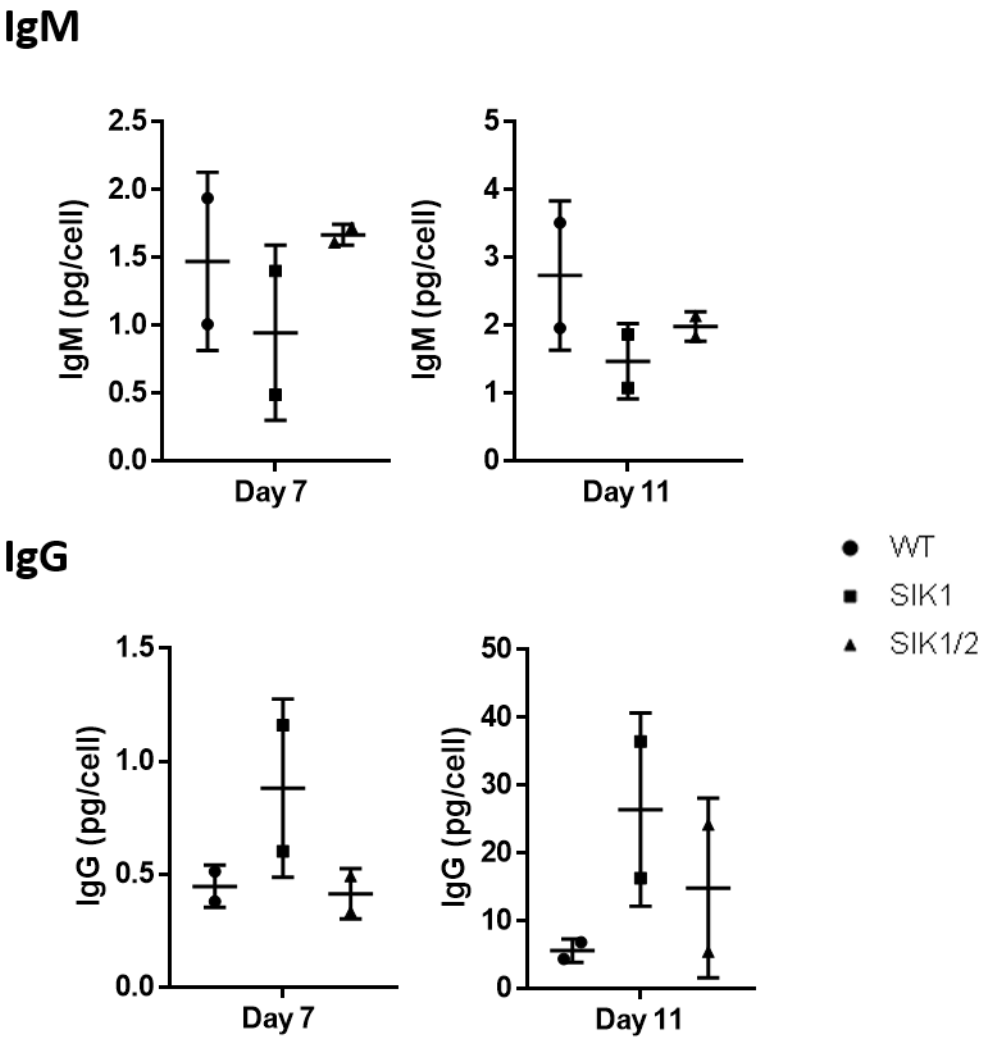

Figure 6.10 The impact of SIK kinase inactivity on immunoglobulin secretion. Supernatant was collected from cells in culture at day 7 and 11. IgM and IgG was quantified using an ELISA. Ig concentrations were divided by cell number to calculate secretion/cell.

6.4 Immunisation with NP-OVA

To explore the in vivo function of SIK catalytic activity, the next step was to assess the ability of SIK KI mice to mount an immune response to a model antigen. Both WT and SIK KI mice were immunised with NP-OVA, an antigen that elicits antibody production in a T-cell-dependent fashion (Matthews *et al.*, 2010). At different time points post-immunisation, the serum levels of antigen specific immunoglobulin were determined by ELISA and 21 days post-immunisation spleens were harvested for phenotypic analysis.

6.4.1 Splenic weight

To determine whether inactivating SIKs had any impact on spleen weight, the weight of each sample was recorded. As would be expected, non-immunised mice had the lowest spleen weight indicative of steady state. 21 days post immunisation, all genotypes displayed an increase in splenic weight. Furthermore, SIK2 KI mice presented a significant increase in splenic weight compared with WT mice.

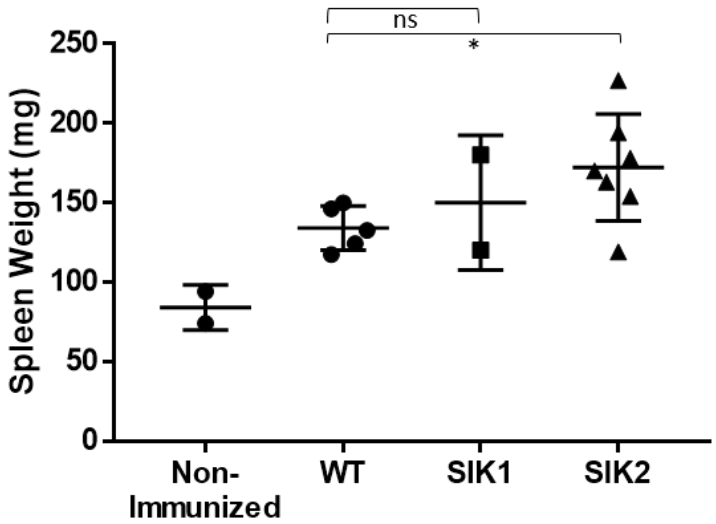

Figure 6.11 The effect of immunization on splenic weight. Spleens were harvested and weighed on a precision balance (Balance SA200). Significance was calculated using a student's t-test (* = $p<0.05$; **=$p<0.01$).

6.4.2 Phenotypical analysis of splenic PBMCs

In addition to weight, spleens were further subjected to phenotypic analysis. Although there was no significant difference, 3 of the SIK2 KI mice had a much lower proportion of B-cells compared with both WT and SIK1 KI mice. Plasmablasts appeared to split into 2 populations of high and low across all the genotypes whereas plasma cells remained consistent. Notably, there was a significant decrease in CD8+ T-cells from SIK2 KI mice, but not SIK1 KI mice and a minimal difference in CD4+ T-cells. Finally, compared with WT there appeared to be an increase in the proportion of non B/T- cells in 5/7 of the SIK2 KI mice.

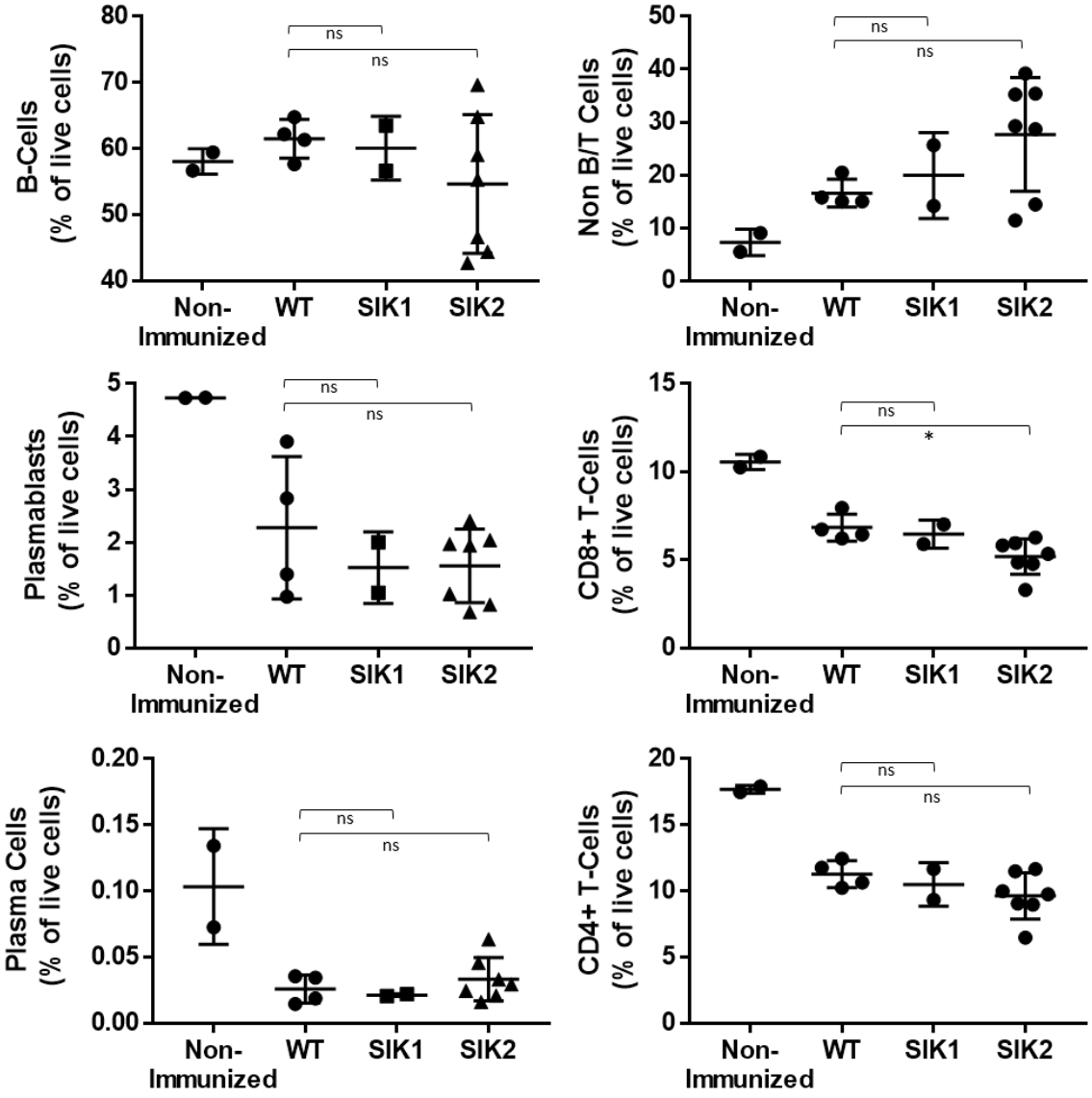

Figure 6.12 The impact of SIK kinase inactivity on splenic PBMCs post-immunization. Splenic tissue was harvested 21 days post-immunization with NP-OVA and homogenised to obtain single cell suspensions. Cells were stained using antibodies against B220, CD138, CD3ε, CD4 and CD8 and analysed using flow cytometry. Non-immunized n=2, WT n=4, SIK1 n=2, SIK2 n=7. Significance was calculated using a student's t-test (* = p<0.05; **=p<0.01)

6.4.3 Immunoglobulin titres

Immunoglobulin titres were assessed in all genotypes 14 days post-immunisation. There were subtle differences in total IgM, however antigen-specific IgM increased significantly in SIK2 KI mice compared with those of WT mice. SIK1 KI mice also appeared to display a similar trend. Although non-significant, SIK1 KI mice and SIK2 KI mice to a lesser extent displayed increased concentrations of total IgG. Antigen-specific IgG1 also appeared elevated in numerous samples in both SIK1 and SIK2 KI mice.

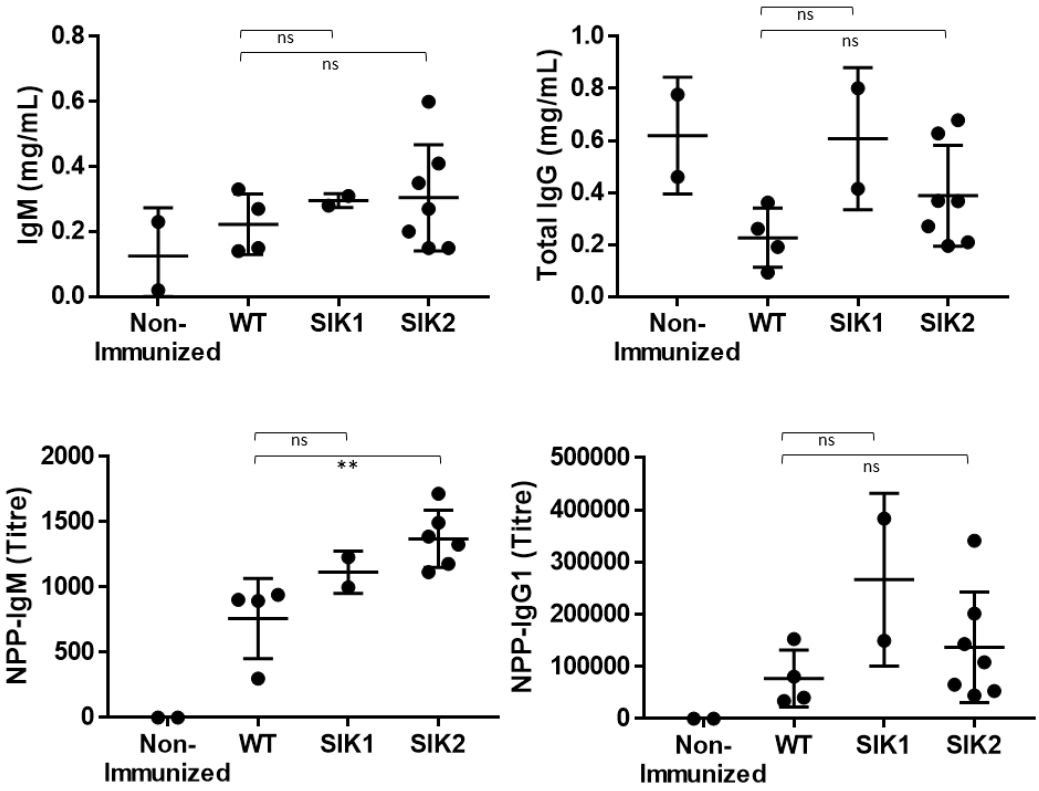

Figure 6.13 The impact of SIK kinase inactivity on antigen-specific immunoglobulin secretion. Serum was extracted from whole blood 14 days post-immunization with NP-OVA and diluted to the appropriate concentration. IgM and IgG concentrations were quantified using an ELISA. Non-immunized n=2, WT n=4, SIK1 n=2, SIK2 n=7 Significance was calculated using a student's t-test (* = $p<0.05$; **=$p<0.01$)

6.4.3.1 Immunoglobulin titres in SIK1 KI mice

In an attempt to further decipher SIK1 involvement during in vivo antibody response, antigen-specific IgM and IgG1 was evaluated in both WT and SIK1 KI mice at additional time points (7, 14 and 21 days post-immunisation). Temporal analysis provided useful insight into the kinetics of each immunoglobulin isotype following immunisation, showing that IgM secretion peaked at day 14 and then decreased whereas IgG1 continued to increase from day 7 to day 21. Of interest, both WT and SIK1 KI mice followed the same trend across the experiment, however antigen-specific IgM and IgG1 from SIK1 KI mice were raised throughout (most prominently at day 14).

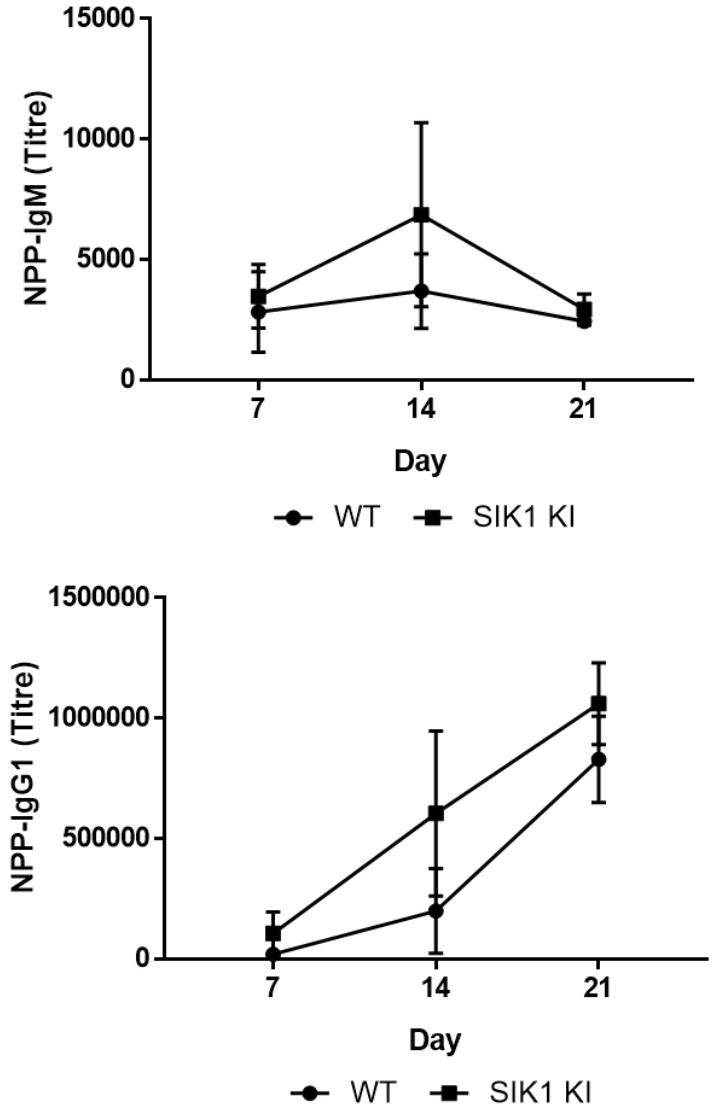

Figure 6.14 The impact of SIK1 kinase inactivity on antigen-specific immunoglobulin secretion. Serum was extracted from whole blood 7, 14 and 21 days post-immunization with NP-OVA and diluted to the appropriate concentration. IgM and IgG concentrations were quantified using an ELISA. WT n=4, SIK1 n=2.

6.5 Discussion

Genetic manipulation of the mouse genome provided additional means of exploration into the role of SIKs during terminal B-cell differentiation. Mice are commonly used as part of in vivo immunological experimentation and in many respects mirror human biology remarkably well. This is reflected by only 300 or so genes which appear to be unique to one species or the other (Chinwalla *et al.*, 2002). However, there are also significant differences between mice and human immune system development, activation, and response to challenge meaning that mice will often not wholly reflect the role of a gene in human pathology (Tellkamp *et al.*, 2014). With this in mind, it may be challenging to draw direct and meaningful comparisons between human and murine data sets.

Phenotypic analysis of B- and T-cell populations revealed a significant decrease in the proportion of splenic plasma cells in SIK1 KI mice at steady state. The presence of normal ratios of plasmablasts in the spleen and plasma cells in the bone marrow could suggest that SIK1 is neither required for the initiation of plasma cell differentiation, migration to the bone marrow or survival of long-lived plasma cells that have successfully reached the optimal supportive niche. Furthermore, plasma cells that arise in the spleen are thought to be short-lived (Jacob and Kelsoe, 1992). The specific reduction in mature splenic plasma cells could be interpreted to mean that SIK1 preferentially affects the survival of those cells destined for short-term antibody production and may be more important for extrafollicular or T-independent antigen responses in vivo (MacLennan *et al.*, 2003). The fact that the double SIK1/2 KI mice did not exhibit the same phenotype suggests a complex interaction between the individual isoforms, whereby SIK2 may be counteracting certain functions of SIK1 or vice versa. Furthermore, SIK1/2 KI mice displayed a significant increase in non B-cells in the spleen suggesting that SIK kinase activity could affect alternative immune populations such as T-cells, myeloid cells and NK cells. This is a novel finding as there has been no previous characterisation of the steady-state or dynamically responding immune cell populations in these mice. It is important to consider that phenotypic analysis in this chapter addressed multiple hypotheses and it is possible that with formal correction for multiple hypotheses, the results described above would become non-significant due to the increased discovery of false positives. If confirmed, this could be down to the fact that either there is no real difference in vivo between WT and SIK KI mice or that the experiments were substantially underpowered. To overcome this uncertainty, it would be necessary to increase the sample size based on a robust priori power calculation (Charan and Kantharia, 2013) and to repeat the experiment again.

In vitro differentiation of B-cells from KI mice revealed a decrease in the proportion of plasma cells ($B220^{-}$ $CD138^{+}$) in relation to the overall population in SIK1/2 mice when using TLR stimuli and a decrease in overall plasma cell number in all KI mice when using BCR stimuli. This highlights the effect that different mechanisms of stimuli can have on SIK utilisation since TLR stimulation appeared to affect rate of differentiation whereas BCR stimulation seemed to impact survival. Collectively, these results suggest that the SIKs may be of most importance when cells approach the latter stages of terminal differentiation as cells at earlier time points appeared phenotypically normal. This was surprising as loss of SIK kinase activity in human B-cells resulted in high numbers of cell death as soon as cells were stimulated to differentiate. This however may be explained by the differential expression of receptors between human and murine systems. For example, IL-5 induces murine splenic B-cells to differentiate into IgM cells and to undergo class switch recombination, resulting in IgG1 production (Horikawa and Takatsu, 2006), however a significant biological effect of IL-5 on human B-cells has been difficult to demonstrate (Baumann and Paul, 1997). Based on this, it is conceivable that the different cytokines within the human and murine in vitro systems combined with the loss of SIK kinase activity may affect the cells differently, however both data sets support the idea that SIKs aid survival of plasma cells.

To explore the in vivo function of SIK catalytic activity, the ability of SIK KI mice to mount an immune response to a model antigen was explored. In order to assess secretory capacity, antigen-specific IgM and IgG1 were investigated at days 7, 14 and 21 post-immunisation in SIK1 KI mice. Both NP-specific IgM and IgG1 were elevated in SIK1 KI mice compared with WT and this was most pronounced at 14 days post-immunisation. An attempt was also made to evaluate whether there were differences in affinity maturation but the results were inconclusive, as the WT mice failed to generate any high-affinity NP antibody and there were no differences seen in the SIK KI mice. Based on this set of results, it is conceivable that SIK1 KI ASCs are simply able to secrete more immunoglobulin suggesting that SIKs may act as a 'brake' in regards to immunoglobulin secretion. This theory would also agree with the gene expression data generated in chapter 4, which point to a role for SIKs in regulating protein processing in the ER and managing metabolic competence and are reminiscent of the effects of mTOR inhibition in plasma cells (Jones *et al.*, 2016; Benhamron *et al.*, 2015). To improve the validity of these findings, further work would include using animals with B-cell specific versions of the KI alleles or adoptively transferred KI B-cells to establish that the impact of SIK1 on increased antibody production is B-cell intrinsic. A quantitative ELISpot would be also be required to measure per cell secretion. As a final consideration, it would be of interest to assess alternative Ig isotypes, and to determine whether the data is replicated in human samples treated with a SIK inhibitor since there are well-known differences in isotype expression between mice and humans. For

example, although both species make four subtypes of IgG, they are not direct homologues of one another and have differing abilities to bind FcR or fix complement (Mestas and Hughes, 2004).

Although the aim of this chapter was to build on the data observed in human samples, the mice were generated from knock-in inactivating mutations, rather than knock-outs meaning that alternative mechanisms of SIK regulation could have contributed to the results including PKA, CaMKI, and other potentially undescribed upstream regulators (Berggreen *et al.*, 2012; Sonntag, Vaughan and Montminy, 2018). Based on this, it would be beneficial to use CD19-Cre mice or ERT2-Cre mice to assess the loss of SIK kinase activity specifically in B-cells or at particular time points during differentiation.

Overall, this chapter provides preliminary investigation into the role of SIKs during terminal B-cell differentiation in mice. Although not conclusive, it provides additional insight that SIKs may be necessary for plasma cell survival and immunoglobulin secretion.

Chapter 7 - Final Discussion

The antigen-dependent phase of B-cell development involves activated B-cell proliferation, differentiation, affinity maturation and antibody class switching, all of which occurs in the germinal centres of secondary lymphoid tissues. Following maturation, B-cells leave the germinal centre as high-affinity plasma cells and memory B-cells, providing adaptive immunity to the host.

Plasma cells are the terminal effectors of the B-cell lineage and devote most of their transcriptional and metabolic resources to antibody production. Therefore, specificity and longevity of plasma cells are the major determinants of durable humoral immunity (Shi *et al.*, 2015). The shortest-lived plasma cells persist only for several days after formation and are mostly localised to the extrafollicular regions of secondary lymphoid organs (Sze *et al.*, 2000). In contrast, long-lived plasma cells are largely bone marrow-resident and can persist for the entire lifespan of the organism (Slifka *et al.*, 1998; Manz, Thiel and Radbruch, 1997). Although there is an in-depth understanding of the factors that control commitment to the ASC fate, less is known about the transition between cycling plasmablasts and quiescent plasma cells. Gene expression profiling indicates that during the transition of human plasmablasts to long-lived plasma cells, a range of cell cycle regulators are induced in a pattern that suggests a quiescence program with potential for cell cycle re-entry (Tooze, 2013).

Initial work using WGCNA identified *SIK1* as a highly connected transcriptional regulator during the window that encompasses transition to quiescence and gene expression data showed that *SIK1* increased as B-cells transitioned to ASCs. Moreover, the upstream kinase LKB1 has been shown to be sequentially activated then inactivated in B-cells during a T-cell dependent response promoting terminal differentiation, although downstream mechanisms remain unclear (Waters, Walsh and Teitell, 2015). This prompted the hypothesis that SIK1 may be critical in the development and maintenance of plasma cells. Moreover, *SIK1* mapped to module 6 of publicly available myeloma data sets and was strongly associated with overall survival. This further suggested that SIK1 may be linked to a particular role in the pathogenesis of myeloma with the prospect of targeted intervention.

7.1 SIK expression

Current literature highlights the importance of all three SIK isoforms in many different aspects of cell biology. For example, SIK1 acts as a resolver of inflammation through repression of pro-inflammatory cytokines, SIK2 as a molecular switch in glucose production and SIK3 as a repressor of myogenesis through HDAC IIa nuclear export (Lombardi *et al.*, 2016; Patel *et al.*, 2014; Walkinshaw *et al.*, 2013). In this project, RNA-Seq data provided evidence that *SIK1* was

compatible with a requirement for differentiation, whereas the expression of *SIK2* and *SIK3* remained relatively static. In light of this, SIK1 became the primary focus of the project, however it was also important to assess the overall contribution of SIK2 and SIK3 due to prior knowledge of isoform redundancy (Abend *et al.*, 2017; Darling *et al.*, 2017). Protein analysis of primary cells showed that all 3 isoforms were induced strongly following B-cell activation (between day 1 and 3), however SIK2 appeared to decrease shortly after day 6 and was not detectable for the remainder of the differentiation. This appeared to suggest that all 3 isoforms could be required immediately post-B-cell activation to regulate either overlapping or distinct functions relating to cell growth, proliferation and mechanisms associated with CSR. Preferential expression of SIK1 was then evident as cells approached terminal differentiation. As the primary function of a plasma cell is to secrete large quantities of immunoglobulin, expression at this time point is consistent with a role in secretion and overall cell survival.

Following establishment of SIK isoform expression during a normal differentiation, it was of interest to determine expression in malignant plasma cells using multiple myeloma cell lines. Expression patterns varied and although no specific isoform could be correlated with sensitivity to SIK inhibition, resistant cell lines appeared to express both SIK1 and SIK2 at high levels whereas sensitive cell lines (OPM2, KMS11 and JJN3) displayed only one (SIK1 or SIK2). Detection of SIK3 proved difficult due to antibody quality, however expression levels were generally less than SIK1 and SIK2 and differed between the cell lines. Collectively, this provided further evidence supporting the differential expression of individual isoforms and suggested that a mechanism downstream of the SIKs could be accountable for differences observed in sensitivity to SIK inhibition. To determine the activation status of each isoform, it was considered appropriate to immunoprecipitate SIK1, SIK2 and SIK3 from both primary cells and myeloma cell lines and determine T182, T175 and T163 phosphorylation respectively (the site of activation of LKB1) as a measure of SIK activation. Initially this did not seem feasible due to poor antibody quality, however recent work in ovarian cells has provided strong evidence that LKB1 is not essential for SIK2 catalytic activity and instead SIK2 auto-phosphorylation at an alternative residue (S358) is triggered by the addition of ATP in vitro (Miranda *et al.*, 2016). This may be similar in the B-cell lineage meaning that the site of LKB1 phosphorylation would provide no further insight, and therefore future work would instead include an in vitro kinase assay to measure the activity of each individual isoform. Furthermore, attempts to assess inhibitory PKA signalling using the cAMP analogue Bt_2-cAMP seemed to suggest that cAMP does not regulate SIK activity in plasmablasts. With this in mind, it is possible that alternative upstream substrates such as CaMKI may regulate SIK activity in this context and therefore further work would focus on investigating these.

7.2 SIK inhibition

Use of the pan-SIK inhibitor HG-9-91-01 demonstrated that B-cells stimulated to differentiate depend on SIK kinase activity regardless of the differentiation stage. This profound effect was somewhat unexpected, given the previous observations using HG-9-91-01 on hepatocytes and macrophages. In both cases, HG-9-91-01 promoted dephosphorylation of CRTC2/3 resulting in enhanced gluconeogenic gene expression and a regulatory macrophage phenotype, but did not kill the cells (Patel *et al.*, 2014; Clark *et al.*, 2012). In contrast, recent work has demonstrated that AML cells rely on SIK activity (SIK3 in a partially redundant manner with SIK2) to proliferate through phosphorylation of HDAC4 and subsequent MEF2C function (Tarumoto *et al.*, 2018) providing insight into a new role for the SIKs.

Although a decrease in viability was the overall consequence of SIK inhibition, the underlying cause of this remained undefined. Intriguingly, SIK inhibition at progressive stages of the differentiation revealed potential differences in SIK regulation. For example, cell counts suggested a proliferative defect in activated B-cells whereas phenotypic analysis of plasmablasts seemed to suggest that cells may be experiencing enhanced differentiation. In plasma cells that have exited cell cycle, SIK inhibition did not appear to affect phenotype and instead appeared to create a survival defect which could be linked to secretory capacity. In addition, the ability to potently target cells stimulated in both a T-independent and T-dependent manner suggests that SIK inhibition might allow targeting of malignant plasma cells that are generated by either polyclonal activation or as a consequence of a GC-related event.

SIK inhibition in myeloma cell lines provided variable results. For example, OPM2 and KMS11 displayed over a 90% reduction in cell viability, whereas in other cell lines this decreased to around 50-75%. To determine the underlying cause for these differences, sequencing of the *SIK1* kinase domain was performed to assess inhibitor binding capability, however sequences were as expected and there were no differences between cell lines. As a further consideration, myeloma cell lines displayed differences in CRTC2 and HDAC4 protein expression, and therefore it is plausible that downstream regulation may confer sensitivity. Taking this into account, further work will include the generation of drug-resistant cell lines from HG-9-91-01 sensitive cell lines using a drug-training technique. This will hopefully reveal key differences in gene expression profile and downstream substrates within clonally related cells, and provide an explanation as to what determines overall sensitivity.

7.2.1 Off-target effects

HG-9-91-01 can target alternative kinases in addition to the SIKs, including Src family members (Src, Lck, and Yes), BTK, FGF and Ephrin receptors due to a threonine residue at the gatekeeper site. In an effort to try to rule out off-target effects contributing to the interpretation of this work, the improved analogue YKL-05-099 was tested on myeloma cell lines (KMS11, OPM2 and H929). Each cell line behaved in a similar manner to HG-9-91-01, however all three cell lines displayed a small decrease in sensitivity to SIK inhibition which is likely to be a consequence of improved specificity. This would seem to suggest that the results generated throughout are due to SIK inhibition, although the development of more specific SIK inhibitors and the use of siRNA would be required to be able to conclude this fully. Furthermore, use of CRISPR-mediated editing in the B-cell lineage was considered to overcome limitations associated with SIK inhibition, however due to the lack of single guide RNA's for SIK1 this was not feasible.

7.3 Downstream substrates

To uncover the potential mechanisms that may account for the observed effects of HG-9-91-01 on proliferation, survival and differentiation, likely downstream substrates were assessed. Although CRTC2 dephosphorylation was visible in both primary cells and myeloma cell lines, fractionation appeared to suggest that SIK inhibition caused cytoplasmic degradation rather than nuclear accumulation. As nuclear localisation is a requirement for CRTC2 regulated transcription and alternative splicing (Altarejos and Montminy, 2011), it seemed likely that CRTC2 may not be the main driver of SIK regulation in differentiating B-cells.

Investigation into class II HDACs revealed surprising results. For example, in activated B-cells class II HDAC expression levels did not change following SIK inhibition, however there was a decrease/loss of total protein in both plasmablasts and plasma cells. In vitro pan-HDAC inhibition (HDACi) with vorinostat has been shown to modify B-cell survival, proliferation and differentiation (Waibel *et al.*, 2015). Furthermore, B-cell and plasma-cell malignancies are sensitive to HDACi treatment, including myeloma plasma cells (Chesi *et al.*, 2012; Lindemann *et al.*, 2007). As HDAC and SIK inhibition produce similar effects on the B-cell lineage, it is possible that class II HDACs could be responsible for mediating SIK regulation. Furthermore, the variable effects of SIK inhibition on class II HDAC expression support the idea of the SIKs having distinct functions as cells differentiate. To further explore this hypothesis, additional work would include testing HDAC inhibitors on differentiating B-cells using the in vitro system. It would then be of interest to compare viability, phenotype and gene/protein expression profiles to determine whether results are comparable to SIK inhibition.

As a further consideration, total loss of class II HDAC protein could be the result of ubiquitin-dependent degradation. It has been documented that the putative 14-3-3 binding sites within class II HDACs are critical for phosphorylation-mediated stabilisation, and that ubiquitin-mediated proteolysis degrades un-phosphorylated forms (Li *et al.*, 2004; Zhou *et al.*, 2008). This could suggest that the SIKs in cooperation with 14-3-3 proteins stabilise class II HDACs, and that the dephosphorylation caused by SIK inhibition leads to degradation, although additional work to investigate this would be necessary.

Furthermore, MEF2 protein in plasmablasts decreased 24 hours post-SIK inhibition and downregulation of *MEF2B* mRNA was predominantly evident in activated B-cells. Members of the MEF2 family are known to have distinct roles within the B-cell lineage and regulate similar functions to those proposed to be regulated by the SIKs. For example, Mef2b has been implicated in germinal centre formation whereas Mef2c has been shown to play a role in B-cell proliferation and survival following BCR stimulation in vitro (Brescia *et al.*, 2018; Wilker *et al.*, 2008). Furthermore, the HDAC-MEF2 axis has been shown to contribute to the regulation of several differentiation-specific functions. For example, VEGF stimulation of HUVEC cells promotes HDAC5 phosphorylation and nuclear export thereby stimulating MEF2 dependent transcription and *in vitro* angiogenesis (Ha *et al.*, 2008) and deletion of HDAC9 in mice leads to exaggerated MEF2-dependent activation and cardiac hypertrophy (Zhang *et al.*, 2002). Collectively, this indicates that the SIK-HDAC-MEF2 axis could be crucial to various aspects of B-cell differentiation.

7.4 Gene expression

Given the alternations in class II HDAC expression levels following SIK inhibition, it seemed highly likely that there would also be equally compelling changes in gene expression. Differential gene expression analysis revealed that SIK inhibition convincingly orchestrated distinct changes in the transcriptome across differentiating cells. Furthermore, striking differences between activated B-cells and ASCs indicated that the SIKs could co-ordinate different downstream signalling mechanisms, highlighting both the complex and time-dependent nature of SIK regulation.

As cells approach terminal differentiation, metabolic reprogramming along with marked ER expansion and increased translation of ER-associated proteins is accompanied by the production of copious amounts of antibodies, with nearly 70% of the transcriptome being devoted to immunoglobulin synthesis (van Anken *et al.*, 2003). Whilst there were differences in regulation of the actin cytoskeleton and cell adhesion signatures, a consistent theme emerged highlighting the dramatic changes in genes related to metabolic fitness. Both plasmablasts and plasma cells displayed downregulation of PI3K/AKT signalling with genes specifically relating to cell survival, cell cycle and metabolism. Furthermore, there was striking downregulation of genes involved in

glycolysis demonstrating profound metabolic collapse and upregulation of genes involved in endocytosis and lysozyme formation suggesting an attempt at nutrient uptake and recovery. There was also downregulation of genes associated with the UPR including *XBP1, EIF2AK3*, *ATF6*, however despite previous findings demonstrating that ER stress-dependent pathways affect in vitro plasma cell death, the differences in lifespan between plasma cell subsets in vivo have not been explained by alterations in the UPR (Auner *et al.*, 2010; Pelletier *et al.*, 2006; Gaudette, Iwakoshi and Boise, 2014).

7.4.1 Plasma cell metabolism

During initial B-cell activation, glucose is used for oxidative phosphorylation, lipid synthesis and the pentose-phosphate pathway, however mature plasma cells primarily divert glucose into the hexosamine pathway to glycosylate antibodies (Doughty *et al.*, 2006). Upon depletion of energy reserves, glucose can be diverted from the hexosamine pathway back to glycolysis, and the resultant pyruvate can be used for respiration (Lam *et al.*, 2016). Glucose thereby maintains energy reserves and survival pathways that promote long-term maintenance of antibody-secreting cells (Lam *et al.*, 2018). Catabolised glucose has also been shown to stabilize the expression of anti-apoptotic Mcl1 which is essential for plasma cell survival (Peperzak *et al.*, 2013). Despite exhibiting similar transcriptomes, short- and long- lived plasma cells display metabolic differences. For example, under limiting nutrient availability and low ATP generation, long-lived plasma cells can expand their basal respiratory capacity to compensate whereas short-lived plasma cells are unable to perform this function and as a result, initiate pathways of programmed cell death. Long-lived plasma cells also take up higher levels of glucose and glutamine under homeostatic conditions (D'Souza and Bhattacharya, 2019). Collectively, this demonstrates that plasma cell longevity is primarily dictated by nutrient uptake and non-transcriptionally regulated metabolic pathways. Collapse of such pathways after SIK inhibition leads to the idea that the SIKs may regulate ASC metabolism in response to low nutrient availability. In addition, it would be of interest to determine whether SIK inhibition predominantly targets short- or long- lived plasma cells which display diverse metabolic profiles.

7.5 Implications for multiple myeloma treatment

As the critical metabolic pathways of plasma cells become defined, it will be important to determine if these same pathways can be targeted to eliminate multiple myeloma although alterations in cellular metabolism are common features of cancers due to excessively high metabolic demands. To both proliferate and secrete immunoglobulin, myeloma cells demonstrate changes in glycolysis, gluconeogenesis, the tricarboxylic acid cycle (glutamine uptake), oxidative phosphorylation and fatty acid/amino acid synthesis and degradation in an attempt to overcome the loss of nutrients (Rizzieri, Paul and Kang, 2019; Caro-Maldonado *et al.*, 2014) (Figure 7.1).

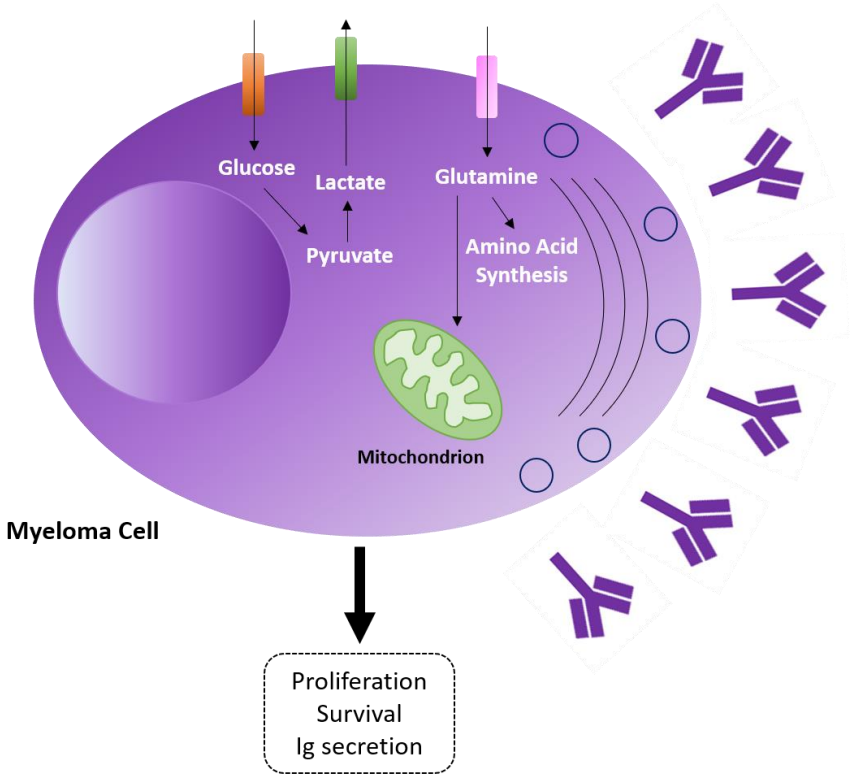

Figure 7.1 Schematic presentation of metabolic pathways utilised in multiple myeloma cells. (Adapted from Arfani *et al.* 2018).

Hexokinase II (HKII) which irreversibly catalyses the first step of glycolysis has been shown to be widely overexpressed enzyme in several cancers including multiple myeloma, indicating increased glucose metabolism (Nakano *et al.*, 2012). As the result of PI3K/AKT signalling, HKII binds to the voltage-dependent anion channel (VDAC) present on the outer membrane of mitochondria leading to the continuous proliferation of malignant cells (Hirschey *et al.*, 2015; Robey and Hay, 2006; Mathupala, Ko and Pedersen, 2006).

Furthermore, pyruvate kinase isozyme 2 (PKM2) which is involved in the final step of glycolysis has been shown to play a supportive role in tumour progression as a suppressor of apoptosis. PKM2 silencing leads to a decrease in multiple myeloma cell growth and cell cycle arrest at the G1/S transition (He *et al.*, 2015). In addition, metabolites do not only affect other metabolic components to benefit cancer development but also interfere with transcription factors involved in proliferation and apoptotic regulation (El Arfani *et al.*, 2018). This highlights the importance of metabolism for cancer cell survival, in particular the use of glycolysis. It also supports the proposal that SIKs may provide a useful therapeutic target in the treatment of myeloma due to the significant downregulation of the glycolytic pathway through PI3K/AKT signalling which ultimately impairs survival, respiration and secretory capacity. To evaluate this further, it would be useful to the measure oxygen consumption rate (OCR) and extracellular acidification rate (ECAR) of cells treated with a SIK inhibitor to determine whether gene expression defects translate into functional effects regarding mitochondrial respiration and glycolysis.

Although sensitivity to SIK inhibition varied when using myeloma cell lines and work to uncover these differences provided no further insight, it is conceivable that sensitivity could be linked to cell lines that have evolved pathways which depend heavily on SIK kinase activity, and those that are less sensitive depend on alternative pathways. Given these results, it would be a priority in the future to evaluate the impact of SIK inhibition on primary human myeloma samples cultured in vitro. Alternatively, transplantation of the spontaneously arising 5TMM cells from aged C57BL/KaLwRij mice into syngeneic younger recipients (Radl *et al.*, 1978) and treatment with YKL-05-099 could provide insight into the relationship between myeloma tumour burden and SIK dependency in vivo.

7.6 SIK KI mouse model

In a further attempt to overcome the off-target effects associated with current SIK inhibitors and to determine isoform specific effects, SIK KI mice were assessed for B- and T-cell populations, the ability to differentiate and immunoglobulin secretion. Initial work included the development of a multi-stage culture system that generates a phenotypically homogenous $B220^{-}CD138^{+}$ population of murine ASCs that have exited cell cycle and secrete class switched immunoglobulin. Work by Shi et al, it demonstrated that there were considerable transcriptional differences between ASCs generated in vivo and in vitro, in particular those generated in vitro were not as fully mature as their in vivo counterparts (Shi *et al.*, 2015). In this work, RNA-sequencing confirmed the specific expression patterns of known drivers of B cell, GC B cell and ASC fate and ASCs convincingly displayed a common gene program consistent with in vivo bone marrow derived plasma cells. Overall, this model system

provides an exciting opportunity to investigate the roles of potential mediators during murine ASC differentiation, including the SIKs.

Analysis of tissues from SIK KI mice at steady state highlighted a decrease in the proportion of splenic plasma cells, suggesting that SIK1 may preferentially affect the survival of cells destined for short term antibody production since populations in the bone marrow appeared normal. In contrast, double SIK1/2 KI mice did not exhibit the same result which suggests a complex interaction between the individual isoforms, whereby SIK2 may be counteracting certain functions of SIK1, or vice versa. In vitro differentiation revealed that SIK KI mice responded differently depending on the type of stimuli. For example, SIK1 KI mice activated with TLR stimuli displayed normal proportions of ASCs (although SIK1/2 KI mice displayed a decreased proportion), whereas BCR signalling resulted in a decreased number of ASCs at all-time points for SIK1 and SIK1/2 mice with no effect on phenotype. This was most likely a consequence of distinct transcriptional regulation of differentiation and demonstrates that activation of discrete signalling pathways influences dependency on SIK kinase activity. Overall, SIK KI mice were able to generate plasma cells, albeit a reduced number/percentage in agreement with what had been seen in splenic tissue at steady state.

Unexpectedly, immunisation revealed no differences in the proportion of splenic plasma cells which could potentially be a consequence of the small sample size (SIK1 n=2) or the time point chosen for analysis (21 days post-immunisation). To overcome this, power calculations have been performed to determine the number of samples required for a significant result (n=15), and in further experiments, tissues would be harvested between 7-10 days post-immunisation. Notably, there was also was a decrease in $CD8^+$ and $CD4^+$ T-cells and an increase in non- B/T cells in SIK2 KI mice, providing evidence that SIK2 may regulate alternative immune cell types. This agrees with recent work by He and colleagues in which SIK kinases were shown to act as critical effectors of LKB1 in maintaining energy homeostasis and survival in T-regulatory cells which are a subset of CD4+ T-cells (He *et al.*, 2017). Future work will also include gene expression profiling of SIK KI mice to determine whether any striking pathways are altered or dysregulated in the absence of SIK kinase activity and whether these overlap with pathways already identified in human cells.

Analysis of immunoglobulin in serum and supernatant provided varying results, however immunisation experiments revealed an increase in NP-specific IgG1 and IgM suggesting that SIK catalytic activity can influence T-cell dependent antibody responses in vivo. In view of this, it is conceivable that rather than displaying an enhanced ability to class switch, SIK KI ASCs are simply able to secrete more immunoglobulin. This implies that the SIKs act as a 'brake' and loss of SIK kinase activity releases this brake. This result is also consistent with a decrease in survival as

observed in both the human SIK inhibition experiments and SIK KI in vitro differentiation. When protein-folding requirements exceed the processing capacity of the ER, the accumulated misfolded and unfolded proteins trigger the UPR, resulting in the adjustment of protein synthesis and the enhancement of ER folding capacity as well as increased degradation of misfolded proteins and enhanced ER biogenesis (Ron and Walter, 2007; Grootjans *et al.*, 2016). However, when these attempts fail and ER stress is persistent, UPR signalling typically switches to a pro-apoptotic mode (Hetz, 2012). Therefore, increased immunoglobulin synthesis in SIK1 KI mice could lead to ER stress/exhaustion and subsequent apoptosis. To clarify these results, it will be necessary to use animals with B-cell specific versions of the KI alleles or B-cell specific SIK1 knockout mice to establish that the impact of SIK1 on antibody production is B-cell intrinsic. Moreover, due to the decrease in cell number observed in vitro, it will be important to quantify immunoglobulin production using a quantitative ELISpot to measure secretion per cell and to assess alternative isotypes. As a final consideration, assessment of immunoglobulin secretion in differentiating human samples will be necessary to determine whether SIK inhibition correlates with the differences seen in murine samples.

7.7 Overall conclusion

In summary, the data presented in this thesis support the initial hypothesis predicting an important role for the SIKs during the final stages of plasma cell differentiation. In addition to this, the SIKs were also shown to be involved during the earlier stages of B-cell differentiation to support functions such as growth and proliferation. Although initial work proposed SIK1 as the main regulator, lack of isoform specific inhibitors/successful knockdowns coupled with the difficult interpretation of data generated from the use of SIK KI mice means that no definitive conclusion can be made regarding individual isoform contribution. However, it is possible that individual isoforms contribute to different functions i.e. growth, proliferation, differentiation etc due to different expression patterns during human differentiation and the variable results observed between SIK KI mice. Although this work provides insight into numerous pathways and proteins which are affected by SIK inhibition, it is difficult to describe a complete mechanism due to the diversity of SIK-mediated functions and pathways which appear to change as the cells differentiate. Overall, it seems reasonable to conclude that the SIKs directly target class II HDACs during the later stages of differentiation to regulate either chromatin accessibility and/or transcription factor activity as outlined in Figure 7.2.

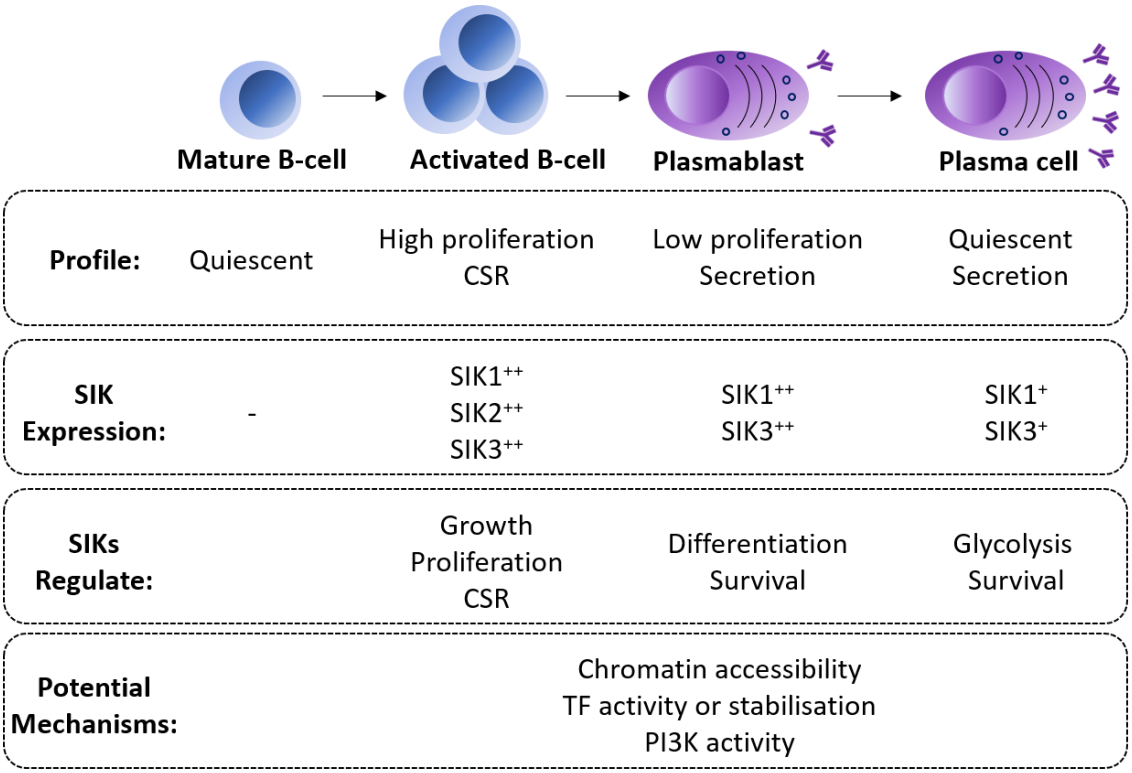

Figure 7.2 Schematic diagram highlighting SIK expression, regulation and the potential underlying mechanisms during terminal differentiation.

Nuclear HDACs make up the catalytic core of chromatin accessibility modulating complexes that are active at *cis*-regulatory elements such as enhancers and promoters (Lee and Young, 2013). In recent times, HDAC inhibitors have been shown to dynamically effect chromatin states. For example, anti-tumour responses to HDAC inhibition in vitro are associated with hyper-acetylation of chromatin and induction of apoptosis or cell-cycle arrest (Bolden, Peart and Johnstone, 2006). From this perspective, it is possible that the SIKs may regulate chromatin accessibility through employment of the HDACs. To investigate this further, it would be of use to apply ATAC-seq to differentiating cells treated with/without a SIK inhibitor in order to compare global chromatin accessibility profiles.

Furthermore, the observed effects may be due to HDAC mediated epigenetic modifications such as transcription factor activity or stabilisation. For example, HDAC inhibitors dramatically decrease HIF-1α protein and transcriptional activity presenting a potential novel approach in the treatment of hepatocellular carcinoma (Kim *et al.*, 2007; Hutt *et al.*, 2014). Furthermore, HDAC inhibition also results in the acetylation of c-Myc at lysine 323, reducing its expression and causing apoptosis (Nebbioso *et al.*, 2017). As HIF-1α is known to enhance glycolytic flux by targeting transporters and enzymes involved in glycolysis (Marin-Hernandez *et al.*, 2009) and HDACs can directly interact with HIF-1α to influence stability (Schoepflin, Shapiro and Risbud, 2016), it is plausible that SIK inhibition alters HIF-1α activity or stabilisation which ultimately

impairs glycolysis leading to nutrient deprivation and cell death. To further explore this theory, HIF-1α protein expression will be evaluated during B-cell differentiation, before and after SIK inhibition.

Alternatively, gene expression analysis uncovered significant downregulation of genes involved in PI3K/AKT signalling which also feeds into the glycolytic pathway through HK2 and PFK2. Miranda and colleagues uncovered a previously unrecognised role of SIK2 in coupling metabolism with survival at the cancer metastatic niche. More specifically, SIK2 directly activated PI3K through phosphorylation of p85α in ovarian cancer cells thus regulating proliferation and survival. As a result, targeting of SIK2 will have the potential to block major pathways that contribute to the establishment and growth of tumour metastasis (Miranda *et al.*, 2016). Furthermore, SIK2 depletion has been shown to reduce AKT phosphorylation which resides downstream of PI3K (Ahmed *et al.*, 2010). Collectively, this suggests that SIKs may regulate PI3K signalling in the B-cell lineage driving cell survival and metabolism and future work will assess the relationship between the SIKs and PI3K. As a final consideration, HDAC inhibitors are known to synergize with PI3K inhibitors to inhibit tumour growth in vivo (Pei *et al.*, 2016) strengthening the case that SIKs would make effective therapeutic targets due to the simultaneous inhibition of multiple downstream pathways.

References

Abbondanza, C., C. De Rosa, A. D'arcangelo, M. Pacifico, C. Spizuoco, G. Piluso, E. Di Zazzo, P. Gazzerro, N. Medici, B. Moncharmont and G. A. Puca. 2012. Identification of a functional estrogen-responsive enhancer element in the promoter 2 of PRDM2 gene in breast cancer cell lines. *J Cell Physiol,* **227**(3), pp.964-75.

Abe, M., K. Hiura, J. Wilde, A. Shioyasono, K. Moriyama, T. Hashimoto, S. Kido, T. Oshima, H. Shibata, S. Ozaki, D. Inoue and T. Matsumoto. 2004. Osteoclasts enhance myeloma cell growth and survival via cell-cell contact: a vicious cycle between bone destruction and myeloma expansion. *Blood,* **104**(8), pp.2484-91.

Abend, A., O. Shkedi, M. Fertouk, L. H. Caspi and I. Kehat. 2017. Salt-inducible kinase induces cytoplasmic histone deacetylase 4 to promote vascular calcification. *EMBO Rep,* **18**(7), pp.1166-1185.

Ahmed, A. A., Z. Lu, N. B. Jennings, D. Etemadmoghadam, L. Capalbo, R. O. Jacamo, N. Barbosa-Morais, X. F. Le, P. Vivas-Mejia, G. Lopez-Berestein, G. Grandjean, G. Bartholomeusz, W. Liao, M. Andreeff, D. Bowtell, D. M. Glover, A. K. Sood and R. C. Bast, Jr. 2010. SIK2 is a centrosome kinase required for bipolar mitotic spindle formation that provides a potential target for therapy in ovarian cancer. *Cancer Cell,* **18**(2), pp.109-21.

Al-Hakim, A. K., O. Göransson, M. Deak, R. Toth, D. G. Campbell, N. A. Morrice, A. R. Prescott and D. R. J. J. O. C. S. Alessi. 2005. 14-3-3 cooperates with LKB1 to regulate the activity and localization of QSK and SIK. **118**(23), pp.5661-5673.

Alessi, D. R., K. Sakamoto and J. R. Bayascas. 2006. LKB1-dependent signaling pathways. *Annu Rev Biochem,* **75**, pp.137-63.

Alexander, A. and C. L. Walker. 2011. The role of LKB1 and AMPK in cellular responses to stress and damage. *FEBS Lett,* **585**(7), pp.952-7.

Alinikula, J., K. P. Nera, S. Junttila and O. Lassila. 2011. Alternate pathways for Bcl6-mediated regulation of B cell to plasma cell differentiation. *Eur J Immunol,* **41**(8), pp.2404-13.

Allman, D. and S. Pillai. 2008. Peripheral B cell subsets. *Curr Opin Immunol,* **20**(2), pp.149-57.

Altarejos, J. Y. and M. Montminy. 2011. CREB and the CRTC co-activators: sensors for hormonal and metabolic signals. *Nat Rev Mol Cell Biol,* **12**(3), pp.141-51.

Amanna, I. J. and M. K. Slifka. 2010. Mechanisms that determine plasma cell lifespan and the duration of humoral immunity. *Immunol Rev,* **236**, pp.125-38.

Anderson, K. A., T. J. Ribar, F. Lin, P. K. Noeldner, M. F. Green, M. J. Muehlbauer, L. A. Witters, B. E. Kemp and A. R. Means. 2008. Hypothalamic CaMKK2 contributes to the regulation of energy balance. *Cell Metab,* **7**(5), pp.377-88.

Aronov, M. and B. J. J. O. C. I. Tirosh. 2016. Metabolic control of plasma cell differentiation-what we know and what we don't know. **36**(1), pp.12-17.

Auner, H. W., C. Beham-Schmid, N. Dillon and P. Sabbattini. 2010. The life span of short-lived plasma cells is partly determined by a block on activation of apoptotic caspases acting in combination with endoplasmic reticulum stress. *Blood,* **116**(18), pp.3445-55.

Backs, J., K. Song, S. Bezprozvannaya, S. Chang and E. N. Olson. 2006. CaM kinase II selectively signals to histone deacetylase 4 during cardiomyocyte hypertrophy. *J Clin Invest,* **116**(7), pp.1853-64.

Bayles, I. and C. Milcarek. 2014. Plasma cell formation, secretion, and persistence: the short and the long of it. *Crit Rev Immunol,* **34**(6), pp.481-99.

Belloni, D., S. Heltai, M. Ponzoni, A. Villa, B. Vergani, L. Pecciarini, M. Marcatti, S. Girlanda, G. Tonon and F. J. H. Ciceri. 2018. Modeling multiple myeloma-bone marrow interactions and response to drugs in a 3D surrogate microenvironment. **103**(4), pp.707-716.

Belnoue, E., M. Pihlgren, T. L. Mcgaha, C. Tougne, A. F. Rochat, C. Bossen, P. Schneider, B. Huard, P. H. Lambert and C. A. Siegrist. 2008. APRIL is critical for plasmablast survival in the bone marrow and poorly expressed by early-life bone marrow stromal cells. *Blood,* **111**(5), pp.2755-64.

Benhamron, S., S. P. Pattanayak, M. Berger and B. Tirosh. 2015. mTOR activation promotes plasma cell differentiation and bypasses XBP-1 for immunoglobulin secretion. *Mol Cell Biol,* **35**(1), pp.153-66.

Benson, M. J., S. R. Dillon, E. Castigli, R. S. Geha, S. Xu, K.-P. Lam and R. J. J. T. J. O. I. Noelle. 2008. Cutting edge: the dependence of plasma cells and independence of memory B cells on BAFF and APRIL. **180**(6), pp.3655-3659.

Berggreen, C., E. Henriksson, H. A. Jones, N. Morrice and O. Goransson. 2012. cAMP-elevation mediated by beta-adrenergic stimulation inhibits salt-inducible kinase (SIK) 3 activity in adipocytes. *Cell Signal,* **24**(9), pp.1863-71.

Bianchi, G. and K. C. Anderson. 2014. Understanding biology to tackle the disease: Multiple myeloma from bench to bedside, and back. *CA Cancer J Clin,* **64**(6), pp.422-44.

Birgegård, G., P. Gascón and H. J. E. J. O. H. Ludwig. 2006. Evaluation of anaemia in patients with multiple myeloma and lymphoma: findings of the European CANCER ANAEMIA SURVEY. **77**(5), pp.378-386.

Bittinger, M. A., E. Mcwhinnie, J. Meltzer, V. Iourgenko, B. Latario, X. Liu, C. H. Chen, C. Song, D. Garza and M. Labow. 2004. Activation of cAMP response element-mediated gene expression by regulated nuclear transport of TORC proteins. *Curr Biol,* **14**(23), pp.2156-61.

Blagih, J., C. M. Krawczyk and R. G. Jones. 2012. LKB1 and AMPK: central regulators of lymphocyte metabolism and function. *Immunol Rev,* **249**(1), pp.59-71.

Bolden, J. E., M. J. Peart and R. W. Johnstone. 2006. Anticancer activities of histone deacetylase inhibitors. *Nat Rev Drug Discov,* **5**(9), pp.769-84.

Bossie, A. and E. S. Vitetta. 1991. IFN-gamma enhances secretion of IgG2a from IgG2a-committed LPS-stimulated murine B cells: implications for the role of IFN-gamma in class switching. *Cell Immunol,* **135**(1), pp.95-104.

Brescia, P., C. Schneider, A. B. Holmes, Q. Shen, S. Hussein, L. Pasqualucci, K. Basso and R. Dalla-Favera. 2018. MEF2B Instructs Germinal Center Development and Acts as an Oncogene in B Cell Lymphomagenesis. *Cancer Cell,* **34**(3), pp.453-465.e9.

Brown, K. A., N. U. Samarajeewa and E. R. Simpson. 2013. Endocrine-related cancers and the role of AMPK. *Mol Cell Endocrinol,* **366**(2), pp.170-9.

Brynjolfsson, S. F., L. Persson Berg, T. Olsen Ekerhult, I. Rimkute, M. J. Wick, L. Mårtensson and O. J. F. I. I. Grimsholm. 2018. Long-lived plasma cells in mice and men. **9**, p2673.

Buchta, C. M. and G. a. J. I. R. Bishop. 2014. Toll-like receptors and B cells: functions and mechanisms. **59**(1-3), pp.12-22.

Calado, D. P., Y. Sasaki, S. A. Godinho, A. Pellerin, K. Kochert, B. P. Sleckman, I. M. De Alboran, M. Janz, S. Rodig and K. Rajewsky. 2012. The cell-cycle regulator c-Myc is essential for the formation and maintenance of germinal centers. *Nat Immunol,* **13**(11), pp.1092-100.

Care, M. A., S. J. Stephenson, N. A. Barnes, I. Fan, A. Zougman, Y. M. El-Sherbiny, E. M. Vital, D. R. Westhead, R. M. Tooze and G. M. Doody. 2016. Network Analysis Identifies Proinflammatory Plasma Cell Polarization for Secretion of ISG15 in Human Autoimmunity. *J Immunol,* **197**(4), pp.1447-59.

Care, M. A., D. R. Westhead and R. M. Tooze. 2019. Parsimonious Gene Correlation Network Analysis (PGCNA): a tool to define modular gene co-expression for refined molecular stratification in cancer. *NPJ Syst Biol Appl,* **5**, p13.

Caro-Maldonado, A., R. Wang, A. G. Nichols, M. Kuraoka, S. Milasta, L. D. Sun, A. L. Gavin, E. D. Abel, G. Kelsoe, D. R. Green and J. C. Rathmell. 2014. Metabolic reprogramming is required for antibody production that is suppressed in anergic but exaggerated in chronically BAFF-exposed B cells. *J Immunol,* **192**(8), pp.3626-36.

Castigli, E., S. A. Wilson, S. Scott, F. Dedeoglu, S. Xu, K. P. Lam, R. J. Bram, H. Jabara and R. S. Geha. 2005. TACI and BAFF-R mediate isotype switching in B cells. *J Exp Med,* **201**(1), pp.35-9.

Catley, L., E. Weisberg, T. Kiziltepe, Y. T. Tai, T. Hideshima, P. Neri, P. Tassone, P. Atadja, D. Chauhan, N. C. Munshi and K. C. Anderson. 2006. Aggresome induction by proteasome

inhibitor bortezomib and alpha-tubulin hyperacetylation by tubulin deacetylase (TDAC) inhibitor LBH589 are synergistic in myeloma cells. *Blood,* **108**(10), pp.3441-9.

Ch'ng, T. H., B. Uzgil, P. Lin, N. K. Avliyakulov, T. J. O'dell and K. C. J. C. Martin. 2012. Activity-dependent transport of the transcriptional coactivator CRTC1 from synapse to nucleus. **150**(1), pp.207-221.

Charan, J. and N. Kantharia. 2013. How to calculate sample size in animal studies? *Journal of Pharmacology and Pharmacotherapeutics,* **4**(4), p303.

Chaudhuri, J., M. Tian, C. Khuong, K. Chua, E. Pinaud and F. W. Alt. 2003. Transcription-targeted DNA deamination by the AID antibody diversification enzyme. *Nature,* **422**(6933), pp.726-30.

Chen-Kiang, S. 2003. Cell-cycle control of plasma cell differentiation and tumorigenesis. *Immunol Rev,* **194**, pp.39-47.

Chen-Kiang, S. J. I. R. 2003. Cell-cycle control of plasma cell differentiation and tumorigenesis. **194**(1), pp.39-47.

Chen, F., L. Chen, Q. Qin and X. Sun. 2019. Salt-Inducible Kinase 2: An Oncogenic Signal Transmitter and Potential Target for Cancer Therapy. **9**(18).

Cheng, H., P. Liu, Z. C. Wang, L. Zou, S. Santiago, V. Garbitt, O. V. Gjoerup, J. D. Iglehart, A. Miron, A. L. Richardson, W. C. Hahn and J. J. Zhao. 2009. SIK1 couples LKB1 to p53-dependent anoikis and suppresses metastasis. *Sci Signal,* **2**(80), pra35.

Chesi, M., G. M. Matthews, V. M. Garbitt, S. E. Palmer, J. Shortt, M. Lefebure, A. K. Stewart, R. W. Johnstone and P. L. Bergsagel. 2012. Drug response in a genetically engineered mouse model of multiple myeloma is predictive of clinical efficacy. *Blood,* **120**(2), pp.376-85.

Cheung, T. H. and T. A. Rando. 2013. Molecular regulation of stem cell quiescence. *Nat Rev Mol Cell Biol,* **14**(6), pp.329-40.

Chinwalla, A. T., L. L. Cook, K. D. Delehaunty, G. A. Fewell, L. A. Fulton, R. S. Fulton, T. A. Graves, L. W. Hillier, E. R. Mardis, J. D. Mcpherson, T. L. Miner, W. E. Nash, J. O. Nelson, M. N. Nhan, K. H. Pepin, C. S. Pohl, T. C. Ponce, B. Schultz, J. Thompson, E. Trevaskis, R. H. Waterston, M. C. Wendl, R. K. Wilson, S.-P. Yang, P. An, E. Berry, B. Birren, T. Bloom, D. G. Brown, J. Butler, M. Daly, R. David, J. Deri, S. Dodge, K. Foley, D. Gage, S. Gnerre, T. Holzer, D. B. Jaffe, M. Kamal, E. K. Karlsson, C. Kells, A. Kirby, E. J. Kulbokas, E. S. Lander, T. Landers, J. P. Leger, R. Levine, K. Lindblad-Toh, E. Mauceli, J. H. Mayer, M. Mccarthy, J. Meldrim, J. Meldrim, J. P. Mesirov, R. Nicol, C. Nusbaum, S. Seaman, T. Sharpe, A. Sheridan, J. B. Singer, R. Santos, B. Spencer, N. Stange-Thomann, J. P. Vinson, C. M. Wade, J. Wierzbowski, D. Wyman, M. C. Zody, E. Birney, N. Goldman, A. Kasprzyk, E. Mongin, A. G. Rust, G. Slater, A. Stabenau, A. Ureta-Vidal, S. Whelan, R. Ainscough, J. Attwood, J. Bailey, K. Barlow, S. Beck, J. Burton, M. Clamp, C. Clee, A. Coulson, J. Cuff, V. Curwen, T. Cutts, J. Davies, E. Eyras, D. Grafham, S. Gregory, T. Hubbard, A. Hunt, M. Jones, A. Joy, S. Leonard, C. Lloyd*, et al.* 2002. Initial sequencing and comparative analysis of the mouse genome. *Nature,* **420**(6915), pp.520-562.

Choi, S., D. S. Lim and J. Chung. 2015. Feeding and Fasting Signals Converge on the LKB1-SIK3 Pathway to Regulate Lipid Metabolism in Drosophila. *PLoS Genet,* **11**(5), pe1005263.

Chu, V. T., A. Frohlich, G. Steinhauser, T. Scheel, T. Roch, S. Fillatreau, J. J. Lee, M. Lohning and C. Berek. 2011. Eosinophils are required for the maintenance of plasma cells in the bone marrow. *Nat Immunol,* **12**(2), pp.151-9.

Chung, J. B., M. Silverman and J. G. Monroe. 2003. Transitional B cells: step by step towards immune competence. *Trends Immunol,* **24**(6), pp.343-9.

Clark, K., K. F. Mackenzie, K. Petkevicius, Y. Kristariyanto, J. Zhang, H. G. Choi, M. Peggie, L. Plater, P. G. Pedrioli and E. J. P. O. T. N. a. O. S. Mciver. 2012. Phosphorylation of CRTC3 by the salt-inducible kinases controls the interconversion of classically activated and regulatory macrophages. **109**(42), pp.16986-16991.

Clocchiatti, A., E. Di Giorgio, F. Demarchi and C. Brancolini. 2013. Beside the MEF2 axis: unconventional functions of HDAC4. *Cell Signal,* **25**(1), pp.269-76.

Clocchiatti, A., E. Di Giorgio, G. Viviani, C. Streuli, A. Sgorbissa, R. Picco, V. Cutano and C. Brancolini. 2015. The MEF2-HDAC axis controls proliferation of mammary epithelial cells and acini formation in vitro. *J Cell Sci,* **128**(21), pp.3961-76.

Cocco, M., S. Stephenson, M. A. Care, D. Newton, N. A. Barnes, A. Davison, A. Rawstron, D. R. Westhead, G. M. Doody and R. M. J. T. J. O. I. Tooze. 2012. In vitro generation of long-lived human plasma cells. **189**(12), pp.5773-5785.

Cohen, P. J. B. J. 2010. Guidelines for the effective use of chemical inhibitors of protein function to understand their roles in cell regulation. **425**(1), pp.53-54.

Coluccia, A. M., T. Cirulli, P. Neri, F. Dammacco, P. Tassone, C. Gambacorti and A. Vacca. 2007. *Dasatinib Inhibits Multiple Myeloma Growth by Blocking PDGF-Rb and c-Src Activity in Patient-Derived Tumor and Endothelial Cells*. Am Soc Hematology.

Commisso, C., S. M. Davidson, R. G. Soydaner-Azeloglu, S. J. Parker, J. J. Kamphorst, S. Hackett, E. Grabocka, M. Nofal, J. A. Drebin, C. B. Thompson, J. D. Rabinowitz, C. M. Metallo, M. G. Vander Heiden and D. Bar-Sagi. 2013. Macropinocytosis of protein is an amino acid supply route in Ras-transformed cells. *Nature,* **497**(7451), pp.633-7.

Corcoran, L. M. and S. L. J. I. Nutt. 2016. Long-Lived Plasma Cells Have a Sweet Tooth. **45**(1), pp.3-5.

D'souza, L. and D. Bhattacharya. 2019. Plasma cells: You are what you eat. *Immunol Rev,* **288**(1), pp.161-177.

Darling, N. J., R. Toth, J. S. Arthur and K. Clark. 2017. Inhibition of SIK2 and SIK3 during differentiation enhances the anti-inflammatory phenotype of macrophages. *Biochem J,* **474**(4), pp.521-537.

Davidson, S. M., O. Jonas, M. A. Keibler, H. W. Hou, A. Luengo, J. R. Mayers, J. Wyckoff, A. M. Del Rosario, M. Whitman, C. R. Chin, K. J. Condon, A. Lammers, K. A. Kellersberger, B. K. Stall, G. Stephanopoulos, D. Bar-Sagi, J. Han, J. D. Rabinowitz, M. J. Cima, R. Langer and M. G. Vander Heiden. 2017. Direct evidence for cancer-cell-autonomous extracellular protein catabolism in pancreatic tumors. *Nat Med,* **23**(2), pp.235-241.

De Silva, N. S. and U. Klein. 2015. Dynamics of B cells in germinal centres. *Nat Rev Immunol,* **15**(3), pp.137-48.

Dentin, R., Y. Liu, S. H. Koo, S. Hedrick, T. Vargas, J. Heredia, J. Yates, 3rd and M. Montminy. 2007. Insulin modulates gluconeogenesis by inhibition of the coactivator TORC2. *Nature,* **449**(7160), pp.366-9.

Di Giorgio, E. and C. Brancolini. 2016. Regulation of class IIa HDAC activities: it is not only matter of subcellular localization. *Epigenomics,* **8**(2), pp.251-69.

Di Giorgio, E., A. Clocchiatti, S. Piccinin, A. Sgorbissa, G. Viviani, P. Peruzzo, S. Romeo, S. Rossi, A. P. Dei Tos, R. Maestro and C. Brancolini. 2013. MEF2 is a converging hub for histone deacetylase 4 and phosphatidylinositol 3-kinase/Akt-induced transformation. *Mol Cell Biol,* **33**(22), pp.4473-91.

Dimenna, L. J., W. F. Yen, L. Nicolas, R. Sharma, Z. N. Saldanha and J. Chaudhuri. 2017. Cutting Edge: The Transcription Factor Sox2 Regulates AID Expression in Class-Switched B Cells. *J Immunol,* **198**(6), pp.2244-2248.

Djouder, N., R. D. Tuerk, M. Suter, P. Salvioni, R. F. Thali, R. Scholz, K. Vaahtomeri, Y. Auchli, H. Rechsteiner, R. A. Brunisholz, B. Viollet, T. P. Makela, T. Wallimann, D. Neumann and W. Krek. 2010. PKA phosphorylates and inactivates AMPKalpha to promote efficient lipolysis. *Embo j,* **29**(2), pp.469-81.

Dobin, A., C. A. Davis, F. Schlesinger, J. Drenkow, C. Zaleski, S. Jha, P. Batut, M. Chaisson and T. R. Gingeras. 2013. STAR: ultrafast universal RNA-seq aligner. *Bioinformatics,* **29**(1), pp.15-21.

Dominguez-Sola, D., G. D. Victora, C. Y. Ying, R. T. Phan, M. Saito, M. C. Nussenzweig and R. Dalla-Favera. 2012. The proto-oncogene MYC is required for selection in the germinal center and cyclic reentry. *Nat Immunol,* **13**(11), pp.1083-91.

Doughty, C. A., B. F. Bleiman, D. J. Wagner, F. J. Dufort, J. M. Mataraza, M. F. Roberts and T. C. Chiles. 2006. Antigen receptor-mediated changes in glucose metabolism in B

lymphocytes: role of phosphatidylinositol 3-kinase signaling in the glycolytic control of growth. *Blood,* **107**(11), pp.4458-65.

Driver, D. J., L. J. Mcheyzer-Williams, M. Cool, D. B. Stetson and M. G. J. T. J. O. I. Mcheyzer-Williams. 2001. Development and maintenance of a B220− memory B cell compartment. **167**(3), pp.1393-1405.

Ehrhardt, R. O., W. Strober and G. R. Harriman. 1992. Effect of transforming growth factor (TGF)-beta 1 on IgA isotype expression. TGF-beta 1 induces a small increase in sIgA+ B cells regardless of the method of B cell activation. *J Immunol,* **148**(12), pp.3830-6.

El Arfani, C., K. De Veirman, K. Maes, E. De Bruyne and E. Menu. 2018. Metabolic Features of Multiple Myeloma. *Int J Mol Sci,* **19**(4).

Ellmeier, W. and C. J. N. R. I. Seiser. 2018. Histone deacetylase function in CD4+ T cells. p1.

Facon, T., X. Leleu, A. K. Stewart, A. Spencer, P. Rowlings, C. Hulin, M. Attal, F. Garzon, E. Bleickardt and K. Gialelis. 2009. *Dasatinib in Combination with Lenalidomide and Dexamethasone in Patients with Relapsed or Refractory Multiple Myeloma: Preliminary Results of a Phase I Study*. Am Soc Hematology.

Feldman, J. D., L. Vician, M. Crispino, W. Hoe, M. Baudry and H. R. J. J. O. N. Herschman. 2000. The salt-inducible kinase, SIK, is induced by depolarization in brain. **74**(6), pp.2227-2238.

Fogarty, S. and D. G. Hardie. 2009. C-terminal phosphorylation of LKB1 is not required for regulation of AMP-activated protein kinase, BRSK1, BRSK2, or cell cycle arrest. *J Biol Chem,* **284**(1), pp.77-84.

Foy, T. M., F. H. Durie and R. J. Noelle. 1994. The expansive role of CD40 and its ligand, gp39, in immunity. *In: Seminars in immunology*: Elsevier, pp.259-266.

Frigo, D. E., M. K. Howe, B. M. Wittmann, A. M. Brunner, I. Cushman, Q. Wang, M. Brown, A. R. Means and D. P. Mcdonnell. 2011. CaM kinase kinase beta-mediated activation of the growth regulatory kinase AMPK is required for androgen-dependent migration of prostate cancer cells. *Cancer Res,* **71**(2), pp.528-37.

Gaudette, B. T., N. N. Iwakoshi and L. H. Boise. 2014. Bcl-xL protein protects from C/EBP homologous protein (CHOP)-dependent apoptosis during plasma cell differentiation. *J Biol Chem,* **289**(34), pp.23629-40.

Geisberger, R., M. Lamers and G. Achatz. 2006. The riddle of the dual expression of IgM and IgD. *Immunology,* **118**(4), pp.429-37.

Ghislat, G., M. Patron, R. Rizzuto and E. Knecht. 2012. Withdrawal of essential amino acids increases autophagy by a pathway involving Ca2+/calmodulin-dependent kinase kinase-beta (CaMKK-beta). *J Biol Chem,* **287**(46), pp.38625-36.

Gil, V. S., G. Bhagat, L. Howell, J. Zhang, C. H. Kim, S. Stengel, F. Vega, A. Zelent and K. Petrie. 2016. Deregulated expression of HDAC9 in B cells promotes development of lymphoproliferative disease and lymphoma in mice. *Dis Model Mech,* **9**(12), pp.1483-1495.

Goldschmidt, H., H. Lannert, J. Bommer and A. D. Ho. 2000. Multiple myeloma and renal failure. *Nephrology Dialysis Transplantation,* **15**(3), pp.301-304.

Goodings, C., E. Smith, E. Mathias, N. Elliott, S. M. Cleveland, R. M. Tripathi, J. H. Layer, X. Chen, Y. Guo, Y. Shyr, R. Hamid, Y. Du and U. P. Dave. 2015. Hhex is Required at Multiple Stages of Adult Hematopoietic Stem and Progenitor Cell Differentiation. *Stem Cells,* **33**(8), pp.2628-41.

Grootjans, J., A. Kaser, R. J. Kaufman and R. S. Blumberg. 2016. The unfolded protein response in immunity and inflammation. *Nat Rev Immunol,* **16**(8), pp.469-84.

Groves, C., J. Carrell, R. Grady, B. Rajan, C. Morehouse, R. Halpin, J. Wang, J. Wu, Y. Shrestha and R. J. B. A. Rayanki. 2018. CD19-positive antibody-secreting cells provide immune memory. **2**(22), pp.3163-3176.

Guo, B. and T. L. Rothstein. 2005. B cell receptor (BCR) cross-talk: IL-4 creates an alternate pathway for BCR-induced ERK activation that is phosphatidylinositol 3-kinase independent. *J Immunol,* **174**(9), pp.5375-81.

Gyory, I., G. Fejer, N. Ghosh, E. Seto and K. L. Wright. 2003. Identification of a functionally impaired positive regulatory domain I binding factor 1 transcription repressor in myeloma cell lines. *J Immunol,* **170**(6), pp.3125-33.

Ha, C. H., B. S. Jhun, H. Y. Kao and Z. G. Jin. 2008. VEGF stimulates HDAC7 phosphorylation and cytoplasmic accumulation modulating matrix metalloproteinase expression and angiogenesis. *Arterioscler Thromb Vasc Biol,* **28**(10), pp.1782-8.

Haberland, M., R. L. Montgomery and E. N. Olson. 2009. The many roles of histone deacetylases in development and physiology: implications for disease and therapy. *Nat Rev Genet,* **10**(1), pp.32-42.

Han, J., E. Li, L. Chen, Y. Zhang, F. Wei, J. Liu, H. Deng and Y. Wang. 2015. The CREB coactivator CRTC2 controls hepatic lipid metabolism by regulating SREBP1. *Nature,* **524**(7564), pp.243-6.

Hanten, J. A., J. P. Vasilakos, C. L. Riter, L. Neys, K. E. Lipson, S. S. Alkan and W. Birmachu. 2008. Comparison of human B cell activation by TLR7 and TLR9 agonists. *BMC Immunol,* **9**, p39.

Harada, T., T. Hideshima and K. C. Anderson. 2016. Histone deacetylase inhibitors in multiple myeloma: from bench to bedside. *Int J Hematol,* **104**(3), pp.300-9.

Hardy, R. R., C. E. Carmack, S. A. Shinton, J. D. Kemp and K. Hayakawa. 1991. Resolution and characterization of pro-B and pre-pro-B cell stages in normal mouse bone marrow. **173**(5), pp.1213-1225.

Hashimoto, Y. K., T. Satoh, M. Okamoto and H. Takemori. 2008. Importance of autophosphorylation at Ser186 in the A-loop of salt inducible kinase 1 for its sustained kinase activity. *J Cell Biochem,* **104**(5), pp.1724-39.

He, L., J. X. Yu, L. Liu, I. M. Buyse, M. S. Wang, Q. C. Yang, A. Nakagawara, G. M. Brodeur, Y. E. Shi and S. Huang. 1998. RIZ1, but not the alternative RIZ2 product of the same gene, is underexpressed in breast cancer, and forced RIZ1 expression causes G2-M cell cycle arrest and/or apoptosis. *Cancer Res,* **58**(19), pp.4238-44.

He, N., W. Fan, B. Henriquez, R. T. Yu, A. R. Atkins, C. Liddle, Y. Zheng, M. Downes and R. M. Evans. 2017. Metabolic control of regulatory T cell (Treg) survival and function by Lkb1. **114**(47), pp.12542-12547.

He, Y., Y. Wang, H. Liu, X. Xu, S. He, J. Tang, Y. Huang, X. Miao, Y. Wu, Q. Wang and C. Cheng. 2015. Pyruvate kinase isoform M2 (PKM2) participates in multiple myeloma cell proliferation, adhesion and chemoresistance. *Leuk Res,* **39**(12), pp.1428-36.

Heise, N., N. S. De Silva, K. Silva, A. Carette, G. Simonetti, M. Pasparakis and U. Klein. 2014. Germinal center B cell maintenance and differentiation are controlled by distinct NF-kappaB transcription factor subunits. *J Exp Med,* **211**(10), pp.2103-18.

Hemmings, B. A. and D. F. Restuccia. 2012. PI3K-PKB/Akt pathway. *Cold Spring Harb Perspect Biol,* **4**(9), pa011189.

Hemminki, A., D. Markie, I. Tomlinson, E. Avizienyte, S. Roth, A. Loukola, G. Bignell, W. Warren, M. Aminoff, P. Hoglund, H. Jarvinen, P. Kristo, K. Pelin, M. Ridanpaa, R. Salovaara, T. Toro, W. Bodmer, S. Olschwang, A. S. Olsen, M. R. Stratton, A. De La Chapelle and L. A. Aaltonen. 1998. A serine/threonine kinase gene defective in Peutz-Jeghers syndrome. *Nature,* **391**(6663), pp.184-7.

Henriksson, E., H. A. Jones, K. Patel, M. Peggie, N. Morrice, K. Sakamoto and O. J. B. J. Göransson. 2012. The AMPK-related kinase SIK2 is regulated by cAMP via phosphorylation at Ser358 in adipocytes. **444**(3), pp.503-514.

Henriksson, E., J. Säll, A. Gormand, S. Wasserstrom, N. A. Morrice, A. M. Fritzen, M. Foretz, D. G. Campbell, K. Sakamoto, M. Ekelund, E. Degerman, K. G. Stenkula and O. Göransson. 2015. SIK2 regulates CRTCs, HDAC4 and glucose uptake in adipocytes. **128**(3), pp.472-486.

Hetz, C. 2012. The unfolded protein response: controlling cell fate decisions under ER stress and beyond. *Nat Rev Mol Cell Biol,* **13**(2), pp.89-102.

Hirschey, M. D., R. J. Deberardinis, A. M. E. Diehl, J. E. Drew, C. Frezza, M. F. Green, L. W. Jones, Y. H. Ko, A. Le, M. A. Lea, J. W. Locasale, V. D. Longo, C. A. Lyssiotis, E. Mcdonnell, M. Mehrmohamadi, G. Michelotti, V. Muralidhar, M. P. Murphy, P. L. Pedersen, B. Poore,

L. Raffaghello, J. C. Rathmell, S. Sivanand, M. G. Vander Heiden and K. E. Wellen. 2015. Dysregulated metabolism contributes to oncogenesis. *Semin Cancer Biol,* **35 Suppl**, pp.S129-s150.

Hoek, K. S., N. C. Schlegel, O. M. Eichhoff, D. S. Widmer, C. Praetorius, S. O. Einarsson, S. Valgeirsdottir, K. Bergsteinsdottir, A. Schepsky, R. Dummer and E. Steingrimsson. 2008. Novel MITF targets identified using a two-step DNA microarray strategy. **21**(6), pp.665-676.

Holmes, M. L., C. Pridans and S. L. Nutt. 2008. The regulation of the B-cell gene expression programme by Pax5. *Immunol Cell Biol,* **86**(1), pp.47-53.

Hong, B., J. Zhang and W. Yang. 2018. Activation of the LKB1SIK1 signaling pathway inhibits the TGFbetamediated epithelialmesenchymal transition and apoptosis resistance of ovarian carcinoma cells. *Mol Med Rep,* **17**(2), pp.2837-2844.

Horikawa, K. and K. J. I. Takatsu. 2006. Interleukin-5 regulates genes involved in B-cell terminal maturation. **118**(4), pp.497-508.

Hoxhaj, G., J. Hughes-Hallett, R. C. Timson, E. Ilagan, M. Yuan, J. M. Asara, I. Ben-Sahra and B. D. J. C. R. Manning. 2017. The mTORC1 signaling network senses changes in cellular purine nucleotide levels. **21**(5), pp.1331-1346.

Hu, H., A. Juvekar, C. A. Lyssiotis, E. C. Lien, J. G. Albeck, D. Oh, G. Varma, Y. P. Hung, S. Ullas and J. J. C. Lauring. 2016. Phosphoinositide 3-kinase regulates glycolysis through mobilization of aldolase from the actin cytoskeleton. **164**(3), pp.433-446.

Hutt, D. M., D. M. Roth, H. Vignaud, C. Cullin and M. Bouchecareilh. 2014. The histone deacetylase inhibitor, Vorinostat, represses hypoxia inducible factor 1 alpha expression through translational inhibition. *PLoS One,* **9**(8), pe106224.

Iourgenko, V., W. Zhang, C. Mickanin, I. Daly, C. Jiang, J. M. Hexham, A. P. Orth, L. Miraglia, J. Meltzer, D. Garza, G. W. Chirn, E. Mcwhinnie, D. Cohen, J. Skelton, R. Terry, Y. Yu, D. Bodian, F. P. Buxton, J. Zhu, C. Song and M. A. Labow. 2003. Identification of a family of cAMP response element-binding protein coactivators by genome-scale functional analysis in mammalian cells. *Proc Natl Acad Sci U S A,* **100**(21), pp.12147-52.

Ise, W., M. Kohyama, B. U. Schraml, T. Zhang, B. Schwer, U. Basu, F. W. Alt, J. Tang, E. M. Oltz, T. L. Murphy and K. M. Murphy. 2011. The transcription factor BATF controls the global regulators of class-switch recombination in both B cells and T cells. *Nat Immunol,* **12**(6), pp.536-43.

Jacob, J. and G. Kelsoe. 1992. In situ studies of the primary immune response to (4-hydroxy-3-nitrophenyl)acetyl. II. A common clonal origin for periarteriolar lymphoid sheath-associated foci and germinal centers. *J Exp Med,* **176**(3), pp.679-87.

Jagannath, A., R. Butler, S. I. H. Godinho, Y. Couch, L. A. Brown, S. R. Vasudevan, K. C. Flanagan, D. Anthony, G. C. Churchill, M. J. A. Wood, G. Steiner, M. Ebeling, M. Hossbach, J. G. Wettstein, G. E. Duffield, S. Gatti, M. W. Hankins, R. G. Foster and S. N. Peirson. 2013. The CRTC1-SIK1 pathway regulates entrainment of the circadian clock. *Cell,* **154**(5), pp.1100-1111.

Jansson, D., A. C. Ng, A. Fu, C. Depatie, M. Al Azzabi and R. A. Screaton. 2008. Glucose controls CREB activity in islet cells via regulated phosphorylation of TORC2. *Proc Natl Acad Sci U S A,* **105**(29), pp.10161-6.

Jellusova, J. and R. C. Rickert. 2016. The PI3K pathway in B cell metabolism. *Crit Rev Biochem Mol Biol,* **51**(5), pp.359-378.

Jiang, G. L. and S. Huang. 2000. The yin-yang of PR-domain family genes in tumorigenesis. *Histol Histopathol,* **15**(1), pp.109-17.

Jones, D. D., B. T. Gaudette, J. R. Wilmore, I. Chernova, A. Bortnick, B. M. Weiss and D. Allman. 2016. mTOR has distinct functions in generating versus sustaining humoral immunity. *J Clin Invest,* **126**(11), pp.4250-4261.

Jourdan, M., A. Caraux, J. De Vos, G. Fiol, M. Larroque, C. Cognot, C. Bret, C. Duperray, D. Hose and B. Klein. 2009. An in vitro model of differentiation of memory B cells into plasmablasts and plasma cells including detailed phenotypic and molecular characterization. *Blood,* **114**(25), pp.5173-81.

Jourdan, M., M. Cren, N. Robert, K. Bolloré, T. Fest, C. Duperray, F. Guilloton, D. Hose, K. Tarte and B. J. L. Klein. 2014. IL-6 supports the generation of human long-lived plasma cells in combination with either APRIL or stromal cell-soluble factors. **28**(8), p1647.

Kallies, A., J. Hasbold, K. Fairfax, C. Pridans, D. Emslie, B. S. Mckenzie, A. M. Lew, L. M. Corcoran, P. D. Hodgkin, D. M. Tarlinton and S. L. Nutt. 2007. Initiation of plasma-cell differentiation is independent of the transcription factor Blimp-1. *Immunity,* **26**(5), pp.555-66.

Kallies, A., J. Hasbold, D. M. Tarlinton, W. Dietrich, L. M. Corcoran, P. D. Hodgkin and S. L. J. J. O. E. M. Nutt. 2004. Plasma cell ontogeny defined by quantitative changes in blimp-1 expression. **200**(8), pp.967-977.

Kaminski, D. A., C. Wei, Y. Qian, A. F. Rosenberg and I. J. F. I. I. Sanz. 2012. Advances in human B cell phenotypic profiling. **3**, p302.

Kanno, Y., B. Z. Levi, T. Tamura and K. Ozato. 2005. Immune cell-specific amplification of interferon signaling by the IRF-4/8-PU.1 complex. *J Interferon Cytokine Res,* **25**(12), pp.770-9.

Katoh, Y., H. Takemori, N. Horike, J. Doi, M. Muraoka, L. Min and M. Okamoto. 2004. Salt-inducible kinase (SIK) isoforms: their involvement in steroidogenesis and adipogenesis. *Mol Cell Endocrinol,* **217**(1-2), pp.109-12.

Kaur, G. and J. M. Dufour. 2012. Cell lines: Valuable tools or useless artifacts. *Spermatogenesis,* **2**(1), pp.1-5.

Kikuchi, S., R. Suzuki, H. Ohguchi, Y. Yoshida, D. Lu, F. Cottini, J. Jakubikova, G. Bianchi, T. Harada, G. Gorgun, Y. T. Tai, P. G. Richardson, T. Hideshima and K. C. Anderson. 2015. Class IIa HDAC inhibition enhances ER stress-mediated cell death in multiple myeloma. *Leukemia,* **29**(9), pp.1918-27.

Kim, S. H., J. W. Jeong, J. A. Park, J. W. Lee, J. H. Seo, B. K. Jung, M. K. Bae and K. W. Kim. 2007. Regulation of the HIF-1alpha stability by histone deacetylases. *Oncol Rep,* **17**(3), pp.647-51.

Kitano, M., S. Moriyama, Y. Ando, M. Hikida, Y. Mori, T. Kurosaki and T. Okada. 2011. Bcl6 protein expression shapes pre-germinal center B cell dynamics and follicular helper T cell heterogeneity. *Immunity,* **34**(6), pp.961-72.

Klein, U., S. Casola, G. Cattoretti, Q. Shen, M. Lia, T. Mo, T. Ludwig, K. Rajewsky and R. Dalla-Favera. 2006. Transcription factor IRF4 controls plasma cell differentiation and class-switch recombination. *Nat Immunol,* **7**(7), pp.773-82.

Klein, U. and R. Dalla-Favera. 2008. Germinal centres: role in B-cell physiology and malignancy. *Nat Rev Immunol,* **8**(1), pp.22-33.

Koo, S. H., L. Flechner, L. Qi, X. Zhang, R. A. Screaton, S. Jeffries, S. Hedrick, W. Xu, F. Boussouar, P. Brindle, H. Takemori and M. Montminy. 2005. The CREB coactivator TORC2 is a key regulator of fasting glucose metabolism. *Nature,* **437**(7062), pp.1109-11.

Krock, B., N. Skuli and M. C. Simon. 2011. The tumor suppressor LKB1 emerges as a critical factor in hematopoietic stem cell biology. *Cell Metab,* **13**(1), pp.8-10.

Kuchen, S., R. Robbins, G. P. Sims, C. Sheng, T. M. Phillips, P. E. Lipsky and R. J. T. J. O. I. Ettinger. 2007. Essential role of IL-21 in B cell activation, expansion, and plasma cell generation during CD4+ T cell-B cell collaboration. **179**(9), pp.5886-5896.

Lam, W. Y., A. M. Becker, K. M. Kennerly, R. Wong, J. D. Curtis, E. M. Llufrio, K. S. Mccommis, J. Fahrmann, H. A. Pizzato, R. M. Nunley, J. Lee, M. J. Wolfgang, G. J. Patti, B. N. Finck, E. L. Pearce and D. Bhattacharya. 2016. Mitochondrial Pyruvate Import Promotes Long-Term Survival of Antibody-Secreting Plasma Cells. *Immunity,* **45**(1), pp.60-73.

Lam, W. Y. and D. J. T. I. I. Bhattacharya. 2018. Metabolic links between plasma cell survival, secretion, and stress. **39**(1), pp.19-27.

Lam, W. Y., A. Jash, C.-H. Yao, L. D'souza, R. Wong, R. M. Nunley, G. P. Meares, G. J. Patti and D. J. C. R. Bhattacharya. 2018. Metabolic and transcriptional modules independently diversify plasma cell lifespan and function. **24**(9), pp.2479-2492. e6.

Langfelder, P. and S. Horvath. 2008. WGCNA: an R package for weighted correlation network analysis. *BMC Bioinformatics,* **9**, p559.

Lanzavecchia, A. J. N. 1985. Antigen-specific interaction between T and B cells. **314**(6011), p537.
Laurent, S. A., F. S. Hoffmann, P.-H. Kuhn, Q. Cheng, Y. Chu, M. Schmidt-Supprian, S. M. Hauck, E. Schuh, M. Krumbholz and H. J. N. C. Rübsamen. 2015. γ-secretase directly sheds the survival receptor BCMA from plasma cells. **6**, p7333.
Le Gallou, S., G. Caron, C. Delaloy, D. Rossille, K. Tarte and T. J. T. J. O. I. Fest. 2012. IL-2 requirement for human plasma cell generation: Coupling differentiation and proliferation by enhancing MAPK–ERK signaling. **189**(1), pp.161-173.
Lebien, T. W. and T. F. Tedder. 2008. B lymphocytes: how they develop and function. *Blood,* **112**(5), pp.1570-80.
Lee, C. H., M. Melchers, H. Wang, T. A. Torrey, R. Slota, C.-F. Qi, J. Y. Kim, P. Lugar, H. J. Kong and L. J. J. O. E. M. Farrington. 2006. Regulation of the germinal center gene program by interferon (IFN) regulatory factor 8/IFN consensus sequence-binding protein. *J.E.M,* **203**(1), pp.63-72.
Lee, J. O., S. K. Lee, N. Kim, J. H. Kim, G. Y. You, J. W. Moon, S. Jie, S. J. Kim, Y. W. Lee, H. J. Kang, Y. Lim, S. H. Park and H. S. Kim. 2013. E3 ubiquitin ligase, WWP1, interacts with AMPKalpha2 and down-regulates its expression in skeletal muscle C2C12 cells. *J Biol Chem,* **288**(7), pp.4673-80.
Lee, T. I. and R. A. Young. 2013. Transcriptional regulation and its misregulation in disease. *Cell,* **152**(6), pp.1237-51.
Li, B. and C. N. Dewey. 2011. RSEM: accurate transcript quantification from RNA-Seq data with or without a reference genome. *BMC Bioinformatics,* **12**, p323.
Li, X., S. Song, Y. Liu, S. H. Ko and H. Y. Kao. 2004. Phosphorylation of the histone deacetylase 7 modulates its stability and association with 14-3-3 proteins. *J Biol Chem,* **279**(33), pp.34201-8.
Li, Y., J. Roberts, Z. Akhavanaghdam and N. Hao. 2017. Mitogen-activated protein kinase (MAPK) dynamics determine cell fate in the yeast mating response. *J Biol Chem,* **292**(50), pp.20354-20361.
Liebig, T. M., A. Fiedler, N. Klein-Gonzalez, A. Shimabukuro-Vornhagen and M. Von Bergwelt-Baildon. 2010. Murine model of CD40-activation of B cells. *J Vis Exp,* (37).
Lin, X., H. Takemori, Y. Katoh, J. Doi, N. Horike, A. Makino, Y. Nonaka and M. Okamoto. 2001. Salt-inducible kinase is involved in the ACTH/cAMP-dependent protein kinase signaling in Y1 mouse adrenocortical tumor cells. *Mol Endocrinol,* **15**(8), pp.1264-76.
Lindemann, R. K., A. Newbold, K. F. Whitecross, L. A. Cluse, A. J. Frew, L. Ellis, S. Williams, A. P. Wiegmans, A. E. Dear, C. L. Scott, M. Pellegrini, A. Wei, V. M. Richon, P. A. Marks, S. W. Lowe, M. J. Smyth and R. W. Johnstone. 2007. Analysis of the apoptotic and therapeutic activities of histone deacetylase inhibitors by using a mouse model of B cell lymphoma. *Proc Natl Acad Sci U S A,* **104**(19), pp.8071-6.
Lizcano, J. M., O. Goransson, R. Toth, M. Deak, N. A. Morrice, J. Boudeau, S. A. Hawley, L. Udd, T. P. Makela, D. G. Hardie and D. R. Alessi. 2004. LKB1 is a master kinase that activates 13 kinases of the AMPK subfamily, including MARK/PAR-1. *Embo j,* **23**(4), pp.833-43.
Lombardi, M. S., C. Gilliéron, D. Dietrich and C. J. J. O. L. B. Gabay. 2016. SIK inhibition in human myeloid cells modulates TLR and IL-1R signaling and induces an anti-inflammatory phenotype. **99**(5), pp.711-721.
Love, M. I., W. Huber and S. Anders. 2014. Moderated estimation of fold change and dispersion for RNA-seq data with DESeq2. *Genome Biol,* **15**(12), p550.
Luan, B., M. O. Goodarzi, N. G. Phillips, X. Guo, Y. D. Chen, J. Yao, M. Allison, J. I. Rotter, R. Shaw and M. Montminy. 2014. Leptin-mediated increases in catecholamine signaling reduce adipose tissue inflammation via activation of macrophage HDAC4. *Cell Metab,* **19**(6), pp.1058-65.
Luan, B., Y. S. Yoon, J. Le Lay, K. H. Kaestner, S. Hedrick and M. Montminy. 2015. CREB pathway links PGE2 signaling with macrophage polarization. *Proc Natl Acad Sci U S A,* **112**(51), pp.15642-7.
Lwin, S. T., C. M. Edwards and R. Silbermann. 2016. Preclinical animal models of multiple myeloma. *Bonekey Rep,* **5**, p772.

Mackay, F. and P. Schneider. 2008. TACI, an enigmatic BAFF/APRIL receptor, with new unappreciated biochemical and biological properties. *Cytokine Growth Factor Rev,* **19**(3-4), pp.263-76.

Mackenzie, K. F., K. Clark, S. Naqvi, V. A. Mcguire, G. Noehren, Y. Kristariyanto, M. Van Den Bosch, M. Mudaliar, P. C. Mccarthy, M. J. Pattison, P. G. Pedrioli, G. J. Barton, R. Toth, A. Prescott and J. S. Arthur. 2013a. PGE(2) induces macrophage IL-10 production and a regulatory-like phenotype via a protein kinase A-SIK-CRTC3 pathway. *J Immunol,* **190**(2), pp.565-77.

Mackenzie, K. F., K. Clark, S. Naqvi, V. A. Mcguire, G. Nöehren, Y. Kristariyanto, M. Van Den Bosch, M. Mudaliar, P. C. Mccarthy, M. J. Pattison, P. G. A. Pedrioli, G. J. Barton, R. Toth, A. Prescott and J. S. C. Arthur. 2013b. PGE₂ Induces Macrophage IL-10 Production and a Regulatory-like Phenotype via a Protein Kinase A–SIK–CRTC3 Pathway. **190**(2), pp.565-577.

Maclennan, I. C., K. M. Toellner, A. F. Cunningham, K. Serre, D. M. Sze, E. Zuniga, M. C. Cook and C. G. Vinuesa. 2003. Extrafollicular antibody responses. *Immunol Rev,* **194**, pp.8-18.

Mahindra, A., T. Hideshima and K. C. Anderson. 2010. Multiple myeloma: biology of the disease. *Blood Rev,* **24 Suppl 1**, pp.S5-11.

Maillet, V., N. Boussetta, J. Leclerc, V. Fauveau, M. Foretz, B. Viollet, J. P. Couty, S. Celton-Morizur, C. Perret and C. Desdouets. 2018. LKB1 as a Gatekeeper of Hepatocyte Proliferation and Genomic Integrity during Liver Regeneration. *Cell Rep,* **22**(8), pp.1994-2005.

Manning, G., D. B. Whyte, R. Martinez, T. Hunter and S. Sudarsanam. 2002. The protein kinase complement of the human genome. *Science,* **298**(5600), pp.1912-34.

Manz, R. A., A. Thiel and A. Radbruch. 1997. Lifetime of plasma cells in the bone marrow. *Nature,* **388**(6638), pp.133-4.

Marin-Hernandez, A., J. C. Gallardo-Perez, S. J. Ralph, S. Rodriguez-Enriquez and R. Moreno-Sanchez. 2009. HIF-1alpha modulates energy metabolism in cancer cells by inducing over-expression of specific glycolytic isoforms. *Mini Rev Med Chem,* **9**(9), pp.1084-101.

Marshall, C. J. 1995. Specificity of receptor tyrosine kinase signaling: transient versus sustained extracellular signal-regulated kinase activation. *Cell,* **80**(2), pp.179-85.

Mathupala, S. P., Y. H. Ko and P. L. Pedersen. 2006. Hexokinase II: cancer's double-edged sword acting as both facilitator and gatekeeper of malignancy when bound to mitochondria. *Oncogene,* **25**(34), pp.4777-86.

Matthews, S. A., M. N. Navarro, L. V. Sinclair, E. Emslie, C. Feijoo-Carnero and D. a. J. B. J. Cantrell. 2010. Unique functions for protein kinase D1 and protein kinase D2 in mammalian cells. **432**(1), pp.153-163.

Mccune, J., R. Namikawa, H. Kaneshima, L. Shultz, M. Lieberman and I. J. S. Weissman. 1988. The SCID-hu mouse: murine model for the analysis of human hematolymphoid differentiation and function. **241**(4873), pp.1632-1639.

Mcheyzer-Williams, L. J., M. Cool and M. G. Mcheyzer-Williams. 2000. Antigen-specific B cell memory: expression and replenishment of a novel B220− memory B cell compartment. *Journal of Experimental Medicine,* **191**(7), pp.1149-1166.

Mestas, J. and C. C. W. Hughes. 2004. Of Mice and Not Men: Differences between Mouse and Human Immunology. **172**(5), pp.2731-2738.

Mihaylova, M. M. and R. J. Shaw. 2011. The AMPK signalling pathway coordinates cell growth, autophagy and metabolism. *Nat Cell Biol,* **13**(9), pp.1016-23.

Mihaylova, M. M. and R. J. Shaw. 2013. Metabolic reprogramming by class I and II histone deacetylases. *Trends Endocrinol Metab,* **24**(1), pp.48-57.

Mihaylova, M. M., D. S. Vasquez, K. Ravnskjaer, P. D. Denechaud, R. T. Yu, J. G. Alvarez, M. Downes, R. M. Evans, M. Montminy and R. J. Shaw. 2011. Class IIa histone deacetylases are hormone-activated regulators of FOXO and mammalian glucose homeostasis. *Cell,* **145**(4), pp.607-21.

Miranda, F., D. Mannion, S. Liu, Y. Zheng, L. S. Mangala, C. Redondo, S. Herrero-Gonzalez, R. Xu, C. Taylor, D. F. Chedom, M. Karaminejadranjbar, A. Albukhari, D. Jiang, S. Pradeep, C.

Rodriguez-Aguayo, G. Lopez-Berestein, E. Salah, K. R. Abdul Azeez, J. M. Elkins, L. Campo, K. A. Myers, D. Klotz, S. Bivona, S. Dhar, R. C. Bast, Jr., H. Saya, H. G. Choi, N. S. Gray, R. Fischer, B. M. Kessler, C. Yau, A. K. Sood, T. Motohara, S. Knapp and A. A. Ahmed. 2016. Salt-Inducible Kinase 2 Couples Ovarian Cancer Cell Metabolism with Survival at the Adipocyte-Rich Metastatic Niche. *Cancer Cell,* **30**(2), pp.273-289.

Mitsiades, C. S., P. J. Hayden, K. C. Anderson and P. G. Richardson. 2007. From the bench to the bedside: emerging new treatments in multiple myeloma. *Best Pract Res Clin Haematol,* **20**(4), pp.797-816.

Miura, Y., M. Morooka, N. Sax, R. Roychoudhuri, A. Itoh-Nakadai, A. Brydun, R. Funayama, K. Nakayama, S. Satomi, M. Matsumoto, K. Igarashi and A. Muto. 2018. Bach2 Promotes B Cell Receptor-Induced Proliferation of B Lymphocytes and Represses Cyclin-Dependent Kinase Inhibitors. *J Immunol,* **200**(8), pp.2882-2893.

Morgan, G. J., B. A. Walker and F. E. Davies. 2012. The genetic architecture of multiple myeloma. *Nat Rev Cancer,* **12**(5), pp.335-48.

Morgan, M. A., E. Magnusdottir, T. C. Kuo, C. Tunyaplin, J. Harper, S. J. Arnold, K. Calame, E. J. Robertson, E. K. J. M. Bikoff and C. Biology. 2009. Blimp-1/Prdm1 alternative promoter usage during mouse development and plasma cell differentiation. **29**(21), pp.5813-5827.

Morgan, M. A., A. W. Mould, L. Li, E. J. Robertson and E. K. Bikoff. 2012. Alternative splicing regulates Prdm1/Blimp-1 DNA binding activities and corepressor interactions. *Mol Cell Biol,* **32**(17), pp.3403-13.

Mujahid, N., Y. Liang, R. Murakami, H. G. Choi, A. S. Dobry, J. Wang, Y. Suita, Q. Y. Weng, J. Allouche, L. V. Kemeny, A. L. Hermann, E. M. Roider, N. S. Gray and D. E. Fisher. 2017. A UV-Independent Topical Small-Molecule Approach for Melanin Production in Human Skin. *Cell Rep,* **19**(11), pp.2177-2184.

Muto, A., K. Ochiai, Y. Kimura, A. Itoh-Nakadai, K. L. Calame, D. Ikebe, S. Tashiro and K. Igarashi. 2010. Bach2 represses plasma cell gene regulatory network in B cells to promote antibody class switch. *Embo j,* **29**(23), pp.4048-61.

Nakano, A., H. Miki, S. Nakamura, T. Harada, A. Oda, H. Amou, S. Fujii, K. Kagawa, K. Takeuchi, S. Ozaki, T. Matsumoto and M. Abe. 2012. Up-regulation of hexokinaseII in myeloma cells: targeting myeloma cells with 3-bromopyruvate. *J Bioenerg Biomembr,* **44**(1), pp.31-8.

Narahara, H., E. Sakai, Y. Yamaguchi, S. Narahara, M. Iwatake, K. Okamoto, N. Yoshida and T. Tsukuba. 2018. Actin binding LIM 1 (abLIM1) negatively controls osteoclastogenesis by regulating cell migration and fusion. *J Cell Physiol,* **234**(1), pp.486-499.

Nebbioso, A., V. Carafa, M. Conte, F. P. Tambaro, C. Abbondanza, J. Martens, M. Nees, R. Benedetti, I. Pallavicini, S. Minucci, G. Garcia-Manero, F. Iovino, G. Lania, C. Ingenito, V. Belsito Petrizzi, H. G. Stunnenberg and L. Altucci. 2017. c-Myc Modulation and Acetylation Is a Key HDAC Inhibitor Target in Cancer. *Clin Cancer Res,* **23**(10), pp.2542-2555.

Nguyen, D. C., S. Garimalla, H. Xiao, S. Kyu, I. Albizua, J. Galipeau, K.-Y. Chiang, E. K. Waller, R. Wu and G. J. N. C. Gibson. 2018. Factors of the bone marrow microniche that support human plasma cell survival and immunoglobulin secretion. **9**(1), p3698.

Novak, A. J., J. R. Darce, B. K. Arendt, B. Harder, K. Henderson, W. Kindsvogel, J. A. Gross, P. R. Greipp and D. F. Jelinek. 2004. Expression of BCMA, TACI, and BAFF-R in multiple myeloma: a mechanism for growth and survival. *Blood,* **103**(2), pp.689-94.

Nutt, S. L., P. D. Hodgkin, D. M. Tarlinton and L. M. J. N. R. I. Corcoran. 2015. The generation of antibody-secreting plasma cells. **15**(3), p160.

Nutt, S. L. and B. L. Kee. 2007. The transcriptional regulation of B cell lineage commitment. *Immunity,* **26**(6), pp.715-25.

O'connor, B. P., V. S. Raman, L. D. Erickson, W. J. Cook, L. K. Weaver, C. Ahonen, L. L. Lin, G. T. Mantchev, R. J. Bram and R. J. Noelle. 2004. BCMA is essential for the survival of long-lived bone marrow plasma cells. *J Exp Med,* **199**(1), pp.91-8.

Ocana, E., I. Gonzalez-Garcia, N. C. Gutierrez, F. Mora-Lopez, J. A. Brieva and A. Campos-Caro. 2006. The expression of PRDI-BF1 beta isoform in multiple myeloma plasma cells. *Haematologica,* **91**(11), pp.1579-80.

Ochiai, K., M. Maienschein-Cline, G. Simonetti, J. Chen, R. Rosenthal, R. Brink, A. S. Chong, U. Klein, A. R. Dinner, H. Singh and R. Sciammas. 2013. Transcriptional regulation of germinal center B and plasma cell fates by dynamical control of IRF4. *Immunity,* **38**(5), pp.918-29.

Oh, K. J., H. S. Han, M. J. Kim and S. H. Koo. 2013. CREB and FoxO1: two transcription factors for the regulation of hepatic gluconeogenesis. *BMB Rep,* **46**(12), pp.567-74.

Ohinata, Y., M. Sano, M. Shigeta, K. Yamanaka and M. J. R. Saitou. 2008. A comprehensive, non-invasive visualization of primordial germ cell development in mice by the Blimp1-mVenus and stella-ECFP double transgenic reporter.

Okamoto, M., H. Takemori and Y. Katoh. 2004. Salt-inducible kinase in steroidogenesis and adipogenesis. *Trends Endocrinol Metab,* **15**(1), pp.21-6.

Oracki, S. A., J. A. Walker, M. L. Hibbs, L. M. Corcoran and D. M. J. I. R. Tarlinton. 2010. Plasma cell development and survival. **237**(1), pp.140-159.

Ozaki, K., R. Spolski, R. Ettinger, H.-P. Kim, G. Wang, C.-F. Qi, P. Hwu, D. J. Shaffer, S. Akilesh and D. C. J. T. J. O. I. Roopenian. 2004. Regulation of B cell differentiation and plasma cell generation by IL-21, a novel inducer of Blimp-1 and Bcl-6. **173**(9), pp.5361-5371.

Ozanne, J., A. R. Prescott and K. Clark. 2015. The clinically approved drugs dasatinib and bosutinib induce anti-inflammatory macrophages by inhibiting the salt-inducible kinases. *Biochem J,* **465**(2), pp.271-9.

Ozcan, E., L. Garibyan, J. Lee, R. J. T. J. O. A. Geha and C. Immunology. 2009. Taci Drives Plasma Cell Differentiation in Lps Activated B Cells: 351. **123**(2), pS94.

Park, J., Y. S. Yoon, H. S. Han, Y. H. Kim, Y. Ogawa, K. G. Park, C. H. Lee, S. T. Kim and S. H. Koo. 2014. SIK2 is critical in the regulation of lipid homeostasis and adipogenesis in vivo. *Diabetes,* **63**(11), pp.3659-73.

Parra-Damas, A., M. Chen, L. Enriquez-Barreto, L. Ortega, S. Acosta, J. C. Perna, M. N. Fullana, J. Aguilera, J. Rodriguez-Alvarez and C. A. Saura. 2017. CRTC1 Function During Memory Encoding Is Disrupted in Neurodegeneration. *Biol Psychiatry,* **81**(2), pp.111-123.

Patel, K., M. Foretz, A. Marion, D. G. Campbell, R. Gourlay, N. Boudaba, E. Tournier, P. Titchenell, M. Peggie, M. Deak, M. Wan, K. H. Kaestner, O. Goransson, B. Viollet, N. S. Gray, M. J. Birnbaum, C. Sutherland and K. Sakamoto. 2014. The LKB1-salt-inducible kinase pathway functions as a key gluconeogenic suppressor in the liver. *Nat Commun,* **5**, p4535.

Paul, W. E. 2013. *Fundamental immunology.* Philadelphia: Wolters Kluwer Health/Lippincott Williams & Wilkins.

Pauls, E., S. K. Nanda, H. Smith, R. Toth, J. S. C. Arthur and P. Cohen. 2013. Two phases of inflammatory mediator production defined by the study of IRAK2 and IRAK1 knock-in mice. *J Immunol,* **191**(5), pp.2717-30.

Pei, Y., K. W. Liu, J. Wang, A. Garancher, R. Tao, L. A. Esparza, D. L. Maier, Y. T. Udaka, N. Murad, S. Morrissy, H. Seker-Cin, S. Brabetz, L. Qi, M. Kogiso, S. Schubert, J. M. Olson, Y. J. Cho, X. N. Li, J. R. Crawford, M. L. Levy, M. Kool, S. M. Pfister, M. D. Taylor and R. J. Wechsler-Reya. 2016. HDAC and PI3K Antagonists Cooperate to Inhibit Growth of MYC-Driven Medulloblastoma. *Cancer Cell,* **29**(3), pp.311-323.

Pellegrini, A., N. Guinazu, M. P. Aoki, I. C. Calero, E. A. Carrera-Silva, N. Girones, M. Fresno and S. Gea. 2007. Spleen B cells from BALB/c are more prone to activation than spleen B cells from C57BL/6 mice during a secondary immune response to cruzipain. *Int Immunol,* **19**(12), pp.1395-402.

Pelletier, N., M. Casamayor-Palleja, K. De Luca, P. Mondiere, F. Saltel, P. Jurdic, C. Bella, L. Genestier and T. Defrance. 2006. The endoplasmic reticulum is a key component of the plasma cell death pathway. *J Immunol,* **176**(3), pp.1340-7.

Pène, J., J.-F. Gauchat, S. Lécart, E. Drouet, P. Guglielmi, V. Boulay, A. Delwail, D. Foster, J.-C. Lecron and H. J. T. J. O. I. Yssel. 2004. Cutting edge: IL-21 is a switch factor for the production of IgG1 and IgG3 by human B cells. **172**(9), pp.5154-5157.

Pennock, N. D., J. T. White, E. W. Cross, E. E. Cheney, B. A. Tamburini and R. M. Kedl. 2013. T cell responses: naive to memory and everything in between. *Adv Physiol Educ,* **37**(4), pp.273-83.

Peperzak, V., I. Vikstrom, J. Walker, S. P. Glaser, M. Lepage, C. M. Coquery, L. D. Erickson, K. Fairfax, F. Mackay, A. Strasser, S. L. Nutt and D. M. Tarlinton. 2013. Mcl-1 is essential for the survival of plasma cells. *Nat Immunol,* **14**(3), pp.290-7.

Peroval, M. Y., A. C. Boyd, J. R. Young and A. L. Smith. 2013. A critical role for MAPK signalling pathways in the transcriptional regulation of toll like receptors. *PLoS One,* **8**(2), pe51243.

Peters, P. J., J. Borst, V. Oorschot, M. Fukuda, O. Krahenbuhl, J. Tschopp, J. W. Slot and H. J. Geuze. 1991. Cytotoxic T lymphocyte granules are secretory lysosomes, containing both perforin and granzymes. *J Exp Med,* **173**(5), pp.1099-109.

Potthoff, M. J., H. Wu, M. A. Arnold, J. M. Shelton, J. Backs, J. Mcanally, J. A. Richardson, R. Bassel-Duby and E. N. Olson. 2007. Histone deacetylase degradation and MEF2 activation promote the formation of slow-twitch myofibers. *J Clin Invest,* **117**(9), pp.2459-67.

Qu, C., He, X. Lu, L. Dong, Y. Zhu, Q. Zhao, X. Jiang, P. Chang, X. Jiang, L. Wang, Y. Zhang, L. Bi, J. He, Y. Peng, J. Su, H. Zhang, H. Huang, Y. Li, S. Zhou, Y. Qu, Y. Zhao and Z. Zhang. 2016. Salt-inducible Kinase (SIK1) regulates HCC progression and WNT/beta-catenin activation. *J Hepatol,* **64**(5), pp.1076-1089.

Qu, C. and Y. Qu. 2017. Down-regulation of salt-inducible kinase 1 (SIK1) is mediated by RNF2 in hepatocarcinogenesis. *Oncotarget,* **8**(2), pp.3144-3155.

Radl, J., C. F. Hollander, P. Van Den Berg and E. De Glopper. 1978. Idiopathic paraproteinaemia. I. Studies in an animal model--the ageing C57BL/KaLwRij mouse. *Clin Exp Immunol,* **33**(3), pp.395-402.

Ravnskjaer, K., H. Kester, Y. Liu, X. Zhang, D. Lee, J. R. Yates, 3rd and M. Montminy. 2007. Cooperative interactions between CBP and TORC2 confer selectivity to CREB target gene expression. *Embo j,* **26**(12), pp.2880-9.

Reya, T. and R. Grosschedl. 1998. Transcriptional regulation of B-cell differentiation. *Curr Opin Immunol,* **10**(2), pp.158-65.

Rizzieri, D., B. Paul and Y. Kang. 2019. Metabolic alterations and the potential for targeting metabolic pathways in the treatment of multiple myeloma. *J Cancer Metastasis Treat,* **5**.

Robey, R. B. and N. Hay. 2006. Mitochondrial hexokinases, novel mediators of the antiapoptotic effects of growth factors and Akt. *Oncogene,* **25**(34), pp.4683-96.

Robinson, J. T., H. Thorvaldsdottir, W. Winckler, M. Guttman, E. S. Lander, G. Getz and J. P. Mesirov. 2011. Integrative genomics viewer. *Nat Biotechnol,* **29**(1), pp.24-6.

Ron, D. and P. Walter. 2007. Signal integration in the endoplasmic reticulum unfolded protein response. *Nat Rev Mol Cell Biol,* **8**(7), pp.519-29.

Rossi, M., C. Abbondanza, A. D'arcangelo, P. Gazzerro, N. Medici, B. Moncharmont and G. A. Puca. 2004. The Zn-finger domain of RIZ protein promotes MCF-7 cell proliferation. *Cancer Lett,* **215**(2), pp.229-37.

Roth, K., L. Oehme, S. Zehentmeier, Y. Zhang, R. Niesner and A. E. J. C. P. A. Hauser. 2014. Tracking plasma cell differentiation and survival. **85**(1), pp.15-24.

Sakamoto, K., L. Bultot, O. J. T. I. E. Göransson and Metabolism. 2018. The salt-inducible kinases: emerging metabolic regulators. **29**(12), pp.827-840.

Sakamoto, K., F. E. Norona, D. Alzate-Correa, D. Scarberry, K. R. Hoyt and K. Obrietan. 2013. Clock and light regulation of the CREB coactivator CRTC1 in the suprachiasmatic circadian clock. *J Neurosci,* **33**(21), pp.9021-7.

Sall, J., A. M. Pettersson, C. Bjork, E. Henriksson, S. Wasserstrom, W. Linder, Y. Zhou, O. Hansson, D. P. Andersson, M. Ekelund, E. Degerman, K. G. Stenkula, J. Laurencikiene and O. Goransson. 2017. Salt-inducible kinase 2 and -3 are downregulated in adipose tissue

from obese or insulin-resistant individuals: implications for insulin signalling and glucose uptake in human adipocytes. *Diabetologia,* **60**(2), pp.314-323.

Sasaki, T., H. Takemori, Y. Yagita, Y. Terasaki, T. Uebi, N. Horike, H. Takagi, T. Susumu, H. Teraoka, K. Kusano, O. Hatano, N. Oyama, Y. Sugiyama, S. Sakoda and K. Kitagawa. 2011. SIK2 is a key regulator for neuronal survival after ischemia via TORC1-CREB. *Neuron,* **69**(1), pp.106-19.

Savage, H. P., V. M. Yenson, S. S. Sawhney, B. J. Mousseau, F. E. Lund and N. J. J. O. E. M. Baumgarth. 2017. Blimp-1–dependent and–independent natural antibody production by B-1 and B-1–derived plasma cells. **214**(9), pp.2777-2794.

Schmidlin, H., S. A. Diehl, M. Nagasawa, F. A. Scheeren, R. Schotte, C. H. Uittenbogaart, H. Spits and B. Blom. 2008. Spi-B inhibits human plasma cell differentiation by repressing BLIMP1 and XBP-1 expression. *Blood,* **112**(5), pp.1804-12.

Schmidt, D., A. Nayak, J. E. Schumann, A. Schimpl, I. Berberich and F. Berberich-Siebelt. 2008. Blimp-1Deltaexon7: a naturally occurring Blimp-1 deletion mutant with auto-regulatory potential. *Exp Cell Res,* **314**(20), pp.3614-27.

Schoepflin, Z. R., I. M. Shapiro and M. V. Risbud. 2016. Class I and IIa HDACs Mediate HIF-1alpha Stability Through PHD2-Dependent Mechanism, While HDAC6, a Class IIb Member, Promotes HIF-1alpha Transcriptional Activity in Nucleus Pulposus Cells of the Intervertebral Disc. *J Bone Miner Res,* **31**(6), pp.1287-99.

Schwanhäusser, B., D. Busse, N. Li, G. Dittmar, J. Schuchhardt, J. Wolf, W. Chen and M. J. N. Selbach. 2011. Global quantification of mammalian gene expression control. **473**(7347), p337.

Sciammas, R., A. L. Shaffer, J. H. Schatz, H. Zhao, L. M. Staudt and H. Singh. 2006. Graded expression of interferon regulatory factor-4 coordinates isotype switching with plasma cell differentiation. *Immunity,* **25**(2), pp.225-36.

Scott, K., P. J. Hayden, A. Will, K. Wheatley and I. J. C. D. O. S. R. Coyne. 2016. Bortezomib for the treatment of multiple myeloma. (4).

Screaton, R. A., M. D. Conkright, Y. Katoh, J. L. Best, G. Canettieri, S. Jeffries, E. Guzman, S. Niessen, J. R. Yates, 3rd, H. Takemori, M. Okamoto and M. Montminy. 2004. The CREB coactivator TORC2 functions as a calcium- and cAMP-sensitive coincidence detector. *Cell,* **119**(1), pp.61-74.

Sebbagh, M., M. J. Santoni, B. Hall, J. P. Borg and M. A. Schwartz. 2009. Regulation of LKB1/STRAD localization and function by E-cadherin. *Curr Biol,* **19**(1), pp.37-42.

Seiffert, M., S. Stilgenbauer, H. Dohner and P. Lichter. 2007. Efficient nucleofection of primary human B cells and B-CLL cells induces apoptosis, which depends on the microenvironment and on the structure of transfected nucleic acids. *Leukemia,* **21**(9), pp.1977-83.

Selvik, L. K., S. Rao, T. S. Steigedal, I. Haltbakk, K. Misund, T. Bruland, W. S. Prestvik, A. Laegreid and L. Thommesen. 2014. Salt-inducible kinase 1 (SIK1) is induced by gastrin and inhibits migration of gastric adenocarcinoma cells. *PLoS One,* **9**(11), pe112485.

Shaffer, A. L., N. C. Emre, L. Lamy, V. N. Ngo, G. Wright, W. Xiao, J. Powell, S. Dave, X. Yu, H. Zhao, Y. Zeng, B. Chen, J. Epstein and L. M. Staudt. 2008. IRF4 addiction in multiple myeloma. *Nature,* **454**(7201), pp.226-31.

Shaffer, A. L., K. I. Lin, T. C. Kuo, X. Yu, E. M. Hurt, A. Rosenwald, J. M. Giltnane, L. Yang, H. Zhao, K. Calame and L. M. Staudt. 2002. Blimp-1 orchestrates plasma cell differentiation by extinguishing the mature B cell gene expression program. *Immunity,* **17**(1), pp.51-62.

Shaffer, A. L., M. Shapiro-Shelef, N. N. Iwakoshi, A. H. Lee, S. B. Qian, H. Zhao, X. Yu, L. Yang, B. K. Tan, A. Rosenwald, E. M. Hurt, E. Petroulakis, N. Sonenberg, J. W. Yewdell, K. Calame, L. H. Glimcher and L. M. Staudt. 2004. XBP1, downstream of Blimp-1, expands the secretory apparatus and other organelles, and increases protein synthesis in plasma cell differentiation. *Immunity,* **21**(1), pp.81-93.

Shapiro-Shelef, M. and K. Calame. 2005. Regulation of plasma-cell development. *Nat Rev Immunol,* **5**(3), pp.230-42.

Shapiro-Shelef, M., K.-I. Lin, L. J. Mcheyzer-Williams, J. Liao, M. G. Mcheyzer-Williams and K. J. I. Calame. 2003. Blimp-1 is required for the formation of immunoglobulin secreting plasma cells and pre-plasma memory B cells. **19**(4), pp.607-620.

Sherman, M. H., A. I. Kuraishy, C. Deshpande, J. S. Hong, N. A. Cacalano, R. A. Gatti, J. P. Manis, M. A. Damore, M. Pellegrini and M. a. J. M. C. Teitell. 2010. AID-induced genotoxic stress promotes B cell differentiation in the germinal center via ATM and LKB1 signaling. **39**(6), pp.873-885.

Shi, W., Y. Liao, S. N. Willis, N. Taubenheim, M. Inouye, D. M. Tarlinton, G. K. Smyth, P. D. Hodgkin, S. L. Nutt and L. M. J. N. I. Corcoran. 2015. Transcriptional profiling of mouse B cell terminal differentiation defines a signature for antibody-secreting plasma cells. **16**(6), p663.

Silbermann, R. and G. D. J. J. O. B. O. Roodman. 2013. Myeloma bone disease: pathophysiology and management. **2**(2), pp.59-69.

Siu, Y. T. and D. Y. Jin. 2007. CREB--a real culprit in oncogenesis. *Febs j,* **274**(13), pp.3224-32.

Slifka, M. K., R. Antia, J. K. Whitmire and R. J. I. Ahmed. 1998. Humoral immunity due to long-lived plasma cells. **8**(3), pp.363-372.

Smith, M. A., M. Maurin, H. I. Cho, B. Becknell, A. G. Freud, J. Yu, S. Wei, J. Djeu, E. Celis, M. A. Caligiuri and K. L. Wright. 2010. PRDM1/Blimp-1 controls effector cytokine production in human NK cells. *J Immunol,* **185**(10), pp.6058-67.

Soneson, C., M. I. Love and M. D. Robinson. 2015. Differential analyses for RNA-seq: transcript-level estimates improve gene-level inferences. *F1000Res,* **4**, p1521.

Sonntag, T., J. J. Moresco, J. M. Vaughan, S. Matsumura, J. R. Yates, 3rd and M. Montminy. 2017. Analysis of a cAMP regulated coactivator family reveals an alternative phosphorylation motif for AMPK family members. *PLoS One,* **12**(2), pe0173013.

Sonntag, T., J. M. Vaughan and M. Montminy. 2018. 14-3-3 proteins mediate inhibitory effects of cAMP on salt-inducible kinases (SIKs). *Febs j,* **285**(3), pp.467-480.

Sorrentino, A., A. Federico, M. Rienzo, P. Gazzerro, M. Bifulco, A. Ciccodicola, A. Casamassimi and C. Abbondanza. 2018. PR/SET Domain Family and Cancer: Novel Insights from the Cancer Genome Atlas. *Int J Mol Sci,* **19**(10).

Sridevi, H. B., S. Rai, P. K. Suresh, M. S. Somesh, J. J. J. O. C. Minal and D. R. Jcdr. 2015. Pancytopenia in multiple myeloma-an enigma: our experience from tertiary care hospital. **9**(11), pEC04.

Stavnezer, J., J. E. Guikema and C. E. Schrader. 2008. Mechanism and regulation of class switch recombination. *Annu Rev Immunol,* **26**, pp.261-92.

Steinman, R. M., S. J. Blumencranz, B. G. Machtinger, J. Fried and Z. A. Cohn. 1978. Mouse spleen lymphoblasts generated in vitro. Their replication and differentiation in vitro. *J Exp Med,* **147**(2), pp.297-315.

Stenstrom, K., H. Takemori, G. Bianchi, A. I. Katz and A. M. Bertorello. 2009. Blocking the salt-inducible kinase 1 network prevents the increases in cell sodium transport caused by a hypertension-linked mutation in human alpha-adducin. *J Hypertens,* **27**(12), pp.2452-7.

Stewart, R., D. Akhmedov, C. Robb, C. Leiter and R. Berdeaux. 2013a. Regulation of SIK1 abundance and stability is critical for myogenesis. *Proc Natl Acad Sci U S A,* **110**(1), pp.117-22.

Stewart, R., D. Akhmedov, C. Robb, C. Leiter and R. J. P. O. T. N. a. O. S. Berdeaux. 2013b. Regulation of SIK1 abundance and stability is critical for myogenesis. **110**(1), pp.117-122.

Su, T. T. and D. J. Rawlings. 2002. Transitional B lymphocyte subsets operate as distinct checkpoints in murine splenic B cell development. *J Immunol,* **168**(5), pp.2101-10.

Sundberg, T. B., H. G. Choi, J. H. Song, C. N. Russell, M. M. Hussain, D. B. Graham, B. Khor, J. Gagnon, D. J. O'connell, K. Narayan, V. Dancik, J. R. Perez, H. C. Reinecker, N. S. Gray, S. L. Schreiber, R. J. Xavier and A. F. Shamji. 2014. Small-molecule screening identifies inhibition of salt-inducible kinases as a therapeutic strategy to enhance immunoregulatory functions of dendritic cells. *Proc Natl Acad Sci U S A,* **111**(34), pp.12468-73.

Sundberg, T. B., Y. Liang, H. Wu, H. G. Choi, N. D. Kim, T. Sim, L. Johannessen, A. Petrone, B. Khor, D. B. Graham, I. J. Latorre, A. J. Phillips, S. L. Schreiber, J. Perez, A. F. Shamji, N. S. Gray and R. J. Xavier. 2016. Development of Chemical Probes for Investigation of Salt-Inducible Kinase Function in Vivo. *ACS Chem Biol,* **11**(8), pp.2105-11.

Sze, D. M., K. M. Toellner, C. Garcia De Vinuesa, D. R. Taylor and I. C. Maclennan. 2000. Intrinsic constraint on plasmablast growth and extrinsic limits of plasma cell survival. *J Exp Med,* **192**(6), pp.813-21.

Tai, Y. T., C. Acharya, G. An, M. Moschetta, M. Y. Zhong, X. Feng, M. Cea, A. Cagnetta, K. Wen, H. Van Eenennaam, A. Van Elsas, L. Qiu, P. Richardson, N. Munshi and K. C. Anderson. 2016. APRIL and BCMA promote human multiple myeloma growth and immunosuppression in the bone marrow microenvironment. *Blood,* **127**(25), pp.3225-36.

Tai, Y. T., B. Y. Chang, S. Y. Kong, M. Fulciniti, G. Yang, Y. Calle, Y. Hu, J. Lin, J. J. Zhao, A. Cagnetta, M. Cea, M. A. Sellitto, M. Y. Zhong, Q. Wang, C. Acharya, D. R. Carrasco, J. J. Buggy, L. Elias, S. P. Treon, W. Matsui, P. Richardson, N. C. Munshi and K. C. Anderson. 2012. Bruton tyrosine kinase inhibition is a novel therapeutic strategy targeting tumor in the bone marrow microenvironment in multiple myeloma. *Blood,* **120**(9), pp.1877-87.

Takemori, H., Y. Katoh, N. Horike, J. Doi and M. Okamoto. 2002. ACTH-induced nucleocytoplasmic translocation of salt-inducible kinase. Implication in the protein kinase A-activated gene transcription in mouse adrenocortical tumor cells. *J Biol Chem,* **277**(44), pp.42334-43.

Tang, H.-M. V., W.-W. Gao, C.-P. Chan, Y.-T. Siu, C.-M. Wong, K.-H. Kok, Y.-P. Ching, H. Takemori and D.-Y. J. R. Jin. 2013. LKB1 tumor suppressor and salt-inducible kinases negatively regulate human T-cell leukemia virus type 1 transcription. **10**(1), p40.

Tarte, K., F. Zhan, J. De Vos, B. Klein and J. J. B. Shaughnessy. 2003. Gene expression profiling of plasma cells and plasmablasts: toward a better understanding of the late stages of B-cell differentiation. **102**(2), pp.592-600.

Tarumoto, Y., B. Lu, T. D. D. Somerville, Y. H. Huang, J. P. Milazzo, X. S. Wu, O. Klingbeil, O. El Demerdash, J. Shi and C. R. Vakoc. 2018. LKB1, Salt-Inducible Kinases, and MEF2C Are Linked Dependencies in Acute Myeloid Leukemia. *Mol Cell,* **69**(6), pp.1017-1027.e6.

Tas, J. M., L. Mesin, G. Pasqual, S. Targ, J. T. Jacobsen, Y. M. Mano, C. S. Chen, J. C. Weill, C. A. Reynaud, E. P. Browne, M. Meyer-Hermann and G. D. Victora. 2016. Visualizing antibody affinity maturation in germinal centers. *Science,* **351**(6277), pp.1048-54.

Tellier, J. and S. L. J. E. J. O. I. Nutt. 2017. Standing out from the crowd: How to identify plasma cells. **47**(8), pp.1276-1279.

Tellier, J., W. Shi, M. Minnich, Y. Liao, S. Crawford, G. K. Smyth, A. Kallies, M. Busslinger and S. L. Nutt. 2016a. Blimp-1 controls plasma cell function through the regulation of immunoglobulin secretion and the unfolded protein response. *Nat Immunol,* **17**(3), pp.323-30.

Tellier, J., W. Shi, M. Minnich, Y. Liao, S. Crawford, G. K. Smyth, A. Kallies, M. Busslinger and S. L. J. N. I. Nutt. 2016b. Blimp-1 controls plasma cell function through the regulation of immunoglobulin secretion and the unfolded protein response. **17**(3), p323.

Tellkamp, F., F. Benhadou, J. Bremer, M. Gnarra, J. Knuver, S. Schaffenrath and S. Vorhagen. 2014. Transgenic mouse technology in skin biology: generation of knockin mice. *J Invest Dermatol,* **134**(12), pp.1-3.

Thomas, M., M. Calamito, B. Srivastava, I. Maillard, W. S. Pear and D. Allman. 2007. Notch activity synergizes with B-cell-receptor and CD40 signaling to enhance B-cell activation. *Blood,* **109**(8), pp.3342-50.

Todd, D. J., L. J. Mcheyzer-Williams, C. Kowal, A. H. Lee, B. T. Volpe, B. Diamond, M. G. Mcheyzer-Williams and L. H. Glimcher. 2009. XBP1 governs late events in plasma cell differentiation and is not required for antigen-specific memory B cell development. *J Exp Med,* **206**(10), pp.2151-9.

Tonegawa, S., C. Steinberg, S. Dube and A. Bernardini. 1974. Evidence for Somatic Generation of Antibody Diversity. **71**(10), pp.4027-4031.

Tooze, R. M. J. F. I. I. 2013. A replicative self-renewal model for long-lived plasma cells: questioning irreversible cell cycle exit. **4**, p460.

Treanor, B. J. I. 2012. B-cell receptor: from resting state to activate. **136**(1), pp.21-27.

Tunyaplin, C., M. A. Shapiro and K. L. Calame. 2000. Characterization of the B lymphocyte-induced maturation protein-1 (Blimp-1) gene, mRNA isoforms and basal promoter. *Nucleic Acids Res,* **28**(24), pp.4846-55.

Vale, A. M. and H. W. Schroeder, Jr. 2010. Clinical consequences of defects in B-cell development. *J Allergy Clin Immunol,* **125**(4), pp.778-87.

Van Anken, E., E. P. Romijn, C. Maggioni, A. Mezghrani, R. Sitia, I. Braakman and A. J. Heck. 2003. Sequential waves of functionally related proteins are expressed when B cells prepare for antibody secretion. *Immunity,* **18**(2), pp.243-53.

Waibel, M., A. J. Christiansen, M. L. Hibbs, J. Shortt, S. A. Jones, I. Simpson, A. Light, K. O'donnell, E. F. Morand, D. M. Tarlinton, R. W. Johnstone and E. D. Hawkins. 2015. Manipulation of B-cell responses with histone deacetylase inhibitors. *Nat Commun,* **6**, p6838.

Walkinshaw, D. R., R. Weist, G. W. Kim, L. You, L. Xiao, J. Nie, C. S. Li, S. Zhao, M. Xu and X. J. Yang. 2013. The tumor suppressor kinase LKB1 activates the downstream kinases SIK2 and SIK3 to stimulate nuclear export of class IIa histone deacetylases. *J Biol Chem,* **288**(13), pp.9345-62.

Walsh, N. C., L. R. Waters, J. A. Fowler, M. Lin, C. R. Cunningham, D. G. Brooks, J. E. Rehg, H. C. Morse, 3rd and M. A. Teitell. 2015. LKB1 inhibition of NF-kappaB in B cells prevents T follicular helper cell differentiation and germinal center formation. *EMBO Rep,* **16**(6), pp.753-68.

Wang, B., N. Moya, S. Niessen, H. Hoover, M. M. Mihaylova, R. J. Shaw, J. R. Yates, 3rd, W. H. Fischer, J. B. Thomas and M. Montminy. 2011. A hormone-dependent module regulating energy balance. *Cell,* **145**(4), pp.596-606.

Wang, Y., X. Du, J. Wei, L. Long, H. Tan, C. Guy, Y. Dhungana, C. Qian, G. Neale, Y. X. Fu, J. Yu, J. Peng and H. Chi. 2019. LKB1 orchestrates dendritic cell metabolic quiescence and anti-tumor immunity. *Cell Res,* **29**(5), pp.391-405.

Wang, Z., G. Qin and T. C. Zhao. 2014. HDAC4: mechanism of regulation and biological functions. *Epigenomics,* **6**(1), pp.139-50.

Wang, Z., H. Takemori, S. K. Halder, Y. Nonaka and M. Okamoto. 1999. Cloning of a novel kinase (SIK) of the SNF1/AMPK family from high salt diet-treated rat adrenal. *FEBS Lett,* **453**(1-2), pp.135-9.

Waters, L. R., N. C. Walsh and M. A. Teitell. 2015. LKB1 regulates germinal center formation and termination. *Cell Cycle,* **14**(14), pp.2183-4.

Wein, M. N., M. Foretz, D. E. Fisher, R. J. Xavier, H. M. J. T. I. E. Kronenberg and Metabolism. 2018. Salt-inducible kinases: physiology, regulation by cAMP, and therapeutic potential.

Wein, M. N., Y. Liang, O. Goransson, T. B. Sundberg, J. Wang, E. A. Williams, M. J. O'meara, N. Govea, B. Beqo, S. Nishimori, K. Nagano, D. J. Brooks, J. S. Martins, B. Corbin, A. Anselmo, R. Sadreyev, J. Y. Wu, K. Sakamoto, M. Foretz, R. J. Xavier, R. Baron, M. L. Bouxsein, T. J. Gardella, P. Divieti-Pajevic, N. S. Gray and H. M. Kronenberg. 2016. SIKs control osteocyte responses to parathyroid hormone. *Nature Communications,* **7**, p13176.

Wilker, P. R., M. Kohyama, M. M. Sandau, J. C. Albring, O. Nakagawa, J. J. Schwarz and K. M. Murphy. 2008. Transcription factor Mef2c is required for B cell proliferation and survival after antigen receptor stimulation. *Nat Immunol,* **9**(6), pp.603-12.

Woods, A., S. R. Johnstone, K. Dickerson, F. C. Leiper, L. G. Fryer, D. Neumann, U. Schlattner, T. Wallimann, M. Carlson and D. Carling. 2003. LKB1 is the upstream kinase in the AMP-activated protein kinase cascade. *Curr Biol,* **13**(22), pp.2004-8.

Wu, Y., N. M. Van Besouw, Y. Shi, M. J. Hoogduijn, L. Wang and C. C. J. F. I. I. Baan. 2016. The biological effects of IL-21 signaling on B-cell-mediated responses in organ transplantation. **7**, p319.

Xu, Z., E. J. Pone, A. Al-Qahtani, S. R. Park, H. Zan and P. Casali. 2007. Regulation of aicda expression and AID activity: relevance to somatic hypermutation and class switch DNA recombination. *Crit Rev Immunol,* **27**(4), pp.367-97.

Yang, M., H. Hase, D. Legarda-Addison, L. Varughese, B. Seed and A. T. Ting. 2005. B cell maturation antigen, the receptor for a proliferation-inducing ligand and B cell-activating factor of the TNF family, induces antigen presentation in B cells. *J Immunol,* **175**(5), pp.2814-24.

Yasuda, T., K. Kometani, N. Takahashi, Y. Imai, Y. Aiba and T. Kurosaki. 2011. ERKs induce expression of the transcriptional repressor Blimp-1 and subsequent plasma cell differentiation. *Sci Signal,* **4**(169), pra25.

Ying, C. Y., D. Dominguez-Sola, M. Fabi, I. C. Lorenz, S. Hussein, M. Bansal, A. Califano, L. Pasqualucci, K. Basso and R. Dalla-Favera. 2013. MEF2B mutations lead to deregulated expression of the oncogene BCL6 in diffuse large B cell lymphoma. *Nat Immunol,* **14**(10), pp.1084-92.

Zan, H. and P. Casali. 2013. Regulation of Aicda expression and AID activity. *Autoimmunity,* **46**(2), pp.83-101.

Zhang, C. L., T. A. Mckinsey, S. Chang, C. L. Antos, J. A. Hill and E. N. Olson. 2002. Class II histone deacetylases act as signal-responsive repressors of cardiac hypertrophy. *Cell,* **110**(4), pp.479-88.

Zhang, X., D. T. Odom, S. H. Koo, M. D. Conkright, G. Canettieri, J. Best, H. Chen, R. Jenner, E. Herbolsheimer, E. Jacobsen, S. Kadam, J. R. Ecker, B. Emerson, J. B. Hogenesch, T. Unterman, R. A. Young and M. Montminy. 2005. Genome-wide analysis of cAMP-response element binding protein occupancy, phosphorylation, and target gene activation in human tissues. *Proc Natl Acad Sci U S A,* **102**(12), pp.4459-64.

Zhou, J., A. Alfraidi, S. Zhang, J. M. Santiago-O'farrill, V. K. Yerramreddy Reddy, A. Alsaadi, A. A. Ahmed, H. Yang, J. Liu, W. Mao, Y. Wang, H. Takemori, H. Vankayalapati, Z. Lu and R. C. Bast, Jr. 2017. A Novel Compound ARN-3236 Inhibits Salt-Inducible Kinase 2 and Sensitizes Ovarian Cancer Cell Lines and Xenografts to Paclitaxel. *Clin Cancer Res,* **23**(8), pp.1945-1954.

Zhou, J. H., J. F. Markham, K. R. Duffy and P. D. J. F. I. I. Hodgkin. 2018. Stochastically Timed Competition Between Division and Differentiation Fates Regulates the Transition From B Lymphoblast to Plasma Cell. **9**.

Zhou, Q., A. T. Agoston, P. Atadja, W. G. Nelson and N. E. Davidson. 2008. Inhibition of histone deacetylases promotes ubiquitin-dependent proteasomal degradation of DNA methyltransferase 1 in human breast cancer cells. *Mol Cancer Res,* **6**(5), pp.873-83.

Zhu, A., J. G. Ibrahim and M. I. Love. 2018. Heavy-tailed prior distributions for sequence count data: removing the noise and preserving large differences. *Bioinformatics*.

Zhu, J. and W. E. Paul. 2008. CD4 T cells: fates, functions, and faults. *Blood,* **112**(5), pp.1557-69.

Appendix

Appendix 1: A plasmid map showing the restriction enzymes chosen to sub-clone HA-SIK1 from pUC57 into pIRES2-EGFP. MCS; multiple cloning site, KanR; kanamycin resistance cassette, IRES; internal ribosome entry site, EGFP; enhanced green fluorescent protein.

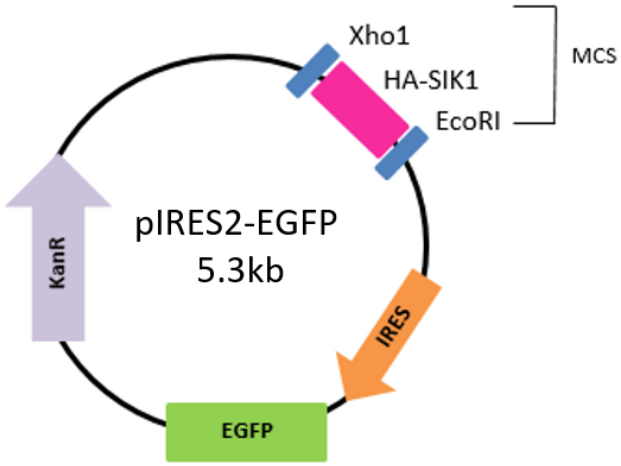

Appendix 2: A plasmid map showing the restriction enzymes chosen to sub-clone HA-SIK1 mutants from pCMV5 into pIRES2-EGFP.

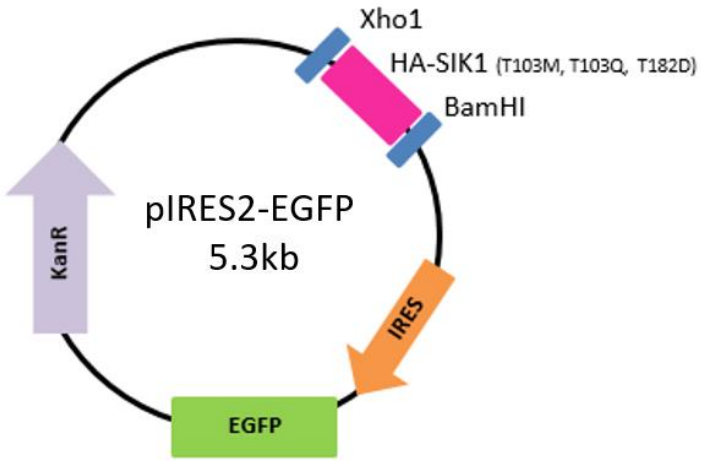

Appendix 3: Determining antibody specificity against SIK1, SIK2 and SIK3. HeLa cells were transfected with vectors encoding HA-SIK1, HA-SIK2 or HA-SIK3. Cells extracts were separated by SDS-PAGE and immunoblotted with the indicated antibodies.

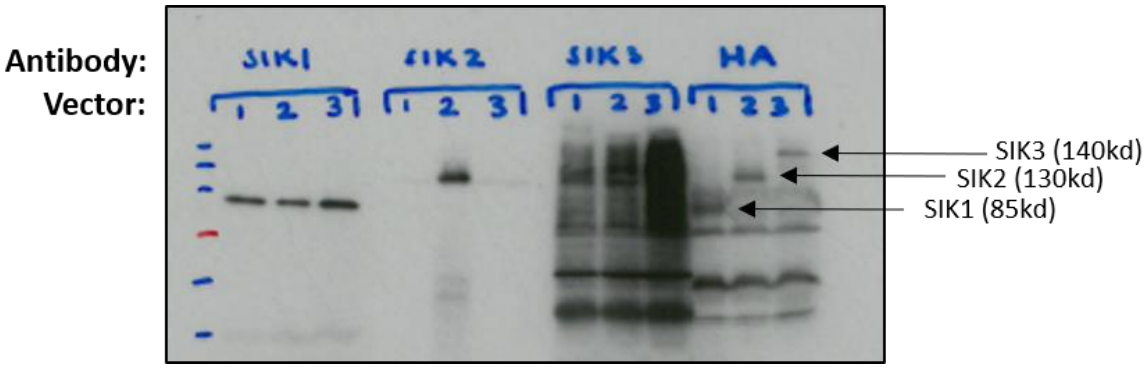

Appendix 4: Detection of HA-SIK1 WT and mutant vector expression in HeLa cells using SIK1 antibody.

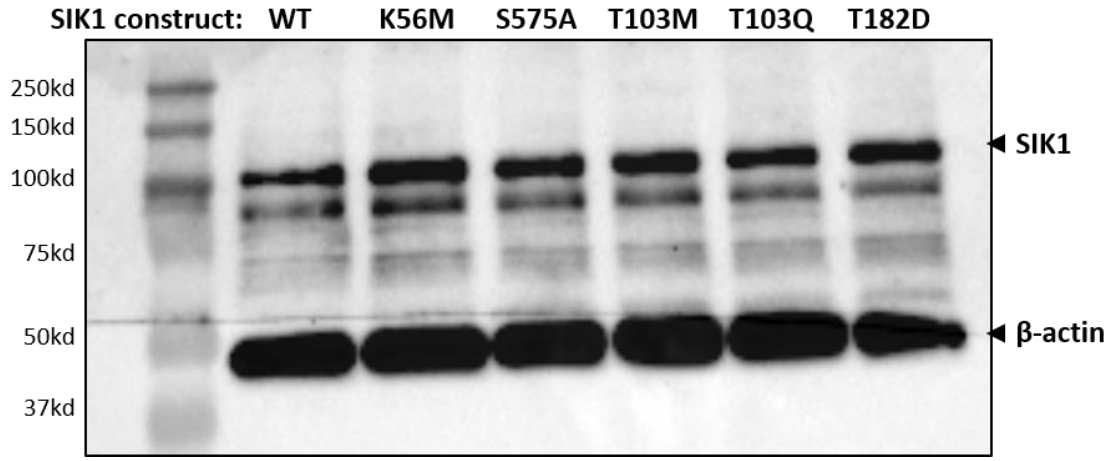

Appendix 5: Splice variants upstream of exon 1 in Δ*ex1A* mice.